Effects of eccentricity, contrast, orientation and the number and length of grating bars on orientation discrimination

Liu Cui

Doctor of Philosophy

School of Optometry and Vision Sciences,
Cardiff University

2010

ProQuest LLC
789 East Eisenhower Parkway
P.O. Box 1346
Ann Arbor, MI 48106-1346

DECLARATION

This work has not previously been accepted in substance for any degree and is not concurrently submitted in candidature for any degree.

Signed ..... (candidate) Date 24-08-10

STATEMENT 1

This thesis is being submitted in partial fulfillment of the requirements for the degree of .....**PhD**.....(insert MCh, MD, MPhil, PhD etc, as appropriate)

Signed ..... (candidate) Date 24-08-10

STATEMENT 2

This thesis is the result of my own independent work/investigation, except where otherwise stated. Other sources are acknowledged by explicit references.

Signed ..... (candidate) Date 24-08-10

STATEMENT 3

I hereby give consent for my thesis, if accepted, to be available for photocopying and for inter-library loan, and for the title and summary to be made available to outside organisations.

Signed ..... (candidate) Date 24-08-10

Summary

E_2 indicates the eccentricity where stimulus size must double to maintain performance equivalent to that at fovea. An over 200-fold range of E_2 has been found using spatial scaling since the introduction of method.

Some later research in orientation discrimination suggested that contrast reduction elevated E_2 (Sally and Gurnesy 2003, 2004 and 2007). However, it was based on very limited data. Therefore, to examine how E_2 changes with contrast, two types of orientation discrimination tasks involving six experiments were studied using spatial scaling in the thesis: (i) orientation discrimination at 10-100% contrasts and 0-10 degree eccentricities using Gaussian-filtered lines and 2-16 cycles-per-image (cpi) gratings, and (ii) contrast thresholds allowing discrimination of 1.5-45 degrees orientation differences (OD) at 0-10 degree eccentricities using the same stimuli for the first task.

Three hypotheses were made: (i) when the effect of contrast was taken into account, the peripheral stimulus size required for performance equivalent to that of the fovea can be obtained at a range of contrasts by spatial scaling, and (ii) for low-cycle-number ($\leq$16 cpi) grating stimulus, the number of cycles played a crucial role on the visual performance across visual field, and (iii) for the threshold contrast of a fixed orientation difference discrimination, the visual process mechanism of the visual task at large orientation difference was different from that at small difference close to orientation discrimination threshold.

The results of the orientation discrimination experiments showed that (i) spatial scaling succeeded in superimposing all the threshold data across contrasts or within a contrast, meaning that there is no qualitative difference between the fovea and periphery, (ii) E_2 was independent of contrast, suggesting that contrast reduction had

no different influence on spatial summation in between foveal and peripheral visual field, (iii) E_2 decreased and saturated with increasing cpi, indicating that for low-cycle-number grating stimulus, the cycle number played a crucial role on the visual performance.

The results of the contrast threshold allowing the fixed orientation discrimination experiments showed that (i) the task complexity resulted in the failure of spatial scaling for superimposing all the threshold data across orientation differences, (ii) spatial E_2 increased and saturated with increasing cpi, suggesting more size scaling needed for achieving foveal levels of performance for smaller cpi stimulus, and (iii) E_2 found in 1.5 deg orientation difference was much smaller than those at other differences, suggesting that the visual process mechanism at large OD was different from that at OD as small as orientation discrimination threshold.

Acknowledgement

This study was carried out at the School of Optometry and Vision Sciences, Cardiff University. I wish to express my sincere gratitude to the following co-workers.

It is difficult to overstate my gratitude to my supervisor Dr Pia Makela, who introduced me to the field of vision science and has been supporting me throughout my PhD research; who has been always close to my heart; who has always had time to share small and big, happy and sad things with me. She provides a stimulating and fun environment in which to learn and know not just knowledge but life. Her understanding, encouragement and personal guidance have carried on through these years. She has contributed to this thesis with a major impact. Without her, I would not have completed this work.

I am deeply grateful to my supervisor, Professor Jyrki Rovamo. His wide knowledge and his logical and creative way of thinking have been of great value for me. With his enthusiasm, his inspiration, and his great efforts to explain things clearly and simply, he helped to make mathematics fun for me. Throughout my thesis-writing period, he provided sound advice, good company, and lots of invaluable ideas. I would have been lost without him.

My special thanks and appreciation goes to my supervisor, Professor Rachel North, who took me under her wings when both of my original supervisors left due to their work commitment; who is always nice to me during these years; who supports me unconditionally when I am most in need.

I wish to express my sincere thanks to: my advisor Dr Tom Margrain for his detailed comments for my first year report and his important support; Dr Fergal Ennis for his constructive advice of my first poster; Dr Christine Purslow for helping to check the

eyesight of my subject.

Finally, I wish to thank my family: I owe my parents for their unconditional love and never-end support. I am indebted to my sister CC, who helped me to finish my experimental work by being a subject when nobody else was available. Particular thanks must go to my husband, Luis, for always believing in me and standing by me.

A journey is easier when you travel together. Interdependence is certainly more valuable than independence.

Table of Contents

List of Figures

List of Tables

Chapter 1 Introduction

1.1 Vision

1.1.1 The structure of the retina

Human eyes resemble a camera in structure. The light enters the eye through the transparent cornea and continues through the pupil and the lens, and is focused onto the retina. Images on the retina are transmitted to the brain via the optic nerve.

The retina is a part of the central nervous system, lining the interior wall of the eyeball. The optic nerve head forms the blind spot, as there are no photoreceptors in the blind spot. The macula is at the posterior pole of the eye. In the middle of the macula is the fovea, which is about 1.25 deg of visual field in diameter. Foveola extending 1 deg of visual field is responsible for the finest central vision.

The retina contains light-sensitive photoreceptor cells, classified as rods and cones. The retina also contains complex layers of ganglion cells, bipolar cells, horizontal cells and amacrine cells (see Fig 1.1).

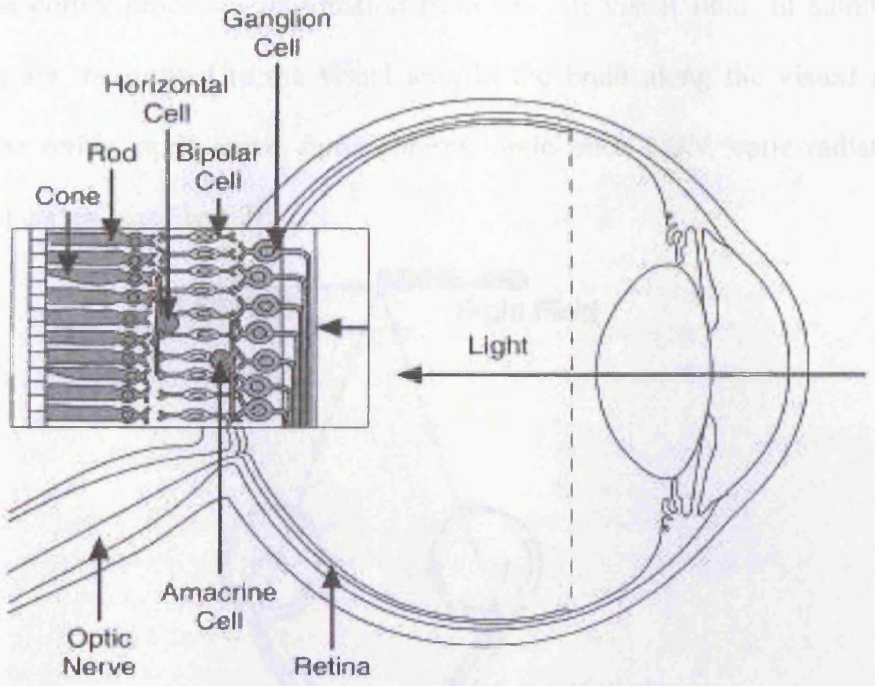

Fig 1.1 A magnified section of the retina (From Schwartz 1999)

1.1.2 Visual pathway

Ganglion cells fire electrical impulses at a constant rate. Inputs from the retinal receptors to the ganglion cell receptive field induce changes in these impulses, generating action potentials that transmit visual information towards the brain along the optic nerve. Some the optic axons in the optic nerve cross at the optic chiasm. The outputs of each eye are split here: the nasal half of each eye's retinal projection crosses to the contralateral side of the brain, while the temporal half remains on the ipsilateral side of the brain. After the chiasm, the axons form the optic tract arrive to the lateral geniculate nucleus (LGN), where the axons synapse for the first time after leaving the ganglion cells. From the LGN, the optic axons travel to primary visual cortex (the striate cortex) at the back of the brain. Thus, the left primary visual cortex processes information from the right visual field, and the right

primary visual cortex processes information from the left visual field. In summary, the visual signals are transmitted to the visual area in the brain along the **visual pathway** formed by: the retina, optic nerve, optic chiasm, optic tract, LGN, optic radiation, and primary visual cortex (see Fig 1.2).

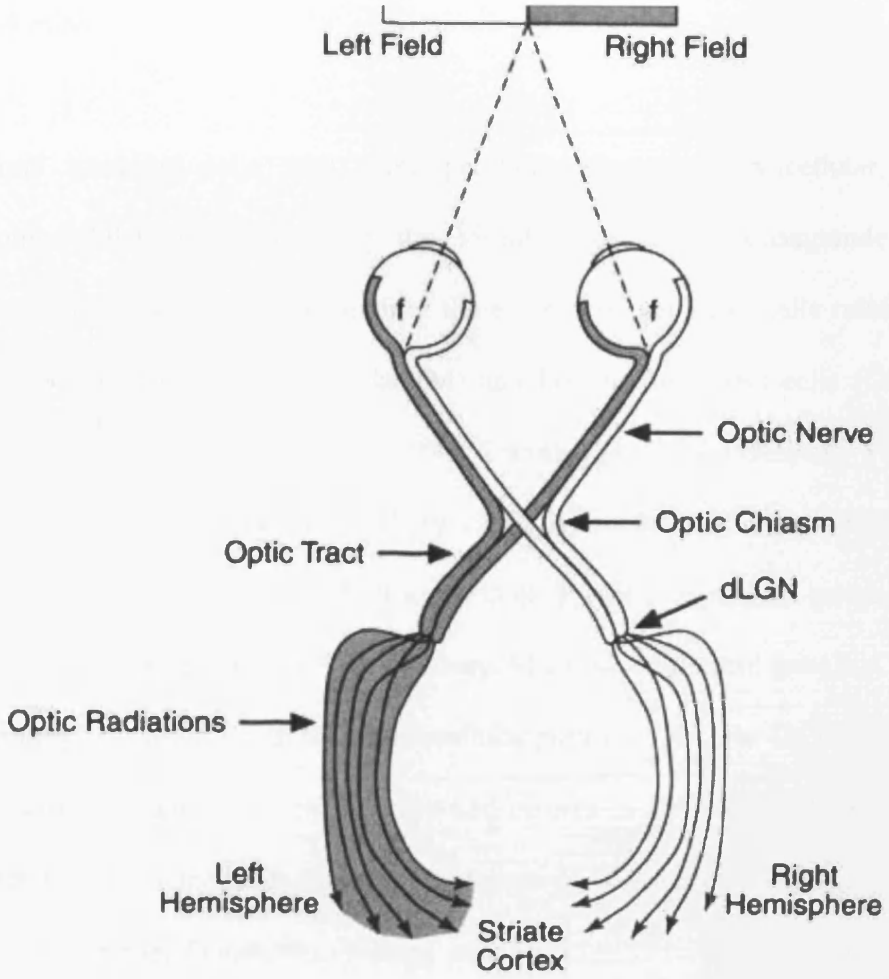

Fig 1.2 The visual pathway: from the retina to the primary visual cortex (From Schwartz 2004)

1.1.3 Ganglion cells and P&M parallel visual pathway

The receptive field of a ganglion cell has a center-surround structure. On the basis of the response of the receptive field to a small spot light, ganglion cells can be divided into two

classes, on- and off- cells. On-center cells are excited when the light is directly applied only to the center of the receptive field, while off-center cells are inhibited. The size of the receptive field of ganglion cells increases linearly with eccentricity. At the fovea of the primate retina, the size of the receptive field centre of a ganglion cell is the smallest, about 2-4 mins.

From ganglion cells start three parallel pathways, parvocellular, magnocelluar and koniocellular, for processing the visual information (Casagrande 1994 and 1999). Correspondingly, there are mainly three types of ganglion cells related to the pathways: parvocellular (P), magnocellular (M) and koniocellular (K) cells (Casagrande 1994 and 1999; Derrington and Lennie 1984; Enroth-Cugell and Robson 1966; Schein and de Monasterio 1987; Shapley and Perry 1986). About 80% of ganglion cells are P cells, about 10% are M cells, and about 10% are K cells. P cells, i.e. midget ganglion cells, show linear summation in the parvocellular pathway. M cells, i.e. parasol ganglion cells, show linear or non-linear summation in the magnocellular pathway. K cells, i.e. bistratified ganglion cells, have been found relatively recently and project to the koniocellular pathway. K cells are involved in color vision and motion processing (Casagrande 1994; Hendry and Reid 2000; Martin, White, Goodchild, Wilder, and Sefton 1997; Morand, Thut, de Peralta, Clarke, Khateb, Landis and Michel 2000; White, Solomon and Martin 2001). The research in this thesis focuses on orientation discrimination and contrast sensitivity mainly based on P and M cells.

The size of the receptive field of P cell is smaller than that of M cell (Drasdo 1989). P and M cells have distinct functions. P cells have high spatial resolution and contribute more to

the recognition of objects (Chalupa and Werner 2004; Kaplan and Shapley 1982; Livingstone and Hubel 1988; Shapley and Perry 1986). P cells are also colour selective and exhibit colour-opponent responses. The firing of P cells is dependent on the wavelength of light in their receptive field. M cells are colour blind and exhibit high temporal resolution. M cells also conduct neural signals faster and contribute to transient processing (motion) (Chalupa and Werner 2004; Enroth-Cugell and Robson 1966; Livingstone and Hubel 1988; Shapley and Perry 1986). M cells fire action potentials when a stimulus is introduced, but quickly fade if the stimulus does not change. M cells have much higher contrast sensitivity than P cells (Kaplan and Shapley 1982).

All the receptive fields of LGN neurons are identical to those of retinal ganglion cells. Anatomically the LGN is composed of 6 distinct layers, where the two bottom layers contain M cells receiving information from the ganglion M cells and the upper four layers are P cells receiving information from the ganglion P cells (see Fig 1.3). In between the six layers are located K-cell layers receiving information from the ganglion K cells. Thus, the M and P pathways separate in the LGN (Derrington and Lennie 1984; Kaplan and Shapley 1982; Livingstone and Hubel 1988; Schein and de Monasterio 1987). The segregation of M and P pathways is maintained from LGN to the primary visual cortex and recombined after the visual cortex. The recombination is detailed in Section 1.2.3 Visual cortex. Table 1.1 generally summarizes the properties of P and M cells (Kaplan and Shapley 1982; Leonova, Pokorny and Smith 2003; Livingstone and Hubel 1988; Nelson 2000; Shapley and Perry 1986).

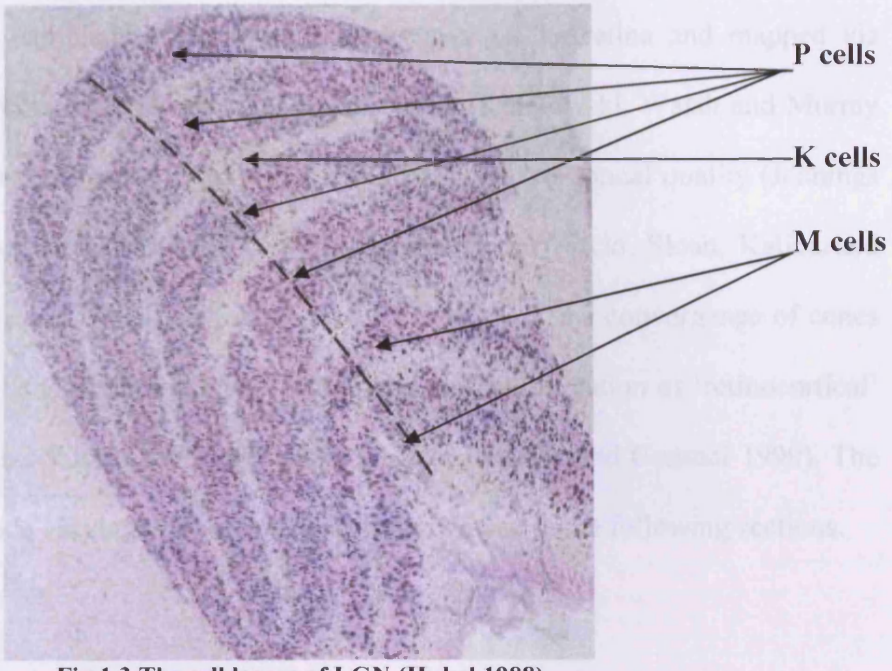

Fig 1.3 The cell layers of LGN (Hubel 1988)

Table 1.1Summary of P and M cells' properties

Name	P cells	M cells
Proportion	80%	10%
Receptive Field	Small	Large
Contrast sensitivity	Low	High
Response to Motion	No	Yes
Response over Time	Sustained	Transient
Colour Sensitive	Yes	No
Information extracted	Color	Motion
Spatial frequency	High	Low
Temporal frequency	Low	High

1.2 Central and peripheral vision

The retinal image is sampled in the photoreceptor layer of the retina and mapped via successive retinal layers and LGN onto the visual cortex (Kulikowski, Walsh and Murray 1991). Visual performance varies with retinal eccentricity due to optical quality (Jennings and Charman 1978 and 1981), density of the photoreceptors (Curcio, Sloan, Kalina and Hendrickson 1990; Drasdo, Millican, Katholi and Curcio 2007), the convergence of cones to retinal ganglion cells (Curcio and Allen 1990), and the magnification of 'retinocortical' connections (Hubel and Wiesel 1974; Sjostrand, Olsson, Popovic and Conradi 1999). The reasons for performance varying with eccentricity are reviewed in the following sections.

1.2.1 Central and peripheral retina

The retina is a seven-layered structure, shown in Fig 1.4. 'Nuclear' layers contain cell bodies, while 'plexiform' layers contain axons and dendrites. There are about 4.6 million cones and about 92 million rods in a human retina (Curcio *et al.* 1990). At the fovea, cone density is up to 200,000 cones per mm^2 (Curcio *et al.* 1990).

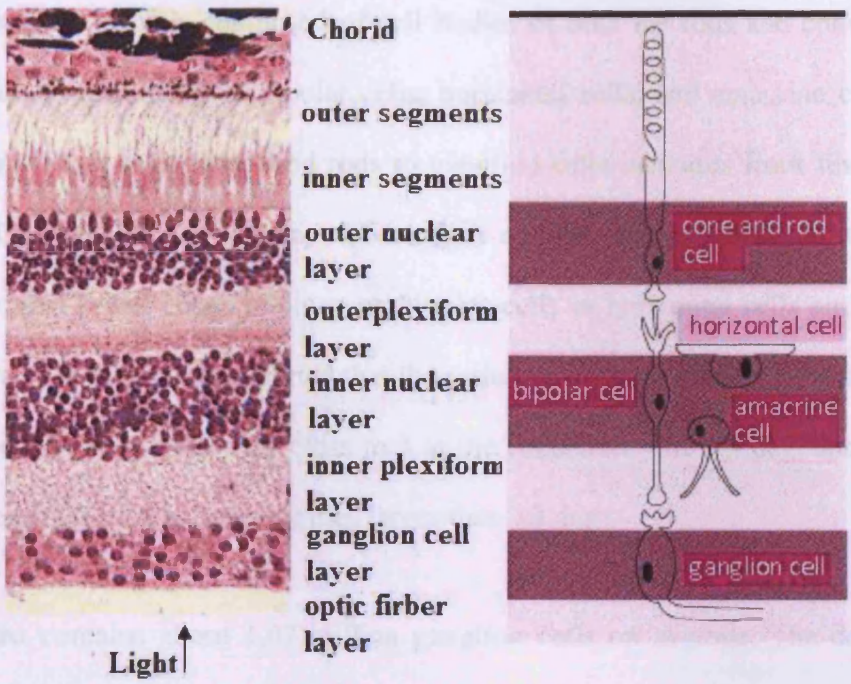

Fig 1.4 Layered structure of the retina (Molavi 1997)

Fig 1.5 shows the cone and rod distribution as a function of eccentricity. Central retina is cone-dominated and peripheral retina is rod-dominated. The density of the cones decreases with increasing eccentricity. The density of rod and all other retinal cells (bipolar, ganglion cells, etc.) first increases and then decreases as eccentricity increases.

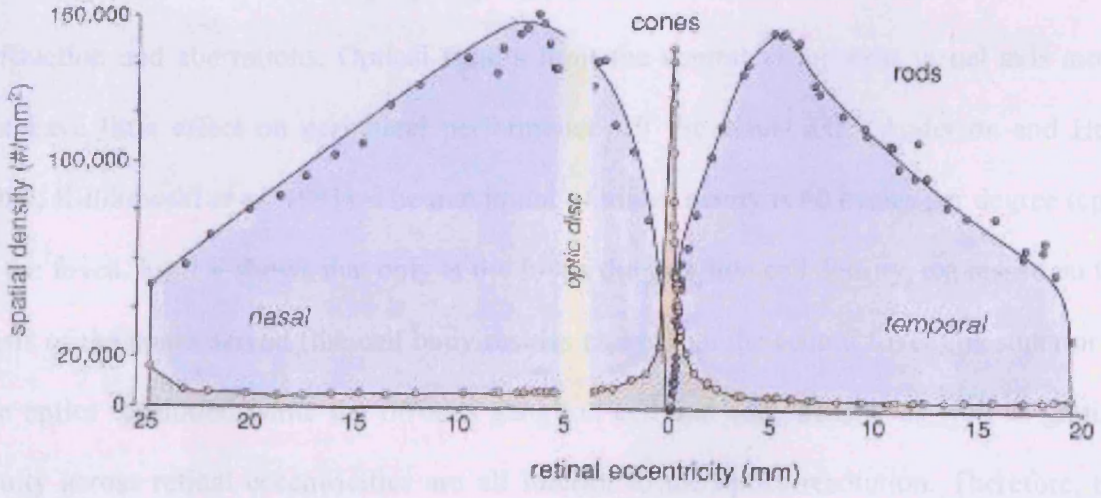

Fig 1.5 The distribution of cone and rod density as a function of retinal eccentricity (Modified by Rodieck 1998)

The outer nuclear layer is composed of cell bodies of both the rods and cones, while the inner nuclear layer consists of bipolar cells, horizontal cells, and amacrine cells (see Fig 1.4). The convergence of cones and rods to ganglion cells increases from fovea to retinal periphery. Cone-connected pathways of neurons are less convergent than rod-connected pathways so that fewer cones impinge on bipolar cells or horizontal cells and to ganglion cells. Sjostrand *et al.* in 1999 reported that the ratio between the number of retinal ganglion cells and their feeding cones was close to 3 at the eccentricity of 2-3 deg, and declined to 1.0 at 7.5 deg and to 0.5 at eccentricities larger than 19 deg.

Human retina contains about 1.07 million ganglion cells on average. The density of the ganglion cell peaks at the retinal eccentricity of about 3.5 - 4 deg. The receptive fields of ganglion cells become larger and more cones connect to each ganglion cell towards retinal periphery.

1.2.2 Optical factors

Ocular optics reduces the image quality of any external stimulus formed on the retina by diffraction and aberrations. Optical factors limit the central vision near visual axis more, but have little effect on peripheral performance off the visual axis (Anderson and Hess 1990; Kulikowski *et al.* 1991). The maximum of visual acuity is 60 cycles per degree (cpd) at the fovea. Fig 1.6 shows that only at the fovea the ganglion cell density, expressed on the basis of the cones served (the cell body resides away from the central fovea), is superior to the optics resolution while the off-axis ganglion cell and cone density as well as grating acuity across retinal eccentricities are all inferior to the optics resolution. Therefore, the maximum of visual acuity is not determined by optics (Anderson, Mullen and Hess 1991;

Campbell and Gubisch 1966).

Fig 1.6 Variations of the optical quality of the eye, cone density, cone-connected ganglion cell density and grating acuity with retina eccentricity.

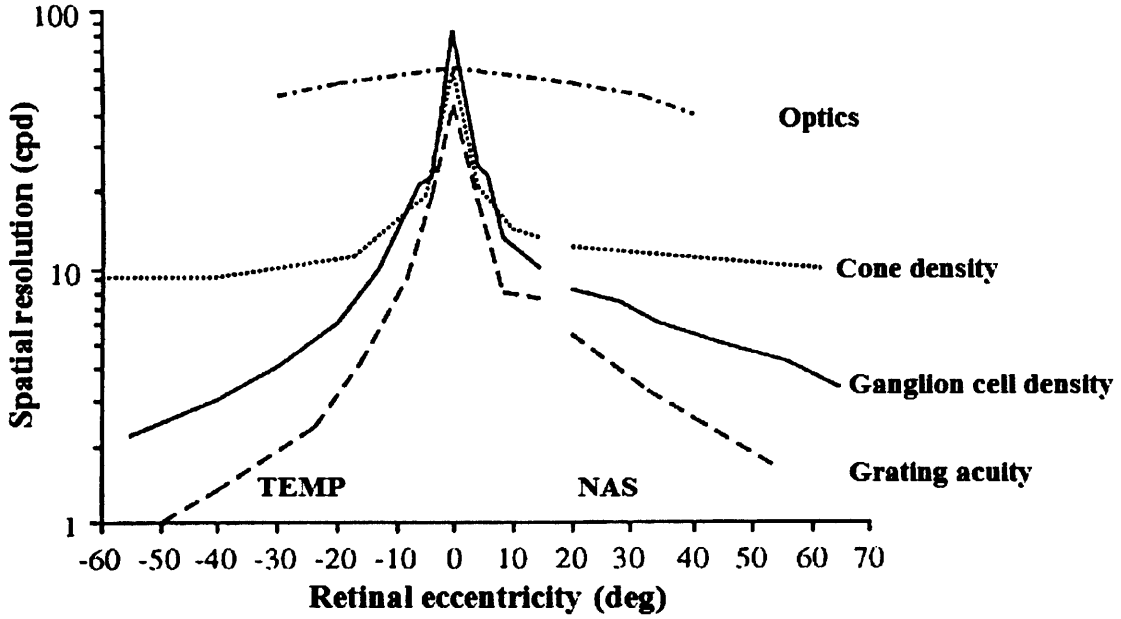

Redrawn by Makela (1994) from Anderson, Mullen and Hess (1991)

Le Grand (1967) reported that peripheral images keep similar structure as the foveal images up to 30 degree eccentricity except that high astigmatism exists. The peripheral visual acuity does not improve by correcting oblique astigmatism and the refractive errors which indicates that neural factors rather than optical factors limit peripheral spatial resolution (see Fig 1.6) (Anderson and Hess 1990; Anderson *et al.* 1991; Williams, Enoch and Essock 1984).

1.2.3 Visual Cortex

The primary visual cortex (see Fig 1.7) is a 2 mm thick grey matter in the occipital lobe around the calcarine sulcus (Hubel 1988). The primary visual cortex is composed of 6

layers. Layer 4 in the monkey is divided into three sub-layers, A, B, and C, while in man layer A is absent. Layer 4C has two sub layers, α and β. The M and P pathways are still preserved separate within the visual cortex. The M pathway projects to layer 4Cα, while the P pathway projects to layer 4A and 4Cβ (Hubel 1988). From there neural information is distributed to higher (1, 2, and 3) and lower (5 and 6) layers. Signals from lower layers are routed back to the LGN and mid-brain (Hubel 1988). Signals from higher layers are routed forward to more specialised areas of visual processing (V2 to V5), which deal with stimulus characteristics such as colour and motion.

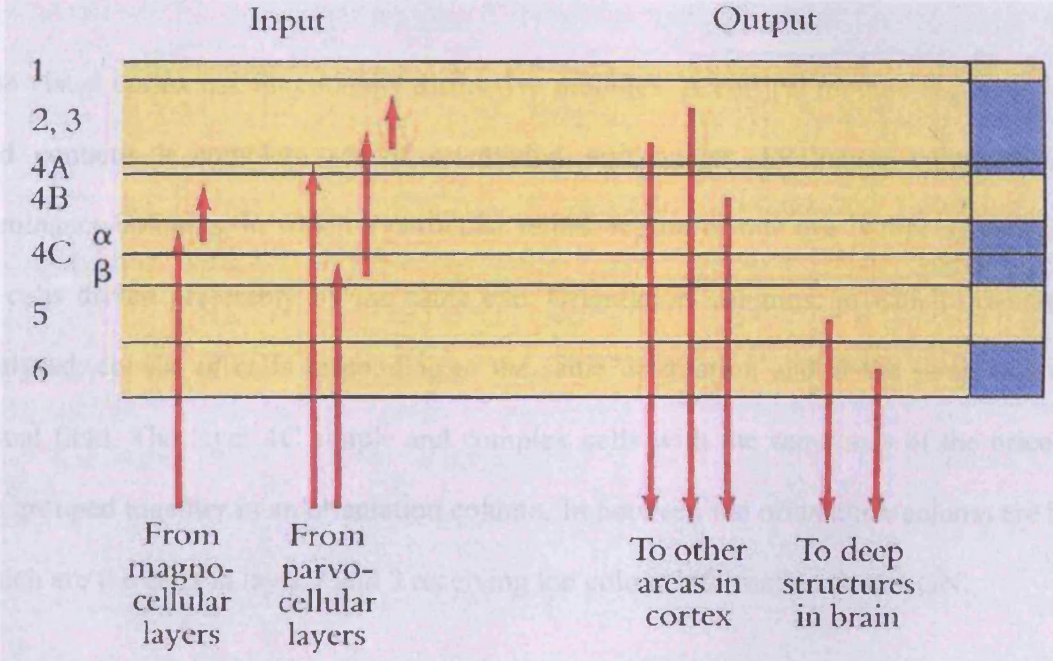

Fig 1.7 A rough indication of the 6 layers of the visual cortex (Hubel 1988)

The visual cortex contains 200 million cells (Hubel 1988). There are three types of cells in visual cortex: simple, complex and hypercomplex cells, according to their receptive field properties. A simple cell receptive field has excitatory and inhibitory areas and responds to

gratings and bars with particular orientations. Simple cells are mainly distributed within layer 4 of the visual cortex. Complex cells are the most common cells in the visual cortex and are found outside layer 4 (Hubel 1988). Complex cells respond to oriented stimuli, while the receptive fields of complex cells cannot be mapped into excitatory and inhibitory areas. The best objects for complex cells are edges, which are tilted in the preferred orientation and moving in the correct direction at the preferred speed. Unlike simple and complex cells whose responses reach a maximum and stay steady, the responses from the hypercomplex cells decrease with increasing stimulus length once the length of the stimulus exceeds the optimal length.

The visual cortex has functionally distinctive modules. A cortical module is 2 mm^2 in area and contains a complete set of orientation and ocular dominance columns. Ocular dominance columns, in which a particular retinal region of one eye is represented, consist of cells driven preferably by the same eye. Orientation columns, in which orientation is analysed, consist of cells responding to the same orientation and at the same area of the visual field. The layer 4C simple and complex cells with the same axis of the orientation are grouped together in an orientation column. In between the orientation column are blobs, which are the cells in layer 2 and 3 receiving the colour information from LGN.

Each location in the visual field corresponds to a well defined region in the visual cortex, resulting in a retinotopic map, a point-for-point copy of the visual field (Adams and Horton 2003; Slotnick and Yantis 2003; Tootell, Switkes, Silverman and Hamilton 1988). From the fovea towards periphery, a progressively smaller and smaller area of visual cortex is devoted to processing of a fixed area of the visual field. This property is called cortical

magnification.

Traditionally, it has been believed that there is a qualitative difference between foveal and peripheral vision: the fovea is specialized for discrimination and the periphery for detection. However, the neural sampling density of the retina decreases with increasing eccentricity, which gives a sensible explanation for the decline in performance for constant size stimuli (Drasdo 1977; Rovamo and Virsu 1979). If the difference between fovea and periphery is in sampling density alone, then the difference between foveal and peripheral visual performance is quantitative and can be equated by providing equal cortical representations for foveal and peripheral stimuli by enlarging stimulus size appropriately with increasing eccentricity.

1.3 Spatial scaling

1.3.1 Cortical magnification

Over half of the primary visual cortex is devoted to dealing with information from the central 10 degrees of the visual field (Connolly and Van Essen 1984; Daniel and Whitteridge 1961). The number of neurones in the visual cortex processing one degree of visual field decreases from the fovea to the periphery. Cortical magnification factor M describes the scale of cortex indicating the linear extent of visual cortex in mm per degree of visual angle (Daniel and Whitteridge 1961).

M_0 represents the greatest value of M at the very centre of visual field. M_0 has been estimated on the basis of data obtained from recordings of cortical response in monkey

(Adams and Horton 2003; Daniel and Whitteridge 1961; Hubel and Wiesel 1974; Tootell *et al.* 1988; Van Essen, Newsom and Maunsell 1984) and human (Brindley and Lewin 1968; Calvert, Manahilov, Simpson and Parker 2005; Drasdo 1989; Rovamo, Virsu and Nasanen 1978). It is also possible to estimate the hypothetical value of M_0 indirectly based on ganglion cell receptive field density (Drasdo 1977; Rovamo and Virsu 1979).

1.3.2 M scaling and spatial scaling

Theoretically, visual performance can be equated between fovea and periphery if stimulus size is scaled in periphery according to *M*. Since the introduction of the concept of *M* scaling (Rovamo *et al.* 1978; Virsu and Rovamo 1979), a significant amount of studies have attempted to equate foveal and peripheral performance using the variable *M* scaling factors. Some attempts have been more successful (Kelly 1984; Popovic and Sjostrand 2001; Rovamo *et al.* 1978; Virsu and Rovamo 1979; Virsu, Rovamo, Laurinen and Nasanen 1982) than others (Jamar, Kwakman and Koenderink 1984; Rovamo and Raninen 1984; Strasburger, Rentschler, and Harvey Jr 1994; Westheimer 1983). It is now recognized that *M* scaling cannot be successfully applied to all types of visual tasks.

Another way to scale the peripheral stimulus size to produce an equivalent performance in periphery to that at the fovea is **spatial scaling** (Johnston and Wright 1986; Levi, Klein and Aitsebaomo 1985; Levi, Makela, Rovamo and Whitaker 1997; Levi and Waugh 1994; Makela, Whitaker and Rovamo 1993; Saarinen, Rovamo and Virsu 1989; Sally and Gurnsey 2003, 2004; Vakrou, Whitaker and McGraw 2007; Watson 1987; Whitaker, Rovamo, MacVeigh and Makela 1992). Visual tasks are conducted using a sequence of

stimuli with increasing magnification to measure performance thresholds both at the fovea and at several retinal eccentricities. Thresholds are then plotted as a function of stimulus size for the fovea and all those eccentricities. The scaling factor at each retinal eccentricity is determined by the shift along the size axis needed to superimpose the foveal and peripheral threshold functions.

The significant difference between *M* scaling and spatial scaling is that spatial scaling is based on the psychophysical experiments, while *M* scaling is based on the anatomical data. Before spatial scaling method is explained in detail in **Section 1.3.4,** it is necessary to define a really important parameter called E_2.

1.3.3 E_2

E_2 indicates the eccentricity at which stimulus needs to be doubled in size in order to produce equal performance to that at the fovea (Levi, *et al.* 1985). In spatial scaling, E_2 values obtained are based on psychophysical experiments. Table 1.2 summarizes the estimates of E_2 values for different visual tasks (vernier acuity, bisection, orientation discrimination, etc.) in various psychophysical experiments. In the next section, the calculation of E_2 and spatial scaling procedure are explained in detail.

Table 1.2 Some estimates of E_2 in psychophysical tasks

Tasks and Researchers		E_2 (deg)
Vernier acuity	Levi *et al.* (1985)	1.06-1.96
	Klein and Levi (1987)	0.19
	Whitaker *et al.* (1992)	1.23-1.78
	Levi, McGraw and Klein (2000a)	0.8/2.5
Spatial interval discrimination	Makela *et al.* (1997)	0.17-0.19
	Yap, Levi and Klein (1989)	0.6-0.8
	Levi and Klein (1990b)	0.68-0.83
Bisection	Makela (1994)	0.07-0.08
	Levi and Klein (1990a)	0.44-0.47
	Klein and Levi (1987)	0.15-0.31
Displacement	Makela *et al.* (1997)	1.0-1.2 (instantaneous displacement)
	Levi *et al.* (1984)	1.3 (motion discrimination)
	Whitaker *et al.* (1992)	13.5-18.5 (gradual displacement) 6.3-11.1 (instantaneous displacement)
	Levi *et al.* (1984)	1.05 (Motion detection)
Orientation discrimination	Makela *et al.* (1993)	1.95
	Westheimer (1982)	1.85, 2.28 *
	Paradiso and Carney (1988)	2.4 *
	Sally and Gurnsey (2003)	1.38-1.64
	Sally and Gurnsey (2004)	3.42-3.50
Visual acuity	Levi and Klein (1990b)	2.1-2.5
	Westheimer (1979)	2.8 *
Contrast sensitivity	Rovamo and Virsu (1979)	2.38-3.45
	Johnston (1987)	5.4 *
	Watson (1987)	4.2 *
	Whitaker, Latham, Makela and Rovamo (1993)	1.84-1.96 (curvature detection) 1.27-1.42 (curvature discrimination)
	Vakrou *et al.*(2007)	2.13-2.65 and 1.62-2.40
	Sally, Poirier and Gurnsey (2005)	5.72-5.92

*calculated by Makela (1994)

1.3.4 Spatial scaling procedure

As mentioned before, unlike M-scaling, spatial scaling method does not depend on pre-determined anatomical or physiological factors. Performance is simply measured over a range of stimulus sizes.

In this section the spatial scaling procedure are presented step by step by using hypothetical data. A set of stimuli (magnified or minified versions of one another) are used to measure performance thresholds for several eccentricities, for example, 0, 2.5, 5, 7.5 and 10 deg. Thresholds are plotted as a function of stimulus size at each eccentricity (see Fig 1.8). The size of stimuli could be, for example, line length or grating diameter.

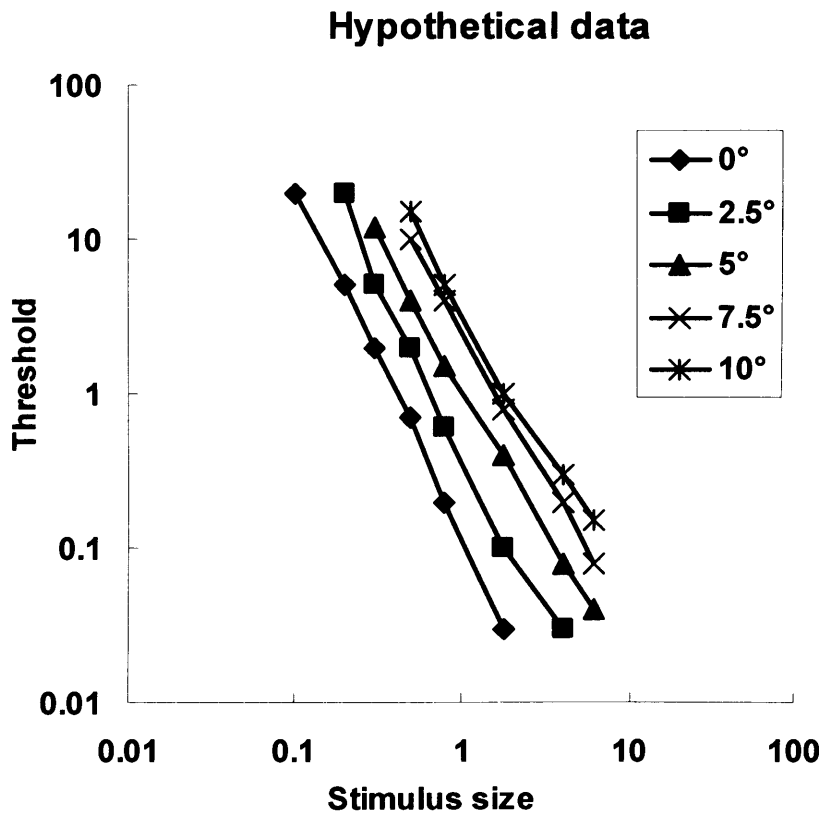

Fig 1.8 Hypothetical data thresholds as a function of size of the stimulus

In Fig 1.8 the threshold sets are displaced from each other along horizontal axis. To equate the threshold performance in an eccentricity (2.5, 5, 7.5 or 10 deg) with that of the fovea (0 deg), the threshold set at the eccentricity has to be shifted along the horizontal size axis to superimpose it with the foveal one. Therefore, the stimulus size at the eccentricity needs to be divided by a scaling factor. The optimal scaling factor minimizes the variance between the foveal and horizontally shifted eccentric data.

The shift is first estimated by eye. An arbitrary, close to 'correct', estimated scaling factor is used to shift the curve at an eccentricity to superimpose with the foveal curve. Then the standard deviation is calculated for the two superimposed curves. This procedure is repeated twice with other estimates of scaling factor. A second-order polynomial regression is fitted to the standard deviations found and the preliminary scaling factor is estimated in which produces the minimum value of the polynomial function, i.e. the minimum standard deviation. Fig 1.9 shows the preliminary scaling factors at each eccentricity for the data of Fig 1.8.

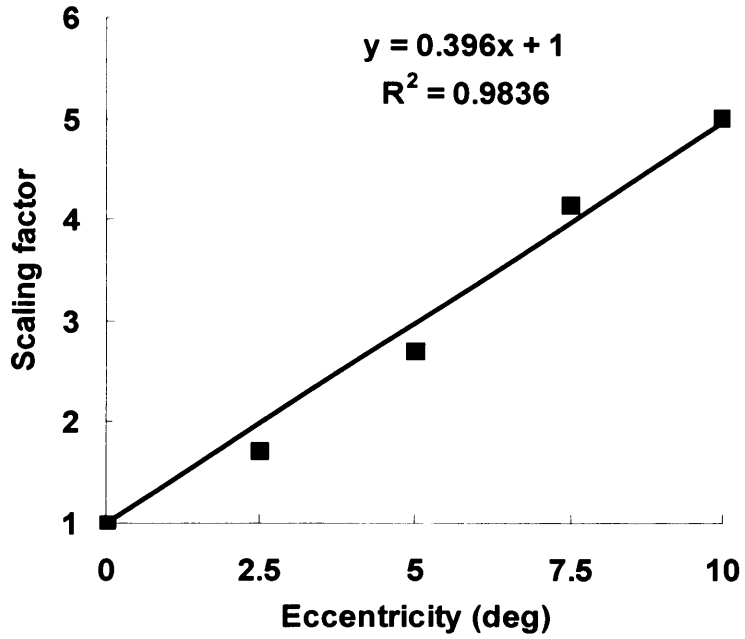

Fig 1.9 The preliminary optimal scaling factors (■) are plotted against eccentricity and are fitted with a linear function. R^2 indicates the goodness of fit.

The final scaling factor for each eccentricity is calculated by a linear function fitted to the preliminary scaling factors in Fig 1.9. The goodness of linear fit is indicated by R^2. The linear function, based on all the preliminary scaling factors at eccentricities of 2.5, 5, 7.5, and 10 deg, is forced to go through point (0, 1), as the scaling factor is 1 at the fovea. Thus, it can be expressed as a simple linear equation:

$$F = 1 + SE. \qquad \textbf{Equation 1.1}$$

The slope of the line reveals how fast the scaling factors increase towards periphery. Fig 1.10 shows the scaled data using the final scaling factors. The solid line is the optimal fit to the original fovea threshold data. The R^2 calculated between the optimal foveal fit and the scaled data set indicates how well all the extra-foveal threshold data are superimposed on the foveal data. The R^2 value of 0.98 implies that the threshold performance could be equated between the fovea and the periphery by magnifying stimulus size.

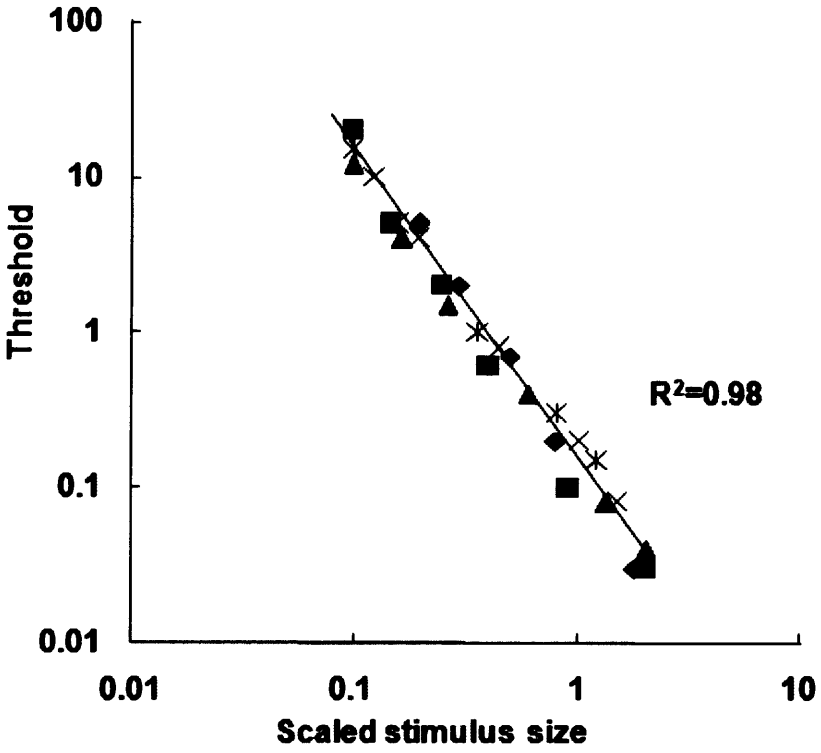

Fig 1.10 Superimposed data after spatial scaling

As previously defined in Section 1.3.3, E_2 is the eccentricity where stimulus size is doubled to maintain performance equivalent with that at the fovea. E_2 is shown to be the inverse of the slope of the linear scaling factor line function as follows:

When $F = 2$, equation (1.1) can be written as

$$2 = 1 + SE_2, \qquad \textbf{Equation 1.2}$$

and where

$$E_2 = 1/S\ . \qquad \textbf{Equation 1.3}$$

1.4 Thresholds of vision

1.4.1 Contrast sensitivity

Contrast sensitivity is a fundamental parameter in assessing vision. A common way to measure contrast threshold is to present a grating at such a low contrast that it cannot be seen and then gradually increase the contrast until the grating is just seen. An alternative way is to first present the grating at a high contrast, and then to decrease the grating contrast until it just disappears. Commonly, these two ways are combined to measure contrast threshold and an average of the results from these is used as the final threshold. Contrast threshold is the contrast level at which the grating is just seen.

Contrast sensitivity is the reciprocal of the contrast threshold. It is limited by many factors, such as luminance level, spatial frequency, and stimulus eccentricity (E). For instance, in Fig 1.11 contrast sensitivity was plotted as a function of stimulus spatial frequency at different eccentricities (Rovamo *et al.* 1978). The stimuli were constant size sinusoidal gratings.

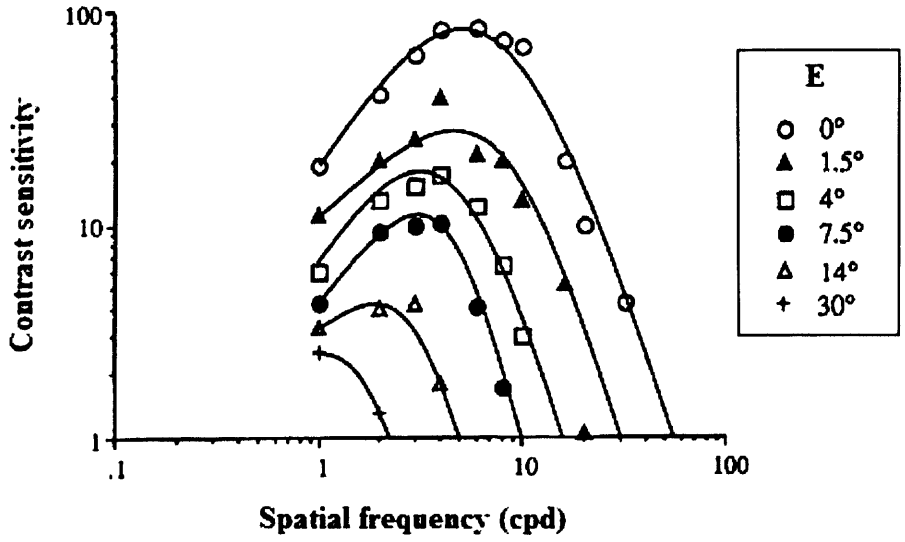

Fig 1.11 Contrast sensitivity as a function of spatial frequency and retinal eccentricity (Rovamo *et al.* 1978).

As shown in the figure, contrast sensitivity decreases with increasing eccentricity and reveals a band-pass function with spatial frequency peaking at about 5 cpd at the fovea. The peak sensitivity shifts towards lower spatial frequencies when the stimulus is placed further towards the peripheral visual field.

Contrast sensitivity varies from 0 to 1 and is calculated differently depending on the stimulus and the background used in the measurements.

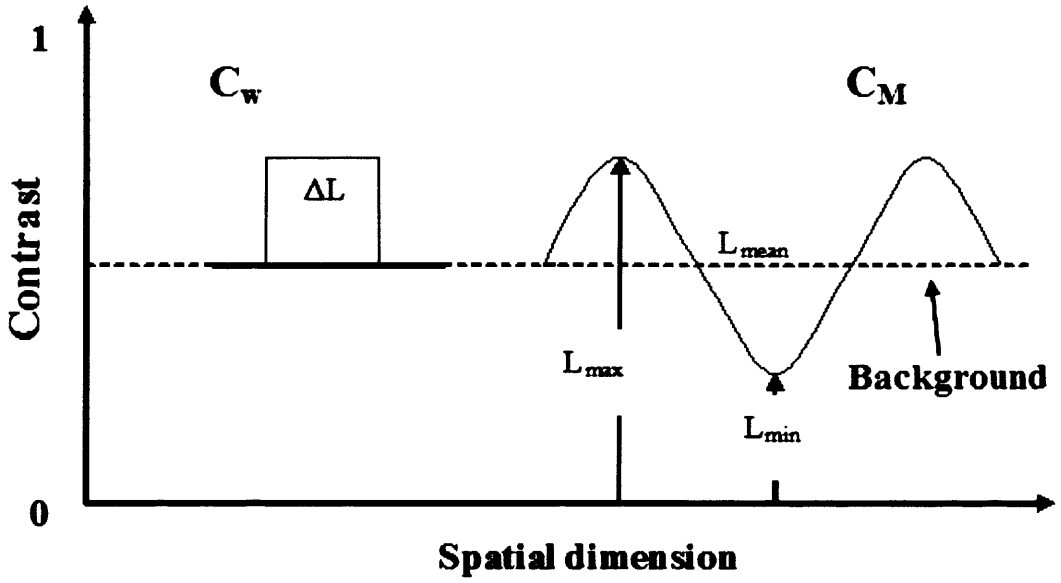

Fig 1.12 Luminance profiles for the *Weber* and *Michelson* contrast defined in text.

Weber contrast is commonly used for defining the contrast of a spot stimulus against a background:

$$C = \frac{\Delta L}{L_{mean}}, \qquad \textbf{Equation 1.4}$$

where L_{mean} represents the mean luminance of the background and ΔL represents the difference of the luminance between the stimulus and the background (see Fig 1.12).

If the stimulus is a simple periodic pattern, for example, a sinusoidal grating, *Michelson contrast* is commonly used to express its contrast:

$$C = \frac{(L_{\max} - L_{\min})}{(L_{\max} + L_{\min})}, \qquad \textbf{Equation 1.5}$$

where $L_{\max}$ and $L_{\min}$ are the maximum and minimum luminance of the stimulus pattern (see Fig 1.12). For complex stimulus patterns, for example, an image, root-mean-square contrast, *r.m.s contrast*, is used:

$$C = \sqrt{\frac{1}{nm}\sum_{i=1}^{n}\sum_{j=1}^{m} c^2(i,j)}\,. \qquad \textbf{Equation 1.6}$$

It is the standard deviation of the luminance distribution of the stimulus divided by the average luminance of the background. In the equation i and j are the pixel indices of the stimulus image, and n and m are the numbers of the pixels in horizontal and vertical direction.

Kukkonen, Rovamo, Tiippana and Nasanen (1993) showed that the contrast measurement method chosen had a significant effect on the appearance of contrast sensitivity functions for different kinds of stimuli.

1.4.2 Resolution

Resolution is the ability to see fine details. The thresholds of resolution are usually expressed as the minimum angle where subjects can discriminate the separation between basic elements of a stimulus pattern such as a two-dot pair or a grating shown in Fig 1.13.

(a) (b)

Fig 1.13 Stimuli for resolution measurements: (a) a two-dot pair, (b) a grating

The minimum angle of resolution (MAR) is a standard visual acuity measurement. For normal observers, MAR is around 30-60 sec of arc. MAR is limited mainly by optical factors (for example, diffraction, aberrations, and scatter of optics reduce resolution) and to

a less extent by neural factors, (for example, retinal cone spacing corresponds to resolution of about 30 sec of arc) (Curcio and Allen 1990; Curcio *et al.* 1990; Popovic and Sjostand 2001). Resolution declines rapidly towards periphery (Wertheim 1891).

1.4.3 Hyperacuity

Unlike resolution, hyperacuity relates to the minimum angle of resolution of the relative location of two objects (Westheimer 1981; Westheimer and McKee 1977). Fig 1.14 explains the difference between resolution and hyperacuity.

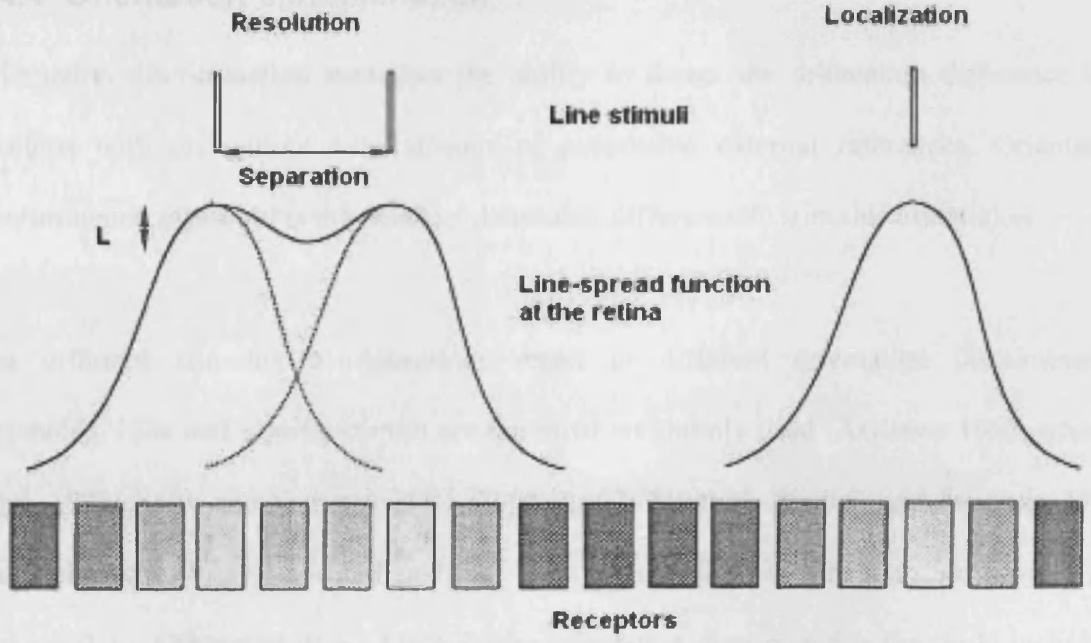

Fig 1.14 Difference between resolution and localization (the diagram from Makela 1994).

To resolve the two line stimuli above, their corresponding retinal image must consist of two luminance peaks which are separated enough to exceed the luminance threshold at the eye's adaptation level. The threshold is dependent on the quality of the optics, the luminance and separation of the stimuli. Furthermore, the differential stimulation in the retina must fall

within different receptors. Compared to resolution which involves the inter-receptor separation, localization is performed by weighting the responses of the receptors underlying the retinal image distribution and so can be more accurate.

Localization acuity, *i.e.* hyperacuity, is defined as any judgement of relative spatial position in optimum condition and is better than resolution limit, *i.e.* under 60 sec of arc (Westheimer 1975, 1981).

1.4.4 Orientation discrimination

Orientation discrimination measures the ability to detect the orientation difference in a stimulus with or without simultaneous or successive external references. Orientation discrimination threshold is the smallest detectable difference in stimulus orientation.

The different stimulus configurations result in different orientation discrimination thresholds. Line and grating stimuli are the most commonly used (Andrews 1967; Makela *et al.* 1993; Sally and Gurnsey 2003, 2004, 2007; Skottun, Bradley and Freeman 1986; Vandenbussche, Vogels and Orban 1986; Westheimer 2003; Westheimer, Shimamura and Mckee 1976). Other stimuli used to measure orientation discrimination threshold include, a pair of dots (Beck and Halloran 1985), 2D filtered noise pattern (Ellemberg, Allen and Hess 2006; Heeley, Buchanan-Smith and Cromwell 1997), and edges (Heeley and Buchanan-Smith 1990).

Fig 1.15 shows a typical orientation discrimination configuration of a line stimulus.

Orientation discrimination threshold is defined either as T in spatial terms (the horizontal separation of the ends of the tilted solid line from the vertical dash line) or α in angular terms (the tilt angle of the solid line from the dash line). Table 1.3 summarizes some foveal orientation discrimination thresholds measured in terms of rotation angle α.

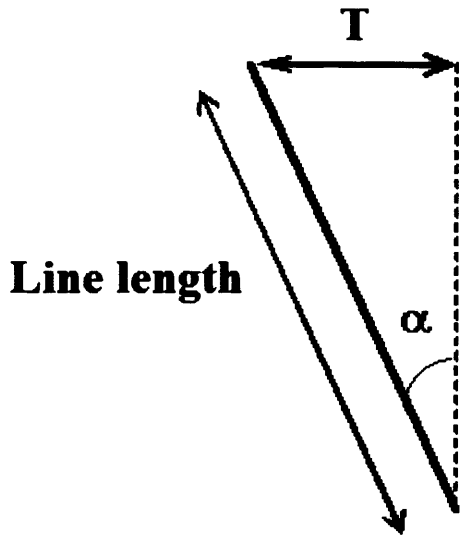

Fig 1.15 The configuration of a typical orientation discrimination line stimulus

Researchers	Threshold (deg)	Stimulus
Andrews (1967)	0.1	Line
Westheimer *et al.* (1976)	0.4	Line
Beck and Halloran (1985)	0.4	Two dots
Vandenbussche *et al.* (1986)	0.7	Line
Skottun *et al.* (1986)	0.5	Grating
Watt (1987)	0.22	Line
Paradiso and Carney (1988)	0.3	Line
Heeley and Buchanan-Smith (1990)	0.6	Edge, line and grating
Heeley *et al.* (1997)	2.1	2D band-pass filtered noise
Westheimer (2003)	0.6	Line
Sally and Gurnsey (2003)	0.56	Line
Ellemberg *et al.* (2006)	1.5	2D band-pass filtered noise
Sally and Gurnsey (2007)	0.6	Line

Table 1.3 Some orientation discrimination thresholds reported by different researchers

The angular difference α was measured as a function of stimulus size in the orientation discrimination experiments conducted in the present thesis (see Figs 3.3, 4.3 and 5.3 in Chapters 3, 4 and 5, respectively). T can be calculated from α using a *sine* equation (1.7) below:

$$T = H \sin \alpha \qquad \textbf{Equation 1.7}$$

where H represents the stimulus size, *e.g.* line length, shown in Fig 1.15 above.

Further, the orientation discrimination threshold in visual angle, θ, can be calculated from T by equation (1.8) (see Fig 1.16),

$$\theta = 2art \tan(\frac{T}{2D}) . \qquad \textbf{Equation 1.8}$$

When T is replace by Hsinα according to equation (1.7),

$$\theta = 2art \tan(\frac{H \sin \alpha}{2D}) . \qquad \textbf{Equation 1.9}$$

From equation (1.9), θ is dependent on orientation discrimination angular threshold α, stimulus size H and viewing distance D so that θ is not proportional to H. In this thesis, θ was presented as a function of stimulus size (as in Makela *et al.* 1993) in Figs 3.2, 4.2 and 5.2 in Chapters 3, 4 and 5, respectively. The function curve of θ against H is generally U-shaped as shown in those figures.

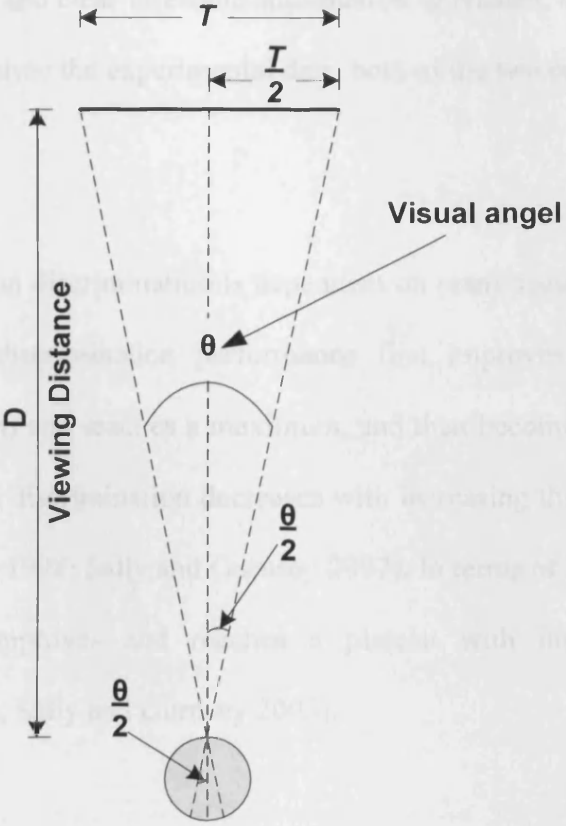

Fig 1.16 The spatial orientation discrimination threshold *T* and its visual angle *θ* in visual field

Both of the threshold presentation methods, *T* or *a vs.* stimulus size are appropriate. The function curve of *T* expressed in visual field, *i.e.* *θ*, against stimulus size shows the spatial extent of the threshold in visual field and whether it is in range of hyperacuity (<60 sec arc) (Makela *et al* 1993; Westheimer *et al.* 1999). The angular threshold *a vs.* size curve is commonly used for the process of spatial scaling due to its shape. The angular threshold decreases and reaches a plateau with increasing stimulus size so that it is convenient for superimposing two threshold curves by a horizontal shift, i.e., spatial scaling (Makela *et al.* 1993; Mareschal and Shapley 2004; Sally and Gurnesy 2003, 2004).

In order to provide complete and clear threshold information to readers, and to process by spatial scaling and further analyse the experimental data, both of the two presentations were used in this thesis.

The performance of orientation discrimination is dependent on many factors. As addressed above, angular orientation discrimination performance first improves with increasing stimulus size (*e.g.*, line length) and reaches a maximum, and then becomes independent of size. Furthermore, orientation discrimination decreases with increasing thickness of stimuli (Heeley and Buchanan-Smith 1998; Sally and Gurnsey 2007). In terms of stimulus contrast, orientation discrimination improves and reaches a plateau with increasing contrast (Mareschal and Shapley 2004; Sally and Gurnsey 2003).

1.4.5 Vernier acuity

Among various hyperacuity tasks, vernier acuity is the most similar task to orientation discrimination and also the most commonly quoted hyperacuity task. To measure vernier acuity, the stimulus configuration can be two lines, two dots, or two gratings (Barrett and Whitaker 2004; Heinrich, Kromeier, Bach and Kommerell 2005; Levi *et al.* 1994; Levi *et al.* 2000a and 2000b; Sullivan, Oatley and Sutherland 1972; Waugh and Levi 1999; Whitaker and MacVeigh 1991; Whitaker *et al.* 1992; Whitaker and Walker 1988). Fig 1.17 shows two samples of stimuli commonly used for measuring vernier acuity.

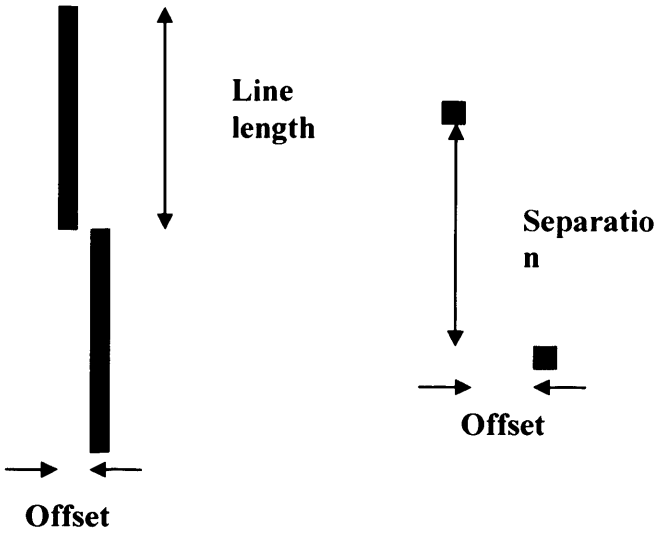

Fig 1.17 Some stimulus configurations of vernier acuity: (a) line stimulus, (b) two-dot stimulus.

Like orientation discrimination, line vernier acuity first improves with increasing stimulus length, and becomes independent of length after it reaches the optimal level (Andrews, Butcher and Buckley 1973; Levi *et al.* 2000a; Sullivan *et al.* 1972; Westheimer and McKee 1977; Whitaker *et al.* 1992). Temporal factors and contrast can affect thresholds too. Waugh and Levi (1993a, 1993b and 1999) found that increasing the duration of the stimulus improved vernier acuity at a low contrast. Some researchers found that vernier acuity improves as contrast increases and eventually reaches to a plateau (Bradley and Freeman 1985; Morgan and Regan 1987). Table 1.4 summarizes some foveal vernier acuity thresholds found previously.

Researchers	Vernier acuity threshold (sec arc)	Stimulus
Berry (1948)	2	Line
Westheimer and McKee (1977)	5	Line
Morgan and Aiba (1985)	5	Line
Wehrhahn and Westheimer (1990)	4-5	Edge
Whitaker *et al.* (1992)	6/5	Line/two-dots
Waugh and Levi (1993)	2/5	1/8cpd grating
Mussap and Levi (1997)	2-3	Line
Heinrich *et al.* (2005)	3-12	Line

Table 1.4 Summary of some vernier acuity thresholds

1.5 Thesis aims and outline

1.5.1 Experiment design

A wide range of E_2 values has been found using spatial scaling since the introduction of the method (See Table 1.2). There are many reasons behind the variations. First the different visual tasks results in a large variation of E_2 values (Whitaker *et al* 1992). For example, Melmoth, Kukkonen, Makela and Rovamo (2000b) obtained an average E_2 of 4.99 deg for detection of phase distortions of faces or gratings. It was much larger than 1.93 deg obtained for orientation discrimination by Makela *et al.* (1993) and 1.90 deg obtained by Whitaker *et al.* (1992) for the curvature detection.

Recently, researchers have obtained different E_2s in the tasks with the same configurations but conducted at different contrasts. For example, Using the same stimulus and experimental configuration, Sally and Gurnsey in 2003 obtained an average E_2 of 1.51 deg between subjects for orientation discrimination at well-above threshold contrast while 3.46 deg was found at near-detection threshold contrast in 2004. Later in 2007, they measured orientation discrimination threshold of line stimuli at 3-48% contrasts and found that E_2 increased as stimulus contrast decreased. However, it should be noted that in their 2007 experiment, the thresholds were measured at the highest contrast only up to 48% and at only two eccentricities of 0 and 10 deg so that the accuracy of E_2 found was comparatively lower.

Therefore, to find out how contrast affects E_2, a systematic study is needed across contrasts and eccentricity. Because orientation selectivity is one of the basic features of the cortical mechanisms, the investigation of the orientation discrimination performance at different contrasts should be able to demonstrate the interaction between E_2 and contrast, further reflecting the dependency of the visual field on contrast.

From the reasons above, the two types of orientation discrimination tasks involving six experiments were designed in this thesis.

- **Orientation discrimination experiments**

In Chapters 3-5, orientation discrimination experiments were carried out using the line and grating stimuli with different cycle-numbers (2, 4, 16 cycles per grating image) at different visual field locations (the eccentricities of 0, 2.5, 5, 7.5 and 10 deg) and different contrasts (10, 30 and 100%).

Firstly, all the threshold data measured across contrasts and eccentricities were superimposed at the fovea and 100% contrast by spatial scaling and 2D scaling[1]. Because both two scaling methods were applied to the threshold data across eccentricities and contrasts, the scaling factors had two independent variables, eccentricity and contrast. By modelling the scaling factors as a function of eccentricity and contrast, the effects of eccentricity and contrast on orientation discrimination were quantified and demonstrated. A

[1] The 2D scaling in this thesis involved a simultaneous vertical and horizontal scaling and its detail was given in each experimental chapter).

global spatial E_2 across contrasts was obtained through spatial scaling procedure. A non-parametric paired statistical test was used to compare the performance between spatial and 2D scaling, and the result indicated whether spatial scaling was good enough for equating the threshold performance across eccentricities and contrasts when both effects of eccentricity and contrast on orientation discrimination were considered.

Secondly, spatial scaling was used to superimpose the orientation discrimination threshold data separately at each contrast, *i.e.* 100%, 30% and 10%. Then the local E_{2C} at each contrast was separately obtained and plotted as a function of contrast, which indicated how contrast affected E_2 and further demonstrated how contrast affected spatial summation in different locations of visual field.

Further, the effects of the number of cycles per image (cpi) on orientation discrimination and E_2 were also investigated. Because E_2 represents how fast performance in a visual task decreases from the fovea to periphery, the dependency of E_2 on cpi can reflect how cpi affects orientation discrimination performance across visual field.

- **Threshold contrast allowing orientation discrimination at a fixed orientation difference experiments**

Due to the limited stimulus size, the orientation discrimination thresholds at lower contrasts (closer to detection-threshold contrast) could not be measured. In Chapters 6-8, the problem was approached from another angle.

The experiments in Chapters 6-8 were designed on the basis of the findings in Chapters 3-5. Contrast thresholds were measured for discriminating two stimuli presented with various orientation differences (1.5, 5, 15 and 45 deg) at the eccentricities of 0-10 deg by using the same stimuli as in Chapters 3-5.

Firstly, all the threshold data were superimposed onto the foveal data at 45 deg orientation difference by spatial scaling and 2D scaling. Performance at the threshold contrast for discriminating a fixed orientation difference was quantitatively equated across 0-10 deg eccentricities and 1.5 to 45 deg orientation differences. Because both spatial and 2D scaling were used to superimpose the threshold data across eccentricities and orientation differences, the spatial and 2D scaling factors were dependent on and estimated as a function of eccentricity and orientation difference, by which the interaction between eccentricity and orientation difference was explained. Performance of spatial and 2D scaling was compared in these experimental chapters to examine whether the thresholds could be equated across eccentricities and orientation differences by the single size scaling, i.e. spatial scaling.

Secondly, spatial scaling was conducted to superimpose the threshold separately at each orientation difference, i.e., 1.5, 5, 15 and 45 deg. The local E_{2OD} at each orientation was obtained and analysed as a function of orientation difference. By Comparing E_{2OD}s, it can be found out whether the visual process mechanism of the detection & discrimination task at large orientation difference (e.g. 45 deg) was different from that at small difference close to orientation discrimination threshold (e.g. 1.5 deg).

Some early studies reported that for the gratings with less than 16 cycles, the number of cycles played a more important role than spatial frequency on threshold contrast (Howell and Hess 1978; Jamar and Koenderink 1983; Savoy and McCann 1975). Therefore, thirdly, by combining the contrast threshold data of the stimuli with different cpi, the effects of cpi on the threshold performance were analyzed so that the importance of cpi on the visual task can be decided for low-cycle-number (≤16) stimuli.

1.5.2 Application, Hypothesis and Question to be answered

Later research suggested that contrast reduction affects the spatial structure of the receptive field of V1 neuron (Kapadia, Westheimer and Gilbert 1999; Sceniak, Ringach, Hawken and Shapley 1999; Sceniak, Hawken and Shapley 2002). Sceniak, *et al.* (1999) found that at low contrast the extent of spatial summation was 2-3 folds greater and the receptive field is 'not size invariant, but depends on stimulus condition'. Based on their research in 2003, 2004, 2007, Sally and Gurnesy suggested that the changes in receptive fields at low contrast were relatively greater at the fovea than periphery due to less spatial scaling, i.e., larger E_2 found at lower contrast. Meanwhile, they also pointed out that the conclusion "is based on very limited data".

Therefore, the investigation of orientation discrimination across contrasts and visual field carried out in this thesis would give a more thorough examination on the contrast-dependent changes from the fovea to periphery. By comparing E_2s obtained at different contrasts (from as high as 100% contrast to as low as the detection threshold contrast), it

can be answered whether the contrast-dependent size changes of the V1 neuron receptive field are different between the fovea and periphery.

Because spatial summation changes with contrast, performance of an orientation discrimination task (or spatial vision task) is affected by contrast. If the effect of contrast is taken into account, spatial scaling may be able to equate the peripheral performance with that of the fovea across contrasts. Therefore, the first hypothesis was that when the effect of contrast is taken into account, the peripheral stimulus size required for performance equivalent to that of the fovea can be obtained at a range of contrasts by spatial scaling. Secondly, it was hypothesized (*i.e.*, the 2nd hypothesis) that for low-cycle-number ($\leq$16) grating stimulus, the number of cycles played a crucial role on the visual performance across visual field.

For the threshold contrast detection, a hypothesis (i.e., the third hypothesis) was made that the visual process mechanism of the visual task at large orientation difference was different from that at as small as orientation discrimination threshold.

Chapter 2 Methods

2.1 Basic concepts

2.1.1 Psychometric function

In psychophysical experiments, an observer responds to physical values (for example, contrast) of stimuli in some way (for example, 'yes' meaning 'visible' or 'no' meaning 'not visible' by pressing the corresponding key such as 'y' or 'n' in the keyboard). The percentage of 'yes' responses as a function of the physical value follows an S-shaped function, called the **psychometric function** (Fig 2.1). The function shows the dependence of an observer's performance relating a physical value of the stimulus, for example, the observer's ability to detect the stimulus. Threshold is usually taken as 50% of 'yes' responses (dashed line).

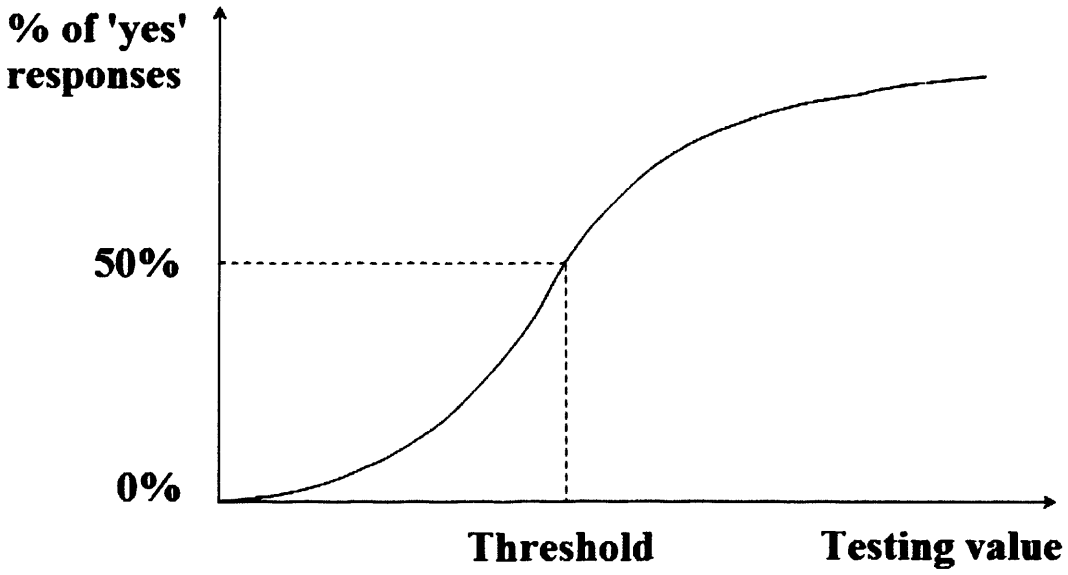

Fig 2.1The psychometric function of a human observer

High contrast, for example, is always visible while low contrast is never visible. The

intermediate contrast is sometimes visible and the percentage of detection increases with contrast. Threshold (50% point) in terms of the physical value is not the same for all observers.

2.1.2 Forced choice procedure

Forced choice procedure is used to minimize the threshold variability. The procedure involves forcing the observers to choose which one is 'correct' among alternatives. Whenever the testing value is below the observer's threshold, the observer needs to make a guess based on any information available. A two-alternative forced choice (2AFC) refers to an experiment where a subject is choosing between two alternatives. As there is already a 50% chance of a correct response with 2AFC, threshold of psychometric function is commonly chosen as 75% (See Fig 2.2).

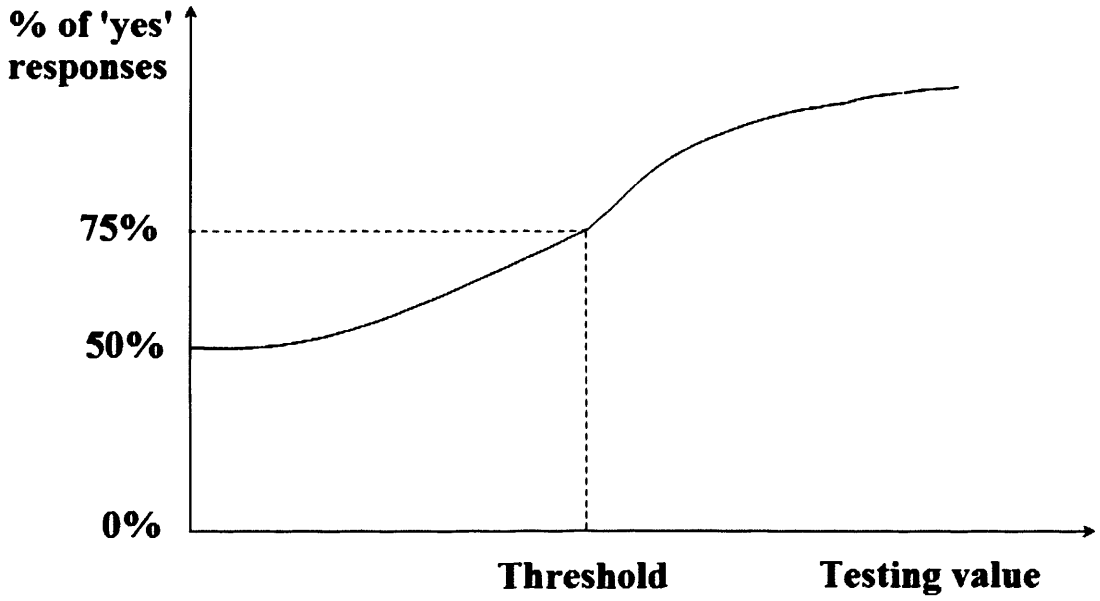

Fig 2.2 Psychometric function for 2AFC. Threshold is taken at 75% correct responses.

2.1.3 Staircase Method

The staircase method estimates the threshold of a testing value by combining ascending and descending limits (Schwartz 2004). With ascending limits a stimulus is first presented below threshold and then the testing value of the stimulus is increased by predetermined steps until threshold is reached. With descending limits a stimulus is first presented well above threshold and then the testing value is decreased by predetermined steps until threshold is reached.

Some parameters need to be determined before conducting an experiment using the staircase method:

1) **Starting value.** A starting value well above threshold results in a long experimental time while a starting value well below threshold causes an inaccurate threshold. An appropriate starting value is above and close to threshold. In order to choose an appropriate starting value, threshold is usually estimated in preliminary experiments.
2) **Step size.** Too large step size results in an inaccurate threshold and too small one makes the experiment inefficient. Cornsweet (1962) introduced logarithmic steps (1.26) in the staircase routine. Step size is sometimes chosen by running pilot experiments to find out an optimal size or as one used in literature.
3) **The number of reversals.** This depends on how accurate the threshold needs to be. The number of reversals must be large enough for a valid threshold. Six to eight reversals are commonly used (for example, in Rovamo, Luntinen and Nasanen 1993, and Nasanen and O'Leary 1998).

2.1.4 Two-alternative forced-choice staircase

Wetherill and Levitt (1965) refined the staircase method and suggested that more than one successive correct or incorrect response could be required before changing the stimulus testing value. Table 2.1 shows some threshold positions of 2AFC staircases commonly used in psychometric functions. For example, in an experiment of contrast detection threshold measurement using a 2AFC combined with the 1:1 staircase procedure, a stimulus is randomly presented in one of the two successive intervals, and subject has to indicate which interval contains the stimulus. With the 1:1 staircase, only one correct (or one wrong) response results in a decrease (or increase) of stimulus contrast in the next stimulus presentation. Fig 2.3 shows a sample of a 4:1 staircase routine starting with an 1:1 staircase.

Table 2.1Threshold positions in psychometric functions of 2AFC staircases

Successive correct responses	Successive incorrect responses	Threshold in psychometric function (%)
1	1	50
2	1	70.7
3	1	79.4
4	1	84.1
5	1	87.0
1	2	29.3
1	3	20.6

Fig 2.3 A 4:1 staircase combined with 1:1 staircase

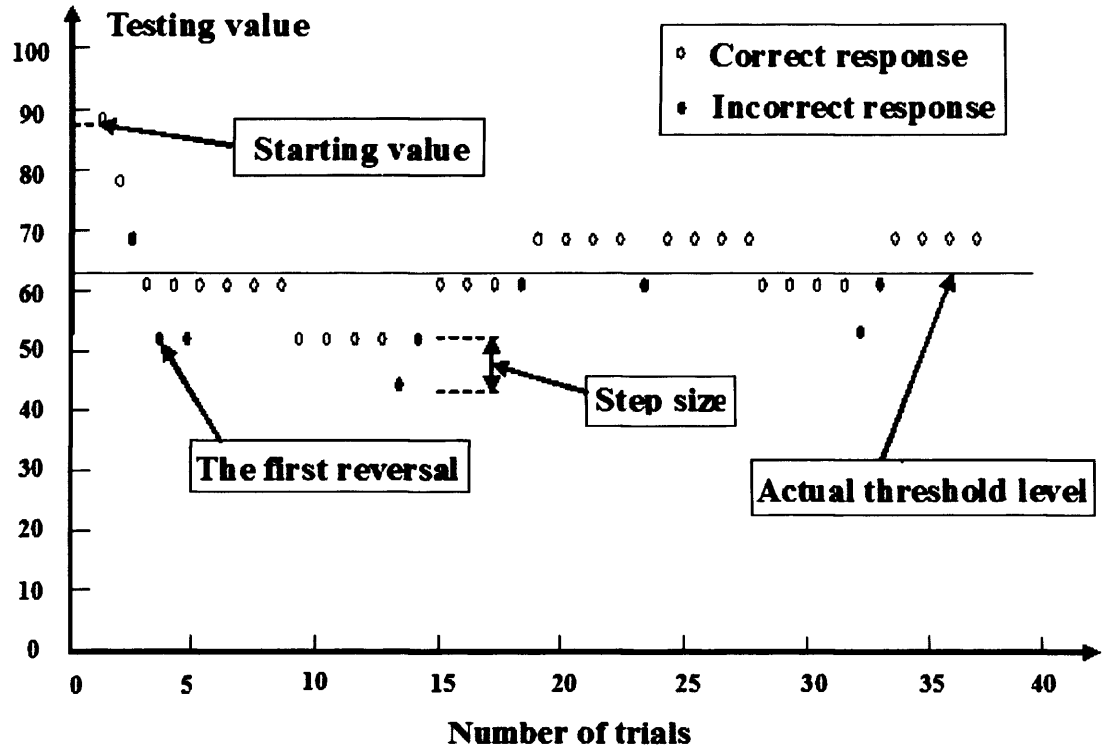

The vertical axis is the value to be tested and the horizontal axis is the trial number. At the beginning of the staircase (1st trial), the testing value of stimulus decreases by a predetermined step from the starting value (well above the actual threshold value) at the top-left of the graph. The first wrong response (marked as filled circle) is ignored and then an 1:1 staircase is initiated, i.e. an increase of the testing value after a wrong response and a decrease of the testing value after a correct response. At the third wrong response, a 4:1 staircase starts, i.e. an increase of the testing value after a wrong response and a decrease of the testing value only after four successive correct responses. The reversal point is where the staircase changes the proceeding direction, from down to up (increasing testing value) or from up to down (decreasing testing value). The actual threshold is calculated as the average of the testing values at a few reversals (for example, the average values of last 6-8 reversals).

2.2 General methods used in this thesis

2.2.1 Apparatus

Stimuli were presented on an Eizo FlexScan F57-M monitor (Eizo, Ishikawa, Japan) with a pixel size 0.485 mm x 0.485 mm, using a Intel Pentium 4 CPU 3.2 MHz computer (RM, Oxfordshire, UK) where a VGA graphics board (NVIDIA GeForce4 MX4000 8X AGP 128MB) is driving the display at 60Hz. The VGA graphics board can simultaneously display 64 (6 bits) luminance levels and 256 (8 bits) colors from a palette of 262144 (3x6 bits) colors. To increase the number of luminance levels available, the color channels of the graphics board were combined via a video summation device (Pelli and Zhang, 1991) and a periodic dither of 2x2 pixels was used (Nasanen, Kukkonen and Rovamo 1993). The arrangement provided a monochrome signal of 1024 intensity levels (10 bits) from a monochrome palette of 16,384 (14 bits) intensity levels.

The average photopic luminance of the screen measured with a Minolta Luminance Meter LS-110 (Minolta, Japan) was 51 cd/m^2. The screen was always covered by a black cardboard with a circular aperture of 20 cm in diameter. All the lights were turned off and subject sat in a dark room lit only by the display.

2.2.2 Stimuli

The stimuli were created and the experiments were conducted using the software developed by Dr Risto Nasanen. The software utilized the graphics subroutine library of Professional HALO 2.0 developed by Media Cybernetics. The stimuli were magnified or minified versions of each other. Thus, the very large or small stimuli could be obtained by varying the viewing distance.

Two types of stimuli were used in this thesis: Gaussian filtered lines and sinusoidal gratings with 2, 4, and 16 cycles per image. Further details of stimuli will be given in the corresponding chapters. In this thesis, the contrasts of all the stimuli were expressed as Michelson contrasts.

2.2.3 Subjects

Traditionally, the number of subjects in psychophysical experiments has been two or three in the literature (e.g., Rovamo and Virsu 1979; Makela *et al* 1993; Whitaker *et al* 1992; Sally and Gurnsey 2003, 2004). In addition to the proceeding training, each experiment in this thesis lasted about 50-70 hours, which also produced a practical limit to the number of subjects used.

In this thesis, subject LC took part in all the experiments while the second subject varied between experiments. For more details of subjects see each chapter and Appendix I. All the subjects had normal or corrected to normal vision. Viewing was always monocular using the dominant eye, which by coincidence was the right eye for all the subjects. Informed

consent was obtained before the experiments were conducted according to Helsinki declaration.

2.2.4 Procedure

Through the entire thesis, thresholds were measured by using a 2AFC method with a 4:1 staircase (see Fig 2.3) thus estimating about 84% correct level from the responses. The step size was 1.26 and the number of the reversals was 8 (excluding the ignored first reversal). Threshold was calculated as the average of the last 6 reversals.

At the beginning of each threshold measurement, the staircase followed the one-correct-down, one-wrong-up rule. The testing value of the stimulus (the tilt angle of the stimulus relative to the vertical reference or the stimulus contrast) progressively decreased by the step size of 1.26. The first wrong response of the subject was ignored. At the second wrong response (the first reversal), the testing value was recorded and then progressively increased by 1.26 until the subject responded correctly. This was the second reversal, from which the value decreased again. The third wrong choice then initiated the staircase with four-correct-down, one-wrong-up rule.

In the experiments, two stimuli were displayed successively for 400 msec with an inter stimulus interval of 84 msec. A sound signal always marked the stimulus appearance. Subjects indicated via the keyboard whether the target stimulus occurred in the first or second interval. There was no time limit for responding. Auditory feedback indicated whether the response was right or wrong after each judgment. Viewing distance was mainly

228 cm but was varied from 28 to 456 cm to obtain more stimulus sizes. For details see each chapter.

For each stimulus, threshold was measured 3, 5 or 7 times and the median was accepted as the final threshold. Thresholds were measured at the fovea and at eccentricities of 2.5, 5, 7.5, and 10 deg in the nasal visual field in all the experiments.

Before data collection began, practice experiments were always conducted in order to familiarise the subjects with the program and to improve their judgments until standard deviations of thresholds remained smaller than half of the threshold itself.

The details of each experimental procedure will be explained in the corresponding chapters.

2.3 Calibration of the monitor

Calibration procedures for the system were carried out using the software written by Dr Risto Nasanen. Programs, 'SHOW', 'LRESP', and 'STIM'. The procedures are given below.

2.3.1 Adjusting the monitor size

The pixel size was 0.485x0.485 mm^2. Two 10x10 cm^2 squares were generated by using the STIM program and displayed using the SHOW program. The vertical and horizontal extents of the display were adjusted until both height and width of the square were exactly 10 cm.

2.3.2 Adjusting the brightness and contrast of the monitor

There are two simple criteria for the adjustments. Firstly the maximum luminance should be about 100 cd/m^2 and a suitable minimum value about 0.3 cd/m^2, which would give a maximum *Michelson contrast* of 99.4%, which is enough for all experiments. The LRESP program was used for brightness and contrast adjustments. The maximum index value (the numerical value corresponding to the maximum output of the graphics card and thus the maximum luminance on the monitor) is set at 63 in LRESP, and the minimum is set at 0.

2.3.3 Gamma correction

Gamma (γ) is the transfer function of Cathode Ray Tubes (CRT). The CRT monitor displays the image signal S received in form of voltage signal V from the VGA graphics card:

$$V = p \times S \qquad \textbf{(}p\textbf{ is a constant).} \qquad \textbf{Equation 2.1}$$

The card has 64 voltage levels for each three primary colours, Red, Green and Blue (RGB). However, monitors do not convert these equally spaced voltage levels into equally spaced luminance levels. Instead, they produce luminance (L) which is related to the input voltage (V) by the following power function:

$$L = k \times V^{\gamma} = k \times (p \times S)^{\gamma}, \qquad \textbf{Equation 2.2}$$

where k is a constant. Most monitors have a gamma (γ) value between 1.7 and 2.7. Because the range of voltage V is between 0 to1, the luminance values of a displayed image are smaller than its actual values.

Gamma correction is introduced to correct this problem. It consists of applying the inverse of the power relationship (between L and V) to image input signal S before loading it to CRT for display. The new input value S' is calculated by equation (2.3):

$$S' = S^{1/\gamma}. \qquad \textbf{Equation 2.3}$$

Equation (2.2) can be rewritten as:

$$L = k \times (p \times (S^{1/r}))^{\gamma} = q \times (S^{1/r})^{r} = q \times S, \qquad \textbf{Equation 2.4}$$

where q is a constant and is equal to k x p.

Thus, the non-linearity is compensated and the luminance value is directly linear to the input voltage values.

2.3.4 Measuring the luminance response of the monitor

The LRESP program was used for measuring luminance response. We measured the luminance in the middle of the screen as a function of the index value from 60 to 0 with a step size of 4 using the Minolta Luminance Meter LS-110.

Generally the luminance response of the monitor obeys the following function:

$$L = b(I - c)^{(1/d)} + a, \qquad \textbf{Equation 2.5}$$

where L is luminance, I is the index value, a, b, c, and d are the constants. A good fit in the mid range can be obtained with a and c set equal to zero. Then the equation can be expressed as

$$L = bI^{(1/d)}. \qquad \textbf{Equation 2.6}$$

With taking the logarithm of both sides, equation (2.6) is rewritten as

$$\log(L) = \log(bI^{(1/d)}). \qquad \textbf{Equation 2.7}$$

It can be fitted using the least squares linear fit in double logarithmic coordinates:

$$\log L = \log b + \log I^{(1/d)}, \qquad \textbf{Equation 2.8}$$

$$\Rightarrow \qquad \log L = \log b + \frac{1}{d}\log I. \qquad \textbf{Equation 2.9}$$

Let y=log$L$, k=1/d, x=log$I$, and g=log$b$, so equation (2.9) can be matched to a linear function:

$$y = g + kx \qquad \textbf{Equation 2.10}$$

It is important that the fit is nearly perfect close to the mid luminance around 50 cd/m^2, so that the small contrasts are displayed correctly. Therefore, some points at both extreme ends may need to be excluded from the fit.

The results of the calibration measurements are shown in Fig 2.4. A valid response function must be approximately linear with R^2 greater than 0.99.

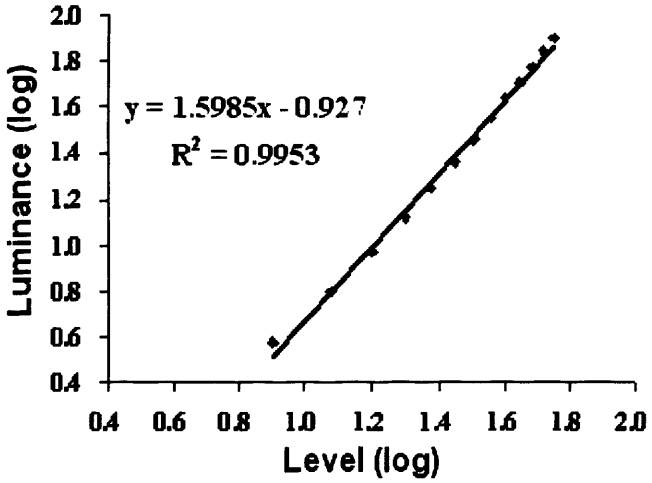

Fig 2.4 Luminance response regression line

2.3.5 Checking the contrast response

Two grating image series of very low spatial frequency (f) were created with contrast ranging from 0.5 to 0.001 using the STIM program. The two series had opposite phase (0 and 180 deg) and were displayed in 10 x 10 cm^2 window using the SHOW program. Luminance was measured in the middle of the square images. The maximum luminance

was obtained from the 0 phase image and the minimum luminance from the 180 phase image. The series were shown alternatively so that contrast decreased until there was no measurable difference between the two series. *Michelson contrast* was calculated and the resulting contrast levels are shown in Fig 2.5. An acceptable response function is linear with R^2 greater than 0.99.

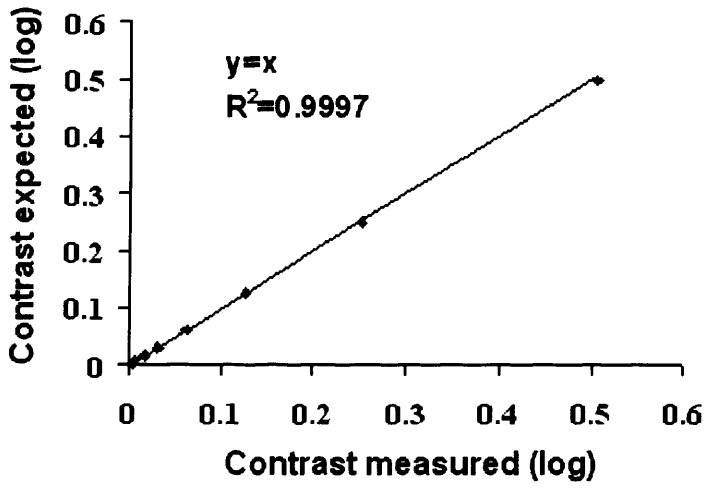

Fig 2.5 Contrast response regression line

Chapter 3 The effects of eccentricity and contrast on orientation discrimination for a Gaussian filtered line

3.1 Introduction

Orientation discrimination threshold indicates the smallest detectable change in the orientation of a stimulus. It can be expressed either in spatial terms or in angular terms (see Fig 1.15 in Section 1.4.4).

Generally, when the threshold is expressed in angular terms, orientation discrimination first improves with increasing stimulus size (for example, line length) and then becomes independent of size (Andrews 1967; Makela *et al.* 1993; Orban, Vandenbussche and Vogels 1984; Sally and Gurnsey 2003, 2004 and 2007; Vandenbussche *et al.* 1986; Watt 1987). Threshold comparisons between studies are difficult because thresholds depend on stimulus dimensions (length and width), exposure duration (Bearse Jr and Freeman 1994; Calvert and Harris 1988), and stimulus contrast (Sally and Gurnsey 2005 and 2007; Westheimer, Brincat, and Wehrhahn 1999). Threshold also depends on stimulus type, including lines (Orban *et al.*1984; Sally and Gurnsey 2003, 2004 and 2007; Westheimer 1982; Westheimer and Li 1996), dots (Beck and Halloran 1985), edges (Heeley and Buchanan-Smith 1990; Morgan 1986), gratings (Heeley and Buchanan-Smith 1990; Morgan 1986; Pardhan 2003; Saylor and Olzak 2006; Skottun, *et al.* 1986), and contours (Bockisch 1998; Westheimer and Li 1996).

Andrew (1967) measured foveal orientation recognition threshold by using a bright thin

line (1 x 5.5 or 1 x 7.4 min) viewed at 1.5 m. In a dark background with a luminance of 3 cd/m^2, the horizontal line stimulus was presented 10 mm above a 1.5 deg long thin reference line. The luminance of the line stimulus was 'sufficient to allow optimal performance' (Andrew 1967). Subjects had to indicate whether the bright line stimulus was clockwise or counter-clockwise tilted from the reference line. The best foveal threshold was found to be 0.1 deg. Westheimer *et al.* (1976) investigated orientation discrimination by using a long bright line with the width of 15 sec in visual field. They measured its foveal orientation discrimination threshold at 75% Michelson contrast and found a threshold of 0.4 deg. Heeley and Buchanan-Smith (1990) measured foveal orientation recognition threshold by using three types of stimuli at 80% contrast :(i) a line 6 min in length in the visual field, (ii) step edge, and (iii) sine wave gratings of 2.5, 5.0 and 10.0 cpd. Subjects were asked to indicate whether the stimulus was titled clockwise or counter-clockwise. All stimuli produced similar thresholds, averaging to 0.6 deg. Thus, very low orientation discrimination thresholds can be obtained at the fovea.

The investigation of orientation discrimination was not limited to the central vision and also has been extended to the peripheral visual field. Vandenbussche *et al.* (1986) conducted orientation discrimination experiments at the fovea and eccentricities of 15 and 30 deg by using very low luminance (0.14 cd/m^2) line stimuli (15 min in width with varying lengths) against a completely dark background (0.006 cd/m^2). The average thresholds obtained between subjects were about 1.5 deg at the fovea, 2.0 deg at the eccentricity of 15 deg, and 2.8 at the eccentricity of 30 deg. Paradiso and Carney (1988) investigated the effects of size and eccentricity on orientation discrimination using a 3 min in width of visual angel line with a luminance of 150 cd/m^2 against a 15 cd/m^2 background. The length of line stimulus

was controlled by placing circular apertures in front of the CRT monitor. Several eccentricities from fovea to 50 deg eccentricity were studied. They found that a very low threshold (about 0.3-0.4 deg) can be obtained from fovea to eccentricity of 20 deg by increasing line length except at the blind point. In comparison, Makela *et al.* (1993) conducted orientation discrimination experiments at the fovea and eccentricities of 2.5, 5, 10 and 15 deg in full contrast using a white line (40 cd/m^2) against a dark background and found an average eccentric threshold of about 0.5 deg from fovea to 15 deg eccentricity.

In recent years, some studies have specifically investigated the effects of contrast variation on orientation discrimination threshold. Westheimer *et al.* (1999) measured foveal orientation discrimination threshold using a circular disk with 30 min in diameter in a uniform background with a Michelson contrast of 10%. A straight edge between the upper and lower halves of the disk was tilted either clockwise or counter-clockwise from the horizontal, and viewed at 4 and 6 m. Subjects had to indicate whether the tilt of the dividing edge was clockwise or counter-clockwise. Orientation discrimination threshold was estimated as a function of stimulus contrast from 3 to 100%. They found that (i) the threshold decreased and reached a plateau with increasing contrast; (ii) and the threshold was about 0.6 deg at 100% and about 4 deg at 3% contrast.

Sally and Gurnsey (2003) investigated the effect of contrast on orientation discrimination by measuring orientation discrimination thresholds of broadband and narrowband line stimuli at eccentricities of 0, 2.5, 5, 10 and 15 deg. The ratio between width and length of line stimulus was 1:9 and line lengths were obtained by varying viewing distances. The background luminance was 26.1 cd/m^2. Orientation discrimination thresholds were

measured at contrasts of 50, 75, 85 and 100%. To calculate E_2 values, they only used the asymptotic thresholds and the corresponding sizes (the length of the line stimuli), where the change of contrast had no influence on the thresholds. The lengths finally used for the calculation of E_2 ranged from 0.25-18 deg for the broadband line and 0.375-12 deg for the narrowband line. The average minimum threshold was about 0.56 deg and a range of 1.29 - 1.83 deg of E_2 values was obtained, which is in good agreement with the 1.95 deg reported by Makela *et al.* in 1993.

After their study of orientation discrimination at high contrast, Sally and Gurnsey continued their investigation at the detection threshold contrast in 2004. They first measured contrast detection and contrast increment thresholds for a 3 deg vertical reference line at the fovea. Then the contrast of the reference line was set to two contrast increment thresholds above its detection threshold and was presented at the fovea. The target stimulus was a Gaussian filtered broadband line and its lengths varied from 0.188 deg to 12 deg. Then subjects were asked to adjust the contrast of the line stimulus presented at the eccentricity of 0, 2.5, 5, 10 and 15 deg to match with that of the reference. Finally orientation discrimination thresholds were measured as a function of line length and eccentricity by using line stimuli of various sizes at their matching contrasts. Threshold was found to decrease and approach a plateau with increasing line length with an average minimum threshold of 1.31 deg. The E_2 values were found to be 3.46 and 3.50 deg for two subjects, which is about two times larger than E_2 values previously found by Sally and Gurnsey (2003) using the same stimulus but at high contrasts.

To investigate the effect of contrast on orientation discrimination further, Sally and

Gurnsey in 2007 measured orientation discrimination thresholds at the fovea and 10 deg eccentricity for Gaussian filtered broadband lines ranging within 0.19-36 deg in length at Michelson contrasts of 3, 12 and 48%. Threshold was estimated as a function of line length. The study showed that (i) the minimum threshold found increased as contrast decreased; and (ii) E_2 values decreased with increasing contrast suggesting that contrast reductions had a stronger effect for small than large stimuli so that performance dropped faster at the fovea where smaller stimulus sizes were used than in the periphery where larger stimulus sizes were used.

For some complex tasks, researchers have suggested both spatial and contrast factors need to be considered when performance is equated between the fovea and the periphery (Melmoth *et al.* 2000a and 2000b; Melmoth and Rovamo 2003; Strasburger *et al.* 1991 and 1994). E_2 values for face identification (Makela *et al.* 2001) or for detecting image distortions (Melmoth *et al.* 2000b) are in fact a lot larger than those obtained from simple tasks, for example, vernier or orientation discrimination (see Chapter 1 Section 1.3.3 Table 1.2).

When studying the effect of contrast on orientation discrimination, it is necessary to compare the performance at high and low contrast. However, comparison across studies or researchers is difficult because of different experimental settings. Therefore, in this chapter, we approached the contrast-dependent changes from the fovea to periphery directly and gave a more thorough examination on the effect of eccentricity and contrast on orientation discrimination. Orientation discrimination thresholds were measured at eccentricities of 0, 2.5, 5, 7.5, and 10 deg, and at contrasts of 100, 30, and 10%. By processing and analyzing

the threshold data with different scaling methods, *i.e.*, spatial scaling across contrasts and within individual contrast, and 2D scaling, it was examined whether spatial scaling can successfully superimpose the threshold data across contrasts and within a contrast. Because E_2 represents how fast performance in a visual task decreases from the fovea to periphery, by observing spatial scaling E_2 found at each contrast, the effect of contrast reduction on spatial scaling (and further, spatial summation at different locations of visual field) was investigated.

3.2 Methods

3.2.1 Apparatus

Stimuli were presented on the monitor described in Section 2.2.1.

3.2.2 Stimuli

A vertical line and a series of counter-clockwise orientated lines with varying amounts of tilt from 0.0005 to 89 deg from the vertical were created at contrast levels of 100, 30 and 10% (see Fig 3.1) using the software developed by Dr Risto Nasanen.

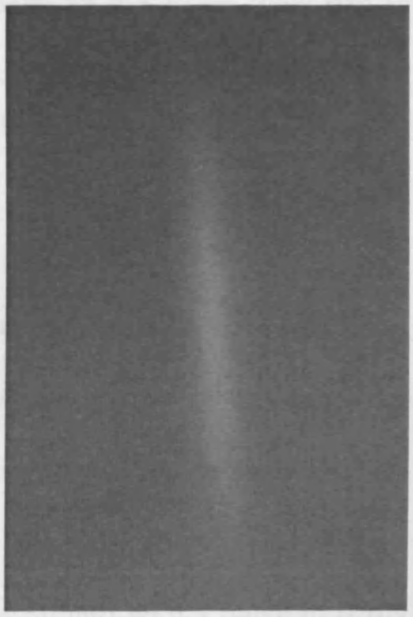

Fig 3.1 An example of the Gaussian filter line stimulus used in the experiment

The ratio between length (height) to width of the unfiltered line was 9:1, and the heights (h) of the lines were 8.7, 17, 35, and 70 mm on the screen. All the lines were magnified

versions of each other. Then the line stimuli were filtered in Fourier space with a Gaussian weighed stimulus window equation:

$$g(x,y) = \exp\{-\ln 2[(x/x_{1/2})^2 + (y/y_{1/2})^2]\}, \qquad \textbf{Equation 3.1}$$

where $x_{1/2} = h/9$ and $y_{1/2} = h$ are coordinates, at which luminance deviation had decreased to half of its maximum value (see Appendix II for further details of the Gaussian filter). At 2.5xh the luminance deviation was so small that it could be cut abruptly without a visual effect.

3.2.3 Subjects

Two subjects, LC and VR, aged 25 and 20 yrs, took part in the experiment. Both subjects had normal or corrected to normal vision (see Appendix I for the details of the subjects).

3.2.4 Procedure

Two line stimuli of the same contrast level were presented successively in random order, one always oriented vertically, and the other tilted counter-clockwise. After the two exposures the subject responded via the keyboard which interval contained the more counter clockwise tilted line stimulus. The viewing distances were 28, 57, 114, 171, 228, 285, and 456 cm, resulting in stimuli with a range of 0.1097-14.22 deg of visual angle in unfiltered line length. The smallest line length (0.1097 deg) was achieved by presenting the smallest 8.7 mm stimulus at the furthest viewing distance of 456 cm and the largest line length (14.22 deg) was achieved by presenting the largest 69.84 mm stimulus at the shortest

viewing distance of 28 cm.

Orientation discrimination thresholds were measured by using the 2AFC procedure explained in Chapter 2. The measurement started from the most tilted stimulus (89 deg from the vertical).

For each stimulus orientation discrimination threshold was measured 3 or 5 times and the median was accepted as the final threshold. Thresholds were measured at the fovea and four eccentricities of 2.5, 5, 7.5, and 10 deg in the nasal visual field. Data collection was started at contrast of 100% then proceeding to contrasts of 30% and 10%.

3.3 Results

In Fig 3.2, orientation discrimination spatial offset thresholds (i.e. θ in Fig 1.16, see Chapter 1 Section 1.4.4) in sec arc in the visual field were plotted against line length in min arc of visual field at contrasts of 100, 30, and 10%, and eccentricities of 0, 2.5, 5, 7.5 and 10 deg for each subject. Spatial offset was chosen to be the distance between the ends of the two lines at 2.5 times the unfiltered length on the screen as this is the location where the filtered stimulus appeared to end on the basis of the visual criterion. The resulting curves tend to be u-shaped, which shows an optimal length for each eccentricity and contrast level. The optimal length increases with increasing eccentricity and decreasing contrast. At the fovea the lowest thresholds (sec arc) are within the hyperacuity range (<60 sec arc) at contrasts of 10-100% (Westheimer 1975 and 1981), except that of 10% contrast for subject VR.

Fig 3.2 Orientation discrimination thresholds (sec arc) for the Gaussian filtered lines

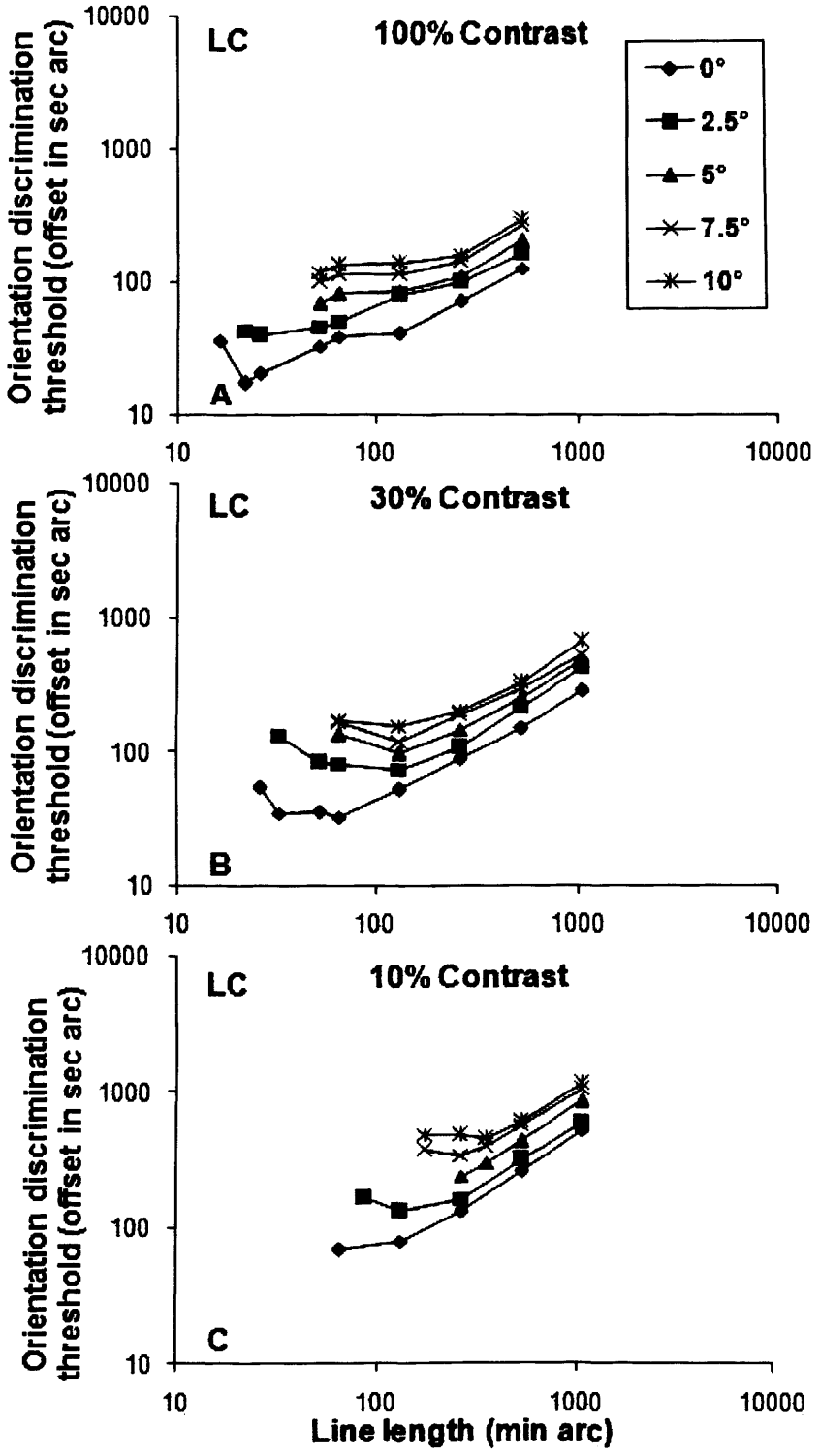

Fig 3.2 (A-C) Orientation discrimination thresholds (spatial offset in the visual field, sec arc) for the Gaussian filtered line stimuli plotted against line length (min arc) at eccentricities of 0, 2.5, 5, 7.5, and 10 deg, and contrasts of 100, 30, and 10% for subject LC.

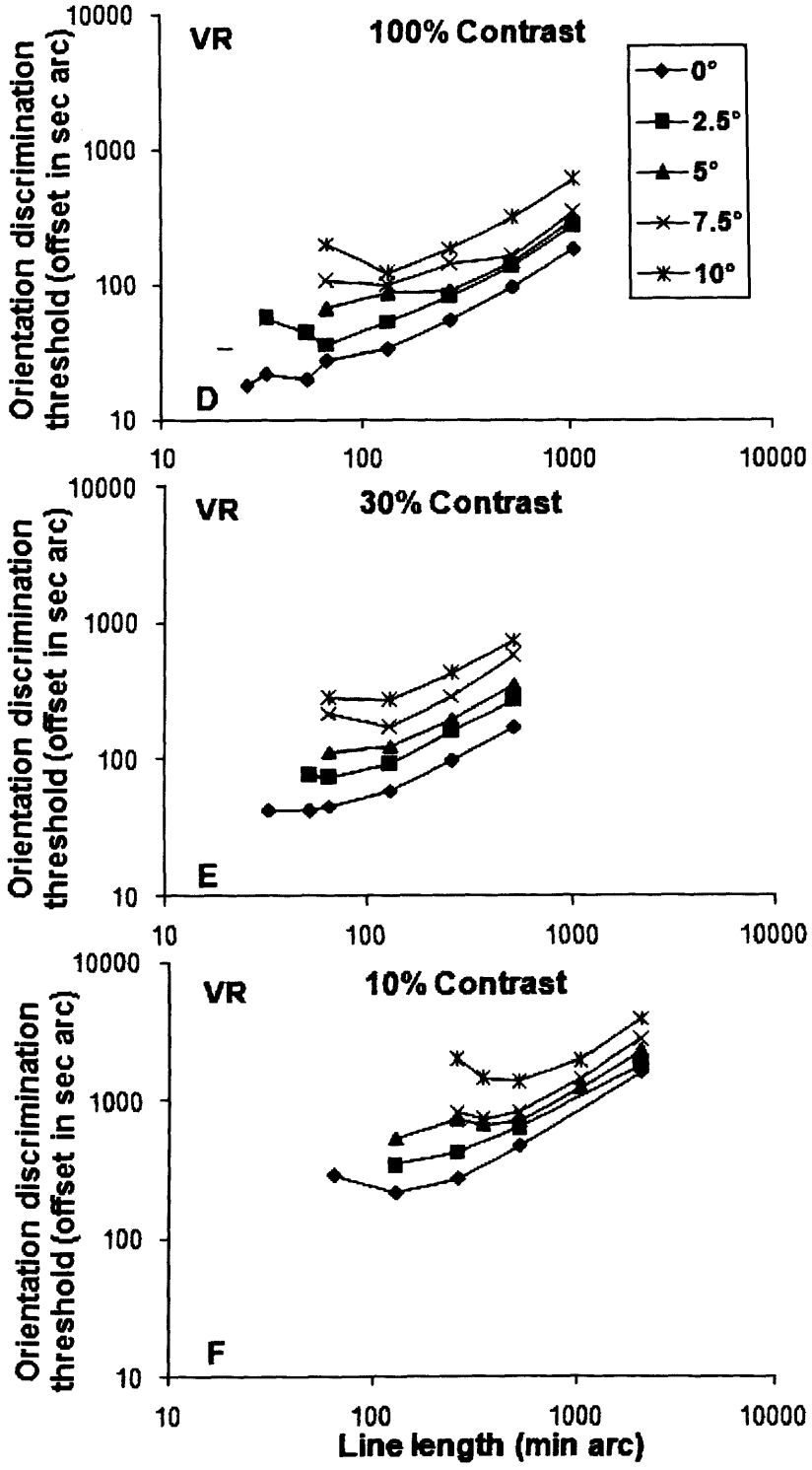

Fig 3.2 (D-F) Orientation discrimination thresholds (spatial offset, sec arc) plotted against line length (min arc) for subject VR. The details are as in Fig 3.2 (A-C).

In Fig 3.3 the orientation discrimination thresholds in rotation angle (deg) (i.e. α in Fig 1.15, see Chapter 1 Section 1.4.4) were plotted as a function of line length in deg of visual field. Threshold first decreases and then reaches a plateau as line length increases. The shapes of the data curves at different eccentricities and contrasts are similar. As shown in the figure, threshold functions are shifted towards right along the horizontal axis revealing the magnification of spatial scale with increasing eccentricity and decreasing contrast.

Due to the similar shapes of the data curves at all eccentricities and contrasts, all the threshold (*Th*) data were fitted with equation (Sally and Gurnsey 2003, 2004):

$$Th = Th_{\min}(1 + H_c / H)^5, \qquad \textbf{Equation 3.2}$$

where Th_{min} is the theoretical minimum threshold, H is line stimulus height (i.e. line length in Fig 1.15) and H_c is the critical stimulus height marking the change from the decrease to plateau(see Appendix V for the details of the exponent determination of the equation). *Th* will always be greater than Th_{min} because the bracket portion of the equation is always greater than one. R^2 was calculated for each data curve to check the accuracy of the fit by Equation (3.2). The R^2 were found to range from 0.90-0.99, with the mean value of 0.96 (see Appendix V Table 5) Therefore, equation (3.2) describes quite accurately all the data curves.

Fig 3.3 Orientation discrimination thresholds (deg) for the Gaussian filtered lines

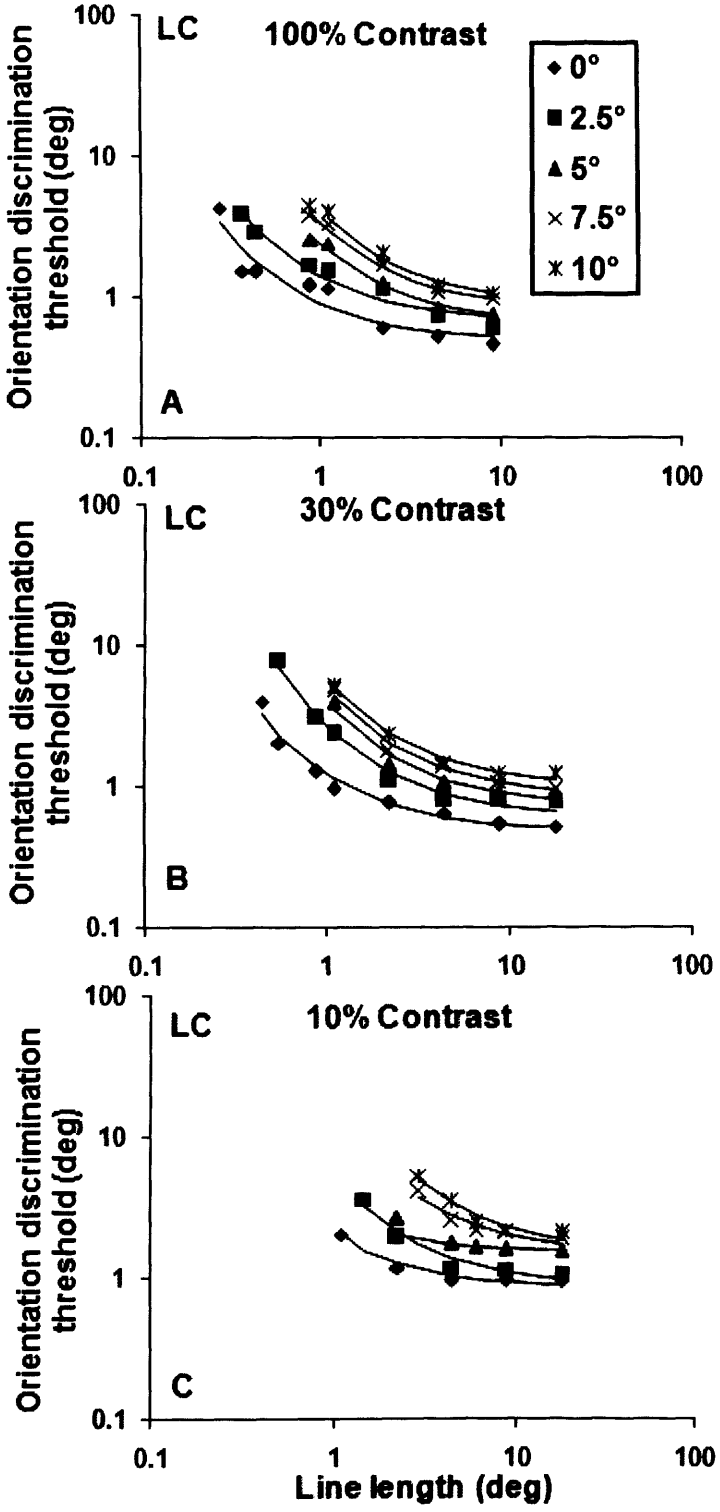

Fig 3.3 (A-C) Orientation discrimination thresholds from Fig 3.2 (A-C) expressed in deg of rotation angle and replotted as a function of line length in deg of visual field. Each data set was fitted with

equation (3.2). The resulting solid line models the decrease and plateau in threshold with increasing line length.

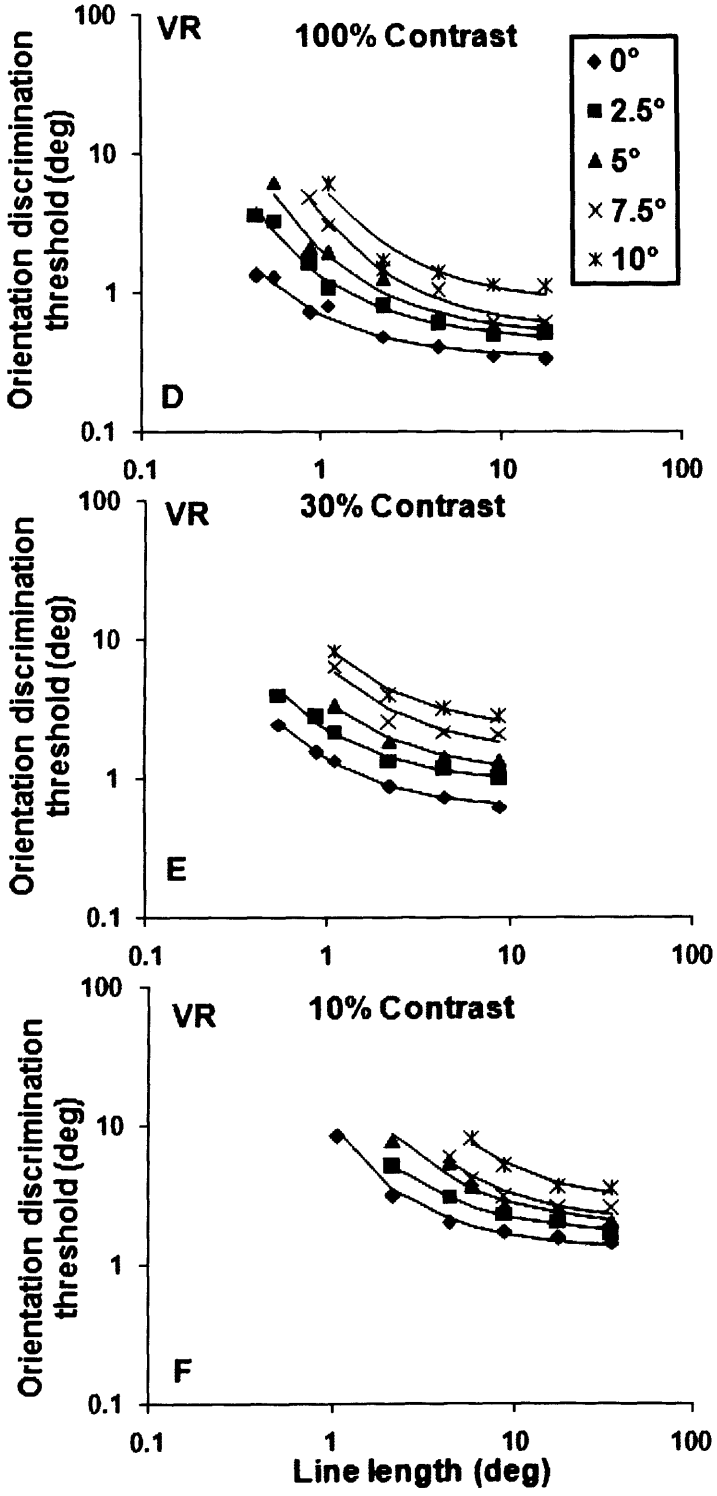

Fig 3.3 (D-F) Orientation discrimination thresholds in terms of rotation angle (deg) plotted against line length (deg) for VR. The details are as in Fig 3.3 (A-C).

3.3.1 Spatial scaling across contrasts

Before applying spatial scaling to equate the peripheral orientation discrimination performance to that of the fovea in this visual task, a basic condition must be chosen, onto which all the threshold data are superimposed.

The foveal orientation discrimination at 100% contrast (E=0, C=1) was chosen as the basic condition and the threshold data at different eccentricities and contrasts were horizontally scaled to it by spatial scaling. The spatial scaling factor at each eccentricity and contrast was obtained by the spatial scaling procedure described in Chapter 1 Section 1.3.4. Because the scaling was applied to each eccentric data across contrasts, the spatial scaling factor was dependent on two variables, eccentricity (E) and contrast (C). Fig 3.4 (A, B) shows the spatial scaling factors plotted against eccentricity and contrast for both subjects. From the figure, spatial scaling factors increase with increasing eccentricity and decreasing contrast.

Thus, the equation for calculating spatial scaling factor F=1+SE (see Chapter 1 Section 1.3.4 equation (1.1)) had be to modified to include the variable of contrast. It was rewritten as equation (3.3) so that the scaling factor is a function of both eccentricity and contrast. The equation included all the necessary 2nd order polynomial parameters involving E and C, and was in the agreement with Melmoth and Rovamo (2003).

$$F_i = 1 + E/E_2 + (\log C)^2/k_1 + \log C/k_2 + E \times \log C/k_3 + E^2/E_2^{'}, \qquad \textbf{Equation 3.3}$$

where F_i represents scaling factor, and E_2, $E^{'}_2$, k_1, k_2 and k_3 are constants: E_2 and $E^{'}_2$ define

the effect of eccentricity on the scaling while k_1 and k_2 together define the effect of contrast. k_3 describes the interaction between eccentricity and contrast. At (E=0, C=1), all the terms involving E and C become 0, which leaves the scaling factor F_i to be equal to unity for the basic condition. However, on the basis of R^2 values and the variances of the constants k_2 and E_2 were found to be either unnecessary or inaccurate (see Appendix III for the details of the procedure obtaining the optimal fitting equation). Thus, equation (3.3) was reduced to equation (3.4):

$$F_s = 1 + E/E_2 + (\log C)^2/k_1 + E \times \log C/k_3, \qquad \textbf{Equation 3.4}$$

where F_s represent spatial scaling factor.

The scaling factor surfaces in Fig 3.4 (A,B) were estimated in Fig 3.4 (C,D) by using equation (3.4), which models the dependency of the spatial scaling factor on eccentricity and contrast with respect of the basic condition (E=0, C=1)

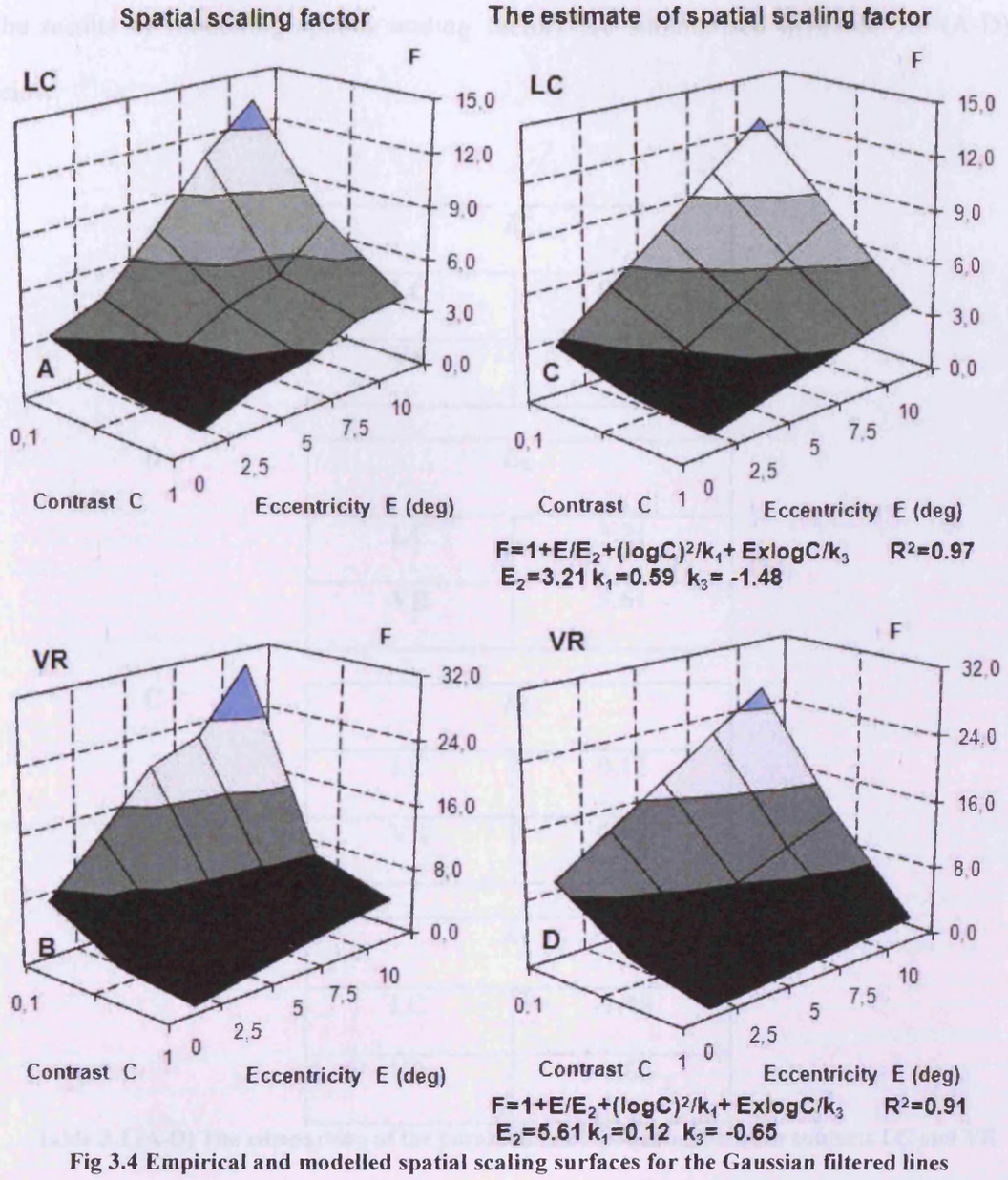

Fig 3.4 Empirical and modelled spatial scaling surfaces for the Gaussian filtered lines

The empirical (left column) and modelled (right column) surfaces showing the spatial scaling factors, *F*, required to quantify performance at any eccentricity (*E*) and contrast (*C*) relative to the basic condition, the fovea&100% contrast data (*E*=0, *C*=1). The columns (A, B) show the empirical scaling surfaces separately for subjects LC and VR, obtained through the procedure of spatial scaling applied to the threshold data in Fig 3.3. The empirical surfaces were fitted with equation (3.4). The equation models the effects of eccentricity (*E*) and contrast (*C*) on *F*. The modelled scaling surfaces calculated by equation (3.4) are shown in the right-hand column (C, D) along with the values of their necessary parameters and R^2s.

The results of modelling spatial scaling factors are summarised in Table 3.1 (A-D) as below.

A

	R^2
LC	0.97
VR	0.91

B

	E_2
LC	3.21
VR	5.61

C

	k_1
LC	0.12
VR	0.59

D

	k_3
LC	-1.48
VR	-0.65

Table 3.1 (A-D) The comparison of the parameters of modelling between subjects LC and VR

To show the distribution of the threshold data across eccentricities (0-10 deg) and contrasts (10-100%), the original experimental orientation discrimination threshold data were plotted against line length in Fig 3.5 (A-B) for subjects LC and VR. Then by the modelled spatial scaling surfaces shown in Fig 3.4 (C, D), the original threshold data were scaled to (E=0, C=1), as shown in Fig 3.6 (A, B).

The change of orientation discrimination performance across all eccentricities and contrasts were explained in quantitative terms in Fig 3.6 (A, B). The smooth curve was the best fit of equation (3.2) to all the scaled threshold data. The R^2 of the curve fitted to the scaled threshold data was 0.82 and 0.61 for subjects LC and VR, respectively.

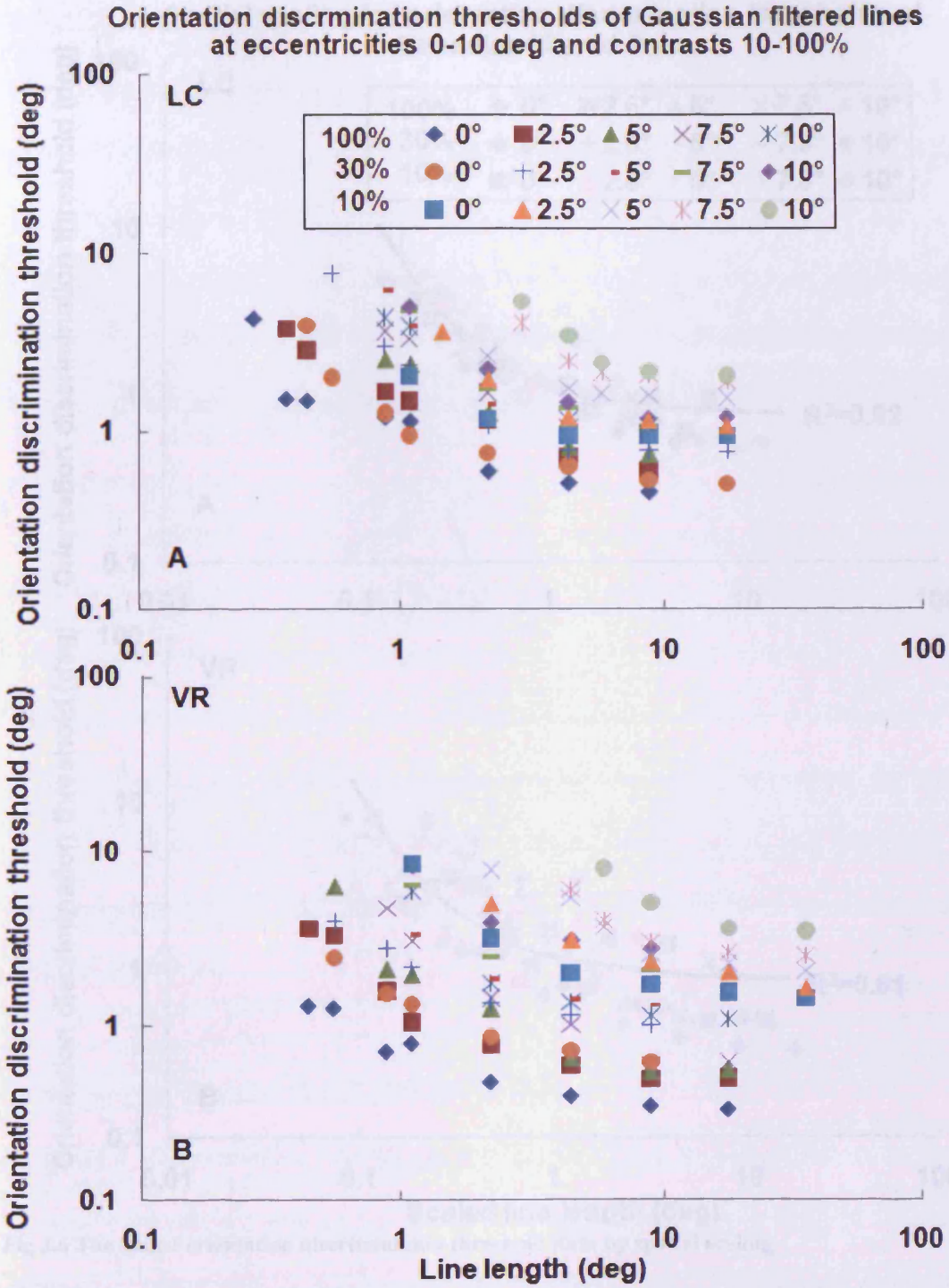

Fig 3.5 The original unscaled orientation discrimination threshold of the Gaussian filtered lines

The original orientation discrimination threshold were plotted against line length (deg) at the eccentricities of 0, 2.5, 5, 7.5 and 10 deg, and contrast of 10, 30 and 100% for LC and VR.

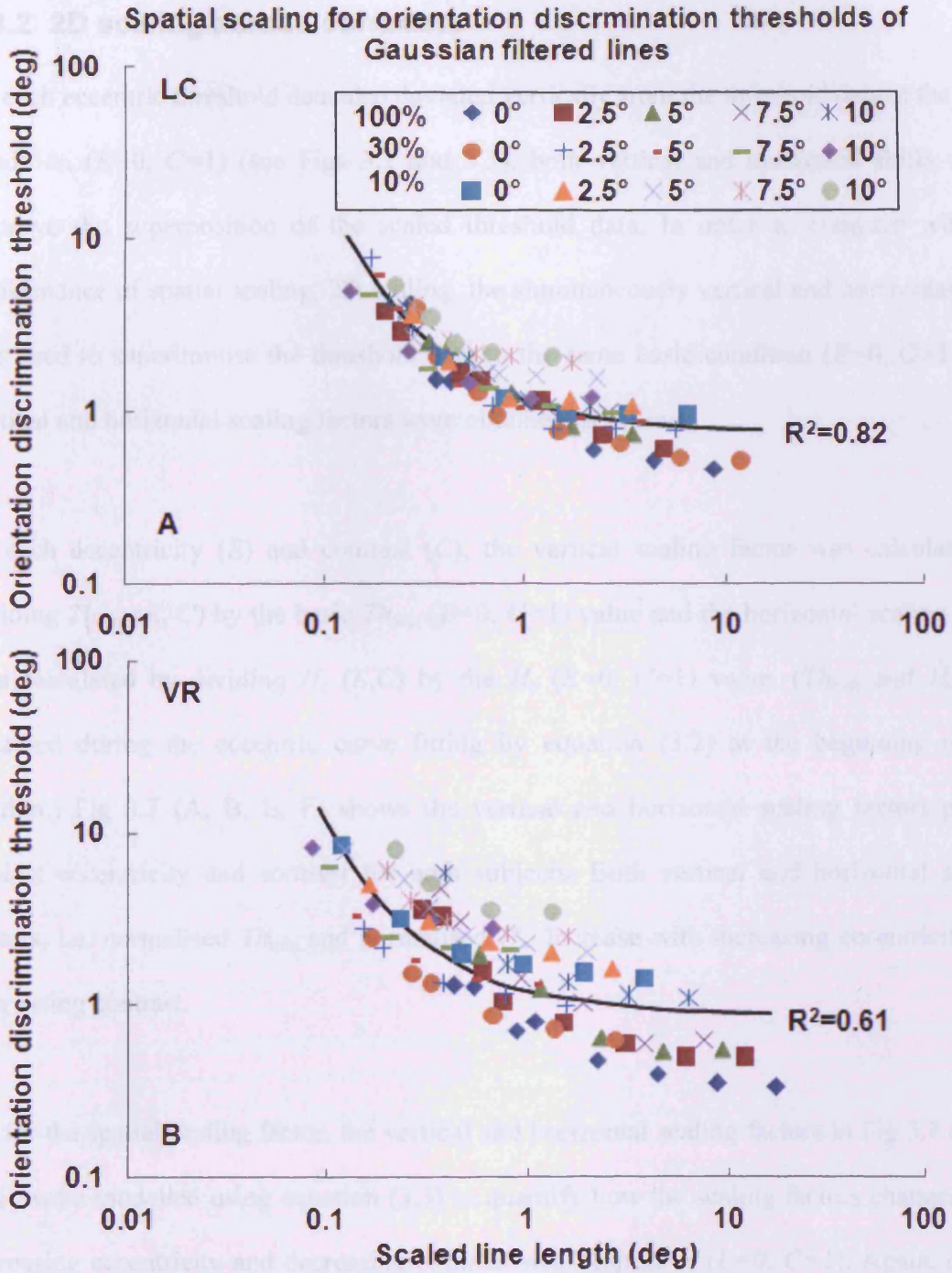

Fig 3.6 The scaled orientation discrimination threshold data by spatial scaling

The original experimental orientation discrimination threshold data in Fig 3.5 (A-B) were scaled using the modelled spatial scaling surfaces in Fig 3.4 (C, D). Data from the eccentricities of 0-10 deg and contrasts of 10-100% collapsed onto (E=0, C=1). The solid curve is the best fit of equation (3.2) to all the superimposed data for subjects LC and VR respectively. The values of R^2 indicate how well all the threshold data were superimposed by spatial scaling.

3.3.2 2D scaling across contrasts

As each eccentric threshold data also deviated vertically from the threshold data at the basic condition (E=0, C=1) (see Figs 3.2 and 3.3), both vertical and horizontal shifts would improve the superposition of the scaled threshold data. In order to compare with the performance of spatial scaling, 2D scaling, the simultaneously vertical and horizontal shift, was used to superimpose the threshold data to the same basic condition (E=0, C=1). The vertical and horizontal scaling factors were obtained as follows.

At each eccentricity (E) and contrast (C), the vertical scaling factor was calculated by dividing Th_{min} (E, C) by the basic Th_{min} (E=0, C=1) value and the horizontal scaling factor was calculated by dividing H_c (E,C) by the H_c (E=0, C=1) value. (Th_{min} and H_c were obtained during the eccentric curve fitting by equation (3.2) at the beginning of this section.) Fig 3.7 (A, B, E, F) shows the vertical and horizontal scaling factors plotted against eccentricity and contrast for both subjects. Both vertical and horizontal scaling factors, i.e. normalised Th_{min} and normalised H_c, increase with increasing eccentricity and decreasing contrast.

As for the spatial scaling factor, the vertical and horizontal scaling factors in Fig 3.7 (A, B, E, F) were modelled using equation (3.3) to quantify how the scaling factors changes with increasing eccentricity and decreasing contrast with respect of (E=0, C=1). Again, on the basis of R^2 values and the variances of the constants, k_2, k_3, and E_2' were dropped. Thus, equation (3.3) was reduced to equation (3.5) for both vertical and horizontal scaling factors:

$$F_l = 1 + E/E_2 + (\log C)^2/k_1 . \qquad \textbf{Equation 3.5}$$

In Fig 3.7 (C, D, G, H), the vertical and horizontal scaling factors were modelled by using equation (3.5) fitted to the data of Fig 3.7 (A, B, E, F).

Fig 3.7 Empirical & modelled 2D scaling surfaces

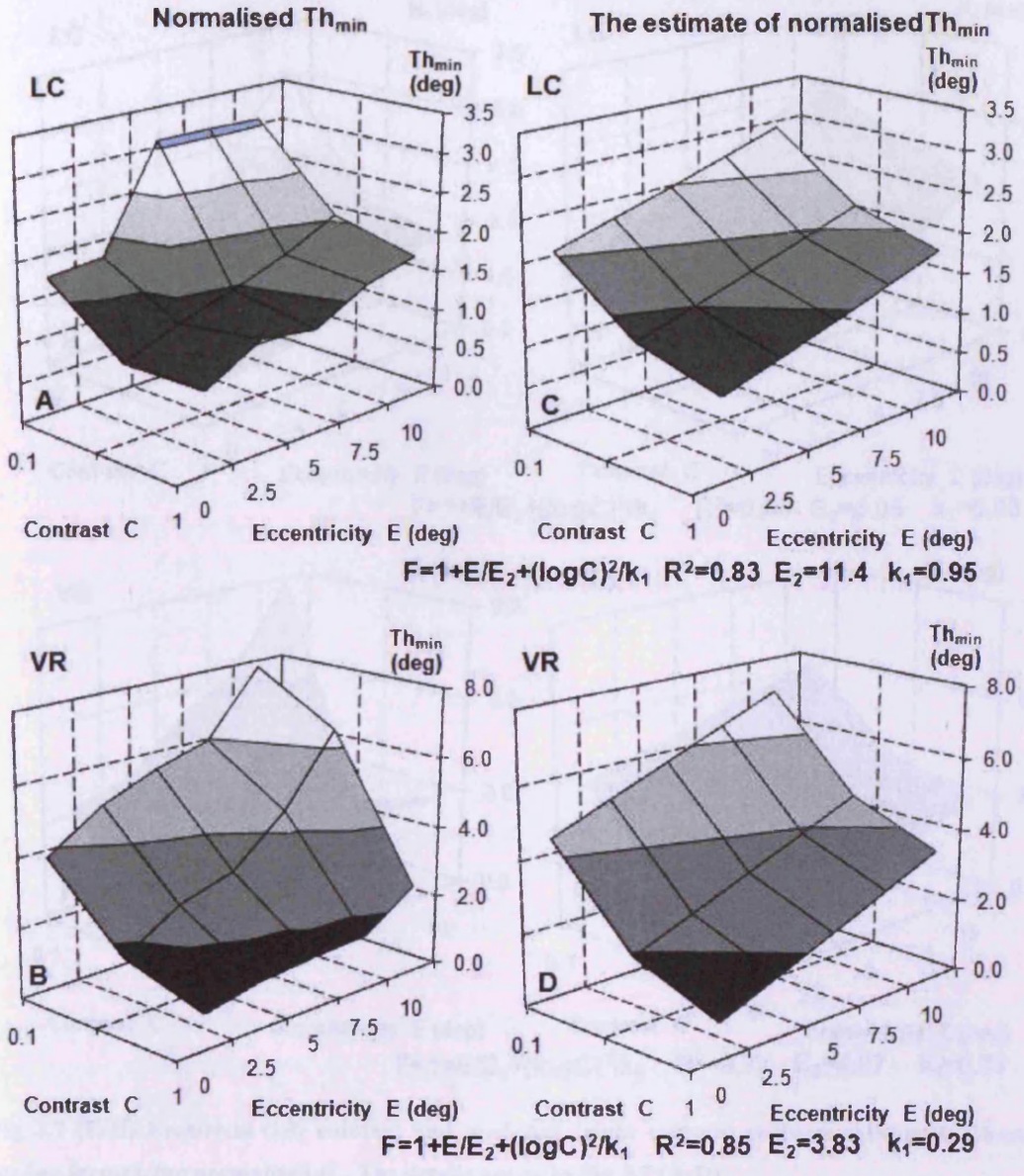

Fig 3.7 (A-D) Empirical (left column) and modelled (right column) surfaces showing the vertical scaling factors of 2D scaling, the normalised Th_{min}, required to quantify performance at any eccentricity (E) and contrast (C) relative to (E=0, C=1). The columns (A-B) show the empirical scaling surfaces separately for subjects LC and VR, calculated from the data in Fig 3.3 by equation (3.2). The empirical surfaces were fitted with equation (3.5). The equation models the effects of eccentricity (E) and contrast (C) on the normalised Th_{min}. The modelled scaling surfaces calculated by equation (3.5) are shown in the right-hand column (C-D) along with the values of their necessary parameters and R^2s.

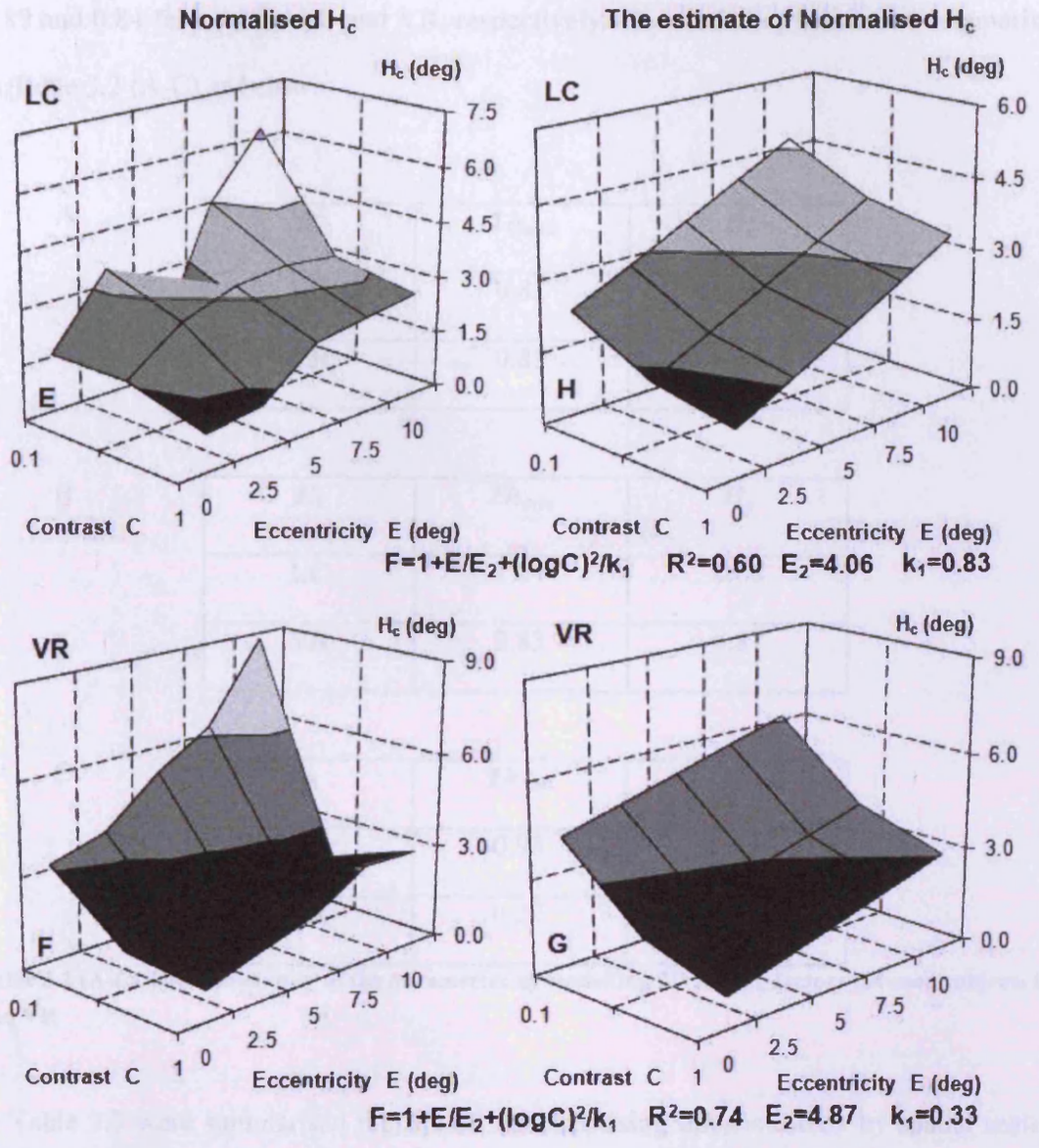

Fig 3.7 (E-H) Empirical (left column) and modelled (right column) surfaces showing the horizontal scaling factors, the normalised H_c. The details are as in Fig 3.7 (A-D).

The original threshold data in Fig 3.5 (A-B) was both horizontally and vertically scaled by the modelled vertical and horizontal scaling surfaces in Fig 3.7 (C, D, G, H). All the data collapsed on to (E=0, C=1) in Fig 3.8 (A-B). The smooth curve was the best fit of equation (3.2) to all the 2D scaled data. The R^2 of the curve fitted to the scaled threshold data was

0.89 and 0.84 for subjects LC and VR, respectively. The modelling results are summarised in Table 3.2 (A-C) as below.

A

R^2	Th_{min}	H_c
LC	0.83	0.60
VR	0.85	0.74

B

E_2	Th_{min}	H_c
LC	11.4	4.06
VR	3.83	4.87

C

k_1	Th_{min}	H_c
LC	0.95	0.83
VR	0.29	0.33

Table 3.2 (A-C) The comparison of the parameters of modelling 2D scaling factors between subjects LC and VR

In Table 3.3 were summarised the R^2s of superimposing threshold data by spatial scaling and 2D scaling.

	Spatial scaling		**2D scaling**	
	LC	**VR**	**LC**	**VR**
R^2	0.82	0.61	0.89	0.84

Table 3.3 The comparison of R^2 between spatial and 2D scaling

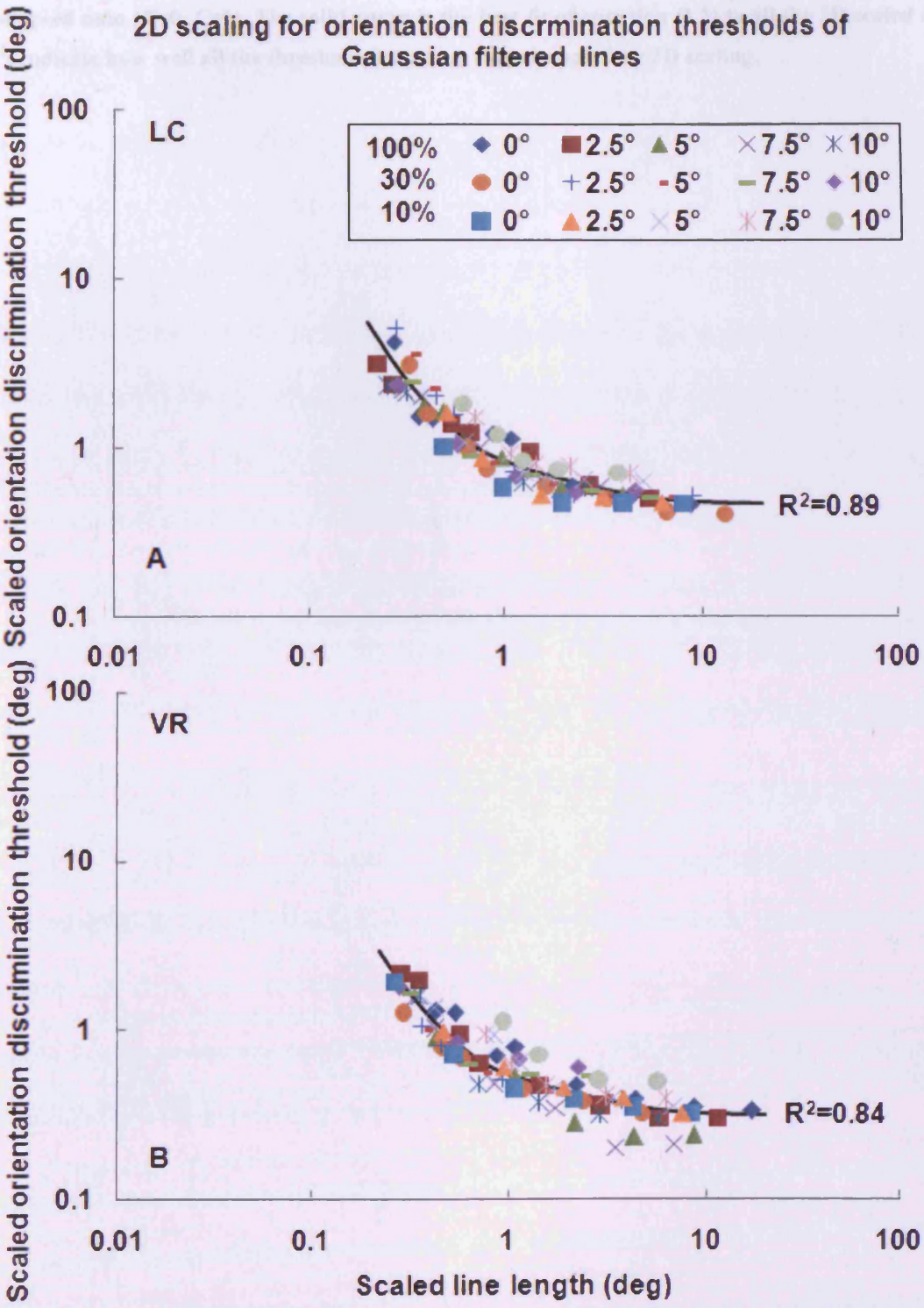

Fig 3.8 The 2D scaled orientation discrimination thresholds for the Gaussian filtered lines

The original orientation discrimination thresholds in Fig 3.5 (A-B) were both horizontally and vertically scaled by using the modelled vertical and horizontal scaling surfaces in Fig 3.7 (C, D, G, H) for subjects LC and VR, respectively. Data from the 0-10 deg eccentricities and 10-100% contrasts

collapsed onto (E=0, C=1). The solid curve is the best fit of equation (3.2) to all the 2D scaled data. The R^2s indicate how well all the threshold data were superimposed by 2D scaling.

3.3.3 Spatial scaling at individual contrast

The performance of spatial scaling of superimposing the threshold data across contrasts (10-100%) were not ideal according to the low R^2 (0.61, see Table 3.3) for subject VR. By observing the superimposition of the scaled threshold data shown in Fig 3.6, the poor R^2 was mainly caused by the considerable vertical offsets of the scaled data across contrasts. Therefore, even though all the horizontal offsets could be made up by more or less horizontal shifts, i.e. spatial scaling, those vertical offsets would still exist and degrade the spatial scaling performance. If the vertical offset of the threshold data was mainly caused by that the data were obtained at different contrasts, spatial scaling should be able to superimpose the data only from the same contrast. Thus, in this section, spatial scaling was conducted separately at individual contrast so that the peripheral threshold performance was equated to that of the fovea from the same contrast level.

As shown in Fig 3.9, at each contrast, a preliminary spatial scaling factor was obtained at each eccentricity through the spatial scaling procedure previously described in Chapter 1 Section 1.3. Then these scaling factors at each contrast were fitted through (0, 1) against eccentricity by an optimal linear function with the corresponding best fit R^2, shown in each sub graph. Final spatial scaling factors were determined by these linear functions.

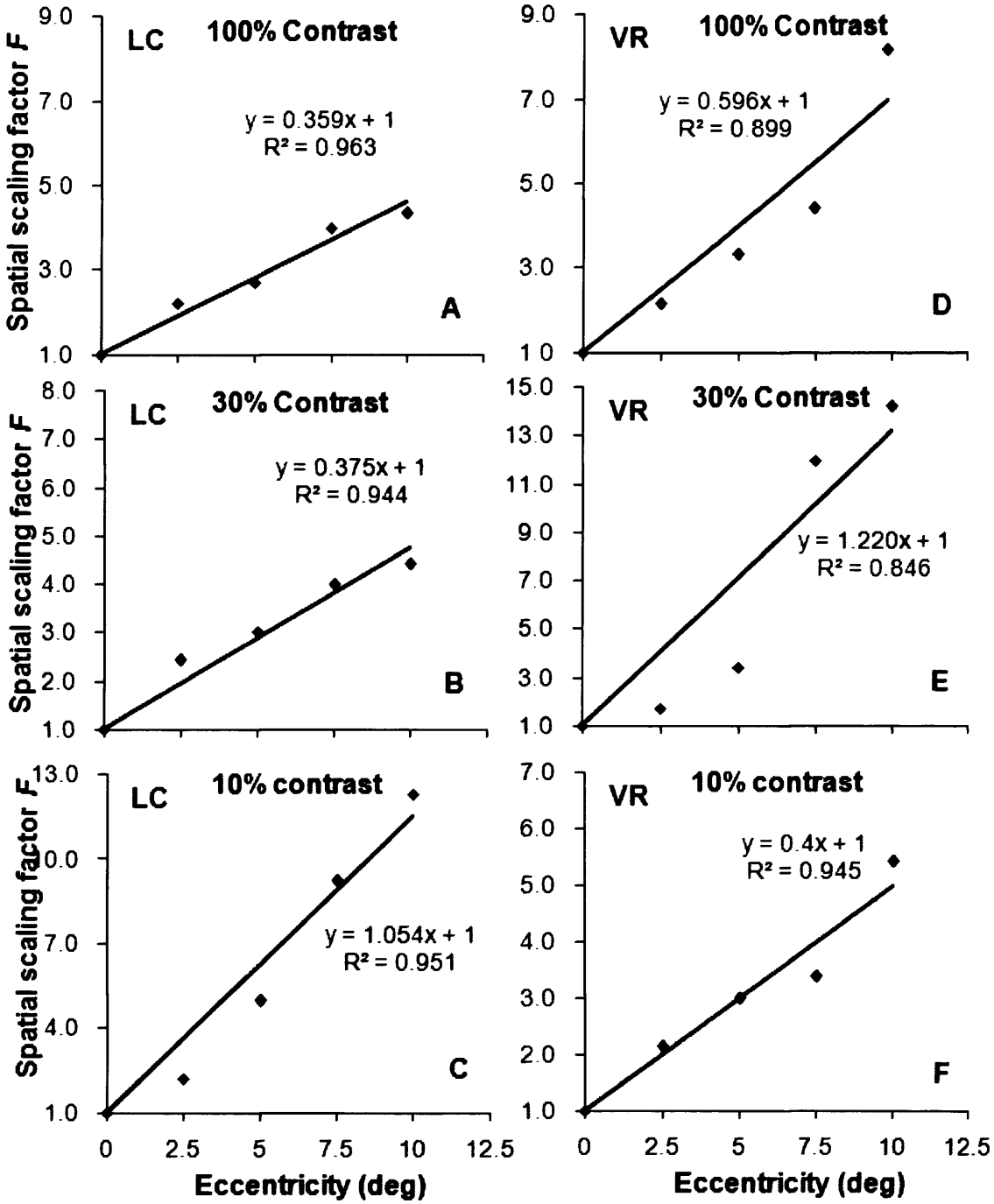

Fig 3.9 (A-F) Spatial scaling factors as a function of eccentricity at each contrast

At each eccentricity and contrast, a preliminary spatial scaling factor (■) was obtained through the spatial scaling procedure previously described in Chapter 1 Section 1.3. At each contrast, the scaling factors were fitted through (0, 1) by an optimal linear function with its best fit R^2, shown in each graphs. Subjects LC and VR are as indicated.

The spatial E_{2c} at each contrast was calculated as the inverse of the slope of the corresponding linear function of Fig 3.9 and shown in Table 3.4.

Table 3.4 Spatial E_{2c} at each contrast

E_{2c}	LC	VR	Average
100%	2.79	1.68	2.23
30%	2.70	0.82	1.76
10%	0.95	2.50	1.72

Further, to show how E_{2c} changes with contrast more clearly, the E_{2c} of each subject and its average between subjects were plotted as a function of contrast in Fig 3.10.

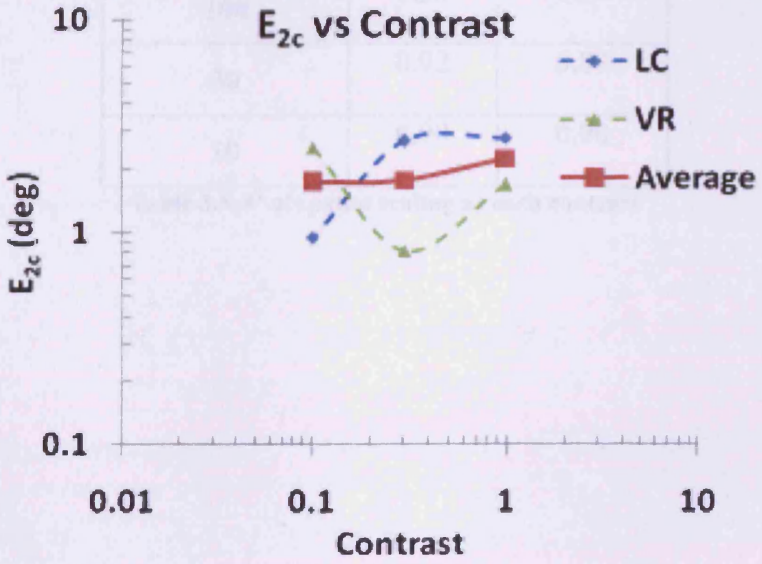

Fig 3.10 Spatial E_{2c} plotted as a function of contrast for subjects LC and VR.

The blue dash smooth curve is the function of E_{2c} vs. contrast for subject LC. The green one is for VR. The average E_{2c} between subjects is plotted against contrast with the red solid smooth curve.

The orientation discrimination threshold data at each contrast (see Fig 3.3) were shifted horizontally by the final spatial scaling factors and shown in Fig 3.11. The eccentric data

was superimposed on to its corresponding fovea curve at each contrast. The R^2 of the best fit to each superimposed threshold set by equation (3.6) was calculated and displayed in each sub-figure. Data collapsed well onto the foveal function at each contrast, shown by the high R^2 values (see Table 3.5).

$$Th = Th_{\min}(1 + H_c / H)^p \qquad \textbf{Equation 3.6}$$

Contrast %	R^2	
	LC	VR
100	0.93	0.97
30	0.92	0.87
10	0.90	0.90

Table 3.5 R^2 of spatial scaling at each contrast

Fig 3.11 Spatial scaling of orientation discrimination threshold at each contrast

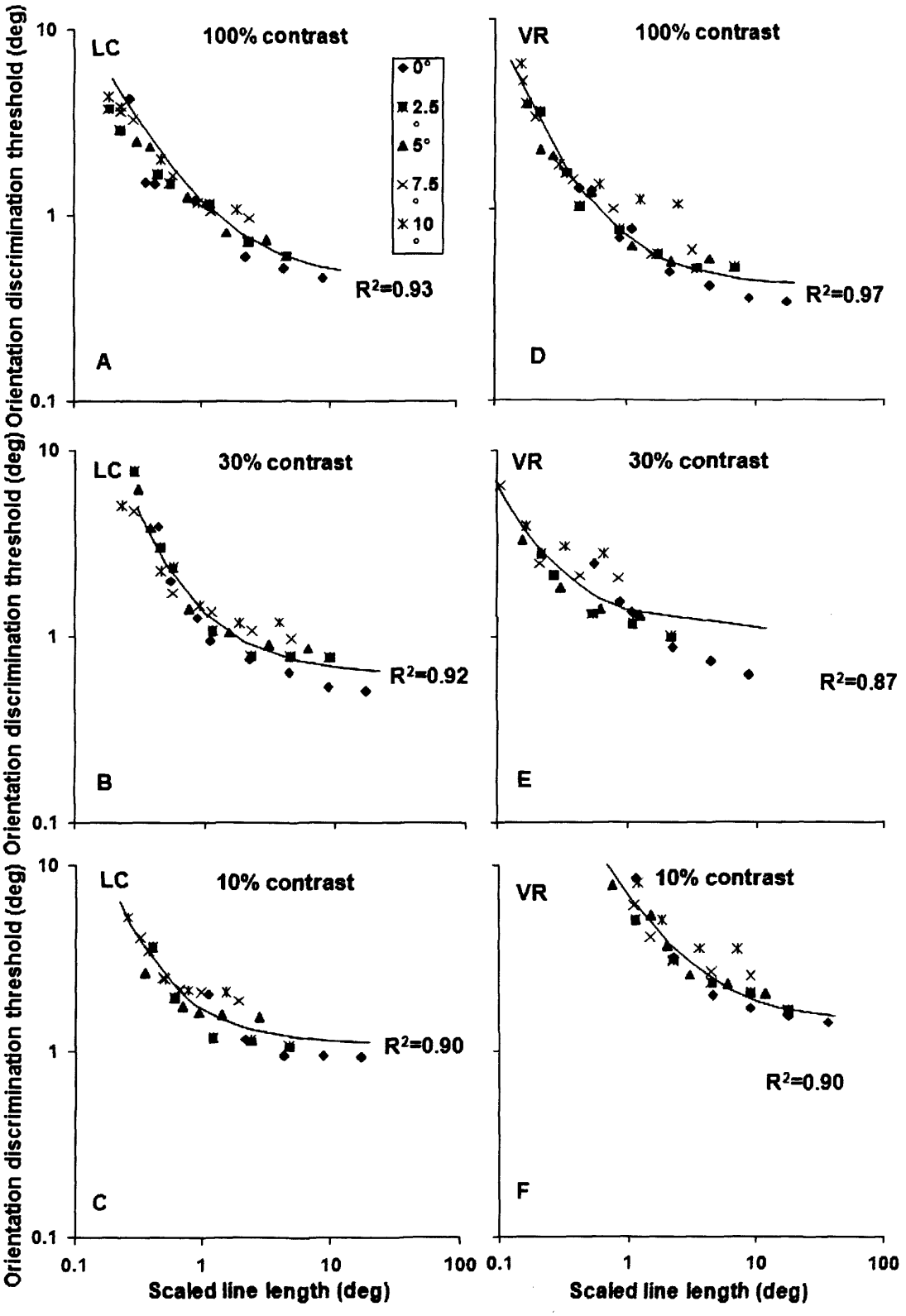

At each contrast, the eccentric orientation discrimination threshold curves at each contrast (shown in Fig 3.3) were horizontally shifted to superimpose onto each fovea curve by spatial scaling factors calculated by using the corresponding linear functions in Fig 3.9. The smooth curve was the best fit to each superimposed threshold set at each contrast by equation (3.6). Data collapsed well onto the foveal function at each contrast, indicating by the high R^2 values.

3.4 Discussion

The analyses of the experimental threshold data show that orientation discrimination performance can be quantitatively described, across the visual field (0-10 deg eccentricity) and across contrasts (10-100%), by both spatial and 2D scaling (see Figs 3.6 and 3.8). However, the great vertical offset of the experimental data distribution resulted in the poor superimposition of the data shifted by spatial scaling for subject VR (see Fig 3.6B).

The foveal thresholds at 100% contrast were found 17.3 sec arc for LC and 17.9 sec arc for VR. Both are within the range of hyperacuity (Westheimer 1981). When expressed in terms of the rotation angle of orientation, the foveal threshold was found to be 0.58 deg for LC and 0.5 deg for VR at 100% contrast. The values are almost identical to (i) 0.5 deg of Makela *et al.* (1993) using a sharp-edged white line at the maximum contrast available, (ii) 0.6 deg of Westheimer *et al.* (1999) using a straight edge between the upper and lower halves of the disk at 100% contrast, and (iii) 0.56 deg of Sally and Gurnsey (2003) using broadband and narrowband line stimuli at contrasts of 51% and 62%, respectively.

According to the R^2 values, all the orientation discrimination threshold curves shown as a function of line length (H) were accurately described with equation (3.2) $Th = Th_{\min}(1 + H_c / H)^5$ irrespective of eccentricity or contrast for both subjects LC and VR. This is consistent with the equation of $Th = \theta_{\min}(1 + L_{crit} / x)^n$ used in Sally and Gurnsey (2003, 2004). The theoretical minimum threshold Th_{min} shown in Fig 3.4 (A-D) was found to increase as contrast decreased, again in agreement with Sally and Gurnsey

(2007).

The spatial scaling factors were modelled as a function of eccentricity and contrast with equation (3.4). In the equation, there was an interaction between eccentricity and contrast, in agreement with Melmoth and Rovamo (2003) who reported the interaction in modelling recognition contrast sensitivities of Times New Roman letters. However, this finding is different from Melmoth *et al.* (2000a) who modelled contrast sensitivity of face recognition.

For 2D scaling, both the vertical and horizontal scaling factors (i.e. normalised Th_{min} and H_c) were modelled as a function of eccentricity and contrast with equation (3.5). According to the equation, there was no interaction between eccentricity and contrast in modelling. It is different from the previous findings for modelling the spatial scaling factor previously.

3.4.1 Global spatial E_2 across contrasts

A spatial scaling E_2 exists at 100% contrast according to equation (3.4). As shown in Fig 3.4 and Table 3.1 (A), E_2 are similar between subjects: 3.21 deg for LC and 5.61 deg for VR with an average 4.41 deg, which is more similar to 3.2 deg reported for the narrowband line stimuli at contrast of 62% than to 2.36 deg reported for the broadband line stimuli at contrast of 51% by Sally and Gurnsey in 2003.

According to equation (3.4), $F_s = 1 + E/E_2 + (\log C)^2/k_1 + E \times \log C/k_3$, the effect of

contrast on E_2 is rather complicated due to the interaction term, i.e. Exlog$C$.

3.4.2 Spatial E_{2c} in individual contrast C

It is difficult to summarise how spatial E_{2c} changes with contrast due to the irregular distribution of the E_{2c} as a function contrast, as shown in Fig 3.10 (see the blue and green dash curves). However, averaged between subjects, E_{2c} shows an independency against contrast (see the solid red curves). The average E_{2c}s are about 2 deg, ranging from 1.72 to 2.23 (see Table 3.4), which are similar to the findings in literature (e.g. 1.93 deg by Makela *et al.*1993).

The finding of E_{2c} being independent of contrast (10-100%) is different from the previous findings by Sally and Gurnsey (2003, 2004 and 2007). In 2003 and 2004, they measured orientation discrimination threshold at the suprathreshold and near-detection contrast using a line stimulus and found that E_2 was greater at lower contrast. In 2007, they measured orientation discrimination threshold of lines stimuli at contrasts of 3-48% and also found that E_2 decreased with increasing contrast. However, it was noted that their conclusion "is based on very limited data" (which were measured at less eccentricities or less contrasts.).

The independency of E_{2c} found in this chapter shows that the contrast reduction has no considerably stronger effect on the fovea than the periphery. More discussion about how contrasts affect E_2 continues in Chapters 5 and 9.

Chapter 4 The effects of eccentricity and contrast on orientation discrimination for a 4 cycles per image grating

4.1 Introduction

Gratings are commonly used for investigating how contrast and size influence orientation perception at various visual field locations (Betts, Sekuler and Bennett 2007; Browne 1990; Burr and Wijesundra 1991; Mareschal and Shapley 2004; Nasanen, Kukkonen and Rovamo 1993; Regan and Beverley 1985; Reisbeck and Gegenfurtner 1998; Spinelli, Bazzeo and Vicario 1984).

Spinelli *et al.* (1984) conducted both orientation setting and matching experiments to investigate orientation sensitivity in the peripheral visual field using sinusoidal gratings at the eccentricities of 10, 20 and 30 deg. All the stimuli were presented against a dark background with a luminance of 30 cd/m^2 and were viewed at a contrast of 40%. In the orientation setting experiments, two occurrences of subject had to set the orientation horizontal when a 1 cpd (3 deg in visual angle) titled grating was presented at the eccentricity measured. The orientation sensitivity was found to linearly decrease with increasing eccentricity. In the orientation matching experiment, the subjects adjusted the orientation of a peripherally presented grating to be equal to a reference grating presented at the fovea. The reference grating was 3.5 cpd, subtended 3 deg in visual angle and tilted at 45 deg from the horizontal. The target grating stimuli were 1-12 times magnified versions of the reference grating. They found that peripheral performance increased and reach a plateau as the magnification increased

Regan and Beverley (1985) used a 12 cpd grating to measure orientation discrimination threshold and found that the thresholds were nearly independent of contrasts from 20 to 60%.

Bowne (1990) investigated the effect of contrast on foveal orientation discrimination using a 4 cpd sinusoidal grating extending 6 x 5 deg of visual angle. Contrasts range was 0.02-0.5. The background luminance was 18 cd/m^2. The orientation discrimination threshold was about 0.7 deg and was nearly independent of contrast.

Burr and Wijesundra (1991) examined the effect of spatial frequency on orientation discrimination. The stimulus was a 4 cycles per image (4cpi) sinusoidal grating presented against a mean background luminance of 12 cd/m^2. The viewing distance ranged from 9 to 57 cm to obtain stimuli of different spatial frequencies. Burr and Wijesundra first measured contrast detection threshold of the grating stimulus at different spatial frequencies. Then orientation discrimination threshold was measured as a function of spatial frequency using stimulus contrast of 3 and 10 times of contrast detection threshold. The study found that orientation discrimination threshold decreased and reached to an asymptote with increasing spatial frequency at both contrasts.

Nasanen *et al.* (1993) measured orientation discrimination threshold by using sinusoidal gratings of 1 to 8 cpd within circular frames of various sizes at contrast levels of 0, 0.1, 0.2, 0.4, and 0.8. They found that as contrasts decreased orientation discrimination performance was degraded less for large than that of small gratings.

Reisbeck and Gegenfurtner (1998) conducted an orientation discrimination experiment by using 1 cpd sinusoidal gratings. The mean luminance of the background was 26.3 cd/m^2. Threshold was estimated as a function of stimulus contrast and was found to first decrease and then saturate with increasing stimulus contrast.

Mareschal and Shapley (2004) measured orientation discrimination thresholds as a function of stimulus contrast, spatial frequency, and area at the fovea and 5 deg eccentricity. The stimulus was a circular sinusoidal grating where spatial frequency was 3 cpd for stimulus sizes of 2, 1 and 0.5 deg; 6 cpd for stimulus size of 0.25 deg; and 12 cpd for stimulus size of 0.12 deg. They found that (i) at both locations orientation discrimination thresholds were basically independent of stimulus area at a very high contrast; (ii) thresholds increased and approached a plateau as contrast and area were decreased.

Betts *et al.* (2007) measured orientation discrimination threshold for 1.5 cpd Gabor patches subtending 2.3 deg. The mean luminance of the background was 61.2 cd/m^2. Threshold was measured at a function of contrast which ranged from 0.05 to 0.80 and was found to decrease and asymptote with increasing contrast.

The previous studies have used variable grating sizes, background luminance and stimulus arrangements. Comparisons between studies are difficult and combining information from them is not very fruitful.

Therefore, to thoroughly examine how contrast and eccentricity affects orientation discrimination for grating stimuli, orientation discrimination was studied in this chapter using 4cpi sinusoidal grating stimuli of different sizes at various contrasts, (100, 30 and

10%) and visual field locations (fovea and eccentricities of 2.5, 5, 7.5, and 10 deg). The aims were to found out (i) whether spatial scaling can equate the threshold performance across contrasts and within a contrast, (ii) by comparing E_2s obtained at different contrasts, the effect of contrast reduction on spatial scaling and spatial summation at different locations of visual field were examined.

4.2 Methods

4.2.1 Apparatus

Stimuli were presented on the monitor previously described in Chapter 2. For details see Section 2.2.

4.2.2 Stimuli

A vertical sinusoidal grating and a series of counter-clockwise orientated gratings with varying amounts of tilt (between 0.0005-89 deg from the vertical) in a circular frame were created at 100, 30 and 10% contrast (see Fig 4.1.) using the software developed by Dr Risto Nasanen (for details see Chapter 2). The circular gratings were magnified versions of each other and diameters ranged 10-160 mm. Each stimulus contained 4 grating cycles, i.e. 4cpi.

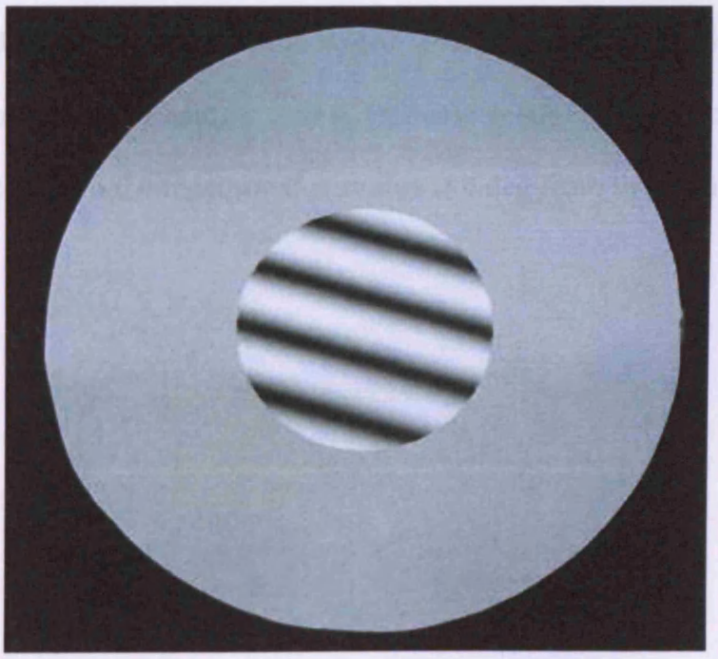

Fig 4.1 An example of a 4cpi grating used in the orientation discrimination experiments

4.2.3 Subjects

Two highly trained subjects, LC and AS (aged 26 and 21 years, respectively), took part in the experiment. Both subjects were fully corrected moderate myopes (see Appendix I for the details of the subjects).

4.2.4 Procedure

The procedure has been explained in detail in Chapter 3. Two grating stimuli of the same contrast level were presented successively in two intervals. One was vertical and the other was tilted counter-clockwise from the vertical at an angle between 0-89 deg. The viewing distances used were 57, 114, 171, 228, 285, 456 cm, producing grating diameters of 0.126-15.8 deg of visual angle. The smallest one (0.126 deg) was achieved by presenting a 10 mm in diameter grating at the furthest viewing distance of 456 cm. Subjects indicated which interval contained the more counter-clockwise tilted grating. Orientation discrimination thresholds were measured by using a 2AFC staircase method explained in Chapter 2. The measurement started from the most tilted stimulus (89 deg from the vertical).

4.3 Results

This section presents the results and corresponding data analysis of orientation discrimination for a 4cpi grating stimulus. The structure of the section is the same as that of Section 3.3.

Fig 4.2 shows orientation discrimination spatial offset thresholds (θ in Fig 1.16), expressed in sec arc in the visual field, plotted against the stimulus size in min arc of diameter of the circular grating at contrasts of 100, 30 and 10%, and eccentricities of 0, 2.5, 5, 7.5 and 10 deg for subjects LC and AS.

Fig 4.2 Orientation discrimination offset thresholds (sec arc) of the 4cpi gratings

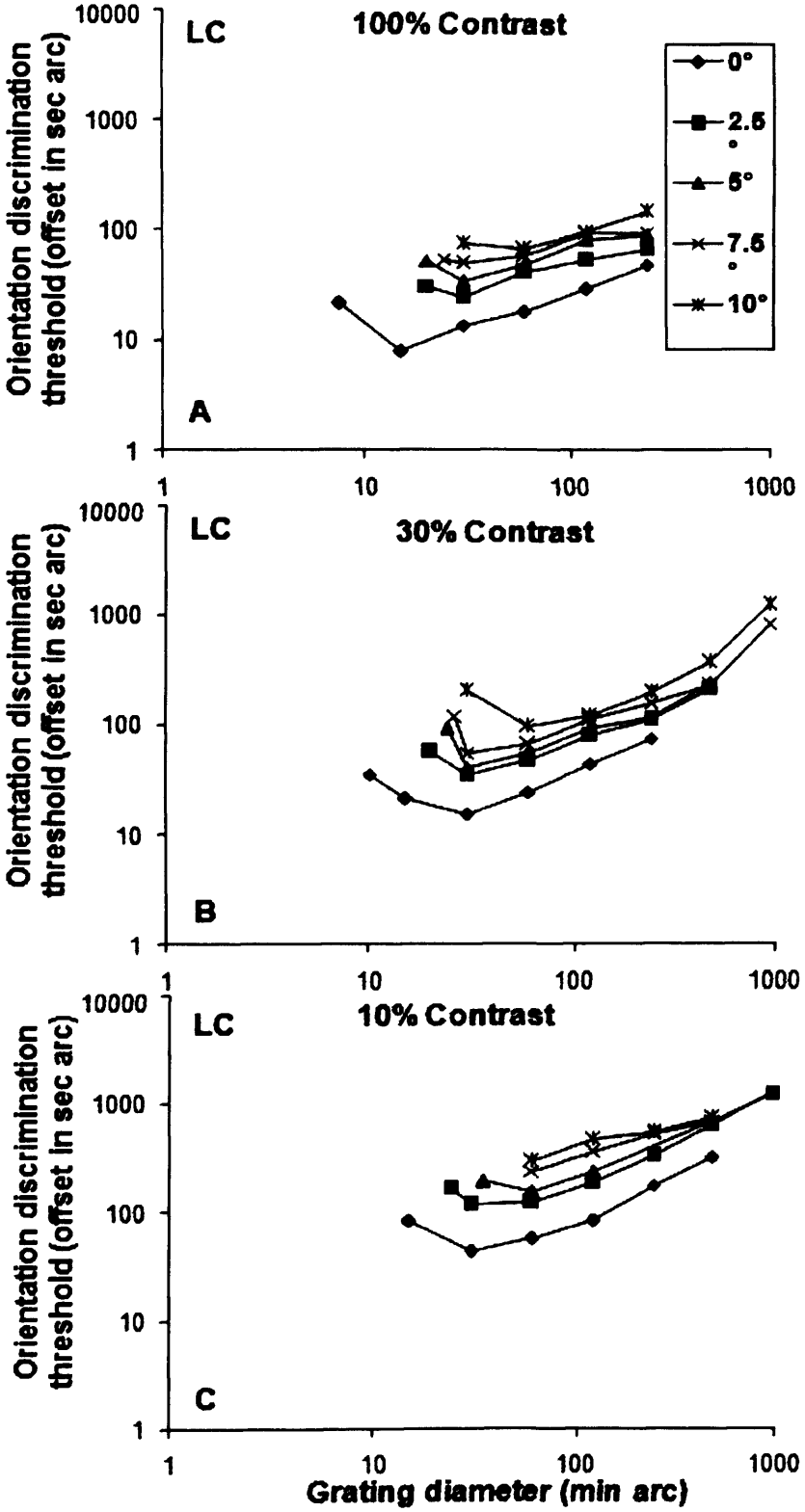

Fig 4.2 (A-C) Orientation discrimination spatial offset thresholds (sec arc) of the 4 cpi gratings were plotted against grating diameter (min arc) at eccentricities of 0, 2.5, 5, 7.5, and 10 deg, and contrasts of 100, 30, and 10% for subject LC.

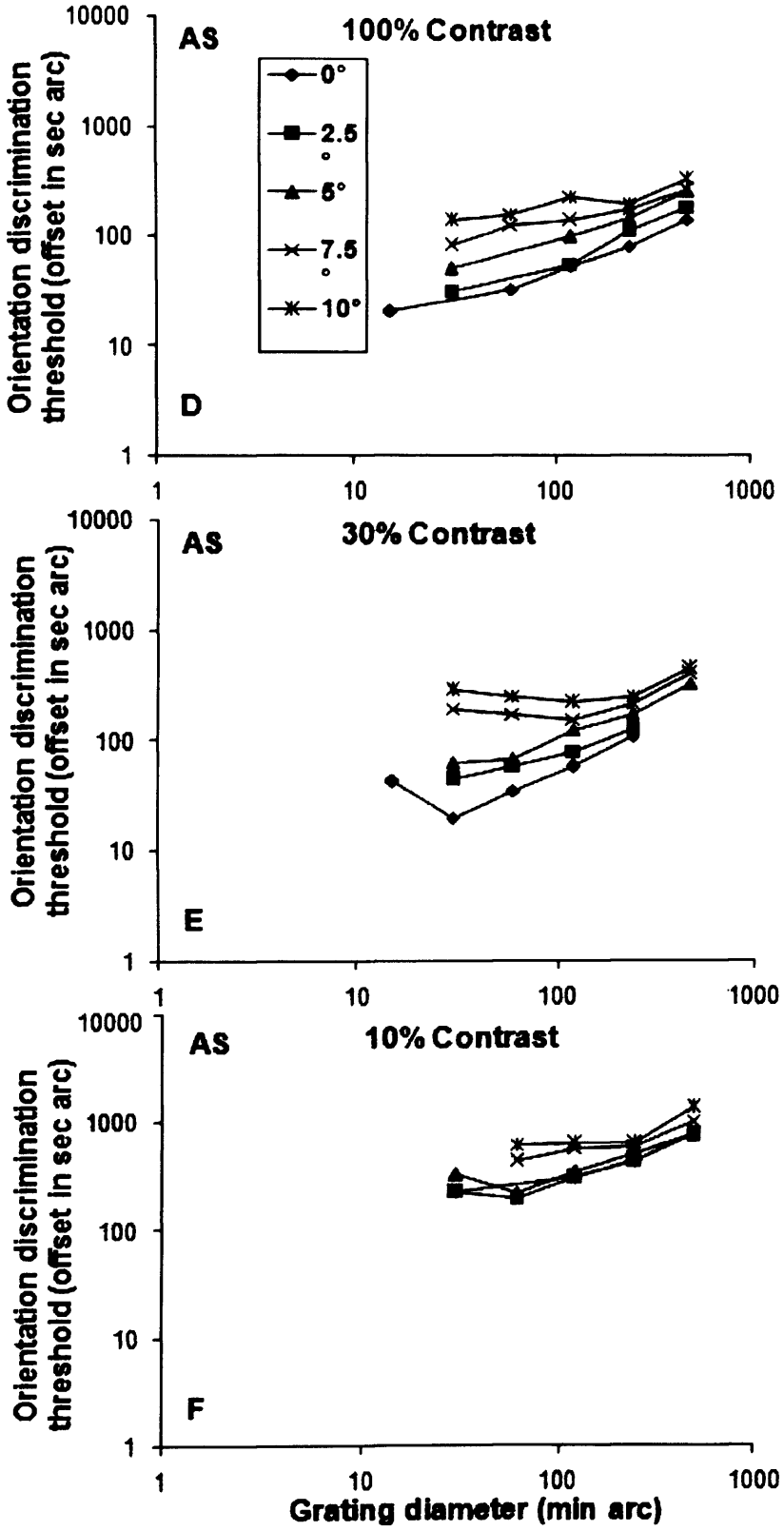

Fig 4.2 (D-F) Orientation discrimination spatial offset thresholds for the 4cpi gratings were plotted against grating diameter (min arc) for subject AS. Other details are as in Fig 4.2 (A-C).

The resulting curves tend to be u-shaped showing an optimal grating diameter for each eccentricity and contrast level. The optimal diameter generally increases with increasing eccentricity and decreasing contrast.

Fig 4.3 shows the orientation discrimination angular thresholds (*a* in Fig 1.15), *i.e.*, the angle (deg) between stimuli, plotted as a function of grating diameter expressed in deg in the visual field. Threshold first decreases and then reaches (or tends to reach) a plateau as grating diameter increases. At all eccentricities and contrasts studied, the shapes of the data curves were similar. Threshold functions appear to move rightwards along the horizontal axis with increasing eccentricity and decreasing contrast.

The threshold data at each contrast and eccentricity were fitted with equation (4.1), which is identical to equation (3.2) in Chapter 3:

$$Th = Th_{\min}(1 + H_c / H)^5, \qquad \textbf{Equation 4.1}$$

where Th_{min} is the theoretical minimum threshold, H represents grating diameter and H_c is the critical grating diameter marking change from decrease to plateau. Th will always greater than Th_{min} because the bracket portion of the equation is always greater than one. R^2 was calculated for each data curve to reveal the accuracy of the fitting. R^2 values ranged from 0.88 to 0.99 with the average of 0.95 across eccentricities, contrasts and subjects (see Appendix V Table 6).

Fig 4.3 Orientation discrimination angular thresholds of the 4cpi gratings in deg

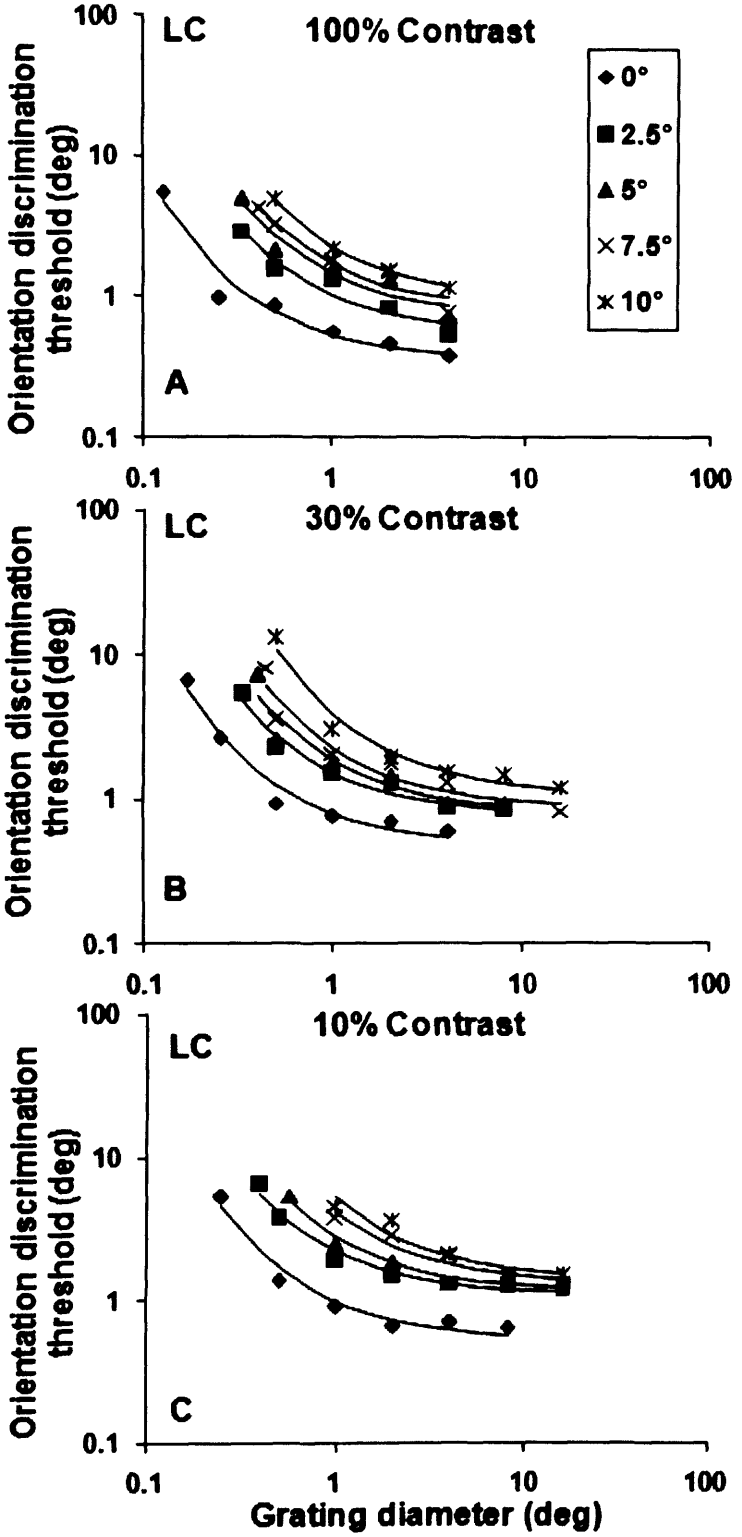

Fig 4.3 (A-C) The orientation discrimination angular thresholds in deg, i.e., the angle between grating stimuli, plotted as a function of grating diameter in deg of visual field for subject LC. Each eccentric data was fitted with equation (4.1) (solid line) to model the decrease and plateau in threshold with increasing grating diameter.

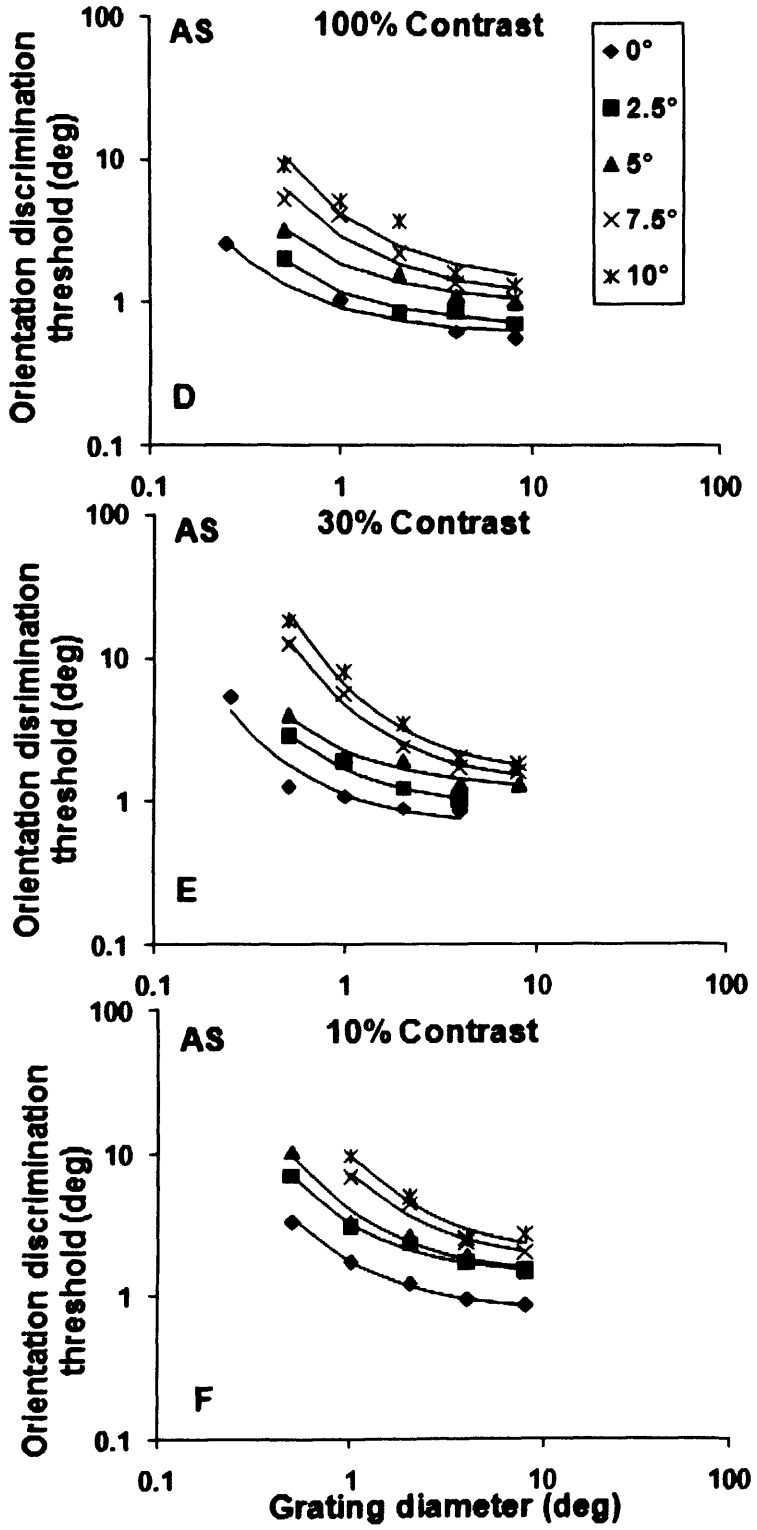

Fig 4.3 (D-F) The orientation discrimination angular thresholds in deg plotted against grating diameter (deg) for subject AS. Other details are as in Fig 4.3 (A-C).

4.3.1 Spatial scaling across contrasts

Spatial scaling was used to shift each eccentric data of the 4cpi gratings from different contrasts to superimpose onto the foveal orientation discrimination at 100% contrast (E=0, C=1). As in Chapter 3 Section 3.3.1, the spatial scaling factor at each eccentricity and contrast was obtained by the spatial scaling procedure explained in Chapter 1 Section 1.3.4. The factor had two independent variables, eccentricity E and contrast C, due to the fact that the spatial scaling was applied to the orientation discrimination threshold data across eccentricities and contrasts.

In Fig 4.4 (A, B), the spatial scaling factor was plotted against eccentricity and contrast for both subjects. It increases with increasing eccentricity and decreasing contrast. As in Chapter 3 Section 3.3.1, the scaling factor F_i was fitted with equation (4.2) to model its dependency on E and C. The equation is equivalent to equation (3.3) and included all the necessary 2nd order polynomial parameters involving E and C (see in Section 3.3.1 for further details of equation).

$$F_i = 1 + E/E_2 + (\log C)^2/k_1 + \log C/k_2 + E \times \log C/k_3 + E^2/E_2' \quad \text{Equation 4.2}$$

Constants k_2 and E'_2 were found to be either inaccurate or redundant on the basis of R^2s for the fitting (see Appendix III for the details of the procedure of selecting parameters). Thus, equation (4.2) was reduced to equation (4.3), which is the same as equation (3.4). Equation (3.4) was used to model the spatial scaling factor of the orientation discrimination threshold

of the Gaussian filtered lines in Chapter 3 Section 3.3.1:

$$F_s = 1 + E/E_2 + (\log C)^2/k_1 + E \times \log C/k_3, \qquad \textbf{Equation 4.3}$$

where F_s represent spatial scaling factor.

In Fig 4.4 (C, D), the scaling factor surfaces in Fig 4.4 (A, B) were modelled by using equation (4.3) to describe how the scaling factors changes with increasing eccentricity and decreasing contrast with respect of the basic condition (E=0, C=1). The resulting parameter and R^2 values of modelling the spatial scaling factors are listed in Table 4.1.

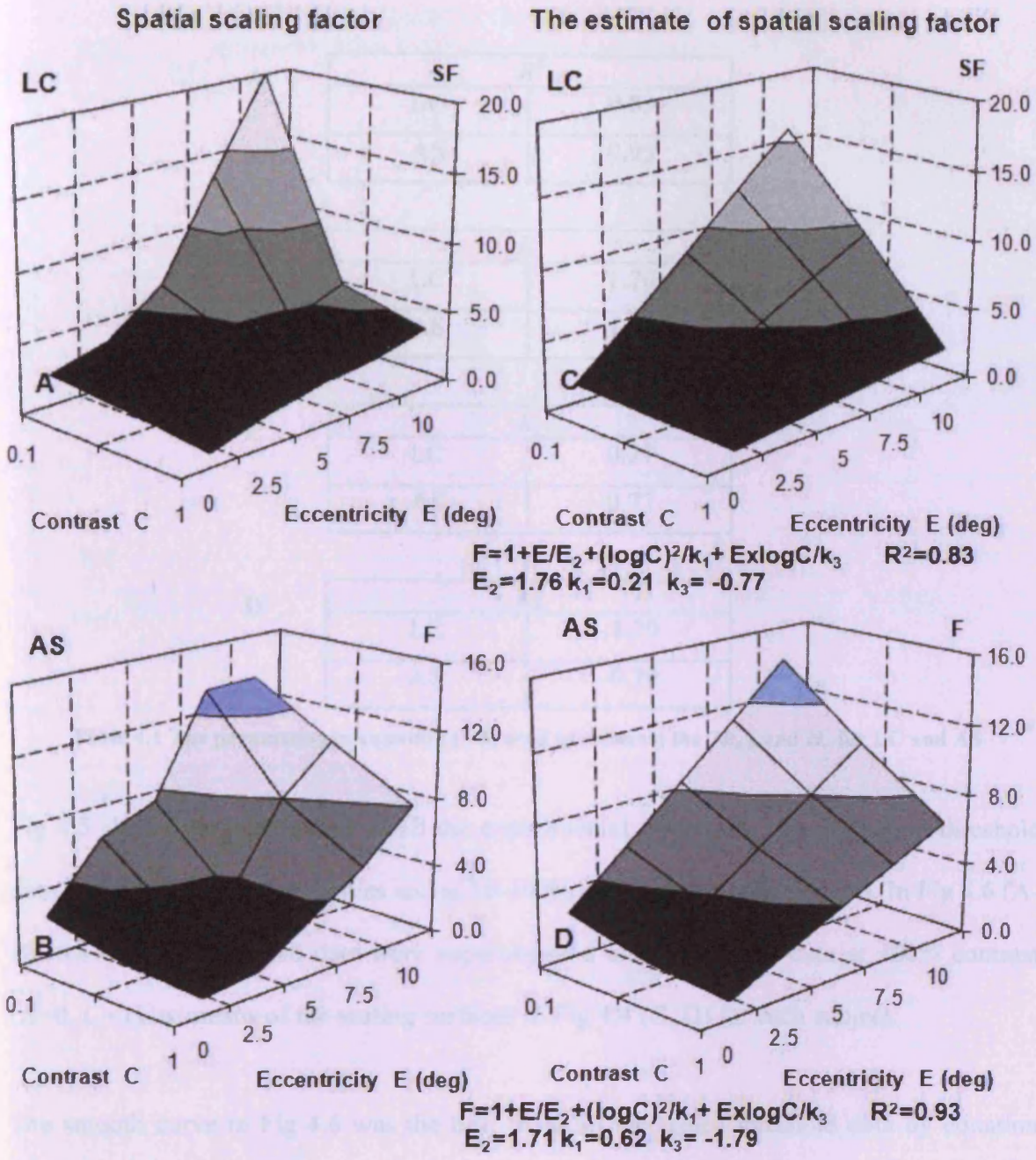

Fig 4.4 Empirical and modelled spatial scaling surfaces for the 4cpi grating

The empirical (left column) and modelled (right column) surfaces showing the spatial scaling factors required to quantify performance at any eccentricity (*E*) and contrast (*C*) relative to the basic condition of foveal 100% contrast data (*E*=0, *C*=1). The left-hand column (A-B) shows the empirical scaling surfaces separately for LC and AS, obtained from the spatial scaling procedure applied to shift the threshold data of Fig 4.3. The empirical surfaces were fitted with equation (4.3) which modelled the effects of eccentricity and contrast on the spatial scaling factor *F*. The modelled scaling surfaces are shown in the right-hand column (C-D) along with the values of their necessary parameters and R^2s.

A

	R^2
LC	0.83
AS	0.93

B

	E_2
LC	1.76
AS	1.71

C

	k_1
LC	0.21
AS	0.77

D

	k_3
LC	-1.79
AS	-0.79

Table 4.1 The parameters in equation (4.3) used to estimate the Th_{min} and H_c for LC and AS

Fig 4.5 shows the distribution of all the experimental orientation discrimination threshold data at the 0-10 deg eccentricities and at 10-100% contrasts for both subjects. In Fig 4.6 (A-B), the original threshold data were superimposed onto the foveal data at 100% contrast (E=0, C=1) by means of the scaling surfaces in Fig 4.4 (C, D) for each subject.

The smooth curve in Fig 4.6 was the best fit to all the scaled threshold data by equation (4.1). The R^2 of the curve to the superimposed data was 0.74 for LC and 0.82 for AS, which demonstrates how well the orientation discrimination performance in this task was equated by spatial scaling across eccentricities and contrasts.

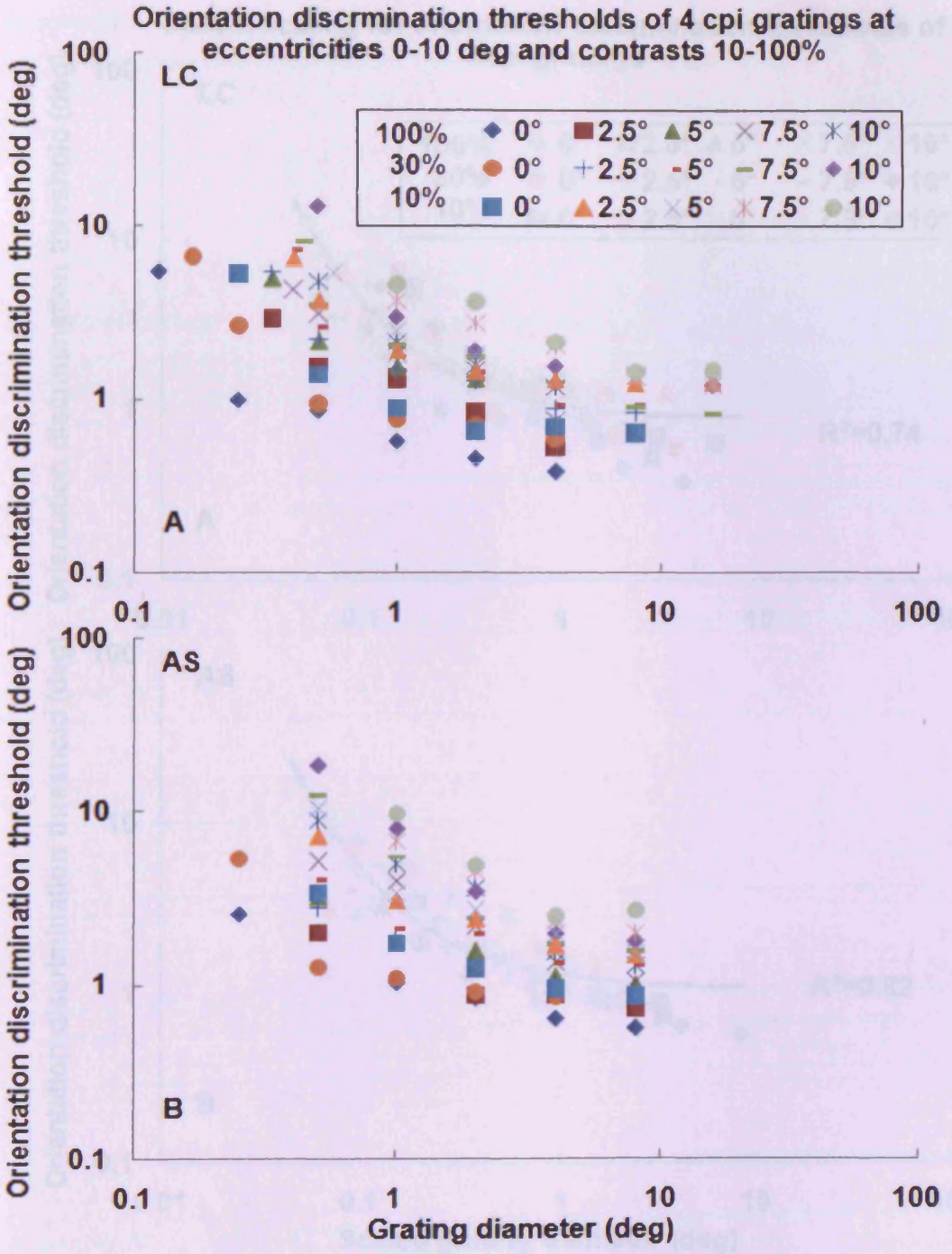

Fig 4.5 The original un-scaled orientation discrimination threshold of the 4cpi grating

The original threshold were plotted against grating diameter (deg) at the eccentricities of 0, 2.5, 5, 7.5 and 10 deg, and contrast of 10, 30 and 100% for subjects LC and AS.

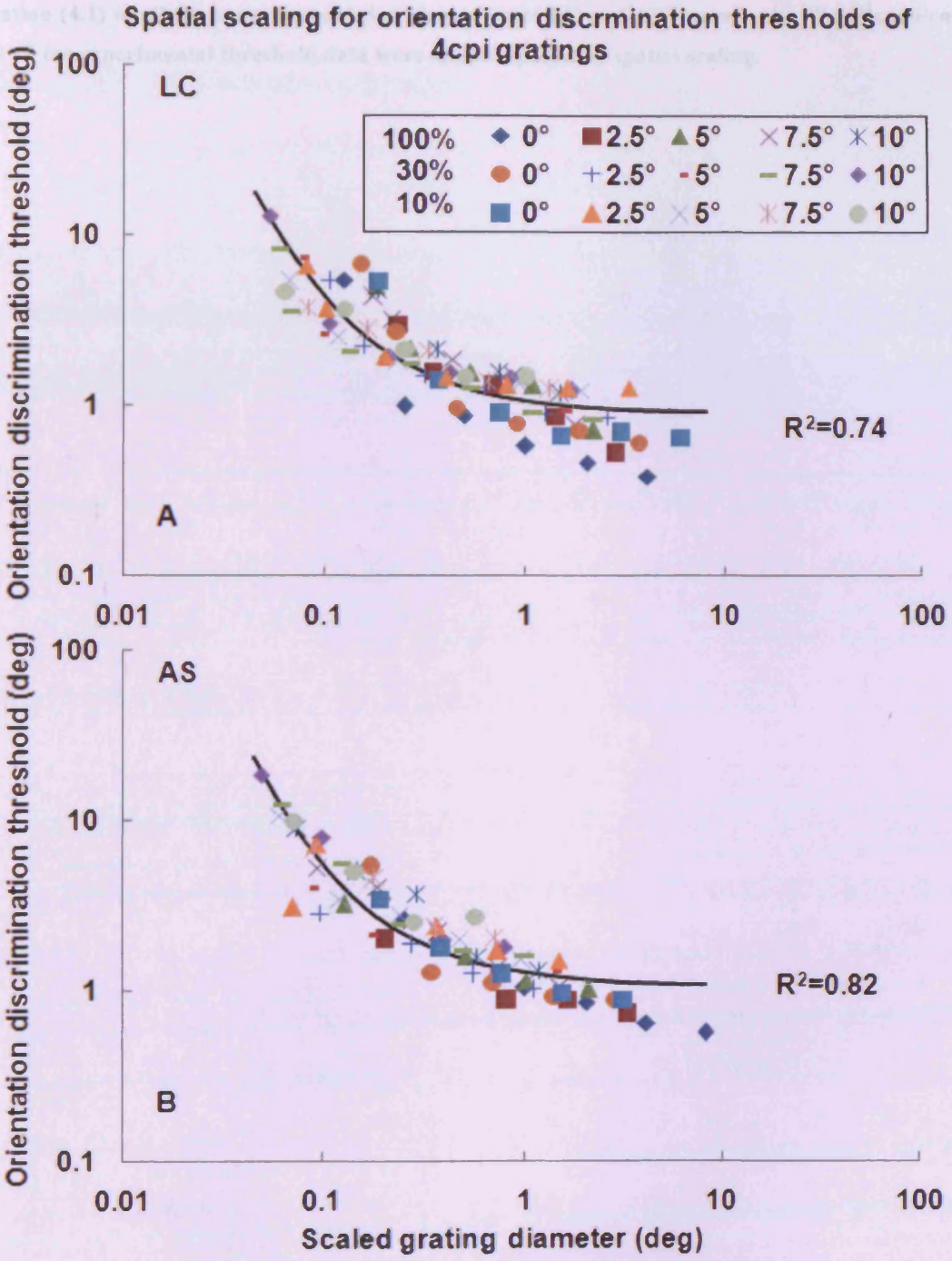

Fig 4.6 The scaled orientation discrimination thresholds of the 4cpi gratings by spatial scaling

The original orientation discrimination threshold data in Fig 4.5 (A-B) were scaled using the modelled spatial scaling surfaces in Fig 4.4 (C, D). Data from the eccentricities of 0-10 deg and contrasts of 10-100% collapsed onto the foveal and 100% contrast data (E=0, C=1). The solid curve is the best fit of

equation (4.1) to all the superimposed data for subjects LC and AS respectively. The R^2s indicate how well all the experimental threshold data were superimposed by spatial scaling.

4.3.2 2D scaling across contrasts

As in Chapter 3 Section 3.3.2, 2D scaling, the simultaneous vertical and horizontal scaling, was applied to scale all the threshold data across eccentricities and contrasts in this section. The foveal threshold data at 100% contrast (E=0, C=1) was chosen to be the basic condition as in Chapter 3.

The vertical and horizontal scaling factors, normalised Th_{min} and H_c, were separately calculated by dividing Th_{min} (E, C) by Th_{min} (E=0, C=1) and H_c (E, C) by H_c (E=0, C=1)} as in Chapter 3 Section 3.3.2. The normalised Th_{min} and H_c increase with decreasing contrast and increasing eccentricity, as shown in Fig 4.7 (A, B, E, F).

To model how the orientation discrimination performance changed with decreasing contrast and increasing eccentricity with respect of the foveal 100% contrast data (E=0, C=1), equation (4.2) was again used to estimate the 2D scaling factors, the normalised Th_{min} and H_c. Constants k_2, k_3 and E_2were discarded because they were found to be either redundant on the basis of R^2 or inaccurate for the fitting (see Appendix III for the procedure of obtaining parameters). Thus, equation (4.2) was reduced to equation (4.4), which was identical to equation (3.5) used to estimate the 2D scaling factors of the orientation discrimination threshold of Gaussian filtered lines in Chapter 3 Section 3.3.2.

$$F_i = 1 + E/E_2 + (\log C)^2/k_1 . \qquad \textbf{Equation 4.4}$$

Thus, the vertical and horizontal scaling factors, i.e., normalised Th_{min} and normalised H_c, were estimated using equation (4.4) in Fig 4.7 (C, D, G, H). The values of the R^2, E_2 and k_1 are listed in Table 4.2. The high R^2s (ranging from 0.87 to 0.94) show equation (4.4) accurately modelled the experimental 2D scaling surfaces in Fig 4.7(A, B, E, F).

Fig 4.7 Empirical & modelled 2D scaling surfaces of the 4cpi gratings

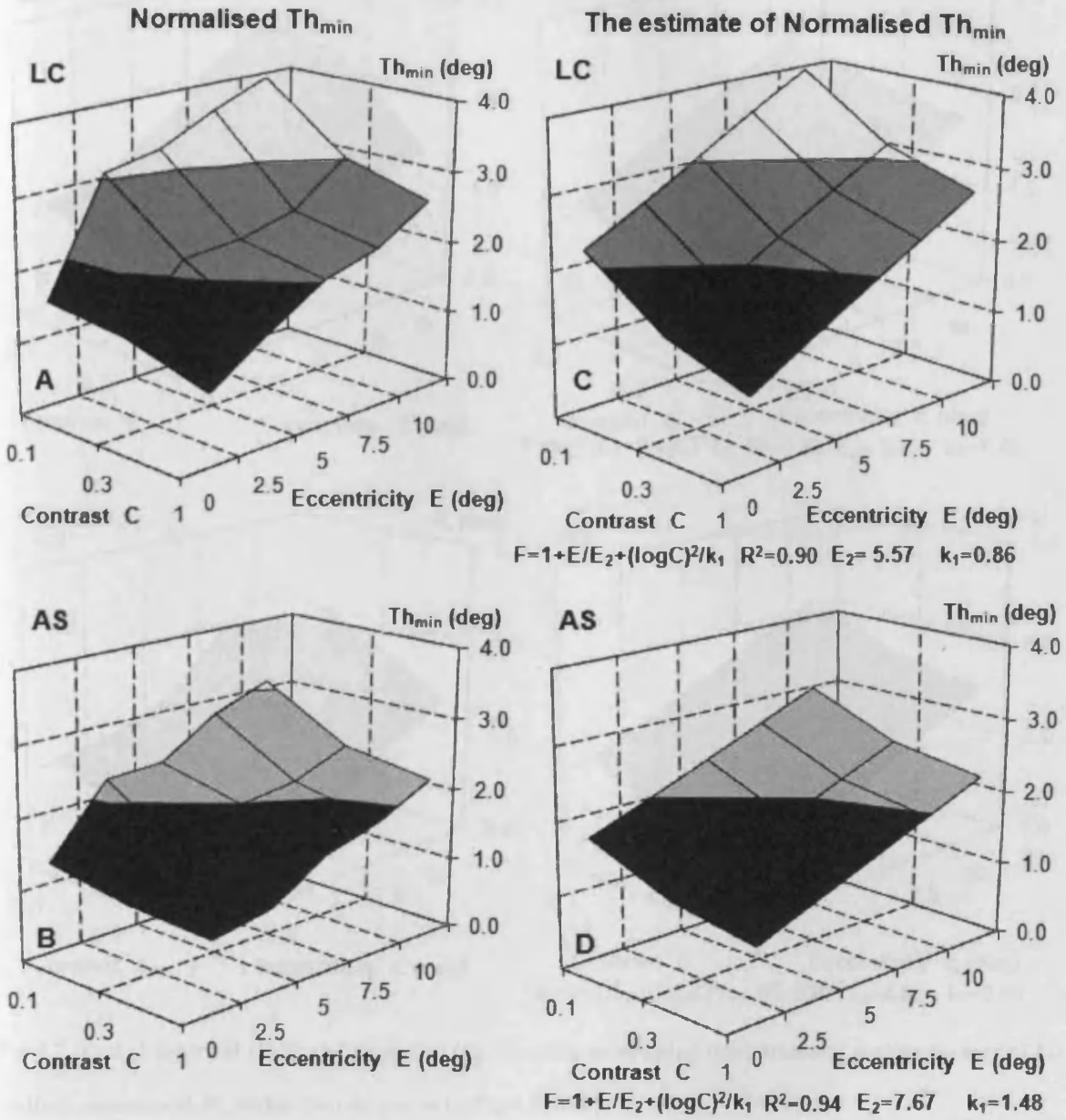

Fig 4.7 (A-D) The empirical (left column) and modelled (right column) surfaces showing the vertical scaling factors of 2D scaling, normalised Th_{min}, required to quantify performance at any eccentricity (E) and contrast (C) relative to the baseline condition (E=0, C=1). The left-hand column (A-B) shows the empirical scaling surfaces separately for subjects LC and AS, calculated from the data in Fig 4.3. The empirical surfaces were fitted with equation (4.4) which modelled the effects of eccentricity and contrast on normalised Th_{min}. The modelled scaling surfaces are shown in the right-hand column (C-D) along with the values of their necessary parameters and R^2s.

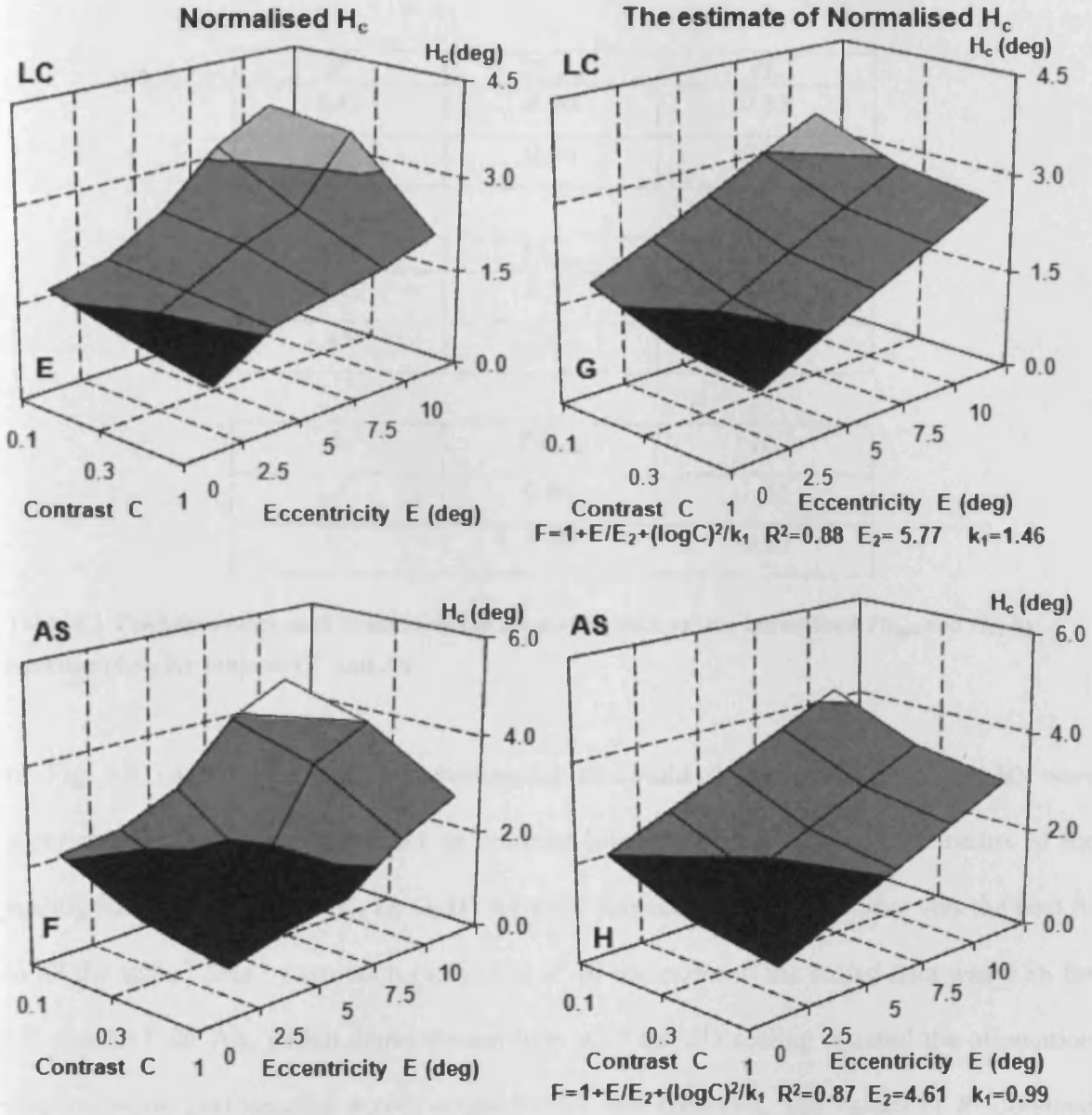

Fig 4.7 (E-H) Empirical (E-F) and modelled (G-H) surfaces showing the horizontal scaling factors of 2D scaling, normalised H_c. Other details are as in Fig 4.7(A-D).

A

R^2	Th_{min}	H_c
LC	0.90	0.88
AS	0.94	0.87

B

E_2	Th_{min}	H_c
LC	5.57	5.77
AS	7.67	4.61

C

k_1	Th_{min}	H_c
LC	0.86	1.46
AS	1.48	0.99

Table 4.2 The parameters used to estimate the 2D scaling factors (the normalised Th_{min} and H_c) by equation (4.4), for subjects LC and AS

In Fig 4.8 (A-B) the original experimental threshold data from Fig 4.5 (A-B) were superimposed onto the foveal data at contrast level 100% (E=0, C=1) by means of the scaling surfaces in Fig 4.7 (C, D, G, H) for each subject. The smooth curve was the best fit to all the scaled data by equation (4.1). The R^2 of the curve to the scaled data was 0.86 for LC and 0.91 for AS, which demonstrates how well the 2D scaling equated the orientation discrimination performance across eccentricities and contrasts. The values of R^2 obtained by spatial and 2D scaling were summarized in Table 4.3.

	Spatial scaling		2D scaling	
	LC	AS	LC	AS
R^2	0.74	0.82	0.86	0.91

Table 4.3 The comparison of R^2 between spatial and 2D scaling

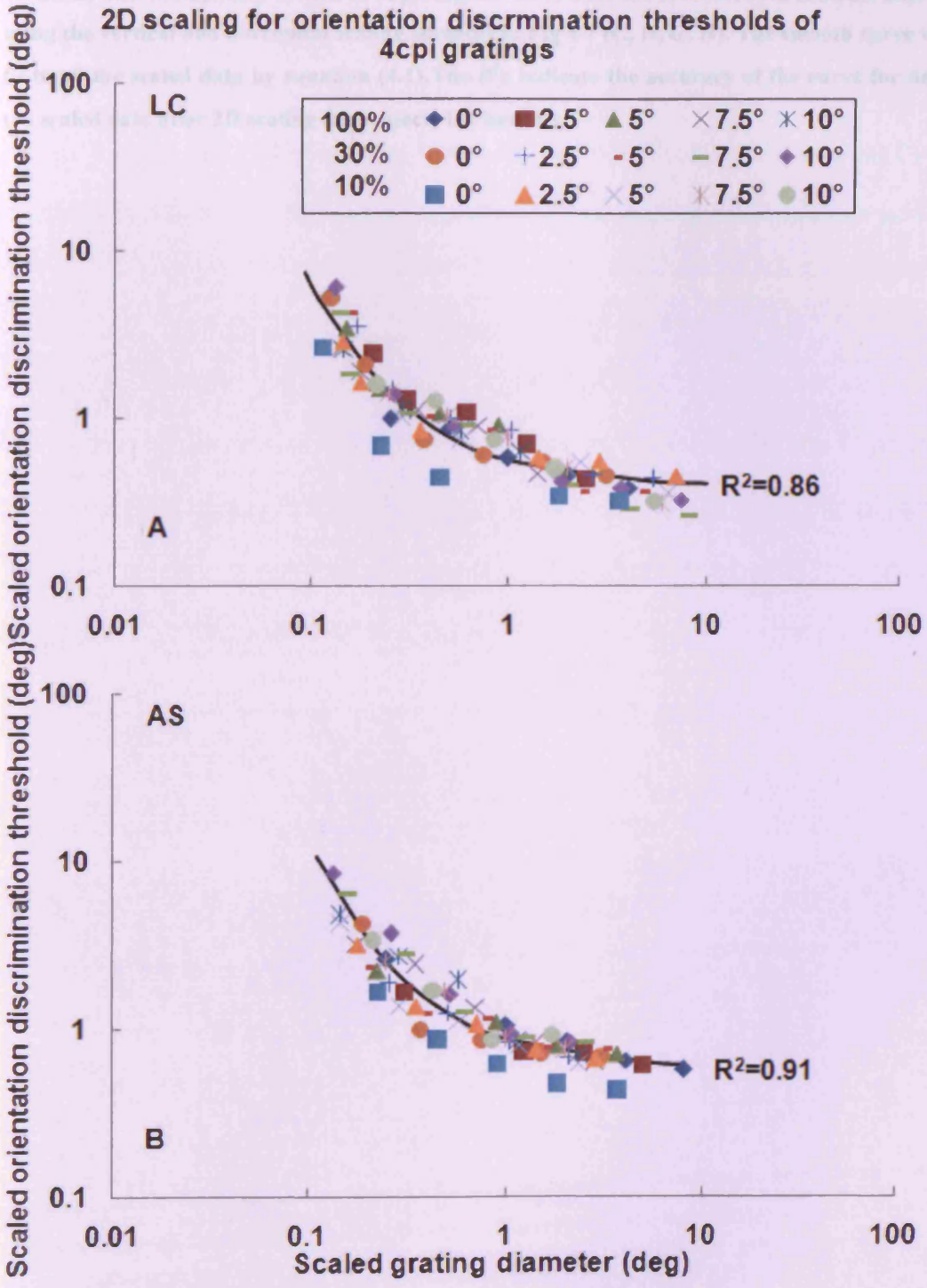

Fig 4.8 (A-B) The 2D scaled orientation discrimination thresholds for the 4cpi gratings

The original experimental orientation discrimination threshold data shown in Fig 4.5 (A-B) were both vertically and horizontally shifted to superimpose on to onto the fovea&100% contrast data (E=0, C=1) using the vertical and horizontal scaling surfaces in Fig 4.7 (C, D, G, H). The smooth curve was the best fit to all the scaled data by equation (4.1).The R^2s indicate the accuracy of the curve for describing all the scaled data after 2D scaling for subjects LC and AS.

4.3.3 Spatial scaling at individual contrast

In this section, spatial scaling was conducted at individual contrast so that the eccentric threshold curves at each contrast were shifted to superimpose onto the fovea curve from the same contrast level.

In Fig 4.9 are shown preliminary spatial scaling factors at each contrast level, which were obtained at each eccentricity through the procedure of spatial scaling (see Chapter 1 Section 1.3). An optimal linear function was fitted to these factors through (0, 1) at each contrast. The R^2 of the fit to the preliminary factors was calculated and displayed in each sub graph of Fig 4.9. The final spatial scaling factor at each eccentricity and contrast was calculated by the linear function.

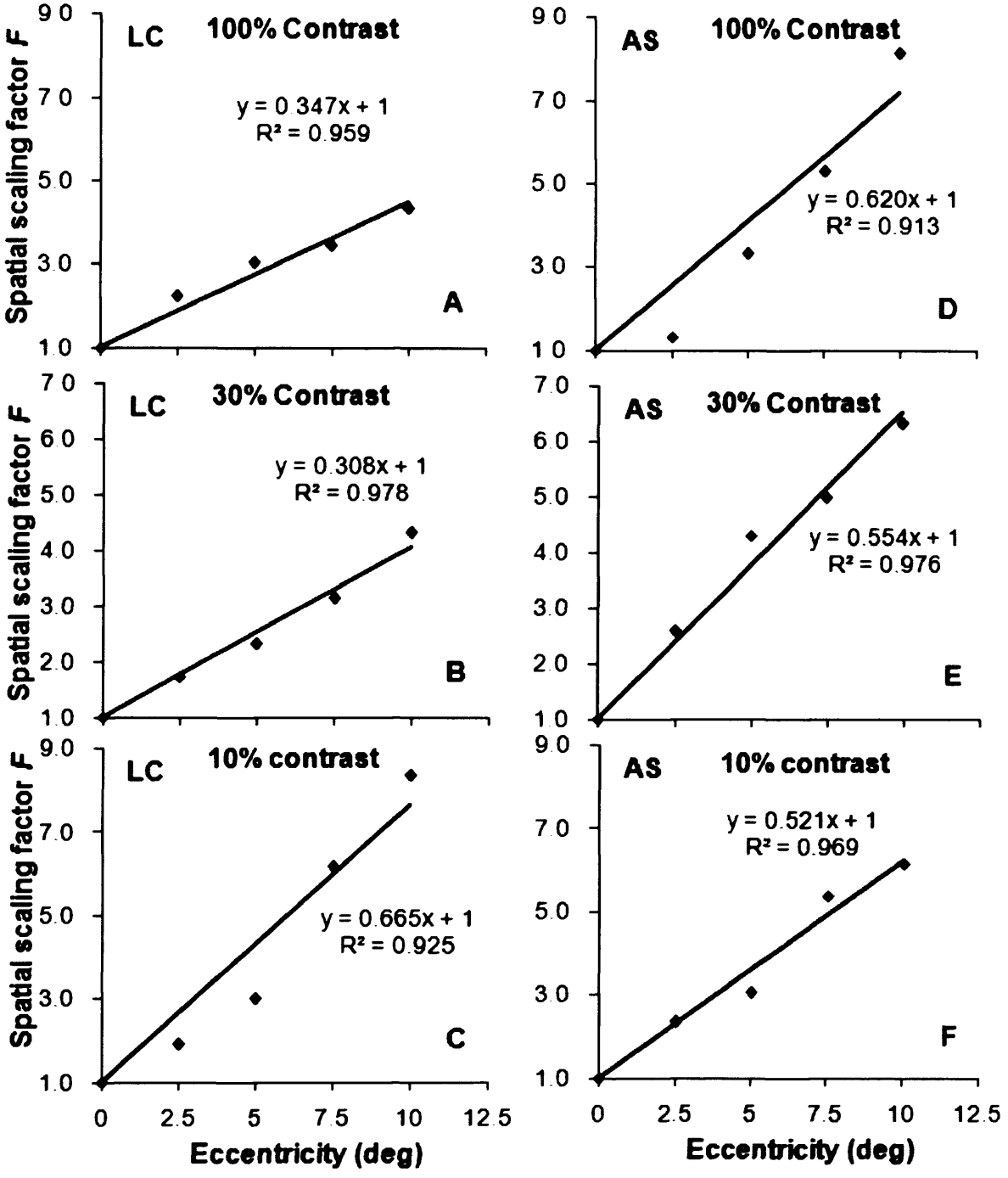

Fig 4.9 (A-F) Spatial scaling factors as a function of eccentricity at each contrast

At each eccentricity and contrast, a preliminary spatial scaling factor (■) was obtained through the spatial scaling procedure previously described in Chapter 1 Section 1.3. At each contrast, the scaling factors were fitted through (0, 1) by an optimal linear function with its fit R^2, shown in each graphs. Subjects LC and AS are as indicated.

The spatial E_{2c} at each contrast was calculated as the inverse of the slope of the corresponding linear function of Fig 4.9 and shown in Table 4.4.

Table 4.4 Spatial E_{2c} at each contrast

E_{2c}	LC	AS	Average
100%	2.88	1.61	2.25
30%	3.25	1.81	2.53
10%	1.50	1.92	1.71

In Fig 4.10 are shown the E_{2c} and its average between subjects.

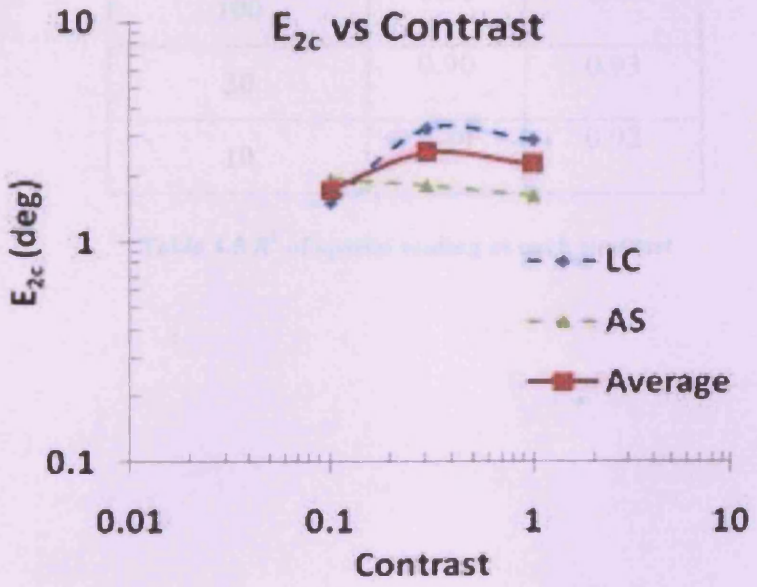

Fig 4.10 Spatial E_{2c} plotted as a function of contrast for subjects LC and AS.

The blue dash smooth curve is the function of E_{2c} vs. contrast for subject LC. The green one is for AS. The average E_{2c} between subjects is plotted against contrast with the red solid smooth curve.

By the final scaling factors calculated with the corresponding linear function at each contrast, the orientation discrimination threshold data at each contrast (see Fig 4.3) were

shifted to superimpose on to the foveal data from the same contrast level in Fig 4.11. The R^2 of the best fit to each scaled threshold data set by equation (4.5) was calculated and shown in each sub-figure. Data collapsed well onto the foveal data at each contrast, indicated by the high R^2 values (see Table 4.5).

$$Th = Th_{\min}(1 + H_c / H)^p \qquad \textbf{Equation 4.5}$$

Contrast %	R^2	
	LC	AS
100	0.91	0.93
30	0.90	0.93
10	0.84	0.92

Table 4.5 R^2 of spatial scaling at each contrast

Fig 4.11 Spatial scaling of orientation discrimination threshold at each contrast

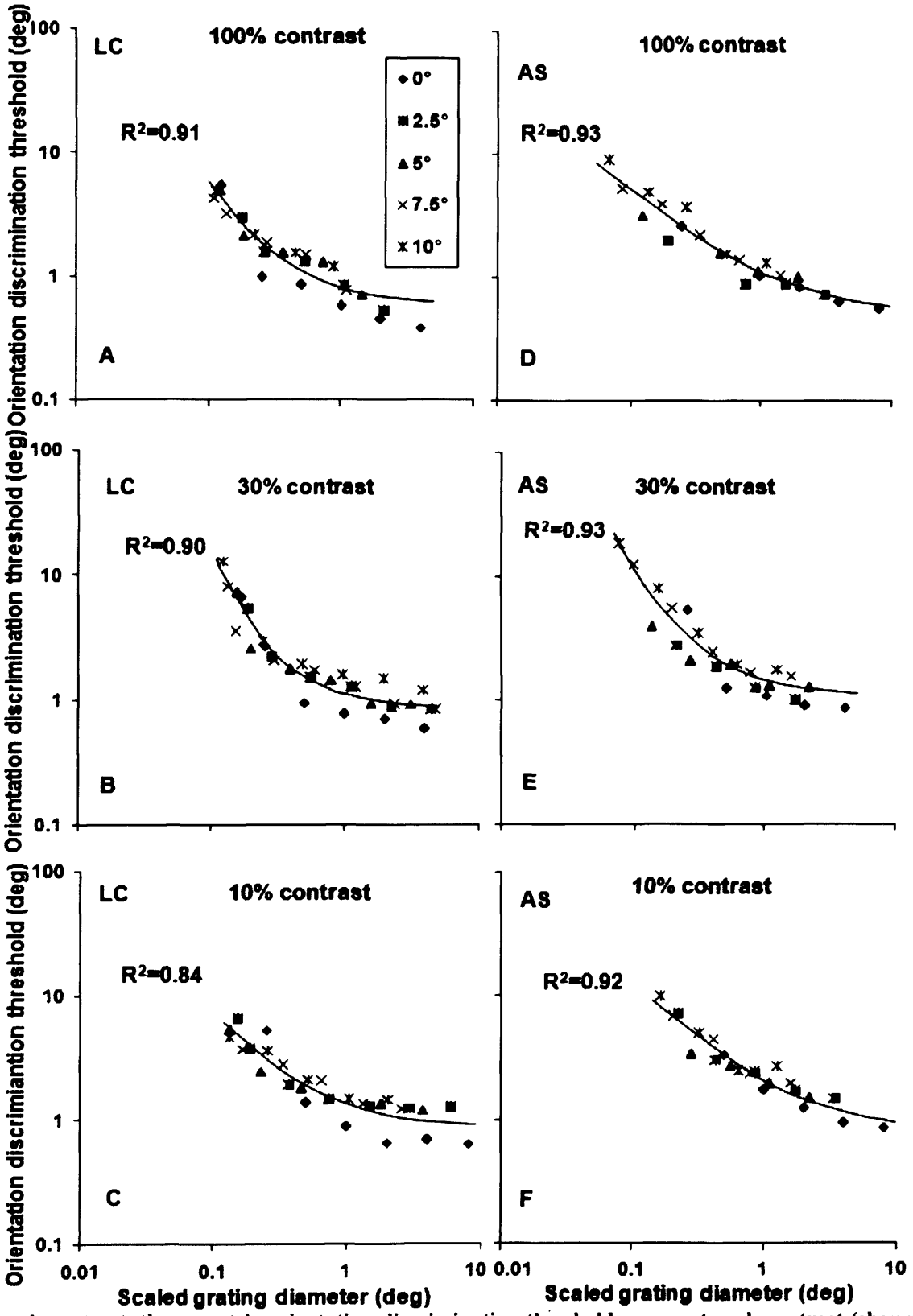

At each contrast, the eccentric orientation discrimination threshold curves at each contrast (shown in

Fig 4.3) were horizontally shifted to superimpose onto each fovea curve by final spatial scaling factors calculated by using the corresponding linear functions in Fig 4.9. The smooth curve was the best fit to each scaled threshold set at each contrast by equation (4.5). Data collapsed well onto the foveal curve at each contrast, indicated by the high R^2 values.

4.4 Discussion

In this chapter, the orientation discrimination thresholds of 4cpi grating stimuli were measured at various contrast levels and eccentricities. Firstly, all the threshold data were superimposed across eccentricities and contrasts on to the foveal 100% contrast condition by spatial and 2D scaling. On the basis of the R^2s in Table 4.1, 2D scaling (0.86 for LC and 0.91 for AS) worked better than spatial scaling (0.74 for LC and 0.82 for AS). However, both scaling methods appropriately scaled the threshold data across eccentricities and contrasts according to their best-fit R^2, which suggested that spatial scaling was adequate to explain the changes across visual field and the peripheral performance was quantitatively different from the foveal one in this visual task, in agreement with Levi *et al.* (2000a), Makela *et al.* (1993), Sally and Gurnsey (2003), Whitaker *et al.* (1992), etc. This was also further proved by the success of spatial scaling within a contrast (with R^2 ranging from 0.84 to 0.93 with an average of 0.91. see Table 4.5).

When expressed in terms of spatial offset, the foveal thresholds at 100% contrast were 15 sec arc for LC and 40 sec arc for AS. Both are well within the range of hyperacuity task (Westheimer 1981). When expressed in terms of the rotation angle of orientation, the foveal thresholds at 100% contrast were found to be 0.38 deg for LC and 0.56 deg for AS. They are similar to 0.5 deg of Makela *et al.* (1993) and 0.6 deg of Westheimer *et al.* (1999), and 0.56 of Sally and Gurnsey (2003) and 0.7 deg found by Bowne (1990). As shown in Figs 4.2 and 4.3, the orientation discrimination threshold increased and reached a plateau with increasing grating diameter, which is in agreement with Betts *et al.* (2007), Mareschal and Shapley (2004), Nasanen *et al.* (1993), Reisbeck and Gegenfurtner (1998) and Spinelli *et*

al. (1984). The minimum threshold was found to increase as eccentricity increased and contrast decreased, as in Chapter 3 and Sally and Gurnsey (2007).

According to the R^2s, all eccentric threshold curves as a function of line length were accurately described with equation (4.1) $Th = Th_{\min}(1 + H_c / H)^5$, irrespective of contrast and eccentricity for both subjects (LC and AS), as in Chapter 3 for describing orientation discrimination threshold of the Gaussian filtered line. This is also consistent with the equation of $Th = \theta_{\min}(1 + L_{crit} / x)^n$ used by Sally and Gurnsey (2003, 2004) for describing orientation discrimination threshold both broadband and narrowband line stimuli.

4.4.1 Global spatial E_2 across contrasts

Equation (4.3) modelled the spatial scaling factors as a function of eccentricity and contrast. In the equation, there is an interaction between eccentricity and contrast in orientation discrimination, which is in agreement with the findings in Chapter 3 for Gaussian filtered line stimulus.

The vertical and horizontal factors of 2D scaling, i.e. the normalised Th_{min} and H_c, were both modelled as a function of eccentricity and contrast with equation (4.4). Based on the equation, there is no interaction between eccentricity and contrast factors in modelling, which is in agreement with Melmoth *et al.* (2000a) who modelled contrast sensitivity of face recognition.

During spatial scaling across contrasts, a global spatial scaling E_2 was found according to

equation (4.3). As shown in Fig 4.4 and Table 4.1 (B), E_2 are different between subjects: 1.76 deg for LC and 1.71 deg for AS, with an average 1.74 deg. It is close to 1.93 deg of Makela *et al.* (1993) and 1.51 deg of Sally and Gurnsey (2003).

During 2D scaling across contrasts, according to equation (4.4), a contrast-non-interacted global E_2 exists for the horizontal scaling components of the 2D scaling. In Table 4.2 (B) the horizontal scaling E_2 are quite similar between subjects: 5.77 deg for LC and 4.61 deg for VR, with an average of 5.19 deg. The horizontal E_2 for 2D scaling is greater than spatial scaling E_2 because in the former case a simultaneous vertical scaling was also applied.

4.4.2 Spatial E_{2c} in individual contrast C

From Table 4.4, the average of E_{2c} between subjects ranges from 1.71 to 2.53 deg and is almost independent of contrast (see the solid red curves in Fig 4.11). The independency suggests that the effect of contrast reduction on performance deterioration of orientation discrimination is not stronger at fovea than the periphery. This is in agreement with the findings in Chapter 3.

Chapter 5 The effects of eccentricity, contrast and cpi on orientation discrimination

5.1 Introduction

When investigating orientation discrimination of grating stimuli, researchers have studied the effects of grating size (Mareschal and Shapley 2004), spatial frequency (Burr and Wijesundra 1991), or contrast (Bowne 1990; Burr and Wijesundra 1991; Mareschal and Shapley 2004). In general, orientation threshold performance improves and saturates with increasing grating size (grating area or grating diameter) (Mareschal and Shapley 2004; Nasanen *et al.* 1993) and contrast (Mareschal and Shapley 2004; Regan and Beverley 1985; Reisbeck and Gegenfurtner 1998). Burr and Wijesundra (1991) found that orientation discrimination threshold first decreased and then reached a plateau with increasing spatial frequency both near the contrast threshold and above. Grating bandwidth affects orientation discrimination threshold as well. Beaudot and Mullen (2006) measured orientation discrimination thresholds of 2D Gaussian patches and found that thresholds increased monotonically with stimulus bandwidth.

In this chapter, firstly, the effects of contrast and eccentricity on orientation discrimination were continually examined. Another two orientation discrimination experiments were conducted using 2 and 16cpi sinusoidal gratings. The threshold data of each stimulus were processed and analyzed as in Chapter 4 for the 4cpi grating.

Then the results from all types of the stimuli were grouped on the basis of the scaling method and a nonparametric paired statistical test, *i.e.* Wilcoxon test, was used to examine whether the difference of R^2s between spatial scaling and 2D scaling was statistically significant. By the test, it can be find out whether the performance difference between the fovea and periphery was qualitative or quantitative.

Finally, in addition to the same analysis as in Chapters 3 and 4, the effect of another factor, *i.e.* cycle per image (cpi) on orientation discrimination was introduced and studied. The aim of this study was to investigate how cpi influenced orientation discrimination performance across visual field.

5.2 Methods

5.2.1 Apparatus

Stimuli were presented on the monitor previously described in Chapter 2. For further details see Section 2.2.1.

5.2.2 Stimuli

The sinusoidal stimuli used in this chapter had 2 and 16cpi and were created as the 4cpi gratings in Chapter 4. Fig 5.1 shows a sample of a 2cpi grating stimulus.

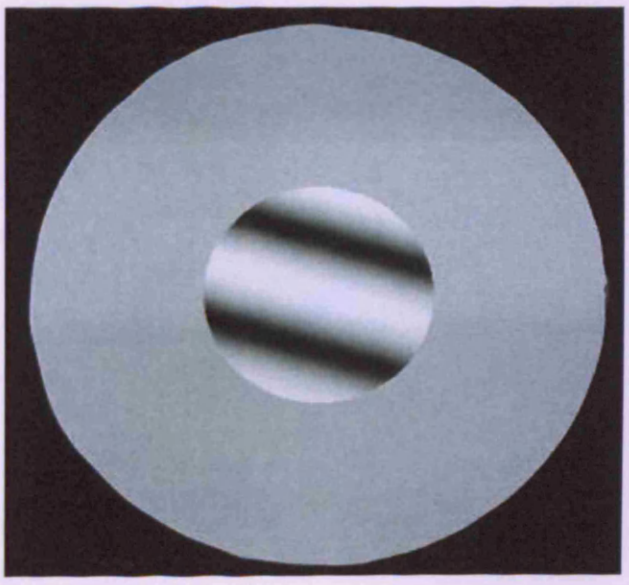

Fig 5.1 A sample of a 2 cpi grating stimulus

5.2.3 Subjects

Subjects LC and AS took part in the experiments, as in Chapter 4.

5.2.4 Procedure

The procedure of the threshold measurements was as in Chapter 4. For the 2 cpi gratings, viewing distances were 114, 171, 228 cm, giving the range of 0.251-8.0 deg of visual angle for the diameter of the grating. For the 16cpi gratings, viewing distances were 57, 114, 171 and 228 cm, giving the range of 0.503-16.0 deg of visual angle for the diameter of the grating. Thresholds were measured at the fovea and 2.5, 5, 7.5, and 10 deg eccentricity in the nasal visual field.

5.3 Results

In Figs 5.2a and 5.2b, orientation discrimination spatial offset thresholds for the 2 and 16 cpi grating stimuli were expressed in sec arc of the visual field (θ in Fig 1.16), and plotted as a function of the diameter (min arc) of the circular grating at contrast levels of 100, 30 and 10% and eccentricities of 0, 2.5, 5, 7.5 and 10 deg for both subjects. The resulting curves tend to be u-shaped showing an optimal length for each eccentricity and contrast level. The optimal size generally increases with increasing eccentricity and decreasing contrast.

Fig 5.2 Orientation discrimination thresholds (sec arc in spatial offset) for the 2 and 16cpi gratings were plotted against grating diameter (min arc)

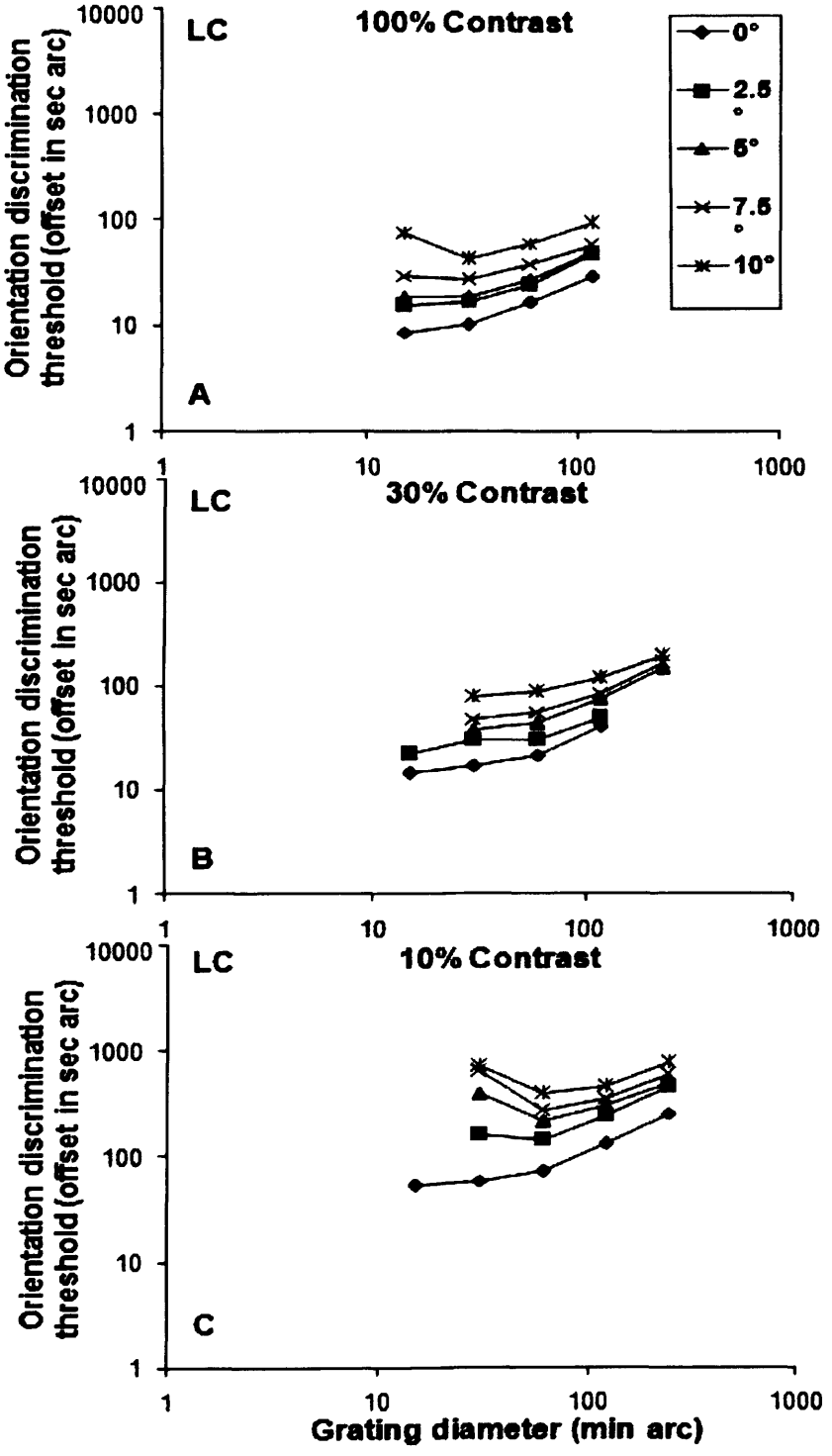

Fig 5.2a (A-C) Orientation discrimination thresholds (sec arc in spatial offset) for the 2cpi gratings were plotted against grating diameter (min arc in visual field) at eccentricities of 0, 2.5, 5, 7.5, and 10 deg and contrasts of 100, 30, and 10% for subject LC.

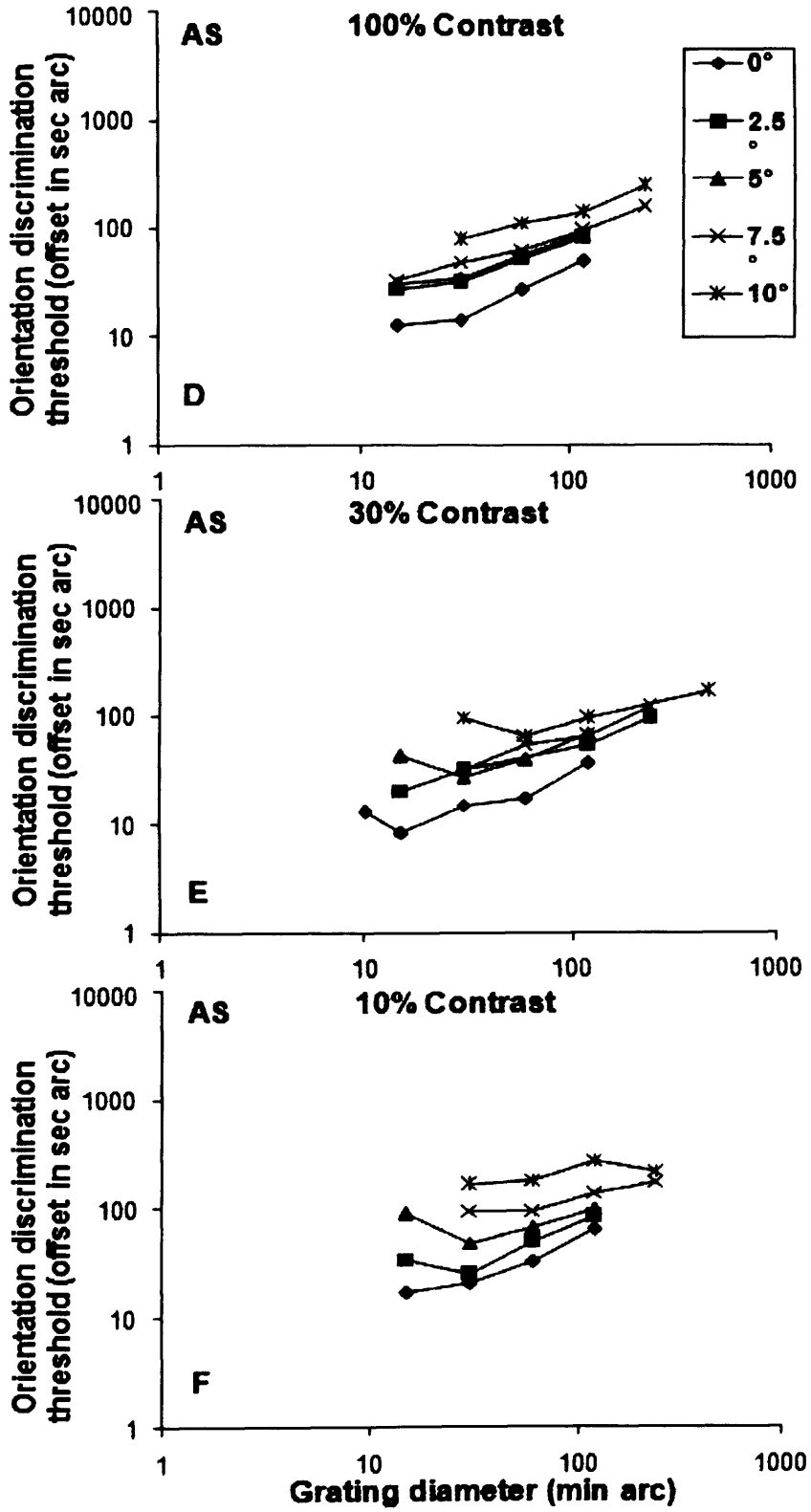

Fig 5.2a (D-F) Orientation discrimination thresholds (sec arc in spatial offset) for the 2cpi gratings were plotted against grating diameter (min arc in visual field) for subject AS as in Fig 5.2a (A-C).

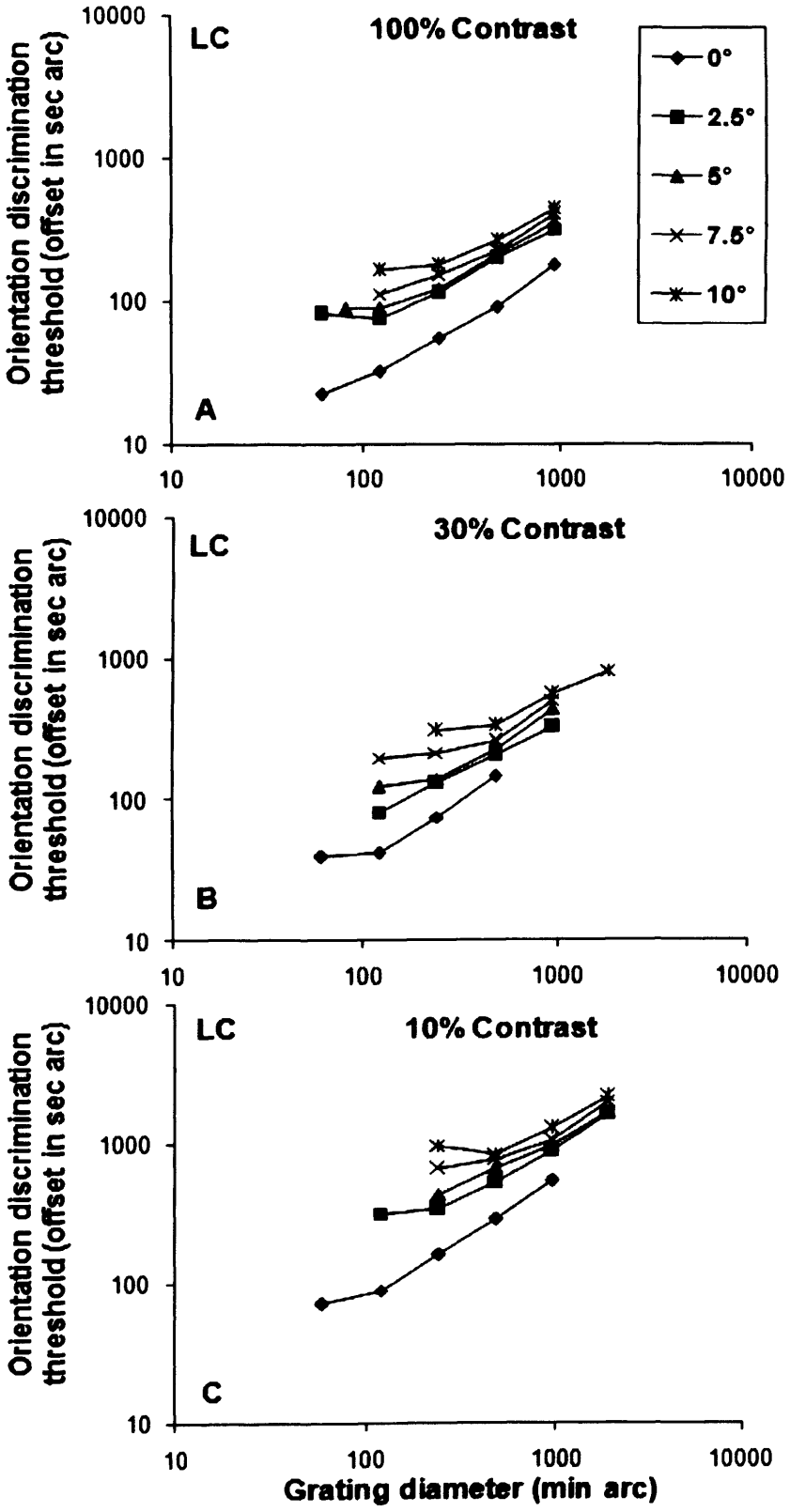

Fig 5.2b (A-C) Orientation discrimination thresholds (sec arc in spatial offset) for the 16cpi gratings were plotted against grating diameter (min arc in visual field) for subject LC as in Fig 5.2a (A-C).

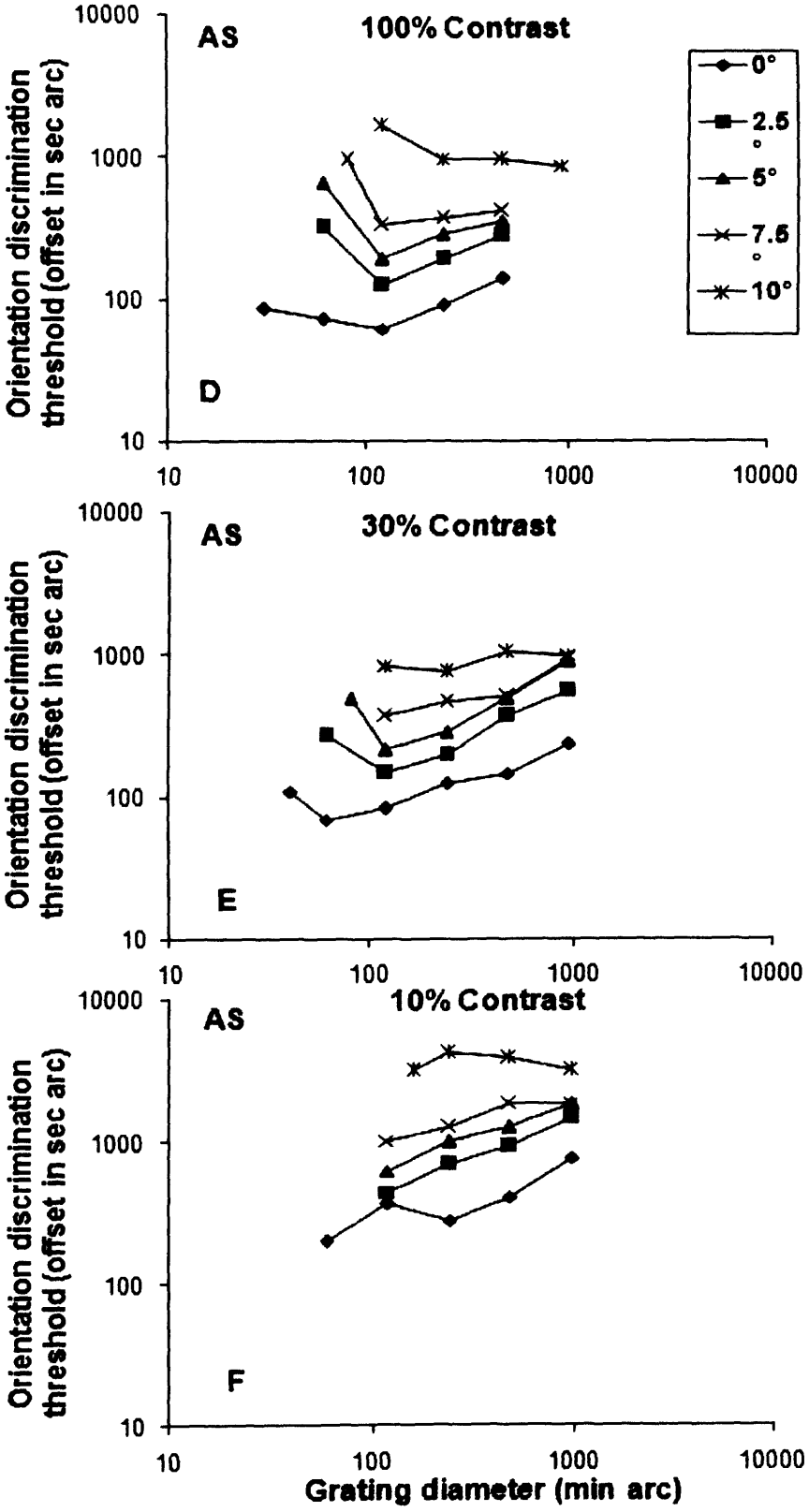

Fig 5.2b (D-F) Orientation discrimination thresholds (sec arc in spatial offset) for the 16cpi gratings were plotted against grating diameter (min arc in visual field) for subject AS as in Fig 5.2a (A-C).

In Figs 5.3a and 5.3b, the orientation discrimination thresholds for the 2 and 16 cpi grating stimuli were expressed in terms of the rotation angle (deg) of grating stimulus orientation (*a* in Fig 1.15), and were replotted as a function of grating diameter (deg) at contrast levels of 100, 30 and 10% and at eccentricities of 0, 2.5, 5, 7.5 and 10 deg for subjects LC and AS.

As in Chapters 3 and 4, each eccentric data set was fitted with equation (5.1), which is identical to equations (3.2) and (4.1):

$$Th = Th_{\min}(1 + H_c / H)^5, \qquad \textbf{Equation 5.1}$$

(see equation (4.1) in Chapter 4 for the details). The R^2 values of fitting ranged from 0.85 to 0.99 with an average of 0.96 for the 2cpi gratings ((see Appendix V Table 7) and from 0.87 to 0.99 for the 16cpi gratings with an average of 0.95 (see Appendix V Table 8).

Fig 5.3 Orientation discrimination thresholds expressed in terms of rotation angle (deg) for 2 and 16cpi grating stimuli were replotted against grating diameter (deg)

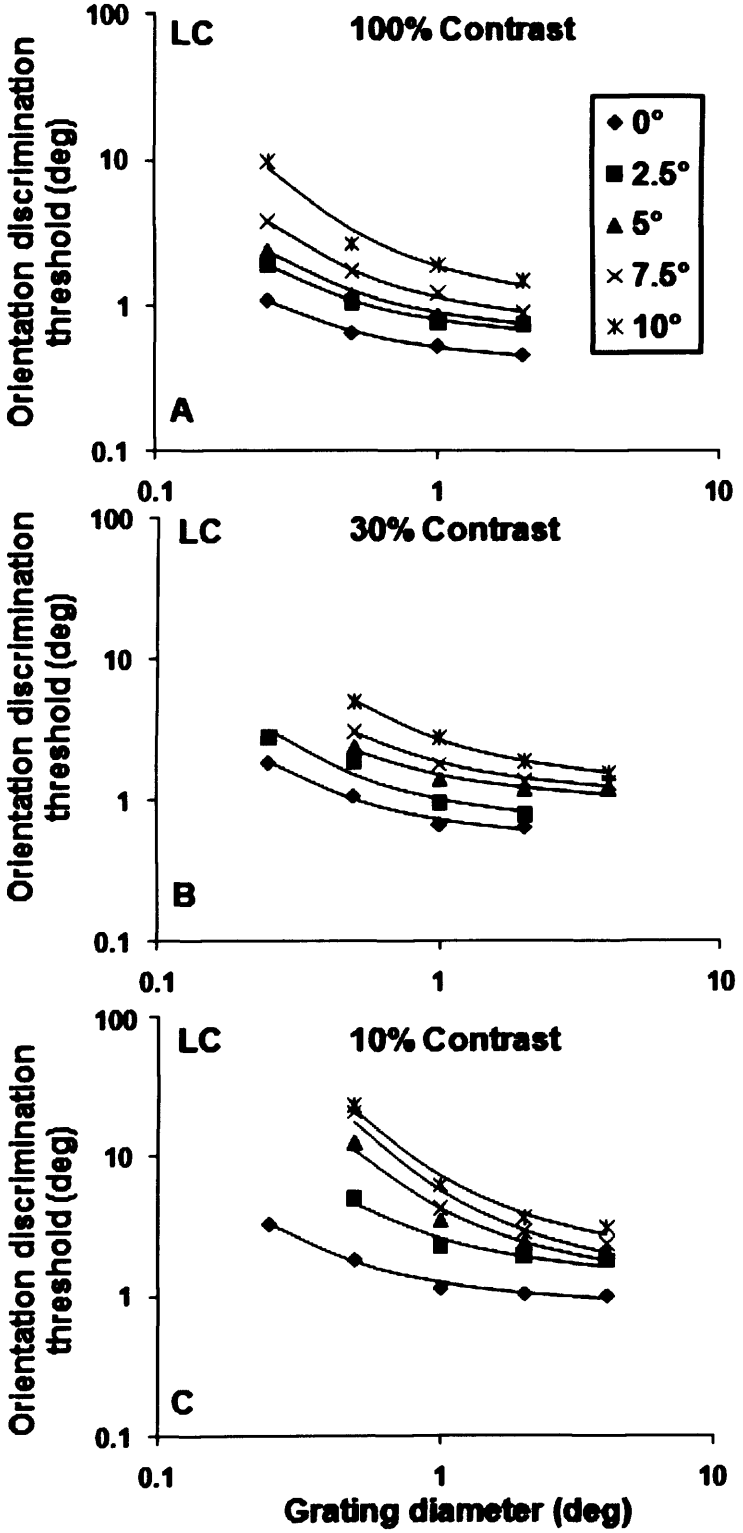

Fig 5.3a (A-C) Orientation discrimination thresholds expressed in terms of rotation angle (deg) for 2cpi grating stimuli were replotted against grating diameter (deg) in the visual field for subject LC. Each

data set was fitted with equation (5.1) (solid line) to model the decrease and plateau in threshold with increasing grating diameter.

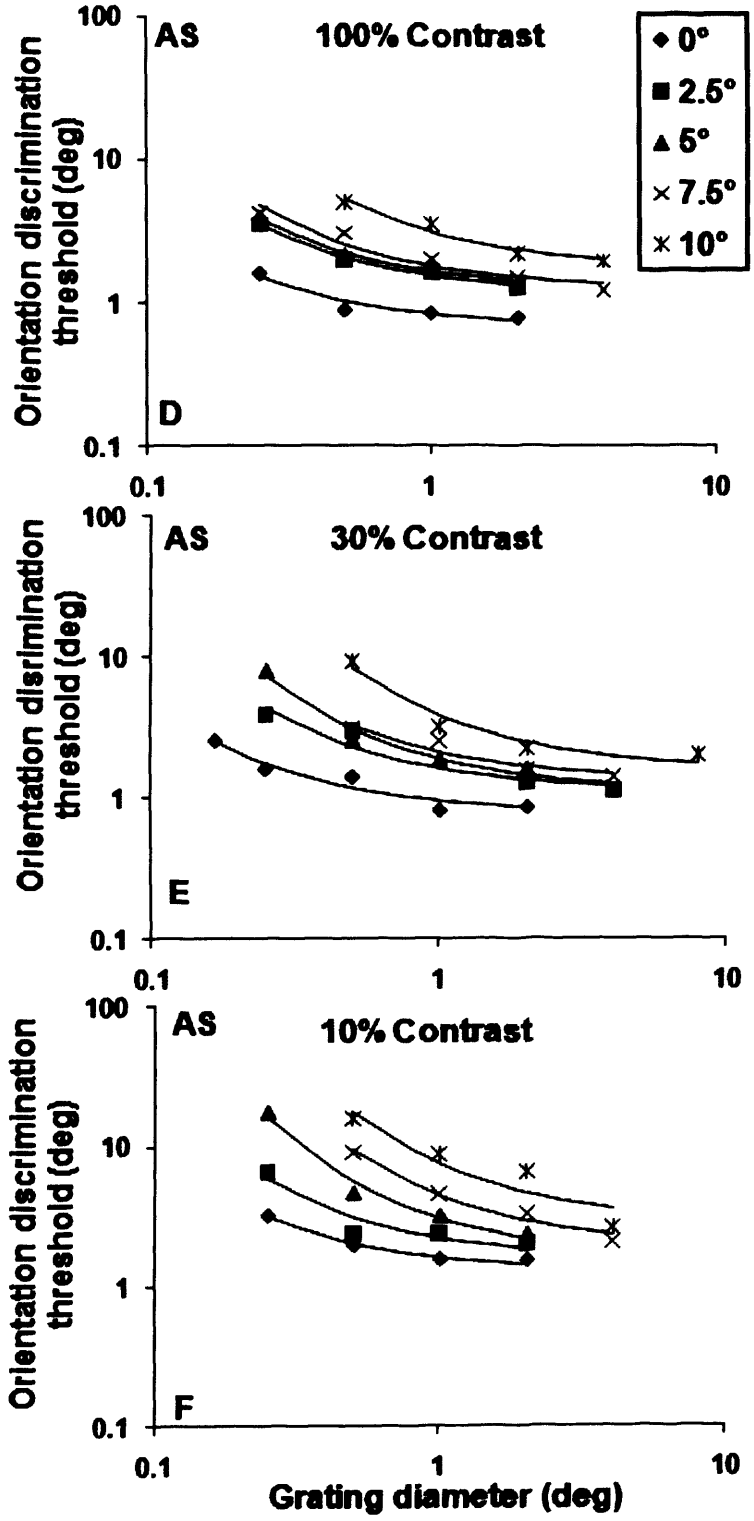

Fig 5.3a (D-F) Orientation discrimination thresholds (deg) for the 2cpi gratings plotted against grating diameter (deg) for subject AS. Other details are as in Fig 5.3a (A-C).

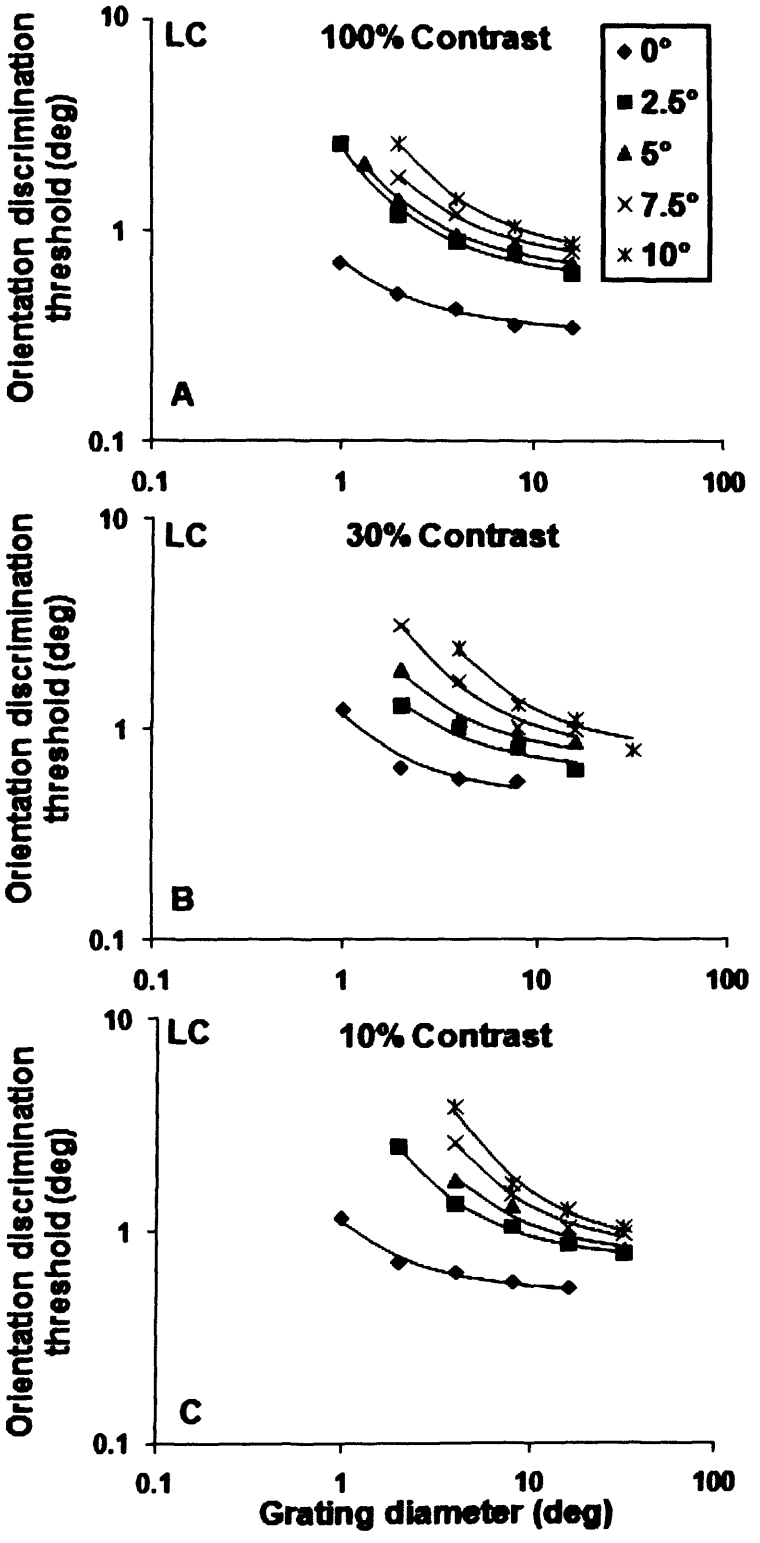

Fig 5.3b (A-C) Orientation discrimination thresholds (deg) for the 16cpi gratings plotted against grating diameter (deg) for subject LC. Other details are as in Fig 5.3a (A-C).

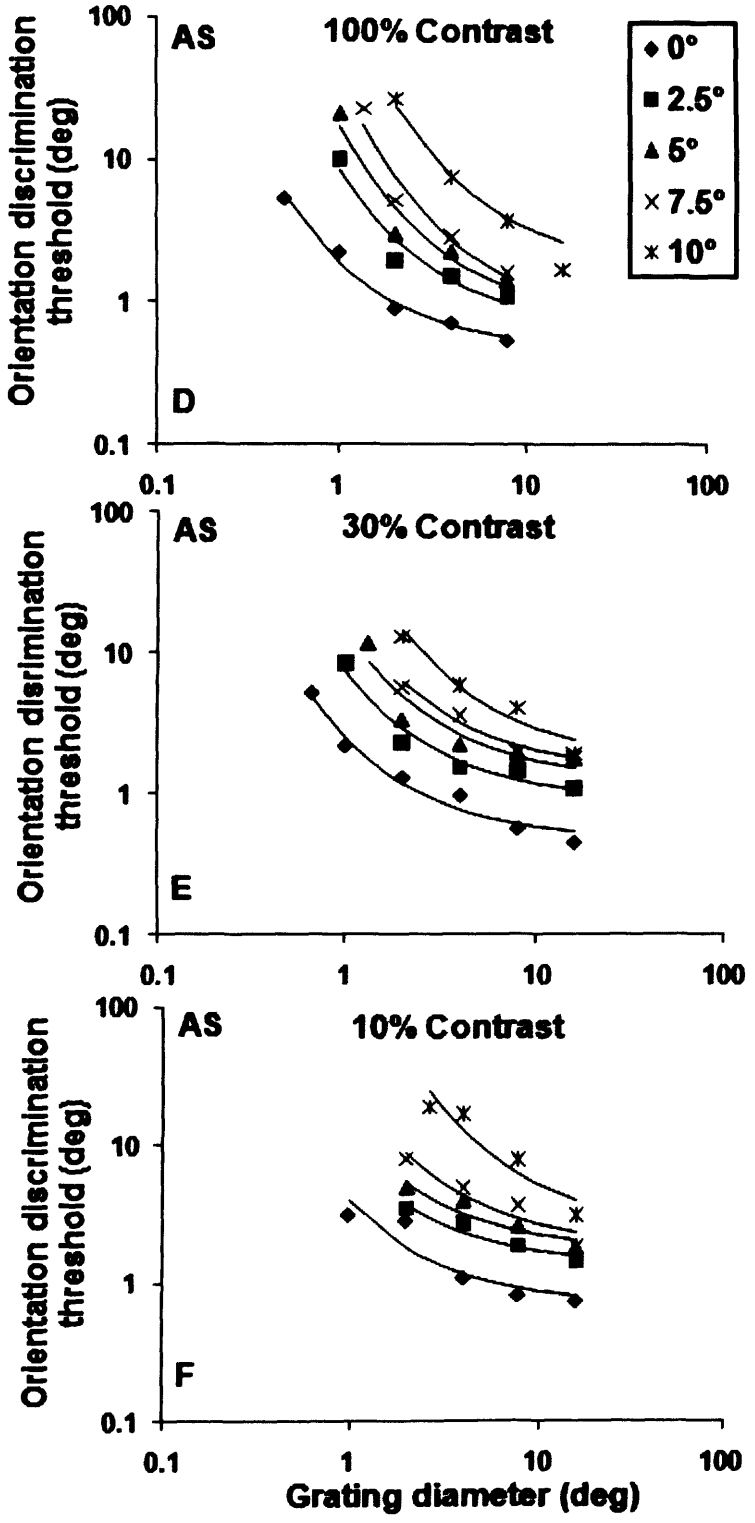

Fig 5.3b (D-F) Orientation discrimination thresholds (deg) for the 16cpi grating plotted against grating diameter (deg) for AS. Other details are as in Fig 5.3a (A-C).

In Fig 5.3 threshold first decreases and then reaches a plateau with increasing grating diameter. The shapes of the threshold curves for the 2 or 16cpi gratings are as for the 4cpi gratings in Chapter 4. Threshold functions tend to shift towards right along the horizontal axis with increasing eccentricity and decreasing contrast.

5.3.1 Spatial scaling across contrasts

In this section, spatial scaling was separately used to shift the orientation discrimination threshold data of 2 and 16cpi gratings for superposition. The foveal threshold data at 100% contrast (E=0, C=1) for each stimulus was chosen as the basic data, to which all other eccentric data were scaled, as in Chapters 3 and 4.

Figs 5.4a and 5.4b (A, B) show the spatial scaling factor surfaces obtained by the procedure of spatial scaling for 2 and 16 cpi gratings, respectively. The spatial scaling factors of both 2 and 16cpi gratings increase with decreasing contrast and increasing eccentricity. Equation (5.2) was used to model the scaling surfaces shown in Figs 5.4a and 5.4b (A, B), as for the Gaussian filtered lines (in Chapter 3 Section 3.3.1) and 4cpi gratings in Chapter 4 Section (4.3.1).

$$F_i = 1 + E/E_2 + \log C/k_2 + (\log C)^2/k_1 + E \times \log C/k_3 + E^2/E_2^{'}. \qquad \textbf{Equation 5.2}$$

The equation is identical to equations (3.3) in Chapter 3 Section 3.3.1 and (4.2) in Chapter 4 Section 4.3.1 (see Chapter 3 Section 3.3.1 for the details of the equation). Parameters k_2 and $E^{'}_2$ were discarded on the basis of their poor accuracy or R^2 values of the fit (see Appendix III for the procedure of obtaining parameters). Therefore, equation (5.2) was

reduced to equation (5.3) to model the experimental spatial scaling factors for both 2 and 16cpi gratings. Equation (5.3) is identical to equations (3.4) (in Chapter 3 Section 3.3.1) and (4.3) (in Chapter 4 Section 4.3.1), which were used to model the spatial scaling factors of the Gaussian filtered lines and 4cpi gratings.

$$F_s = 1 + E/E_2 + (\log C)^2/k_1 + E \times \log C/k_3, \qquad \textbf{Equation 5.3}$$

where F_s represent spatial scaling factor.

The spatial scaling surfaces estimated by equation (5.3) are shown in Figs 5.4a and 5.4b (C, D) for 2 and 16cpi gratings, respectively. Thus, the spatial scaling factor as a function of contrast and eccentricity was modelled with respect of the foveal 100% contrast data (E=0, C=1).

Fig 5.4 Empirical and modelled spatial scaling surfaces for the 2 and 16cpi grating as a function of eccentricity and contrast

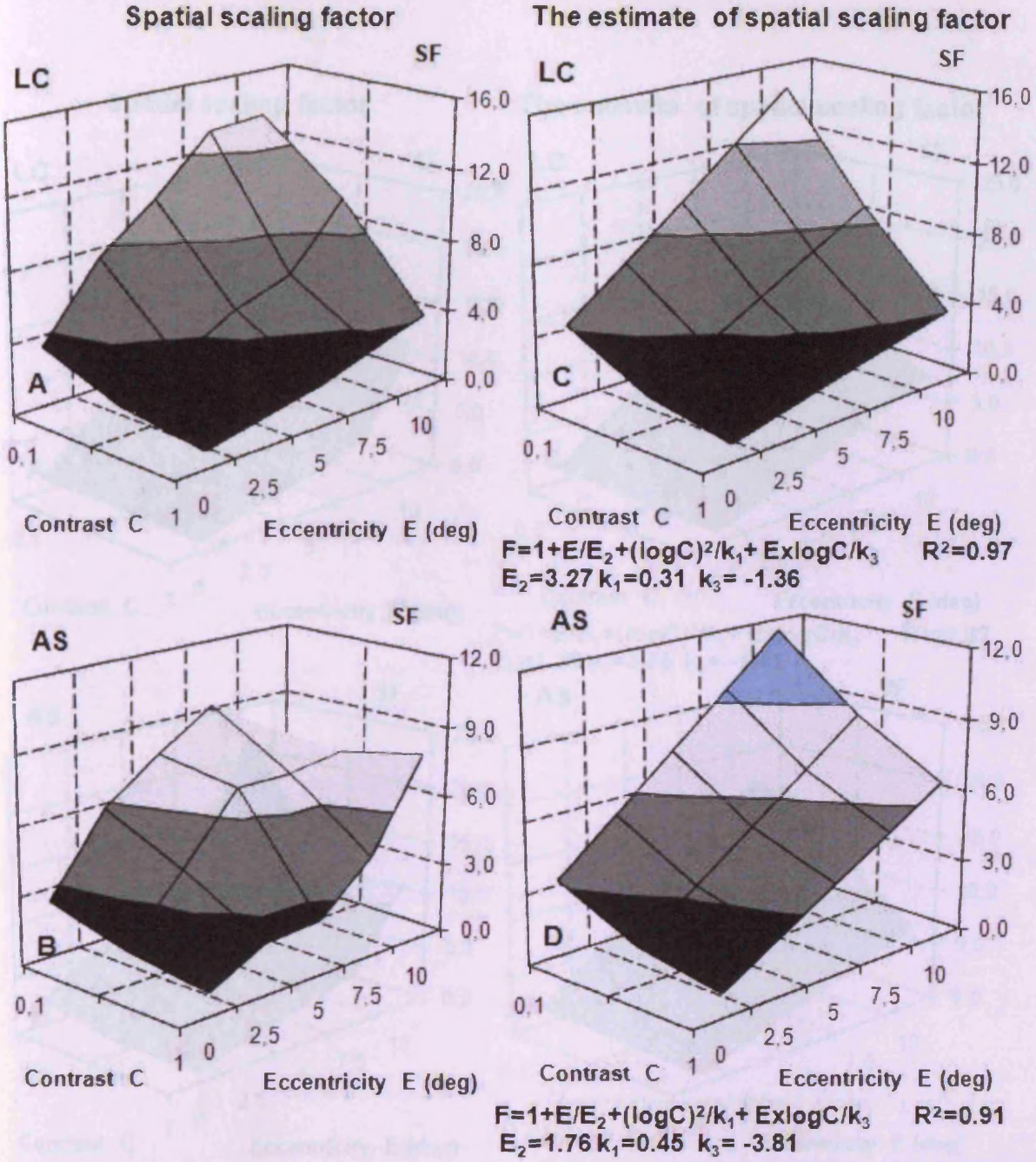

Fig 5.4a (A-D) Empirical (left column) and modelled (right column) spatial scaling surfaces as a function of eccentricity (E) and contrast (C) relative to the basic condition, i.e. foveal 100% contrast data (E=0, C=1) for the 2cpi gratings. The left-hand column (A-B) shows the empirical scaling surfaces separately for LC and AS. The empirical surfaces were fitted with equation (5.3) which modelled the effects of eccentricity and contrast on the scaling factor. The modelled scaling surfaces are shown in the

right-hand column (C-D) along with the fitting equation (5.3) with the necessary parameters and corresponding R^2s.

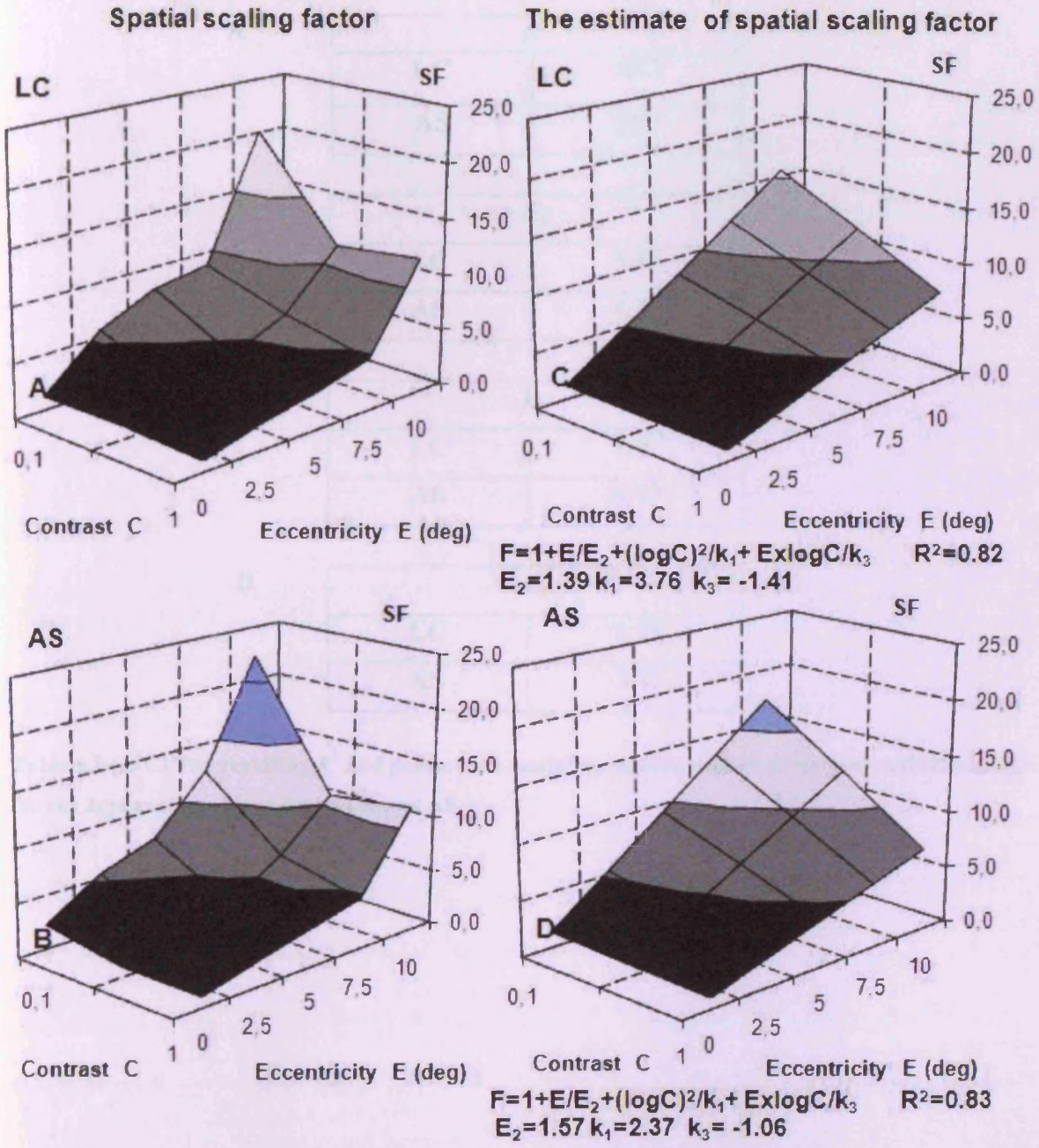

Fig 5.4b (A-D) Empirical (left column) and modelled (right column) spatial scaling surfaces of the 16cpi gratings for subjects LC and AS. Other details are as in Fig 5.4a (A-D).

Tables 5.1 and 5.2 show the values of the parameters and R^2s of equation (5.3) modelling the spatial scaling factors for the 2 and 16cpi gratings, respectively.

A

	R^2
LC	0.97
AS	0.91

B

	E_2
LC	3.27
AS	1.76

C

	k_1
LC	0.31
AS	0.45

D

	k_3
LC	-1.36
AS	-3.81

Table 5.1 (A-C) The resulting R^2 and parameters modelling spatial scaling surfaces by equation (5.3) for the 2cpi gratings for subjects LC and AS.

A

	R^2
LC	0.82
AS	0.83

B

	E_2
LC	1.39
AS	1.57

C

	k_1
LC	3.76
AS	2.37

D

	k_3
LC	-1.41
AS	-1.06

Table 5.2 (A-C) The resulting R^2 and parameters modelling spatial scaling surfaces by equation (5.3) for the 16cpi gratings for subjects LC and AS.

In Figs 5.5 and 5.6 are shown the unscaled experimental orientation discrimination threshold data of 2 and 16cpi gratings, respectively.

By the spatial scaling surfaces shown in Fig 5.4a (C, D), the unscaled threshold data of 2cpi gratings were superimposed onto its basic condition (E=0, C=1), as shown in Fig 5.7. By the spatial scaling surfaces shown in Fig 5.4b (C, D), the unscaled threshold data of 16cpi gratings were superimposed onto its basic condition (E=0, C=1), as shown in Fig 5.8. R^2s were calculated to demonstrate how well the spatial scaling equates performance across eccentricities and contrasts.

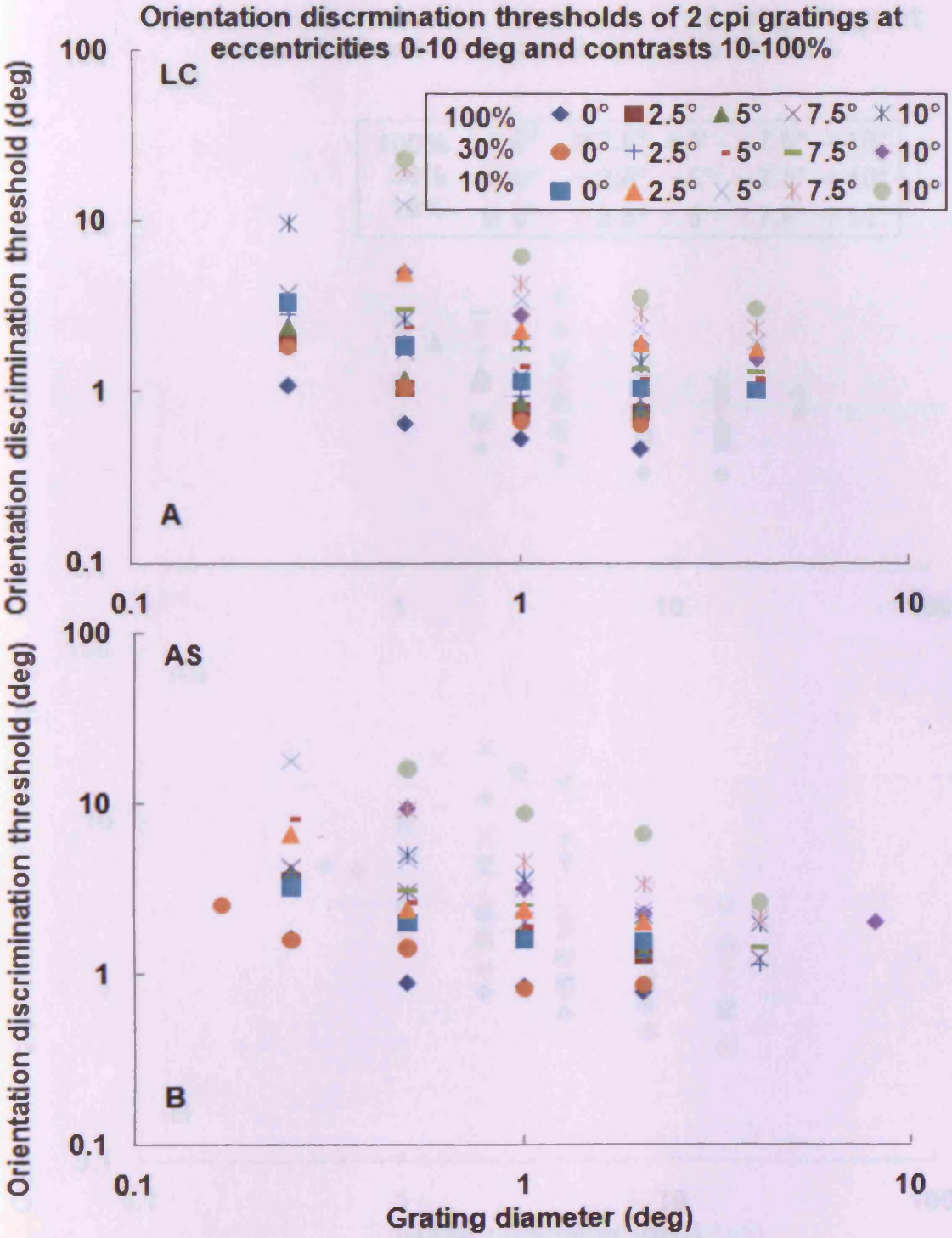

Fig 5.5 (A-B) The unscaled experimental orientation discrimination threshold of the 2cpi gratings

The original orientation discrimination threshold data of the 2cpi gratings were plotted against grating diameter at eccentricities of 0, 2.5, 5, 7.5 and 10 deg, and contrast levels of 10, 30 and 100% for subjects LC and AS.

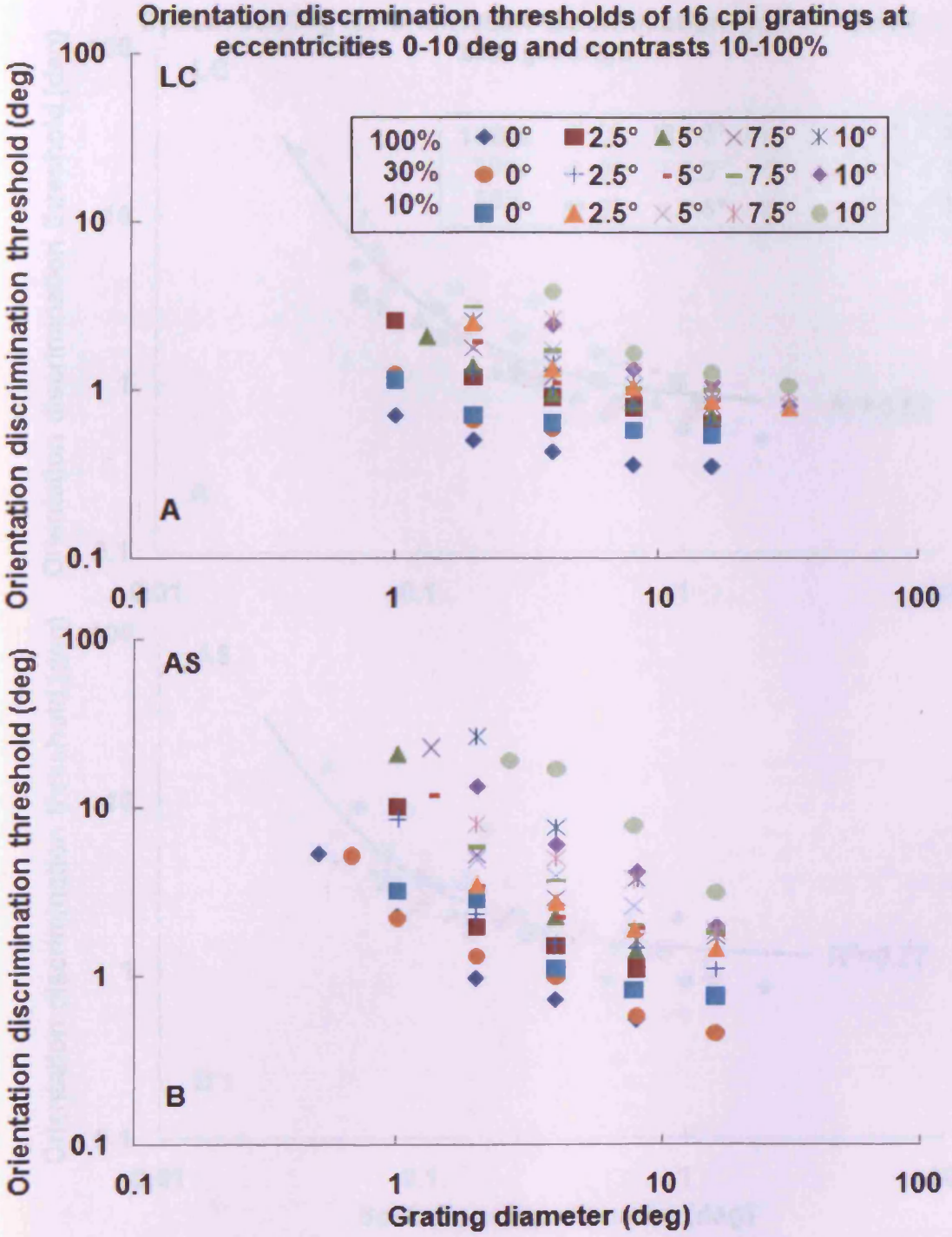

Fig 5.6 (A-B) The unscaled experimental orientation discrimination threshold of the 16cpi gratings

The original orientation discrimination threshold data of the 16cpi gratings plotted against grating diameter as in Fig 5.5 (A-B).

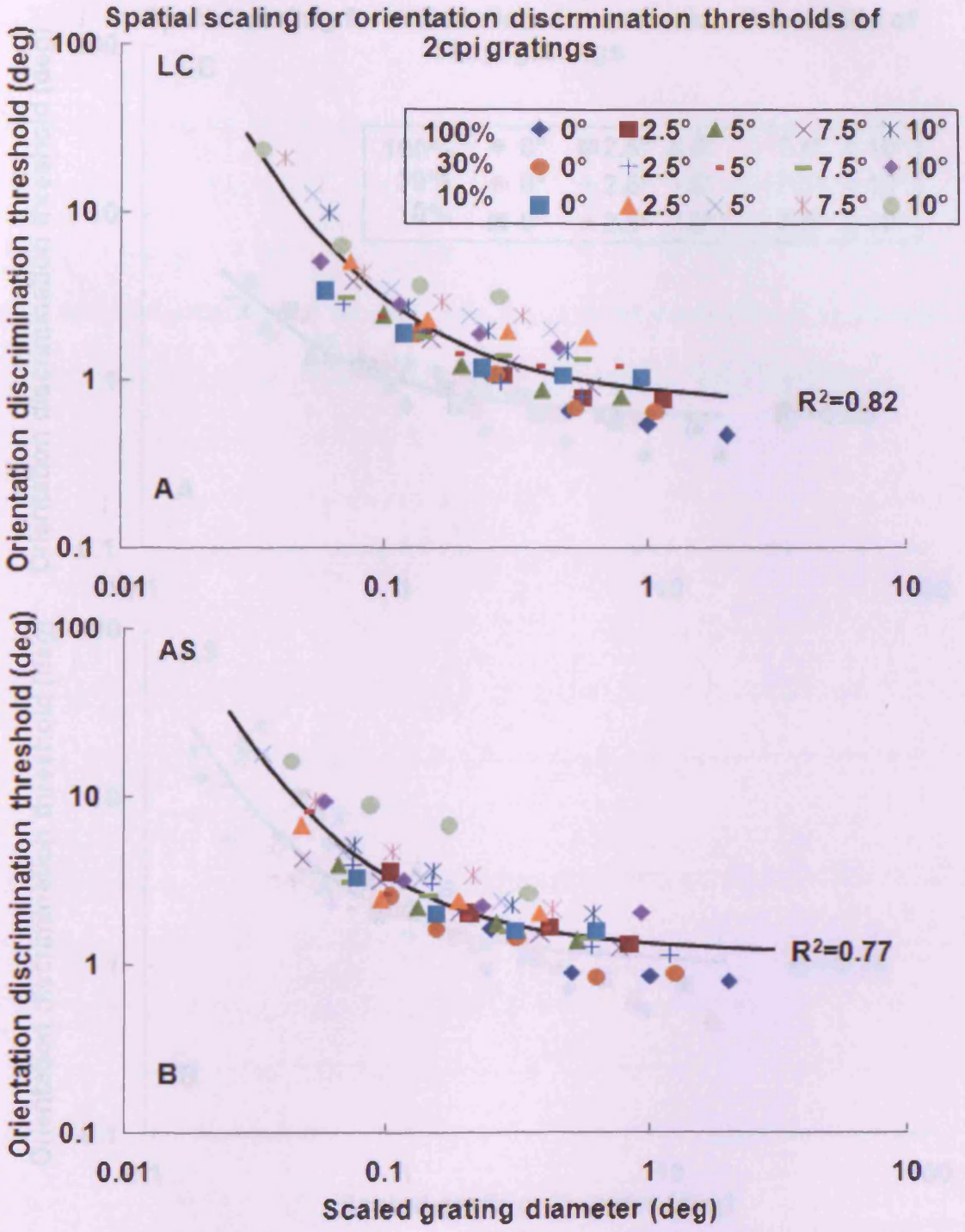

Fig 5.7 (A-B) The scaled orientation discrimination thresholds of the 2cpi gratings by spatial scaling

The original discrimination threshold data of the 2cpi gratings from Fig 5.5 (A-B) were scaled by means of the modelled spatial scaling surfaces of Fig. 5.4a (C, D). Data from the eccentricities of 0-10 deg and contrasts of 10-100% collapsed onto the foveal 100% contrast data (E=0, C=1). The data for subjects LC and AS are as indicated. The smooth curve was the best fit of equation (5.1) to the scaled threshold data. R^2 indicates how accurately the curve describes all the data after spatial scaling.

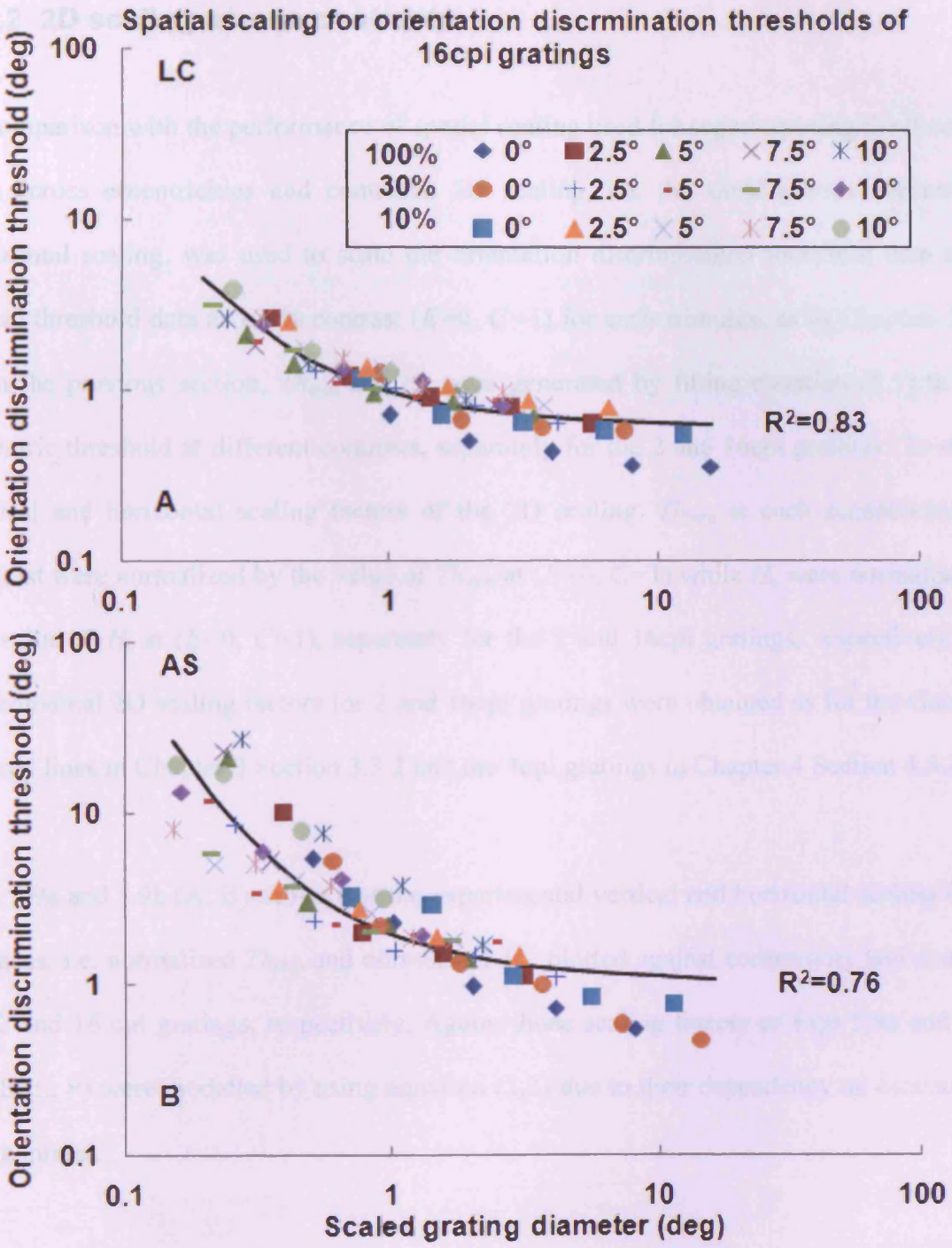

Fig 5.8 (A-B) The scaled orientation discrimination thresholds of the 16cpi gratings by spatial scaling

The original discrimination threshold data of the 16cpi gratings in Fig 5.6 (A-B) were scaled by means of the modelled spatial scaling surfaces of Fig 5.4b (C, D). Other details are as in Fig 5.7 (A-B).

5.3.2 2D scaling across contrasts

In comparison with the performance of spatial scaling used for superimposing the threshold data across eccentricities and contrasts, 2D scaling, i.e. the simultaneous vertical and horizontal scaling, was used to scale the orientation discrimination threshold data to the foveal threshold data at 100% contrast (E=0, C=1) for each stimulus, as in Chapters 3 and 4. In the previous section, Th_{min} and H_c were generated by fitting equation (5.1) to each eccentric threshold at different contrasts, separately for the 2 and 16cpi gratings. To obtain vertical and horizontal scaling factors of the 2D scaling, Th_{min} at each eccentricity and contrast were normalized by the value of Th_{min} at (E=0, C=1) while H_c were normalised by the value of H_c at (E=0, C=1), separately for the 2 and 16cpi gratings, respectively. The experimental 2D scaling factors for 2 and 16cpi gratings were obtained as for the Gaussian filtered lines in Chapter 3 Section 3.3.2 and the 4cpi gratings in Chapter 4 Section 4.3.2.

Figs 5.9a and 5.9b (A, B) shows that the experimental vertical and horizontal scaling factor surfaces, i.e. normalised Th_{min} and normalised H_c, plotted against eccentricity and contrast, for 2 and 16 cpi gratings, respectively. Again, those scaling factors of Figs 5.9a and 5.9b (A, B, E, F) were modelled by using equation (5.2) due to their dependency on eccentricity and contrast.

Parameters k_2, k_3 and E'_2 were found to be unnecessary because of their poor accuracy or R^2s of the fit (see the procedure of selecting parameters in Appendix III). Thus, equation (5.2) was reduced to equation (5.4), identical to equation (3.5) in Section 3.3.2 of Chapter 3 and equation (4.4) in Section 4.3.2 of Chapter 4 used for modeling the 2D scaling factors of

the Gaussian filtered lines and 4cpi gratings.

$$F_t = 1 + E/E_2 + (\log C)^2/k_1 . \qquad \textbf{Equation 5.4}$$

Then the modelled 2D scaling surfaces were calculated by equation (5.4) and shown in Figs 5.9a and 5.9b (C, D, G, H) for the 2 and 16cpi gratings, respectively.

Fig 5.9 Empirical & modelled 2D scaling surfaces of the 2 and 16cpi gratings

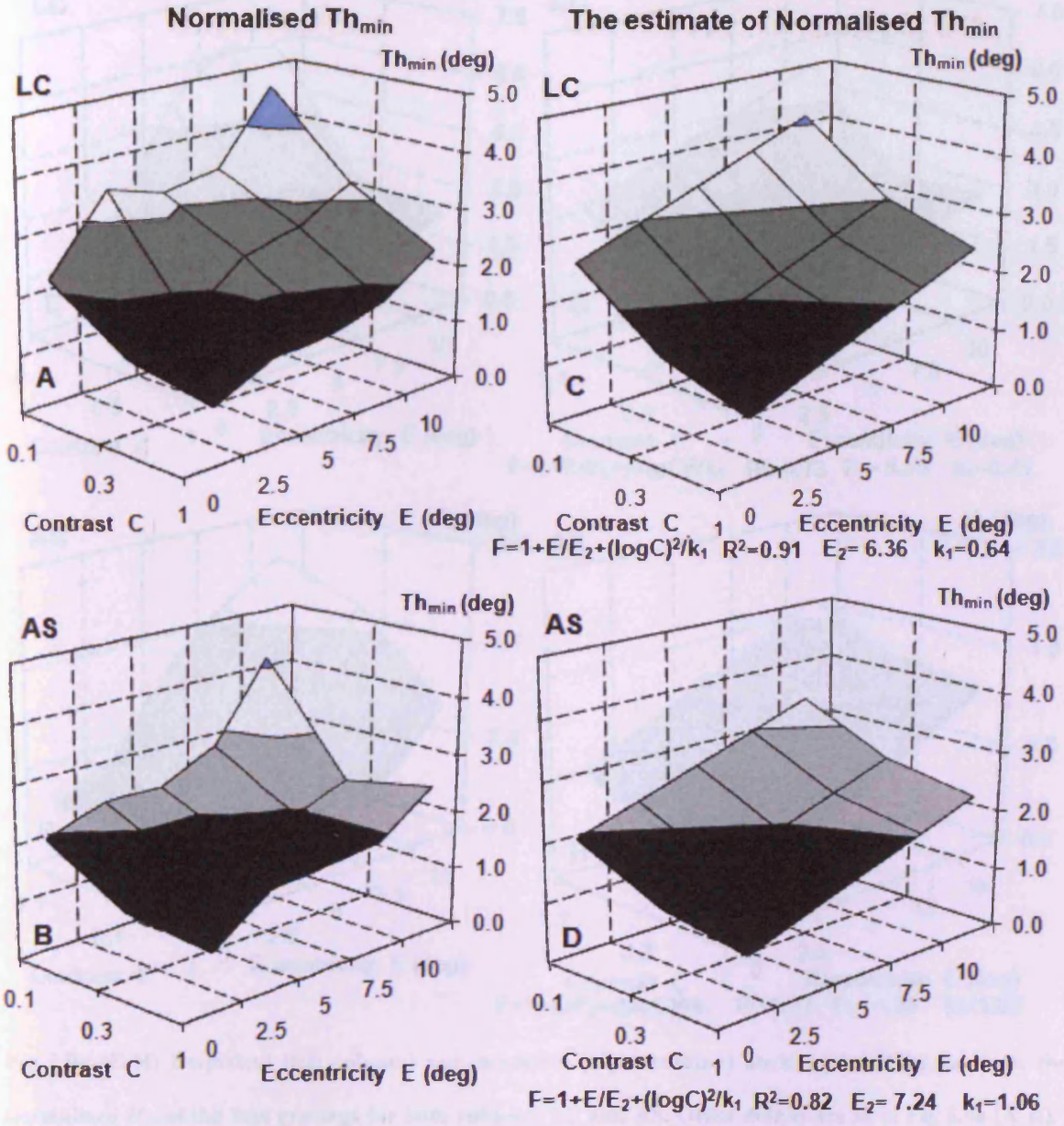

Fig 5.9a (A-D) Empirical (left column) and modelled (right column) vertical scaling surfaces, the normalised Th_{min}, at any eccentricity (E) and contrast (C) relative to the basic condition foveal 100% contrast data (E=0, C=1) for the 2cpi gratings. The left-hand column (A-B) shows the empirical scaling surfaces separately for LC and AS. The empirical surfaces were fitted with equation (5.4) which modelled the effects of eccentricity and contrast on the normalised Th_{min}. The modelled scaling surfaces are shown in the right-hand column (C-D) along with the fitting equation (5.4) with the necessary parameters and the corresponding R^2 values.

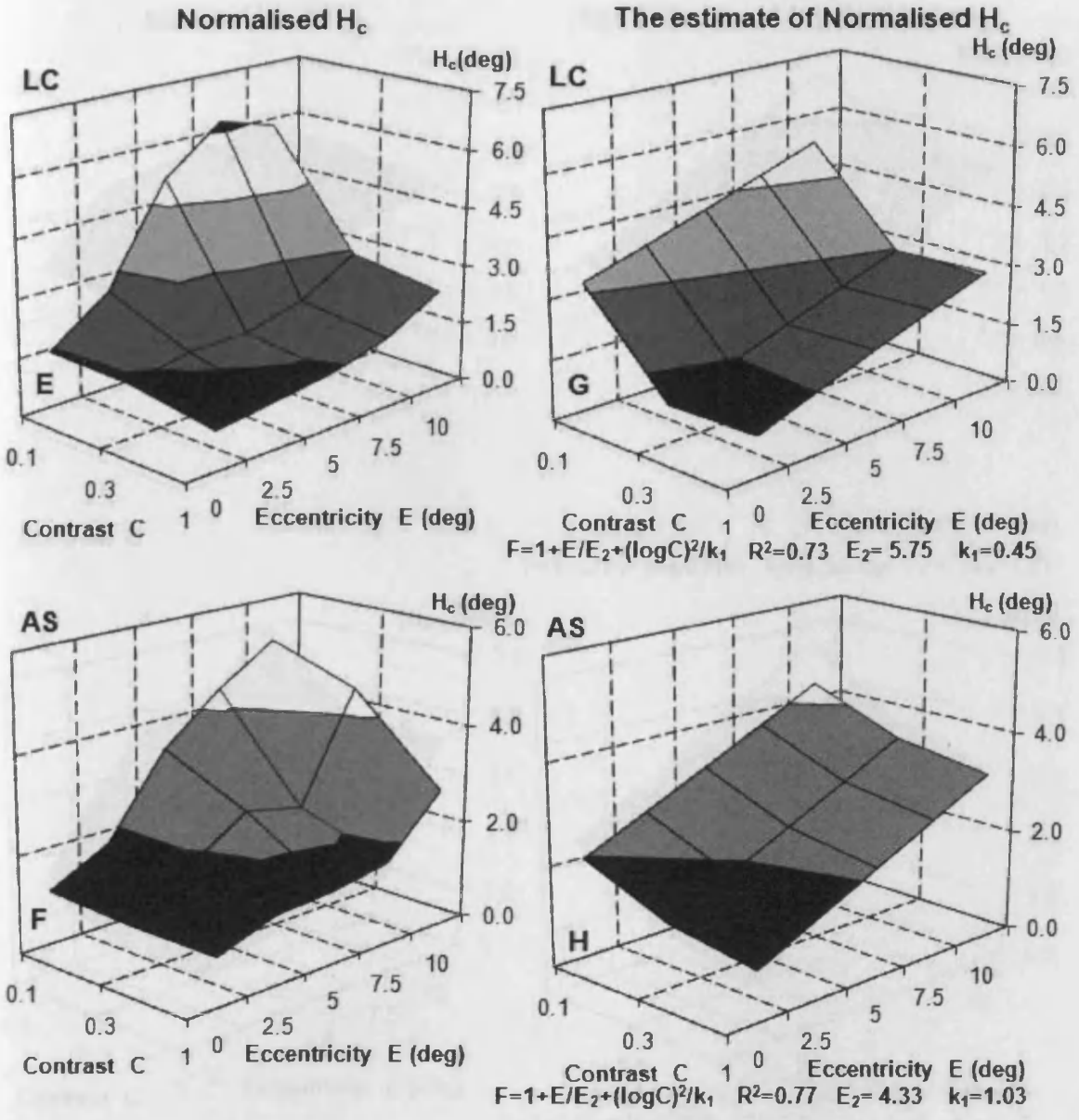

Fig 5.9a (E-H) Empirical (left column) and modelled (right column) horizontal scaling surfaces, the normalised H_c, of the 2cpi gratings for both subjects LC and AS. Other details are as in Fig 5.9a (A-D).

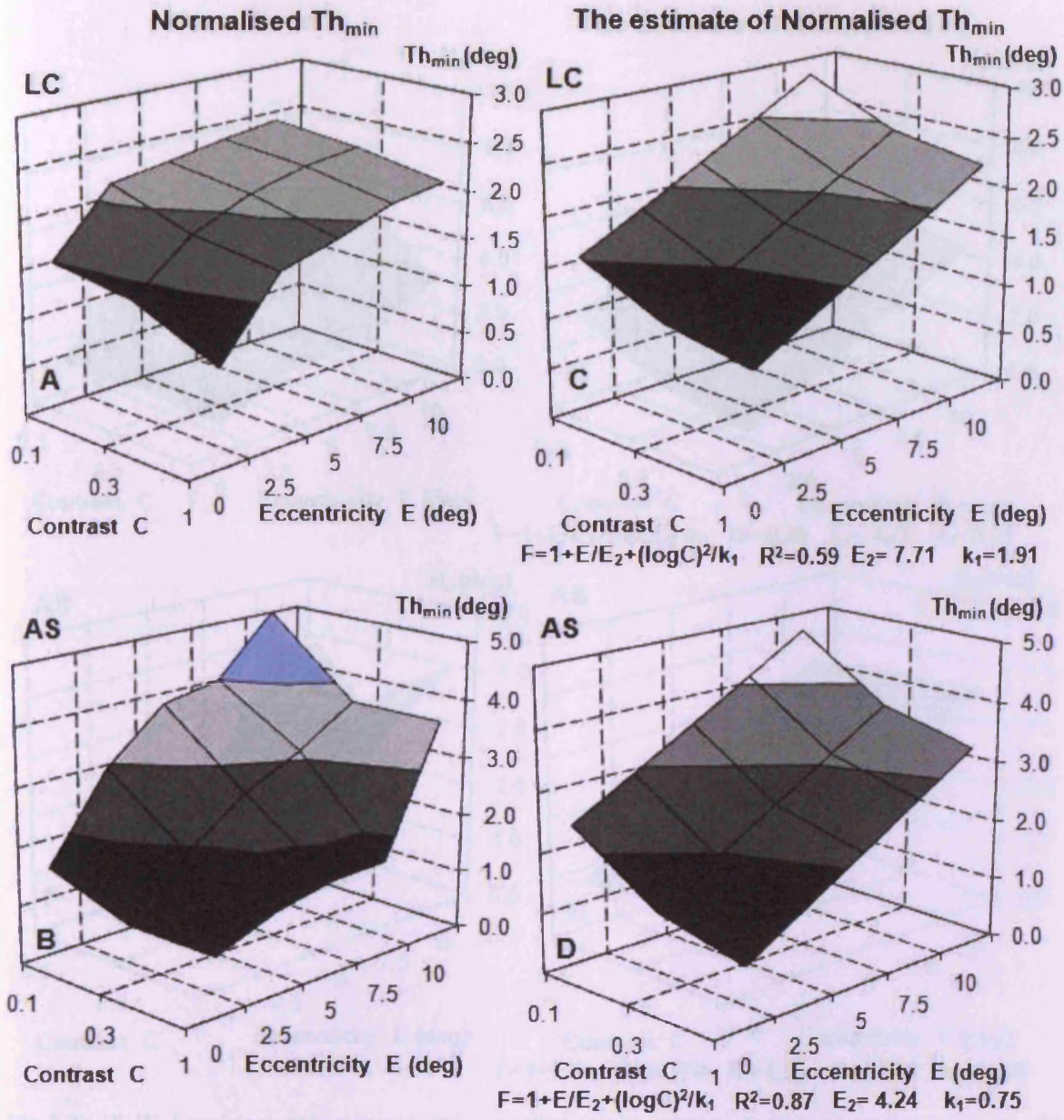

Fig 5.9b (A-D) Empirical (left column) and modelled (right column) vertical scaling surfaces, the normalised Th_{min}, of the 16cpi gratings for subjects LC and AS. Other details are as in Fig 5.9a (A-D).

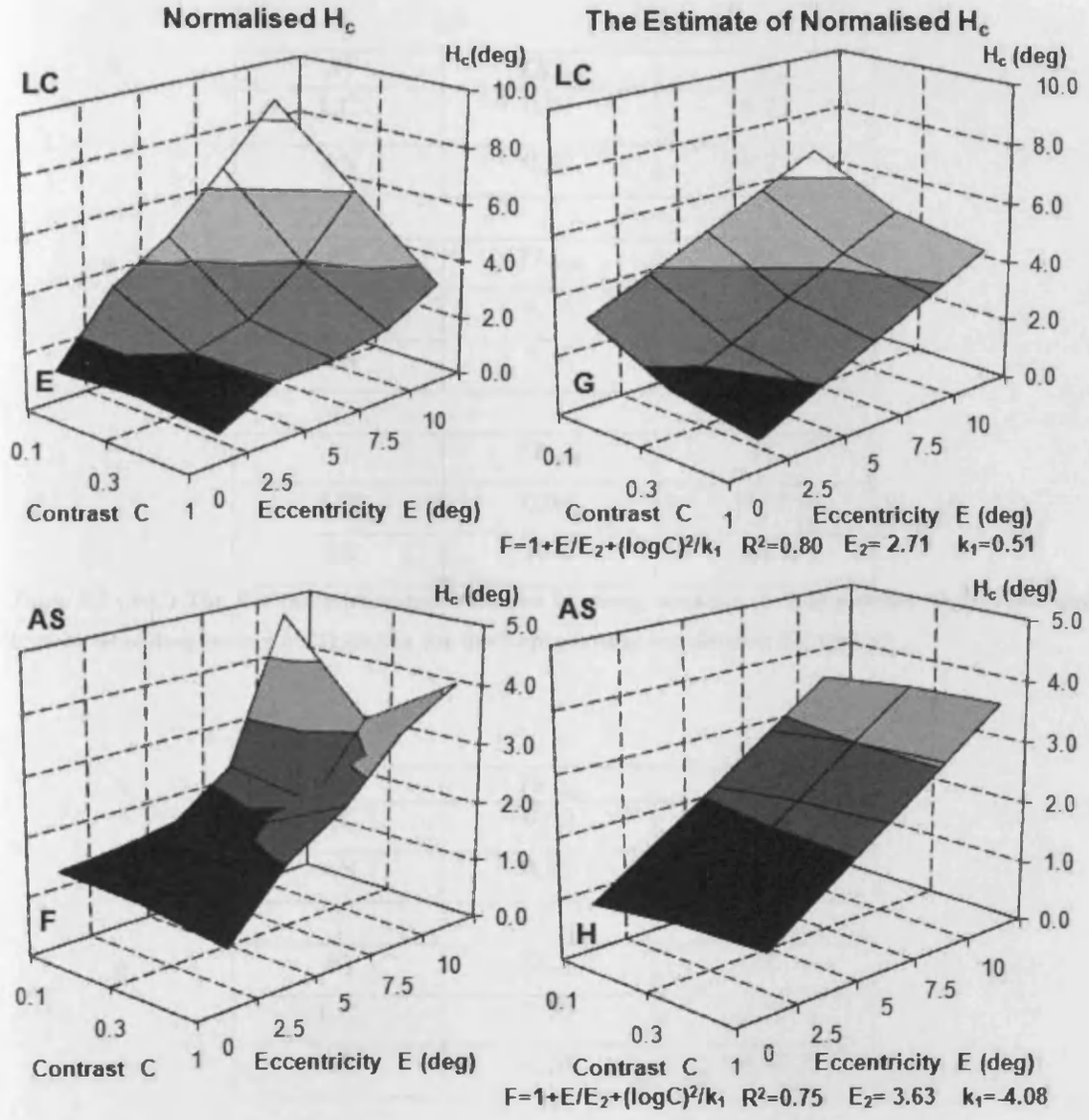

Fig 5.9b (E-H) Empirical (left column) and modelled (right column) horizontal scaling surfaces, the normalised H_c, of the 16cpi gratings for subjects LC and AS. Other details are as in Fig 5.9a (A-D).

Tables 5.3 and 5.4 show the parameters and R^2s obtained by using equation (5.4) to model both the vertical and horizontal scaling surface, normalised $Th_{\min}$ and normalised H_c, for the 2 and 16cpi gratings, respectively.

A

R^2	Th_{min}	H_c
LC	0.91	0.73
AS	0.82	0.77

B

E_2	Th_{min}	H_c
LC	6.36	5.75
AS	7.24	4.33

C

k_1	Th_{min}	H_c
LC	0.64	0.45
AS	1.06	1.03

Table 5.3 (A-C) The R^2s and parameters obtained by using equation (5.4) to estimate the vertical and horizontal scaling factors of 2D scaling for the 2 cpi gratings for subjects LC and AS.

A

R^2	Th_{min}	H_c
LC	0.59	0.80
AS	0.87	0.75

B

E_2	Th_{min}	H_c
LC	7.71	2.71
AS	4.24	3.63

C

k_1	Th_{min}	H_c
LC	1.91	0.51
AS	0.75	-4.08

Table 5.4 (A-C) The R^2s and parameters obtained by using equation (5.4) to estimate the vertical and horizontal scaling factors of 2D scaling for the 16 cpi gratings for subjects LC and AS.

By using the estimated vertical (normalised Th_{min}) and horizontal (normalised H_c) scaling surfaces in Fig 5.9a (C, D, G, H), all the original experimental threshold data for the 2cpi

gratings shown in Fig 5.5, were superimposed onto the foveal 100% contrast data (E=0, C=1) in Fig 5.10. The R^2 of the best fit to the superimposed threshold data was calculated to demonstrate how well the 2D scaling equates performance across eccentricities and contrasts. The scaling surfaces in Fig 5.9b (C, D, G, H) were applied in similar way to the original threshold data of the 16cpi grating data shown in Fig 5.6 and the 2D scaling results are shown in Fig 5.11.

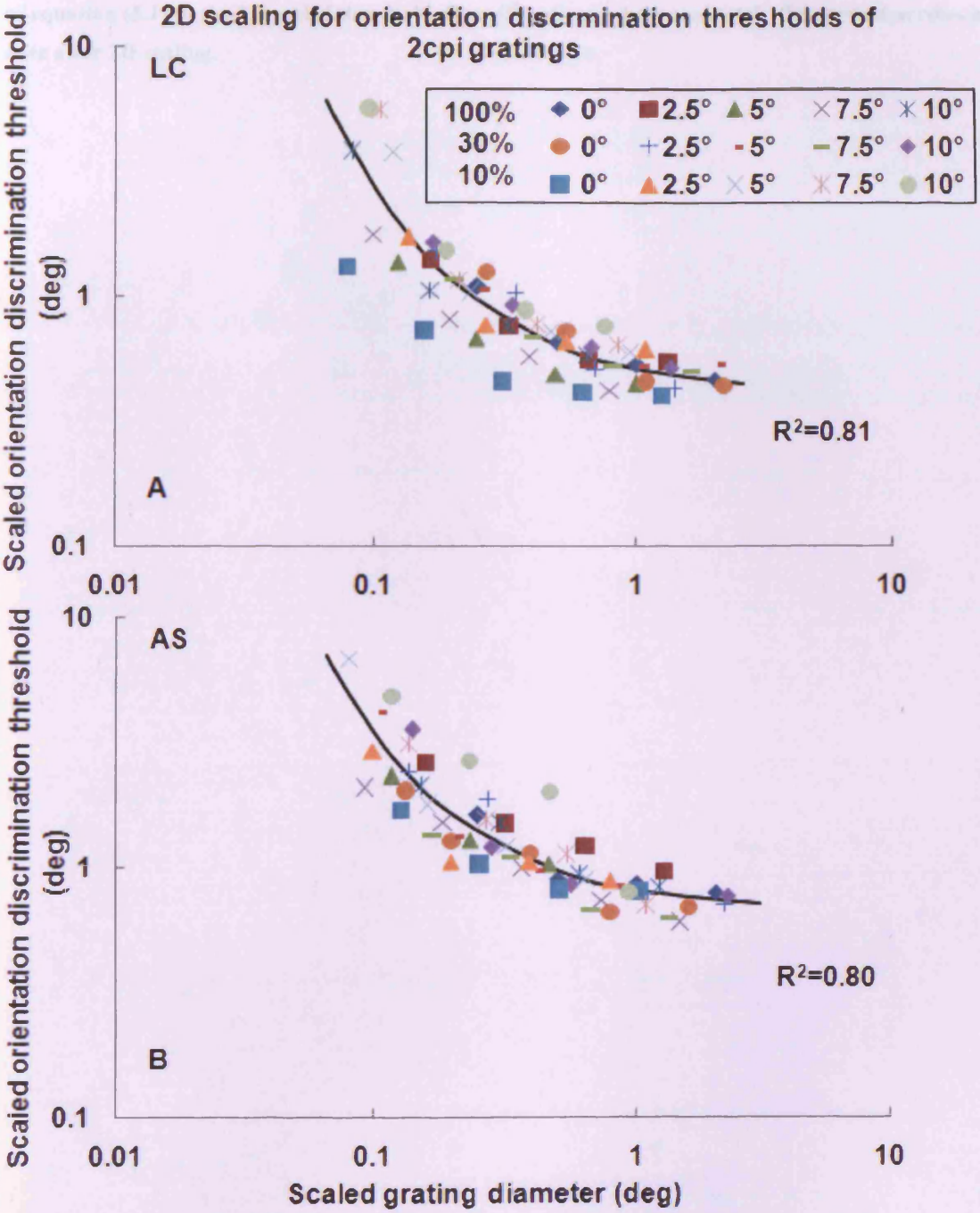

Fig 5.10 (A-B) The 2D scaled orientation discrimination thresholds for the 2cpi gratings

The original discrimination threshold data of the 2cpi gratings from Fig 5.5 (A-B) were both vertically and horizontally scaled by means of the estimated 2D scaling surfaces of Fig 5.9a (C, D, G, H). Data from the eccentricities of 0-10 deg and contrasts of 10-100% collapsed onto the foveal 100% contrast data (E=0, C=1). The data for subjects LC and AS are as indicated. The smooth curve was the best fit

of equation (5.1) to the 2D scaled threshold data. R^2 indicates how accurately the curve describes all the data after 2D scaling.

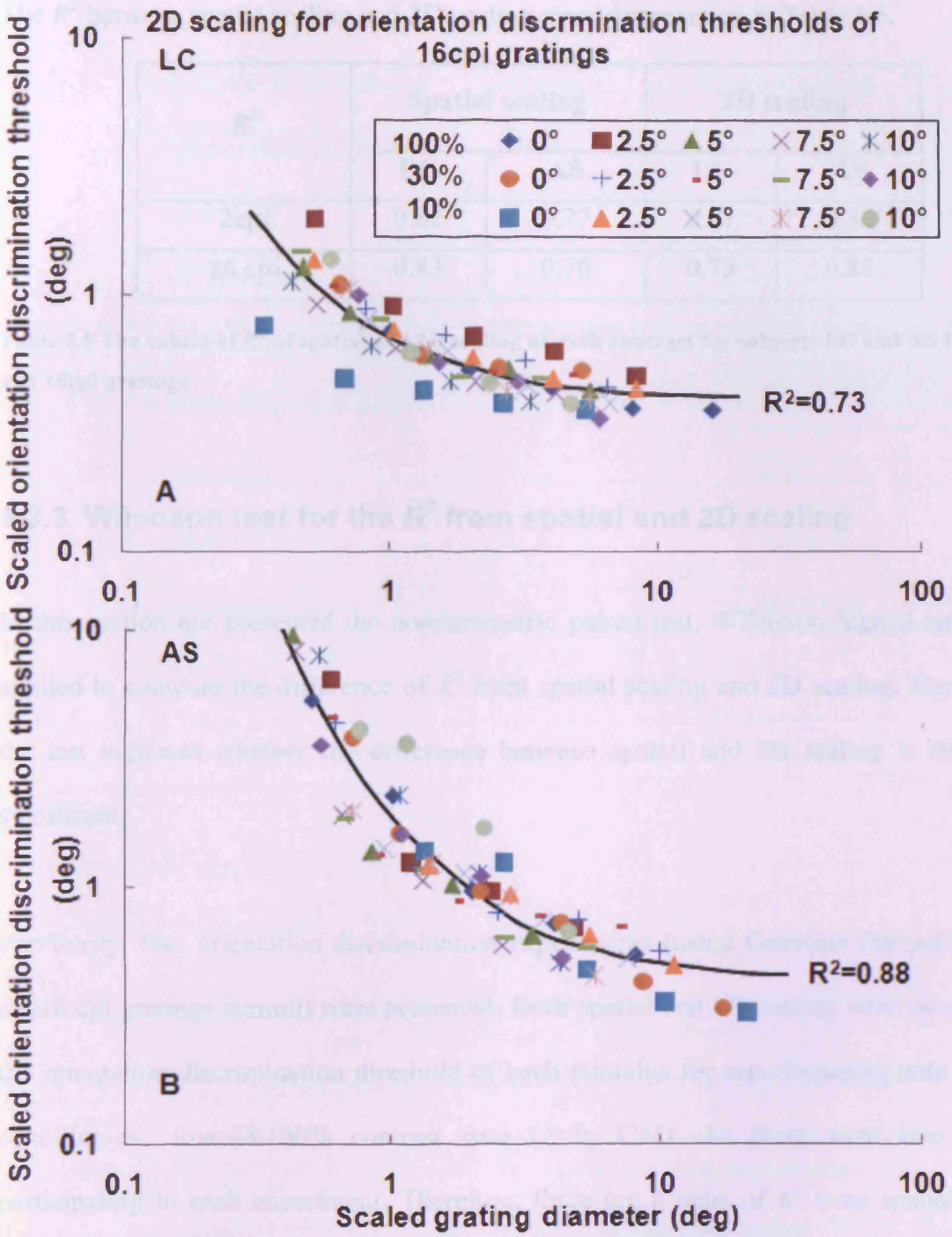

Fig 5.11 (A-B) The 2D scaled orientation discrimination thresholds for the 16cpi gratings

The original discrimination threshold data of the 16cpi gratings from Fig 5.6 (A-B) were both vertically and horizontally scaled by means of the estimated 2D scaling surfaces of Fig 5.9a (C, D, G, H). Other details are as in Fig 5.10 (A-B).

The R^2 between spatial scaling and 2D scaling were summarized in Table 5.5.

R^2	Spatial scaling		2D scaling	
	LC	AS	LC	AS
2cpi	0.82	0.77	0.81	0.80
16 cpi	0.83	0.76	0.73	0.88

Table 5.5 The values of R^2 of spatial and 2D scaling at each contrast for subjects LC and AS for the 2 and 16cpi gratings

5.3.3 Wilcoxon test for the R^2 from spatial and 2D scaling

In this section are presented the nonparametric paired test, Wilcoxon Signed-ranked test, applied to compare the difference of R^2 from spatial scaling and 2D scaling. The result of the test indicates whether the difference between spatial and 2D scaling is statistically significant.

Previously, four orientation discrimination experiments (using Gaussian filtered lines, 2,4 and16 cpi gratings stimuli) were presented. Both spatial and 2D scaling were used to scale the orientation discrimination threshold of each stimulus for superimposing onto its basic condition-the foveal&100% contrast data (E=0, C=1). As there were two subjects participating in each experiment. Therefore, there are 8 pairs of R^2 from spatial and 2D scaling, shown in Table 5.6.

Subject & Stimulus	2D scaling	Spatial scaling
LC& Gaussian line	0.89	0.82
LC&2cpi	0.81	0.82
LC&4cpi	0.86	0.74
LC&16cpi	0.73	0.83
VR& Gaussian line	0.84	0.61
AS&2cpi	0.80	0.77
AS&4cpi	0.91	0.82
AS&16cpi	0.88	0.76
Average	0.82	0.77

Table 5.6 The 8 paired of R^2s resulting from spatial and 2D scaling

The hypotheses of the test are:

4) The null hypothesis H_0: the R^2 resulting from 2D scaling is as good as that of spatial scaling,

5) H_1: the R^2 resulting from 2D scaling is better than that of spatial scaling.

The value of Wilcoxon test statistic was found to be 6 and the significance level p obtained was 0.11. It is greater than the critical value 5 (for 8 paired data set) needed for the Wilcoxon test at the 5% significance level, which suggests that we can accept the null hypothesis H_0, i.e. that the R^2 of 2D scaling is not significantly better than that of spatial scaling at the 5% significance level.

5.3.4 Spatial scaling E_2 across contrasts and cpi

In Table 5.7, the values of global spatial scaling E_2 obtained by spatial scaling across contrasts were summarised for all subjects and stimuli. (According to the configuration of the Gaussian line stimulus, it is regarded as **0.5** cpi grating for the convenience of data analysis.) From the table, the spatial E_2 tends to decrease with increasing cpi. To show the tendency clearly, E_2 and its average between subjects were plotted as a function of cpi in Fig 5.12.

cpi	0.5	2	4	16
LC	3.21	3.27	1.76	1.39
VR&AS	5.61	1.76	1.71	1.57
Average	4.41	2.515	1.735	1.485

Table 5.7 The global spatial E_2 at each cpi for different subjects

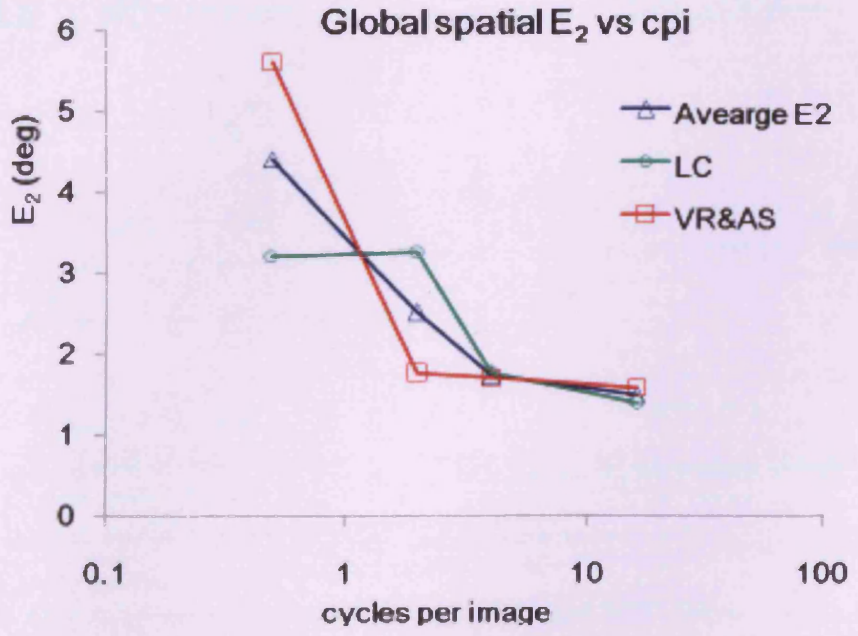

Fig 5.12 (A-B) The global spatial E_2s for subjects and their average between subjects plotted as a function of cpi

Note that the Gaussian filtered line was regarded as 0.5cpi grating.

5.3.5 Spatial scaling at individual contrast

By individual contrast, the eccentric threshold curves at each contrast were shifted to superimpose onto the fovea curve from the same contrast level by spatial scaling in this section.

Fig 5.13 (for 2cpi gratings) and Fig 5.14 (for 16 cpi gratings) show preliminary spatial scaling factors at each contrast level, which were obtained at each eccentricity through the procedure of spatial scaling (see Chapter 1 Section 1.3) separately at each contrast. An optimal linear function was fitted to these factors through (0, 1) at each contrast. The R^2 of the fit to the preliminary factors was calculated and shown in each sub graph of these figures. The final spatial scaling factor at each eccentricity and contrast was determined by the linear function.

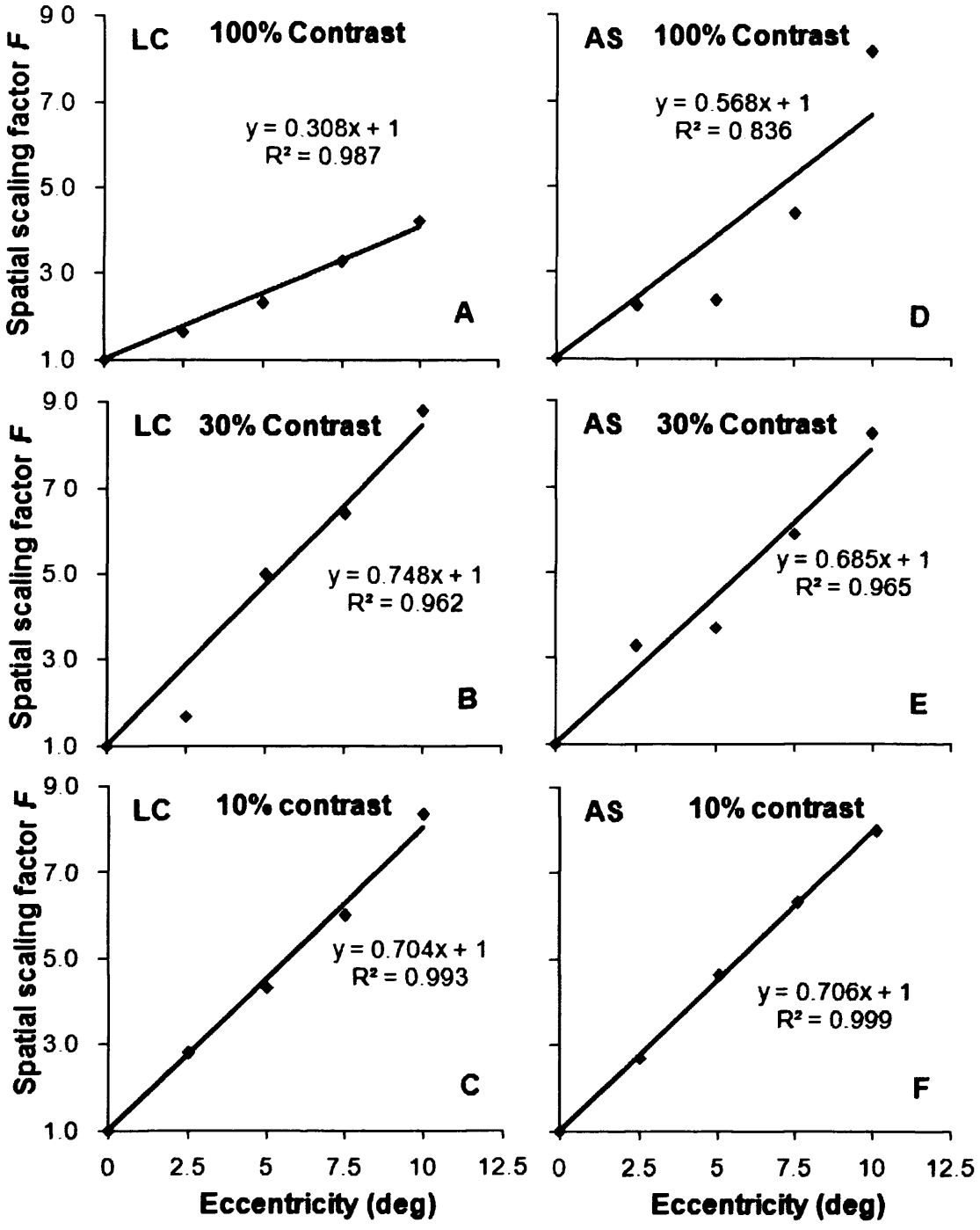

Fig 5.13 (A-F) Spatial scaling factors as a function of eccentricity at each contrast for 2cpi gratings

At each eccentricity and contrast, a preliminary spatial scaling factor (■) was obtained through the spatial scaling procedure previously described in Chapter 1 Section 1.3. At each contrast, the scaling factors were fitted through (0, 1) by an optimal linear function with its fit R^2, shown in each graphs. Subjects LC and AS are as indicated.

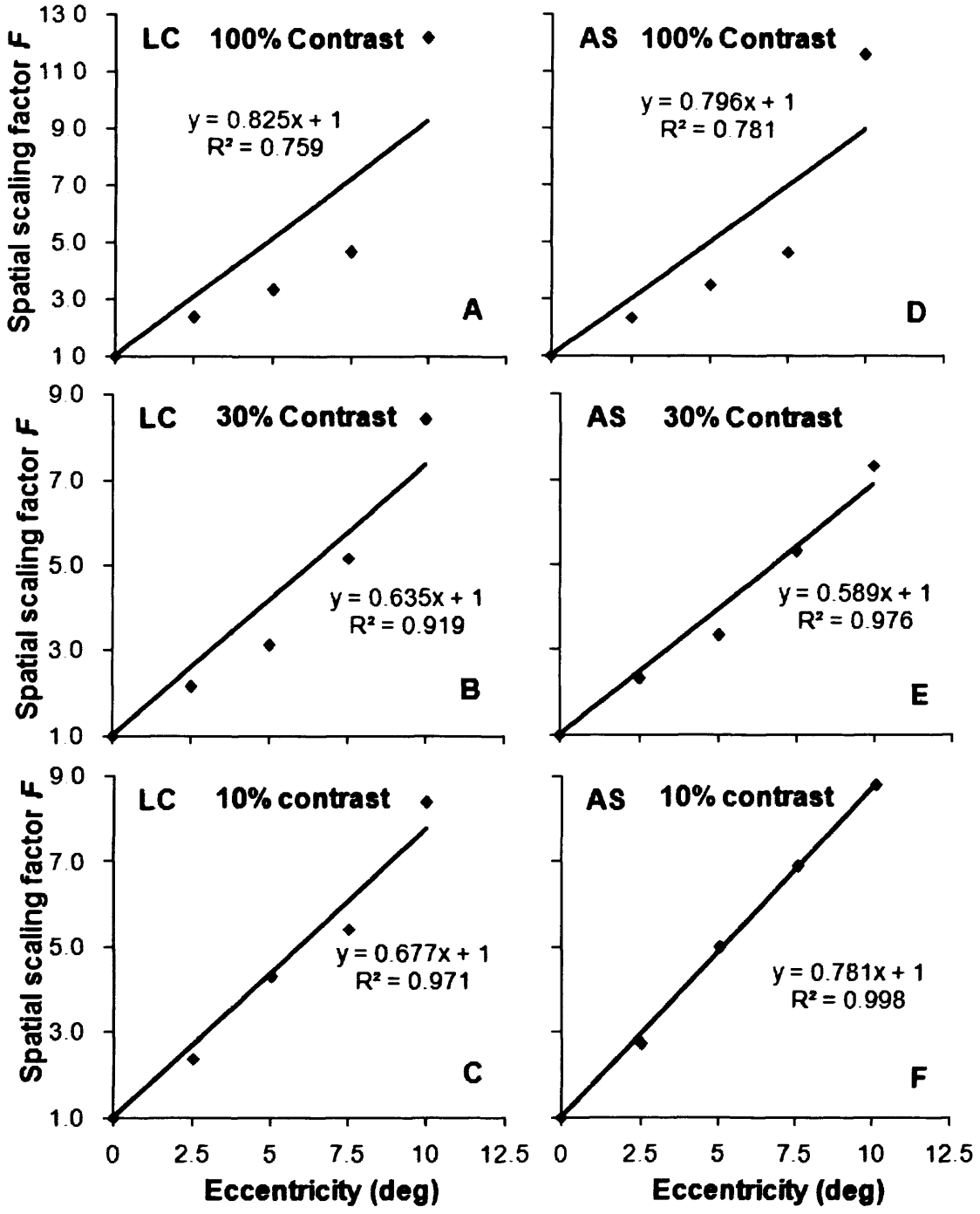

Fig 5.14 (A-F) Spatial scaling factors as a function of eccentricity at each contrast for 16cpi gratings

At each eccentricity and contrast, a preliminary spatial scaling factor (■) was obtained through the spatial scaling procedure previously described in Chapter 1 Section 1.3. At each contrast, the scaling factors were fitted through (0, 1) by an optimal linear function with its fit R^2, shown in each graphs. Subjects LC and AS are as indicated.

The spatial E_{2c} at each contrast was calculated as the inverse of the slope of the corresponding linear function of Figs 5.13 and 5.14 and shown in Tables 5.8 and 5.9 for 2 and 16cpi gratings, respectively.

Table 5.8 Spatial E_{2c} at each contrast for 2cpi gratings

E_{2c}	LC	AS	Average
100%	3.25	1.76	2.51
30%	1.34	1.46	1.40
10%	1.42	1.42	1.42

Table 5.9 Spatial E_{2c} at each contrast for 16cpi gratings

E_{2c}	LC	AS	Average
100%	1.21	1.26	1.21
30%	1.57	1.70	1.57
10%	1.50	1.28	1.50

In Figs 5.15 and 5.16 are shown the E_{2c} from each subject and its average between subjects, for 2 and 16cpi gratings, respectively.

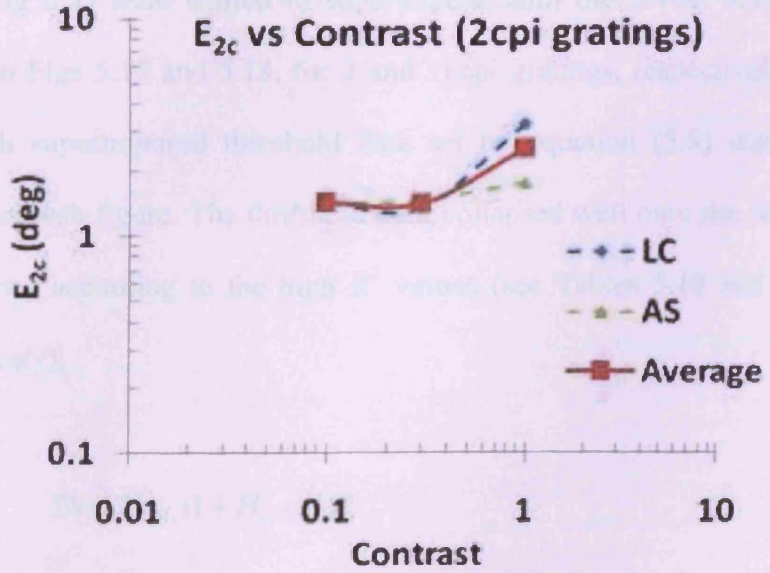

Fig 5.15 Spatial E_{2c} plotted as a function of contrast for subjects LC and AS for 2cpi gratings.

The blue dash smooth curve is the function of E_{2c} vs. contrast for LC. The green one is for AS. The average E_{2c} between subjects is plotted against contrast with the red solid smooth curve.

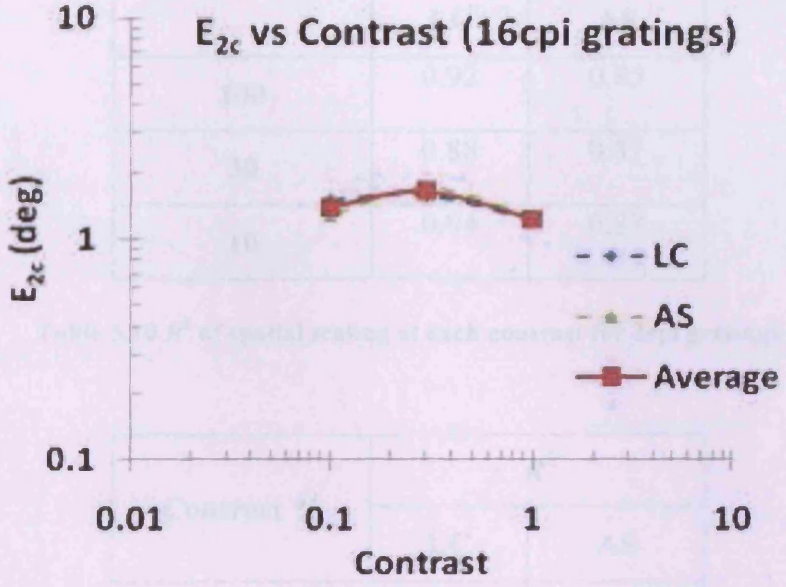

Fig 5.16 Spatial E_{2c} plotted as a function of contrast for subjects LC and AS for 16cpi gratings. The details are as in Fig 5.15.

At each contrast, by spatial scaling, the orientation discrimination threshold data at each contrast (see Fig 5.3) were shifted to superimpose with the foveal data from the same contrast level in Figs 5.17 and 5.18, for 2 and 16cpi gratings, respectively. The R^2 of the best fit to each superimposed threshold data set by equation (5.5) was calculated and displayed in each sub figure. The threshold data collapsed well onto the foveal curve from the same contrast according to the high R^2 values (see Tables 5.10 and 5.11, for 2 and 16cpi, respectively).

$$Th = Th_{\min}(1 + H_c / H)^p \qquad \textbf{Equation 5.5}$$

Contrast %	R^2	
	LC	AS
100	0.92	0.85
30	0.88	0.87
10	0.94	0.87

Table 5.10 R^2 of spatial scaling at each contrast for 2cpi gratings

Contrast %	R^2	
	LC	AS
100	0.89	0.91
30	0.93	0.88
10	0.85	0.84

Table 5.11 R^2 of spatial scaling at each contrast for 16cpi gratings

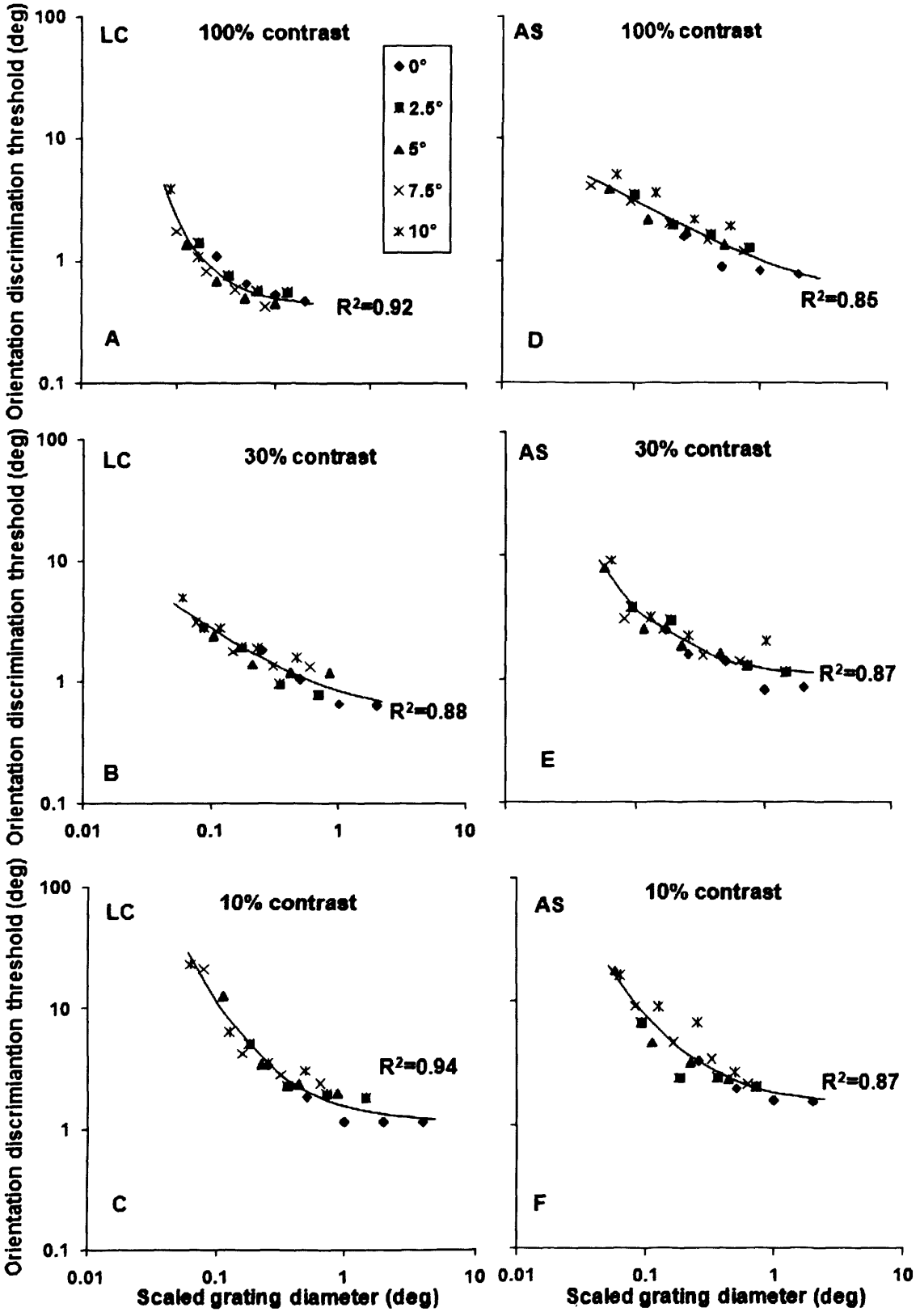

Fig 5.17 Spatial scaling of orientation discrimination threshold at each contrast for 2cpi gratings

At each contrast, the eccentric orientation discrimination threshold curves at each contrast (shown in Fig 5.3a) were horizontally shifted to superimpose onto each fovea curve by final spatial scaling factors calculated by using the corresponding linear functions in Fig 5.15. The smooth curve was the best fit to each scaled threshold set at each contrast by equation (5.5). Data collapsed well onto the foveal curve at each contrast, indicated by the high R^2 values.

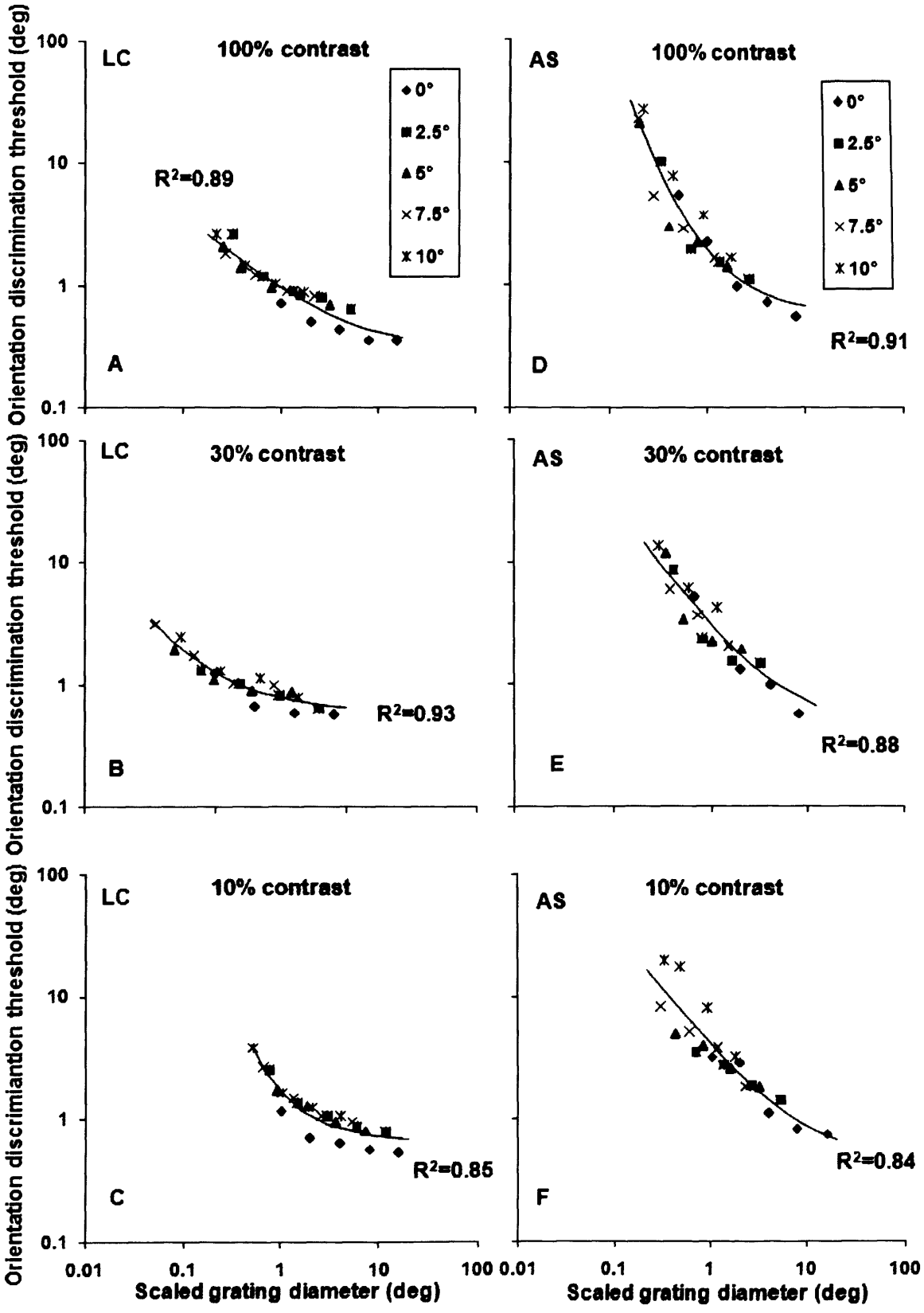

Fig 5.18 Spatial scaling of orientation discrimination threshold at each contrast for 16cpi gratings

At each contrast, the eccentric orientation discrimination threshold curves at each contrast (shown in Fig 5.3b) were horizontally shifted to superimpose onto each fovea curve by final spatial scaling factors calculated by using the corresponding linear functions in Fig 5.16. The smooth curve was the best fit to each scaled threshold set at each contrast by equation (5.5). Data collapsed well onto the foveal curve at each contrast, indicated by the high R^2 values.

5.3.6 Individual spatial scaling E_{2c} and contrast

In Table 5.12 was summarized spatial scaling E_{2c}s obtained at each contrast for all types of stimuli (Gaussian filtered lines, 2, 4, and 16cpi). The average of E_{2c}s across contrasts ranges from 1.48 to 2.53 and from 1.41 to 2.54 deg across stimuli, which are similar to the previous findings in literature (Makela *et al.* 1993, Paradiso and Carney 1988; Sally and Gurnsey 2003; see Chapter 1 Section 1.3 Table 1.2) Further, E_{2c} and its average for all stimuli were plotted as a function of contrast in Fig 5.19.

LC	100%	30%	10%	Average
Gaussian lines	2.79	2.70	1.78	2.42
2cpi	3.25	1.34	1.42	2.00
4cpi	2.88	3.25	1.50	2.54
16cpi	1.21	1.57	1.50	1.43
Average	2.53	2.21	1.55	
VR&AS	**100%**	**30%**	**10%**	**Average**
Gaussian lines	1.68	0.82	2.50	1.67
2cpi	1.76	1.46	1.42	1.55
4cpi	1.61	1.81	1.92	1.78
16cpi	1.26	1.70	1.28	1.41
Average	**1.58**	**1.45**	**1.78**	

Table 5.12 E_2 of spatial scaling at each contrast for all stimuli and subjects

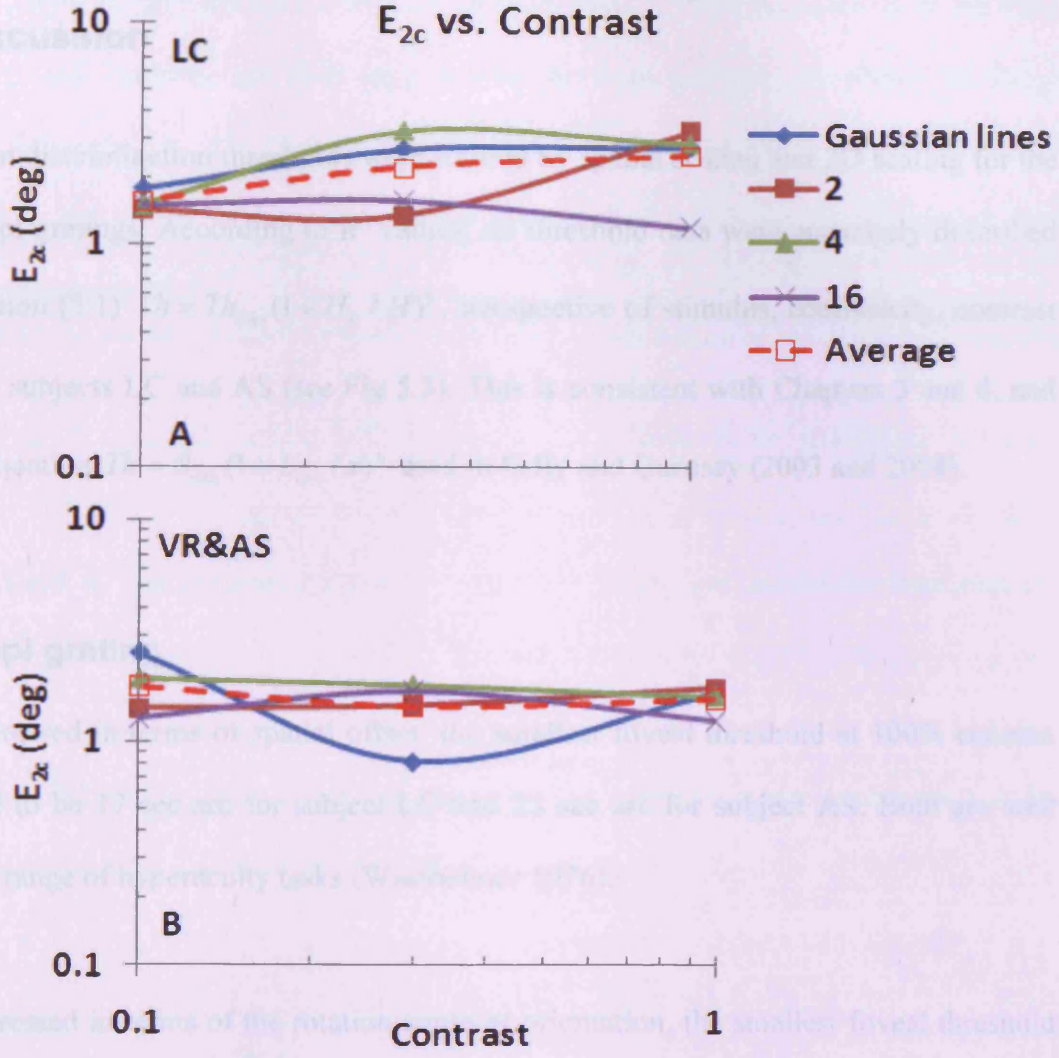

Fig 5.19 Spatial E_{2c}&its averages plotted as a function of contrast for all types of stimuli and subjects. Each E_{2c} data curve is indicated with a unique symbol and color.

5.4 Discussion

Orientation discrimination thresholds were studied by spatial scaling and 2D scaling for the 2 and 16cpi gratings. According to R^2 values, all threshold data were accurately described with equation (5.1) $Th = Th_{\min}(1 + H_c / H)^5$, irrespective of stimulus, eccentricity, contrast or cpi, for subjects LC and AS (see Fig 5.3). This is consistent with Chapters 3 and 4, and with the equation $Th = \theta_{\min}(1 + L_{crit} / x)^n$ used in Sally and Gurnsey (2003 and 2004).

5.4.1 2cpi grating

When expressed in terms of spatial offset, the smallest foveal threshold at 100% contrast was found to be 17 sec arc for subject LC and 25 sec arc for subject AS. Both are well within the range of hyperacuity tasks (Westheimer 1976).

When expressed in terms of the rotation angle of orientation, the smallest foveal threshold at 100% contrast averaged between subjects was 0.64 deg (0.45 deg for LC and 0.79 deg for AS) and similar to 0.45 deg threshold for 4 cpi grating in Chapter 5, 0.5 deg of Makela *et al.* (1993) and 0.6 deg of Westheimer *et al.* (1999), and 0.56 deg of Sally and Gurnsey (2003) and 0.7 deg found by Bowne (1990).

In modelling spatial scaling factors with equation (5.3), spatial E_2 are 3.27 deg for LC and 1.76 deg for AS (see Table 5.1), with an average 2.52 deg which is similar to 2.4 deg of

Paradiso and Carney (1988) (estimated by Makela in 1994) and 1.93 deg of Makela *et al.* (1993). k_1, representing the sole effect of contrast, and k_3, the interaction term between eccentricity and contrast, are both very similar between subjects, as shown in Table 5.1(C,D). According to R^2s of 0.97 for LC and 0.91 for AS shown in Table 5.1 the modelling of the spatial scaling factor as a function of eccentricity and contrast was accurate by equation (5.3).

In modelling 2D scaling factors with equation (5.4), there is no interaction between eccentricity and contrast, in agreement with the Gaussian filtered lines and 4cpi gratings in Chapters 3 and 4. The horizontal E_2s shown in Table 5.3(B) are similar for both subjects (5.75 for LC and 4.43 deg for AS) scaling. The same is true for the vertical E_2s (6.36 deg for LC and 7.24 deg for AS). In Table 5.3 (C) k_1 represents the effect of contrast on modelling of 2D scaling factors and its values are very similar within each subject (0.64 and 0.45 for LC; 1.06 and 1.03 for AS). On the basis of R^2 values of 0.73-0.91 in Table 5.3(A), the modelling of 2D scaling factors was reasonable for subjects LC and AS.

According to R^2 (ranging from 0.85 to 0.94, see Table 5.10), by spatial scaling, the peripheral orientation discrimination performance (at 0-10 deg eccentricity) was successfully equated with that of the fovea at each contrast. This further confirms that the difference of the visual task between the fovea and periphery is quantitative but not qualitative. Spatial scaling E_{2c} found at each contrast ranges from 1.42 to 2.51 deg (Table 5.8), which is similar to the previous findings in literature (see Chapter 1 Section 1.3 Table 1.2). E_{2c}s are similar between subjects (see Fig 5.15). At 100% contrast, the average E_{2c} is slightly higher than those of other contrasts, which is a bit different from the findings of E_2

being independent of contrast for Gaussian filtered lines (see Chapter 3 Fig 3.10) and 4cpi grating (see Chapter 4 Fig 4.10).

5.4.2 16cpi grating

When expressed in terms of spatial offset, the smallest foveal threshold at 100% contrast was found to be 45 sec arc for LC, which is well within the range of hyperacuity tasks (Westheimer 1976). However, the smallest foveal threshold was 121 sec arc for AS, which is not in the range of hyperacuity.

When expressed in terms of the rotation angle of orientation, the average smallest foveal threshold at 100% contrast between subjects was 0.45 deg (0.35 deg for LC and 0.54 deg for AS). It was the same as 0.45 deg threshold of the 4cpi grating and similar to 0.64 deg threshold of the 2cpi gratings.

Equation (5.3) was used to model the spatial scaling factors depending on both eccentricity and contrast. Spatial E_2 (see Table 5.2(B)) was found to be really similar between subjects (1.39 deg for LC and 1.57 deg for AS), averaging 1.43 deg, which are almost the same as 1.51 deg of Sally and Gurnsey (2003), and similar to 1.93 deg of Makela *et al.* (1993). According to equation (5.3), eccentricity and contrast interact for 16cpi gratings as for the 2 and 4cpi gratings and Gaussian filtered lines. Judging by R^2s of 0.82 for LC and 0.83 for AS shown in Table 5.4(A), the spatial scaling factor was successfully modelled by equation (5.3).

In modelling 2D scaling factors with equation (5.4), there is again no interaction between eccentricity and contrast. The horizontal E_2s shown in Table 5.4(B) are similar between subjects (2.71 deg for LC and 3.63 deg for AS). The modelling of normalised Th_{min} of subject LC by equation (5.4) is poor according to its R^2 value of 0.59 shown in Table 5.4 (A). The reason for the poor results of modelling is the fact that the scaling surface of Th_{min} is too flat to be modelled, compared with other surfaces. During the experiment, subject LC subjectively found that the threshold collection became suddenly more difficult when the 16cpi grating stimulus was present in the further periphery, i.e. 7.5 and 10 deg eccentricity.

According to R^2 (ranging from 0.84 to 0.93, see Table 5.11), the peripheral orientation discrimination performance (at 0-10 deg eccentricities) was successfully equated with that of the fovea at each contrast by spatial scaling. Therefore, the difference of the orientation discrimination task between the fovea and periphery is not qualitative. Spatial scaling E_{2c} found at each contrast ranges from 1.21 to 1.70 deg (Table 5.9), which is similar to (but a bit smaller than) the previous findings in literature (see Chapter 1 Section 1.3 Table 1.2). E_{2c}s are almost the same between subjects (see Table 5.9 and Fig 5.16). For each subject, the E_{2c} was found to be independent of contrast. This is in agreement with the findings in the previous chapter for Gaussian filtered lines (see Chapter 3 Fig 3.10) and 4cpi grating (see Chapter 4 Fig 4.10).

5.4.3 Spatial scaling and 2D scaling across contrasts

Both spatial and 2D scaling were generally successfully used to superimpose the orientation discrimination threshold onto the foveal 100% contrast discrimination data for each type stimulus, the Gaussian filtered lines, 2, 4 and 16cpi gratings (their R^2s is greater than 0.70 in Table 5.6), except for the spatial scaling applied to superimpose the threshold data of the Gaussian filtered lines for subject VR (with a R^2 of 0.61).

According to the R^2s obtained for different stimuli, 2D scaling generally performed better than spatial scaling. (The average of R^2s for 2D scaling is 0.82 and 0.77 for spatial scaling.) However, based on the Wilcoxon Sign-Ranked test conducted in Section 5.3.3, the difference of R^2 between spatial and 2D scaling is not statistically significant even at 5% level. It suggests that spatial scaling alone is good enough to equate the peripheral orientation discrimination performance to the foveal one, and the fovea is not qualitatively different from the periphery, in agreement with Makela *et al.* (1993), Makela *et al.* (1997), Levi *et al.* (2000a), Vakrou *et al.* (2007), Whitaker *et al.* (1992) and Whitaker *et al.* (1993). It proves the 1st hypothesis made in Chapter 1 Section 1.5.2.

The spatial E_2s are generally smaller than horizontal E_2s of 2D scaling due to the simultaneously applied vertical scaling (see Table 5.13 below).

	Global Spatial E_2	Horizontal E_2 of 2D scaling
LC&Gaussian	3.21	4.93
VR&Gaussian	5.61	4.02
LC&2cpi	3.27	5.77
AS&2cpi	1.76	4.61
LC&4cpi	1.76	5.75
AS&4pi	1.71	4.33
LC&16cpi	1.39	2.71
AS&16cpi	1.58	3.63
Average	**2.54**	**4.47**

Table 5.13 The comparison of Spatial E_2 of spatial scaling and Horizontal E_2 of 2D scaling

Comparing the equations used in spatial scaling and 2D scaling to model the dependency of the scaling factors on eccentricity and contrast, an interaction between eccentricity and contrast exists for modelling spatial scaling factors but not for modelling 2D scaling horizontal scaling factors for all types of stimuli. From this point of view, the vertical scaling of 2D scaling could be seen to compensate for the loss of the interaction term (*ExlogC*) in the horizontal scaling.

5.4.4 Cpi and global spatial scaling E_2

As Table 5.7 and Fig 5.12 show, the global spatial E_2 drops sharply with increasing cpi and tends to reach a plateau as the cycle number is greater than 4. The result suggests that cpi has a stronger effect on the orientation threshold performance when the cycle number is smaller; while as cpi increases to greater than 4, the effect becomes weaker and tends to reach to the same, which proves the 2nd hypothesis in Chapter 1 Section 1.5.2, *i.e.*, for low-cycle number gratings, the number of cycles played a crucial role on the visual performance across visual field. This resembles to some earlier spatial integration studies in which it was found out that the contrast sensitivity first increased with cpi but then saturated (e.g. Hoekstra, van der Goot, van den Brink, and Bilsen 1974; Jamar and Koenderink 1983; Savoy and McCann 1975 and Virsu *et al.* 1978).

5.4.5 Spatial scaling and E_{2c} by individual contrast

No matter what stimuli, subject, and contrast, the peripheral orientation discrimination performance could be equated with that of the fovea by spatial scaling. It proves that the peripheral performance is only quantitatively different from that of fovea in this visual task.

E_{2c} found is generally about 2 deg, which is similar to the findings in literature. Its average between subjects is almost independent of contrast (see Fig 5.19). The independency of E_{2c} against contrast, which was found for all types of stimuli in Chapters 3-5, answers the question in Chapter 1 Section 1.5.2, *i.e.*, that the contrast-dependent size change of the V1

neuron receptive field caused by contrast reduction are not different between the foveal and peripheral visual field.

Chapter 6 Contrast threshold allowing fixed orientation difference discrimination for Gaussian filtered lines

6.1 Introduction

In Chapter 3 the effects of contrast and eccentricity on orientation discrimination were investigated as a function of stimulus length for Gaussian filtered lines by conducting orientation discrimination experiments at contrasts of 100, 30, and 10% and eccentricities of 0-10 deg. To carry on the investigation of the effect of contrast on orientation discrimination, we first intended to further measure orientation discrimination threshold at the contrast lower than 10%. However, the direct threshold measurement even at 5% contrast was not applicable at the eccentricities over 5 deg due to the lack of stimulus size.

Therefore, the experiments in this and the following two chapters, *i.e.* in Chapters 6-8 were redesigned. The relationship between orientation, contrast, and eccentricity was investigated further from another point of view, namely by measuring threshold contrasts allowing discrimination of constant orientation differences of 45, 15, 5, and 1.5 deg between stimuli, instead of orientation discrimination at constant contrasts as in Chapters 3-5. The effects of eccentricity (0-10 deg) and orientation difference (45-1.5 deg) on contrast threshold were modelled and the accuracy of the model was tested by superposition of all contrast threshold data using spatial scaling across contrasts and within individual contrast, and 2D scaling.

The performance of spatial and 2D scaling across contrasts was compared to examine whether the thresholds can be equated across eccentricities and orientation differences by the single size scaling, i.e. spatial scaling.

Further by comparing E_2 found at each orientation difference by spatial scaling, we examined whether the visual process of the task at large orientation difference (45 deg) was different from that of small orientation difference near the orientation discrimination threshold (1.5 deg).

6.1.1 Various types of contrast threshold measurements in literature

Contrast thresholds for detecting a stimulus and for discriminating between the values of a stimulus feature (for example, orientation or motion.) are different. When measuring contrast threshold for discrimination, the subject has to discriminate one stimulus from another when the two stimuli differ in terms of a stimulus feature but are otherwise similar (for example, a vertical line and a line tilted 45 deg counter-clockwise with the same size and at the same contrast). As the subject first has to be able to see the stimuli and then discriminate between them, contrast detection threshold cannot be higher than the absolute threshold allowing discrimination.

Human vision has been modelled by means of stimulus specific detectors (Carlson, Cohen and Gorog 1977; Gegenfurtner and Kiper 1992; Jamar and Koenderink 1985; Watson and Robson 1981). These detectors are directly related to the physical stimulus characteristics

(for example, size, motion, orientation or brightness.). Each detector responds best to a specific luminance distribution. At least one detector has to be active for us to see the stimulus (Campbell and Robson 1968; Kelly 1977; Kulikowski and Tolhurst 1973; Watson, 1980). The discrimination between two closer orientations requires more contrast because the detectors are noisy and the stimuli are not orthogonal thus disturbing the perception of each other.

Contrast detection threshold depends on stimulus features including spatial frequency (Chung, Legge and Tjan 2002; Nasanen and O'Leary 1998), area (Vassilev 1973), length and width (Sullivan *et al.* 1972). It is also influenced by other factors, such as visual defects (Levi and Harwerth 1980; McKee, Levi and Movshon 2003; Polat, Bonneh, Ma-Naim, Belkin, and Sagi 2005), boundary (Vassilev 1973), exposure time (Whittle 1986), and inducers (Wehrhahn and Dresp 1998). Some of these studies and some other studies are described in more detail below.

Sullivan *et al.* (1972) measured contrast detection thresholds for 1.5 deg long bars at different widths using the method of adjustment. The bar contrast was defined as Weber contrast, *i.e.*, the increment of the intensity above the background (which had a mean luminance of 8.5 cd/m^2) divided by the background intensity. The stimulus was displayed in a screen masked with an 8 deg diameter circular aperture. The results showed that the threshold remained almost the same at bar widths from 5 to 40 min arc.

Vassilev (1973) measured foveal contrast increment threshold as a function of distance between the bar stimulus and the boundary of a long strip presented beside it. The contrast

increment (or decrement) threshold is different from the absolute threshold. When the contrast increment (or decrement) threshold is measured, a stimulus is presented on a background of a certain luminance. Subject has to increase (or decrease) the stimulus luminance until it is just visible (or invisible) and the difference between the just-visible (or just-invisible) stimulus and background luminance is taken as the contrast increment (or decrement) threshold. The area of bars ranged from 1x6 to 6.30x47 min^2. The background luminance varied between 63.7 and 95.5 cd/m^2 and the luminance of the stripe was about 20 times lower than that of the background. The study found that (i) the threshold decreased with increasing distance and the decrease became faster as the bar length increased; (ii) and threshold decreased with increasing stimulus area.

Nasanen and O'Leary (1998) measured contrast thresholds for the recognition of hand-written Fourier filtered numerals 0-9 with central spatial frequencies ranging 1.2-17.7 cycles per object at the fovea and eccentricities of 5, 10 and 20 deg. The stimuli were presented on a 17 in monitor with an average luminance of 50 cd/m^2. The contrast threshold functions plotted against object spatial frequency are generally u-shaped, revealing the lowest threshold at about 4 cycles per object at all eccentricities studied. At higher object spatial frequencies the foveal contrast threshold is noticeably better than thresholds in the periphery.

Melmoth *et al.* (2000a) measured contrast detection and identification thresholds faces as a function of face size (4-10 deg of visual angle) at the eccentricities of 0, 2.5, 5, and 10 deg. Contrast sensitivity for detection and identification was correspondingly calculated as the inverse of the detection and identification threshold expressed in terms of *r.m.s* contrast.

They found (i) contrast sensitivity for both detection and identification first increased to a maximum and saturated with increasing stimulus size; (ii) and the size in which the saturation of sensitivity occurred increased with increasing eccentricity while the maximum sensitivity decreased with increasing eccentricity; (iii) both stimulus size and contrast scalings were needed for equating the performance across eccentricities.

Melmoth *et al.* (2000b) measured *r.m.s.* contrast thresholds for detecting the image distortion at the eccentricities of 0, 2.5, 5 and 10 deg. The mean luminance of the background is 50 cd/m^2. The original stimulus images were polar-circular gratings and band-pass filtered faces while the distorted images were created by randomly adding Fourier components to the original ones. Stimulus size ranged from 0.55 to 10 deg of visual angle. Subjects had to identify whether the stimulus presented was the original or the distorted one. Threshold was estimated as a function of stimulus size. Melmoth *et al.* found that (i) thresholds for both gratings and faces first decreased and then saturated as stimulus size increased; (2) the size where threshold saturated increased with increasing eccentricity for both gratings and faces; (3) the foveal performance could be obtained at the periphery with spatial scaling both for gratings and faces, which made Melmoth *et al.* (2001a) suggest that it was the complexity of the visual task that makes contrast scaling necessary.

Makela *et al.* (2001) measured contrast sensitivity for face identification as a function of image size at the eccentricities of 0-10 deg. The greyscale face stimuli were created at varying *r.m.s.* contrasts. The mean luminance of the background was 50 cd/m^2. The contrast sensitivity for face identification was measured as a function of stimulus size. They found that (i) contrast sensitivity first increased and then saturated with increasing stimulus

size; (ii) sensitivity decreases with increasing eccentricity so that sole size scaling was not sufficient to superimpose all the sensitivity data; and (iii) scaling of both size and contrast dimensions were necessary for equalising performance across eccentricities.

Chung *et al.* (2002) measured contrast thresholds for identifying single, band-pass filtered Times-Roman lower-case letters as a function of center frequency of the band-pass filter at the eccentricities from 0 to 10 deg. The contrast sensitivity (calculated as the inverse of contrast threshold) functions are generally band-pass shaped. The peak sensitivity decreases with increasing eccentricity but occurs at around 3 cycles per letter at all eccentricities and stimulus sizes. Based on the results, they postulated that the spatial-frequency characteristics of letter identification were fundamentally identical in central and peripheral vision.

Melmoth and Rovamo (2003) measured contrast detection and identification thresholds of Times New Roman letters as a function of letter size at the eccentricities of 0, 2.5, 5, and 10 deg. The results showed that for different tasks (i) contrast sensitivity (as the inverse of *r.m.s.* contrast threshold) first increased to a maximum and then decreased with increasing stimulus size; (ii) the maximum sensitivity decreased with increasing eccentricity; (iii) sole size scaling was not adequate to model performance deterioration across eccentricities; (iv) scaling of both stimulus size and contrast successfully normalised performance across eccentricities; and (v) contrast scaling played a more important role than spatial scaling in letter perception.

Sally *et al.* (2005) measured contrast threshold for discriminating a 1.5 deg tilted Gaussian

filtered line stimulus from a vertical one with the same configuration at the eccentricities of 0, 2.5, 5, and 10 deg. The stimuli identical to those of Sally and Gurnsey (2003) were reviewed in Chapter 3. Two stimuli, a vertical line and a 1.5 deg tilted line, were presented in two sequential intervals. Subjects indicated which interval contained the tilted line. Contrast threshold was measured as a function of line length. They found that (i) the threshold decreased and saturated with increasing line length; (ii) and the size where threshold saturated increased with increasing eccentricity; (iii) the minimum threshold allowing orientation discrimination increased with increasing eccentricity; (iv) the average E_2 value for size scaling was 5.85 deg for two subjects; and (v) the average of the E_2 values of two subjects for contrast scaling was 184 deg, which suggests that little contrast scaling is needed for large stimuli in order to equate performance between fovea and periphery.

6.2 Methods

6.2.1 Apparatus

Apparatus used in this experiment has been previously described in Chapter 2.

6.2.2 Stimuli

A series of magnified versions of a vertical line and four series of magnified versions of lines tilted 45, 15, 5 and 1.5 deg counter-clockwise from the vertical were created at various contrast levels using the software described in Chapter 2 and developed by Dr Risto Nasanen. All line stimuli were Gaussian filtered and had the same configuration as the line stimuli used for the orientation discrimination experiments in Chapter 3.

6.2.3 Subjects

Subjects LC and YC, 27 and 24 years old, participated in the experiments. Both were corrected moderate myopes with no ocular abnormality (see Appendix I for the details of the subjects).

6.2.4 Procedure

Two line stimuli of the same size, one vertical and the other tilted counter-clockwise 45, 15, 5 or 1.5 deg, were presented in random order in two successive intervals. Subjects had to indicate by means of the keyboard in which interval the more counter clockwise tilted line was displayed. The viewing distances were 28, 57, 85.5, 114, 171 and 228 cm, resulting in stimuli with a range of 0.1097-14.22 deg of visual angle in unfiltered line heights. The

smallest one (0.1097 deg) was produced by presenting the smallest 8.7 mm stimulus at the furthest viewing distance of 456 cm.

The contrasts thresholds for orientation discrimination were measured separately at orientation differences of 45, 15, 5 and 1.5 deg by using 2AFC method described previously in Chapter 2. Data collection started with 45 deg difference, and then continued with 15, 5 and 1.5 deg differences.

6.3 Results

In Fig 6.1, contrast thresholds were plotted as a function of line length (deg) at orientation differences of 45, 15, 5 and 1.5 deg, and eccentricities of 0, 2.5, 5, 7.5 and 10 deg for each subject. As shown in the figure, the threshold functions generally decrease and reach to a plateau with increasing line length. The asymptotic threshold level increases with increasing eccentricity and decreasing orientation difference. Contrast thresholds for the orientation difference of 1.5 deg could not be measured at the eccentricities of 7.5 and 10 deg for subject YC, because the subject was not able to conduct the discrimination at these eccentricities. Threshold functions move to the right along the horizontal axis with increasing eccentricity, thus implying a magnification of spatial scale.

The shapes of all the eccentric data curves are similar irrespective of eccentricity and orientation difference for both subjects, as shown in Fig 6.1. The eccentric threshold (*Th*) at each orientation difference was fitted with a single equation due to the similarity:

$$Th = Th_{\min}(1+(H_c / H)^2)^{2.5}, \qquad \textbf{Equation 6.1}$$

where Th_{min} is the theoretical minimum threshold, H is line stimulus height (or length) and H_c is the critical height marking change at the threshold curve from the decrease to the plateau (Makela *et al.* 2001; Melmoth *et al.* 2000a; Sally *et al.* 2005) (see Appendix VI for the procedure of obtaining the optimal equation and results of curve fitting). Since the portion of the equation in brackets is always greater than one, *Th* is always greater than $Th_{\min}$. To check the fitting accuracy of equation (6.1), R^2 was calculated for each data curve.

The values of R^2 across eccentricities, orientation differences and subjects ranged from 0.85-0.99 with an average of 0.92 (see Appendix VI Table 5). Thus, equation (6.1) described accurately all the eccentric threshold data curves. In the previous experiments, the equation $Th = Th_{\min}(1+(H_c / H)^1)^5$ was used to fit with the orientation discrimination threshold (see Chapters 3-5), while here in equation (6.1) the exponent of 5 was divided across brackets so that the exponent of (H_c/H) was 2. This difference is discussed later in Section 6.4.

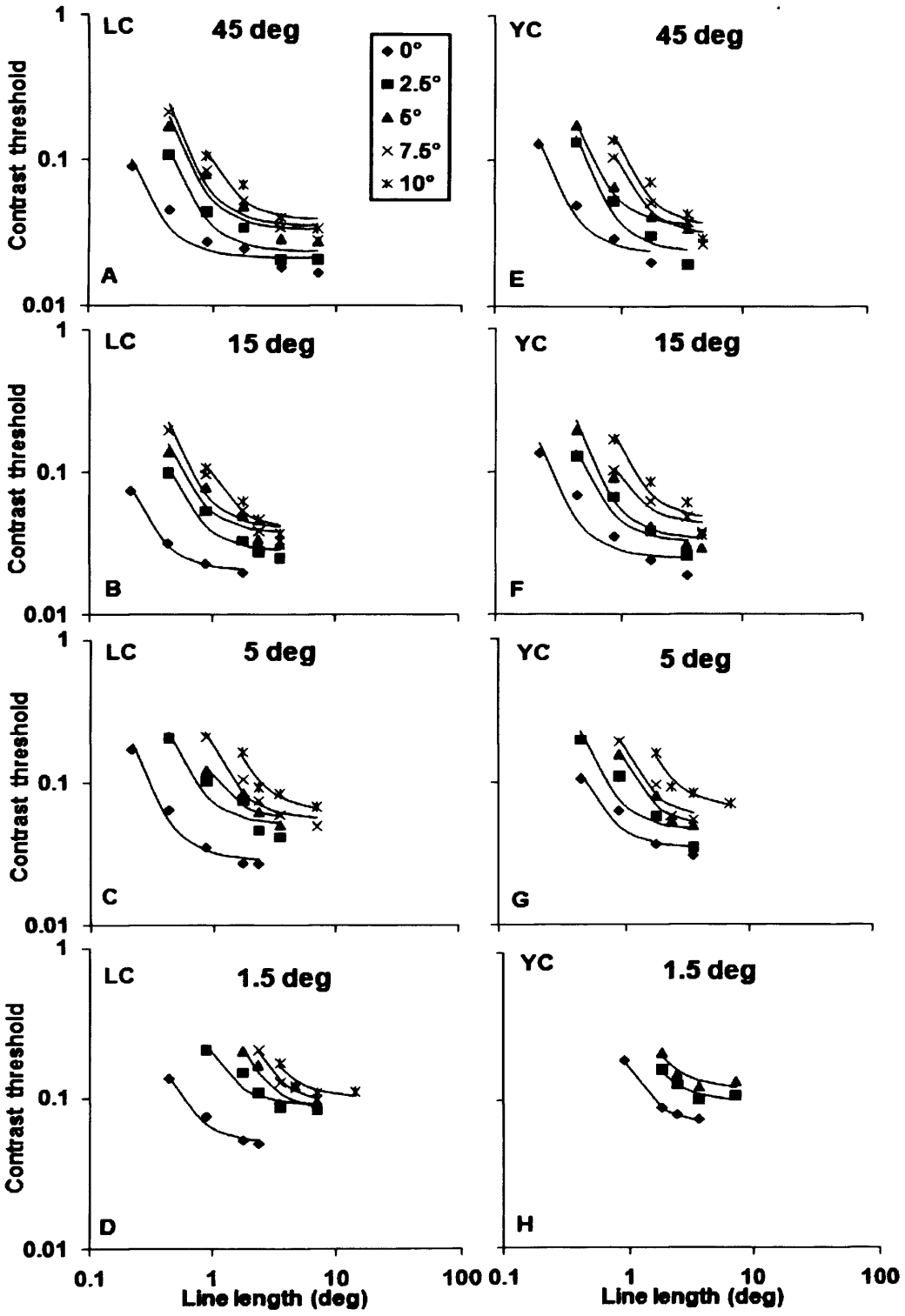

Fig 6.1 Contrast thresholds for orientation discrimination of the Gaussian filtered lines tilted 45, 15, 5 and 1.5 deg

The thresholds were plotted against line length (deg) at eccentricities of 0, 2.5, 5, 7.5 and 10 deg and

orientation differences of 45, 15, 5 and 1.5 deg for subjects LC and YC. Each data set was fitted with equation (6.1) (solid line) to model the decrease and plateau in threshold with increasing line length.

6.3.1 Spatial scaling across orientation differences from 45-1.5 deg

In this section, spatial scaling was used to shift all the contrast threshold data from different eccentricities and orientation differences for superimposing. The threshold data at fovea and 45 deg orientation difference (E=0, OD=45) was chosen as the baseline where all threshold data curves were superimposed. The procedure of spatial scaling was as previously explained in Chapter 1. Because the spatial scaling was across eccentricities and orientation differences, the scaling factors obtained were dependent on two variables, eccentricity (E) and orientation difference (OD), shown in Fig 6.2 (A,B). The spatial scaling factors increase with increasing eccentricity and decreasing orientation difference. Equation (6.2) below was used to model the factors as a function of E and OD, including all the 2nd order polynomial parameters involving eccentricity (E) and orientation difference $(OD)^{-1}$:

$$F_i = 1 + E/E_2 + (OD^{-2} - 45^{-2})/k_1 + E \times (OD)^{-2}/k_2 + (OD^{-1} - 45)^{-1}/k_3 + E \times (OD)^{-1}/k_4 + E^2/E_2'$$

Equation 6.2

where F_i represents for the scaling factor, while parameters E_2, E'_2, k_1, k_2, k_3 and k_4 are constants. E_2 and E'_2 together define the effect of eccentricity on spatial scaling factor while k_1 and k_3 define the effect of orientation difference. Constants k_2 and k_4 describe the interaction between the independent variables, i.e. eccentricity (E) and orientation

difference (OD). When E=0 and OD=45, all the terms involving E and OD become equal to 0, which leaves F_i to be equal to unity.

On the basis of R^2 values and the accuracy of the constants (see Appendix IV for the procedure of obtaining the parameters), the parameters k_3 and E'_2 were discarded. Thus, equation (6.2) was reduced to equation (6.3) for estimate the spatial scaling factor:

$$F_s = 1 + E/E_2 + (OD^{-2} - 45^{-2})/k_1 + E \times (OD)^{-2}/k_2 + E \times (OD)^{-1}/k_4 ,$$

Equation 6.3

where F_s represent spatial scaling factor.

Thus, the spatial scaling factors were estimated by equation (6.3) fitted to the data of Figs. 6.2(A) and (B) separately and plotted in Figs 6.2 (C) and (D). The high R^2 values show that equation (6.3) successfully estimated spatial scaling factors across eccentricities and orientation differences. The resulting constants and R^2 values are summarised in Table 6.1.

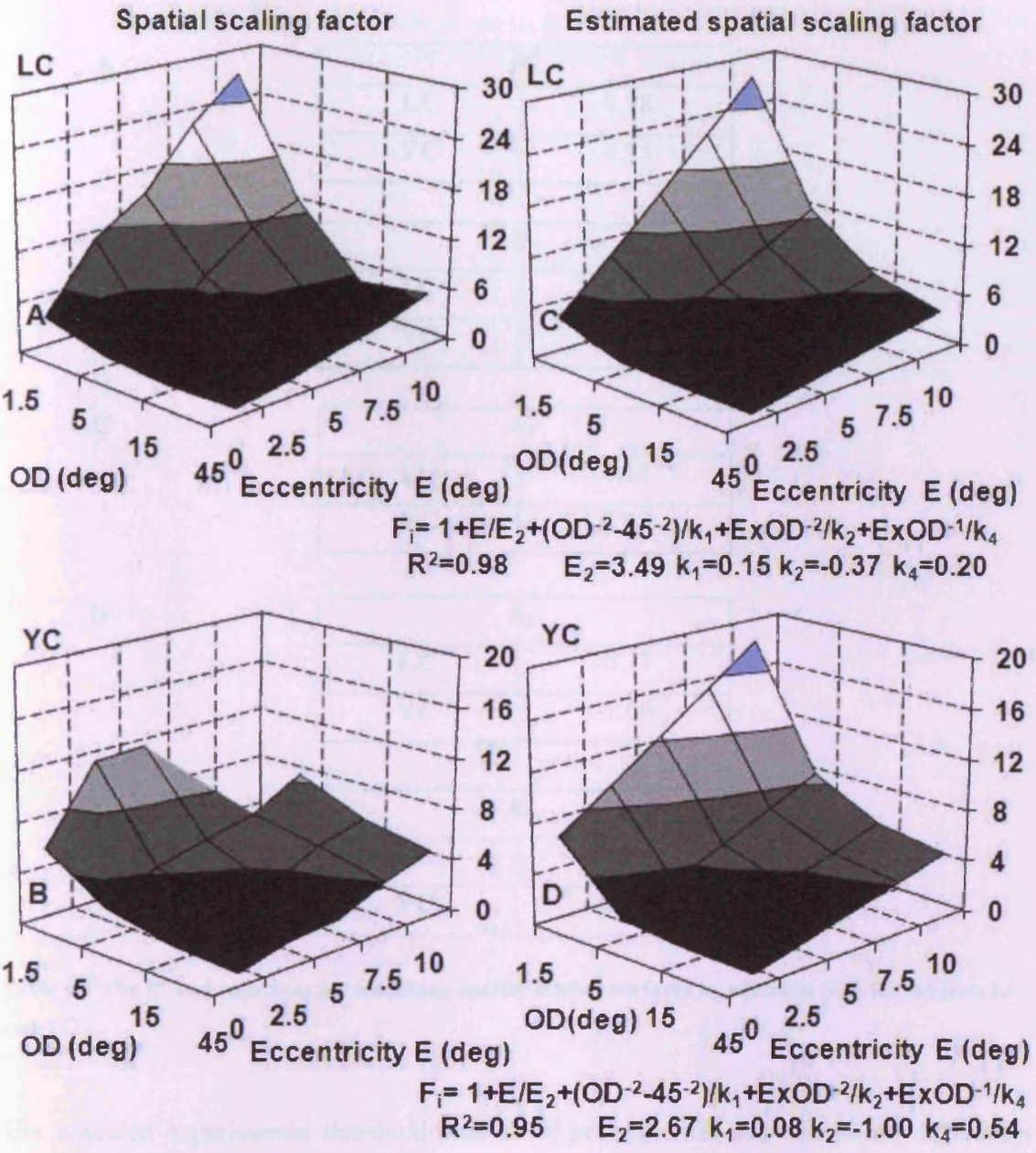

Fig 6.2(A-D) Empirical and modelled spatial scaling surfaces for the Gaussian filtered lines

The empirical (left column) and modelled (right column) spatial scaling surfaces at any eccentricity (*E*) and orientation difference (*OD*) of the Gaussian filtered lines for subjects LC and YC. The left-hand column (A, B) shows the empirical scaling surfaces separately for LC and YC. The empirical surfaces were fitted with equation (6.3) which modelled the effects of eccentricity and orientation difference on the scaling factor F_s. The modelled scaling surfaces are shown in the right-hand column (C, D) along with the fitting equation (6.3), the corresponding parameters used and R^2.

A

R^2	
LC	0.98
YC	0.95

B

E_2	
LC	3.49
YC	2.67

C

k_1	
LC	0.15
YC	0.08

D

k_2	
LC	-0.37
YC	-1.00

E

k_4	
LC	0.20
YC	0.54

Table 6.1 The R^2 and constants for modelling spatial scaling surfaces by equation (6.3) for subjects LC and YC.

The unscaled experimental threshold data at all eccentricities and orientation differences were plotted against line length in Fig 6.3 for subjects LC and YC.

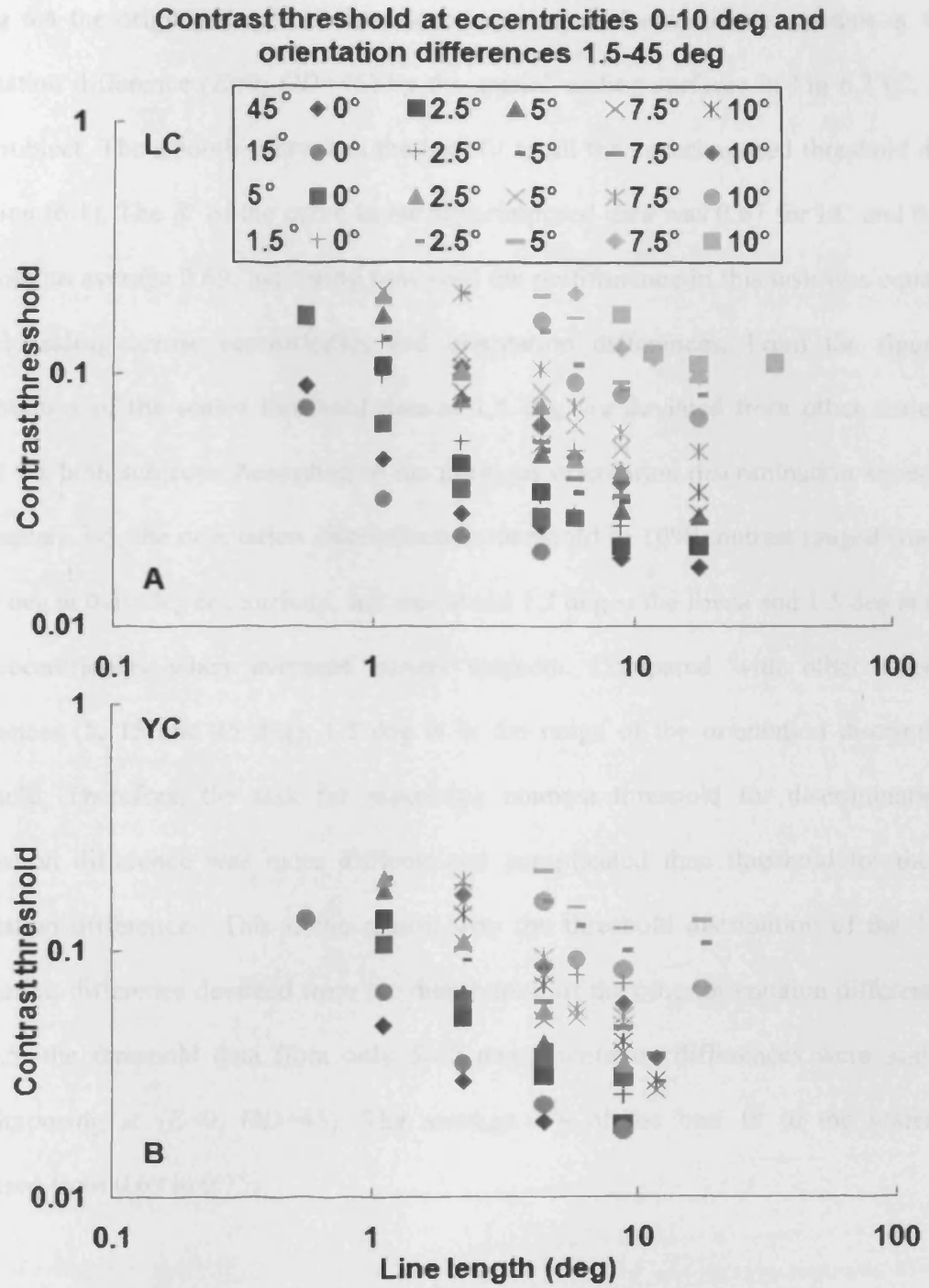

Fig 6.3 The unscaled experimental contrast threshold data of the Gaussian filtered lines

The unscaled experimental contrast threshold data were plotted against line length (deg) at the eccentricities of 0-10 deg and orientation differences of 1.5-45 deg for subjects LC and YC.

In Fig 6.4 the original threshold data were superimposed onto the foveal data at 45 deg orientation difference (E=0, OD=45) by the spatial scaling surfaces in Fig 6.2 (C, D) for each subject. The smooth curve was the best fit to all the superimposed threshold data by equation (6.1). The R^2 of the curve to the superimposed data was 0.67 for LC and 0.71 for YC with an average 0.69, indicating how well the performance in this task was equated by spatial scaling across eccentricities and orientation differences. From the figure, the distributions of the scaled threshold data at 1.5 deg are deviated from other scaled data points for both subjects. According to the previous orientation discrimination experiments in Chapters 3-5, the orientation discrimination threshold in 10% contrast ranged from 0.94 to 3.5 deg at 0-10 deg eccentricity, and was about 1.2 deg at the fovea and 1.5 deg at the 2.5 deg eccentricities when averaged across subjects. Compared with other orientation differences (5, 15 and 45 deg), 1.5 deg is in the range of the orientation discrimination threshold. Therefore, the task for measuring contrast threshold for discriminating 1.5 orientation difference was more difficult and complicated than threshold for the other orientation differences. This is the reason why the threshold distribution of the 1.5 deg orientation difference deviated from the distribution of the other orientation differences. In Fig 6.5, the threshold data from only 5-45 deg orientation differences were scaled for superimposing at (E=0, OD=45). The average R^2s of the best fit to the scaled data increased from 0.69 to 0.75.

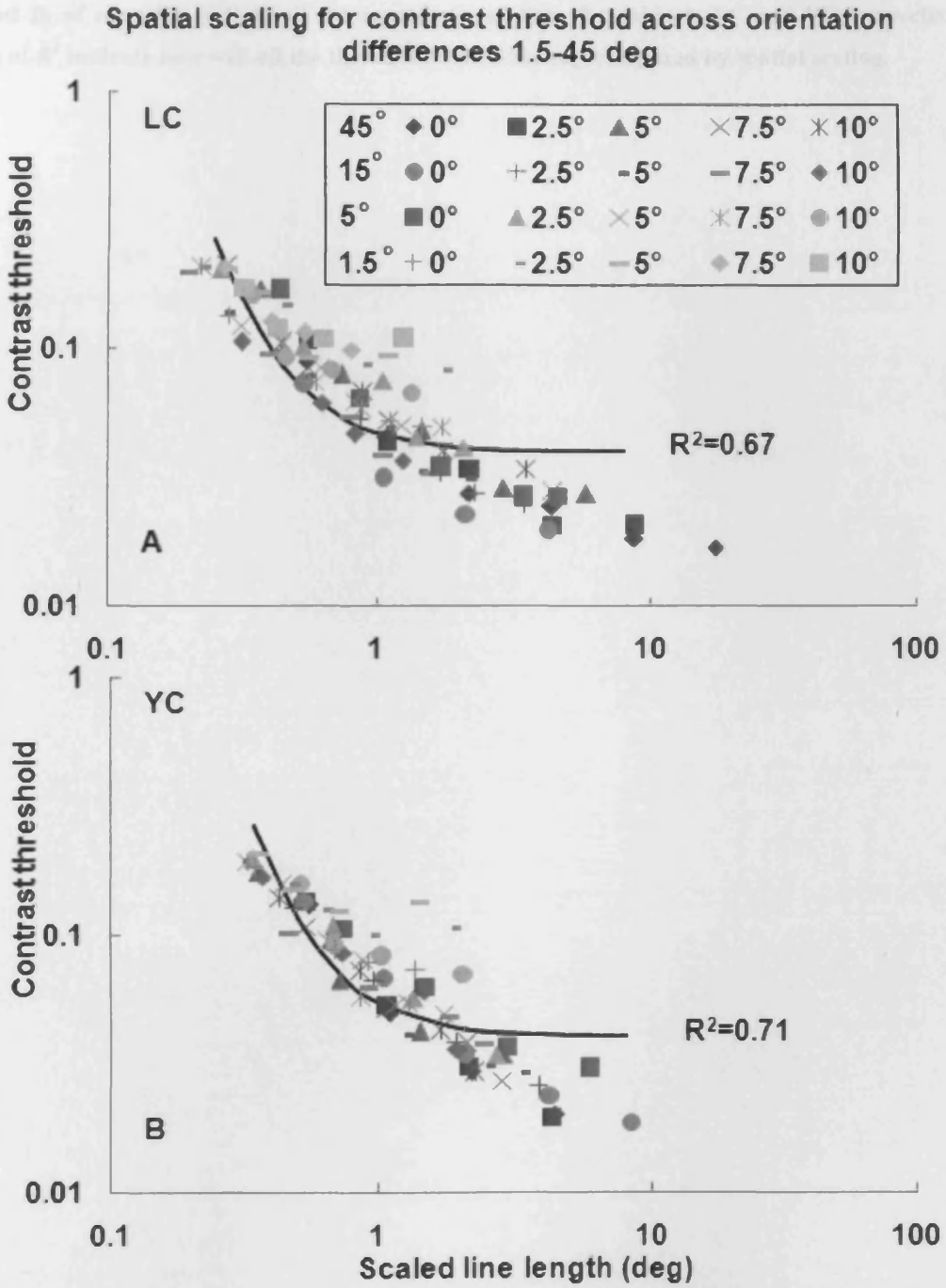

Fig 6.4 The contrast threshold data of the Gaussian filtered lines at 0-10 deg eccentricity and 1.5-45 deg orientation differences were superimposed by spatial scaling

The original contrast threshold data in Fig 6.3 (A, B) were scaled by using the estimated spatial scaling surfaces in Fig 6.2 (C, D). Data from the eccentricities of 0-10 deg and orientation differences of 1.5-45 deg collapsed onto the foveal and 45 deg orientation difference data (*E*=0, *OD*=45). The solid curve is

the best fit of equation (6.1) to all the superimposed data for subjects LC and YC, respectively. The values of R^2 indicate how well all the threshold data were superimposed by spatial scaling.

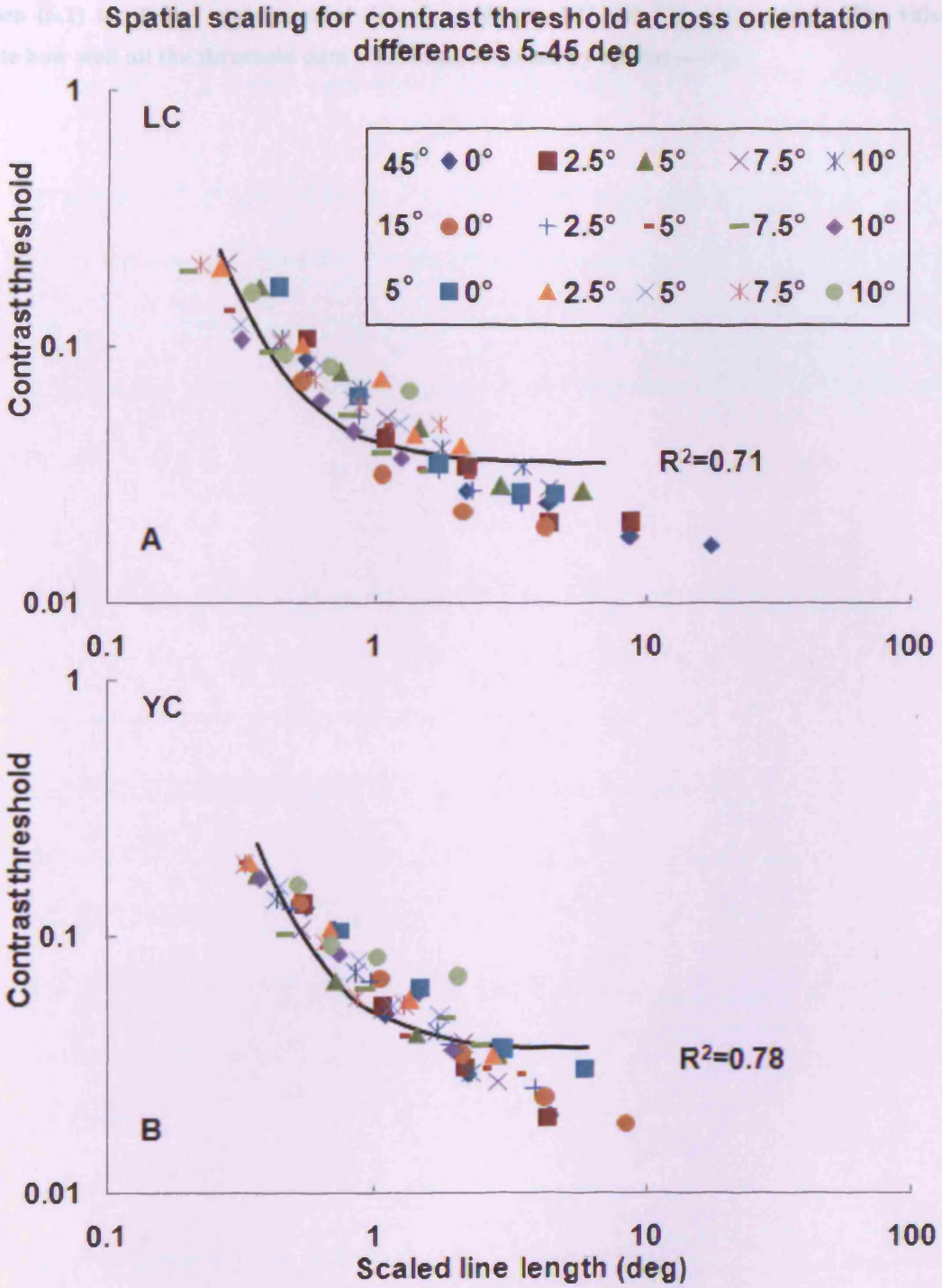

Fig 6.5 The contrast threshold data of the Gaussian filtered lines at 0-10 deg eccentricity and 5-45 deg orientation differences were superimposed by spatial scaling

The threshold data from the eccentricities of 0-10 deg and orientation differences of 5-45 deg collapsed onto the foveal and 45 deg orientation difference data (*E*=0, *OD*=45). The solid curve is the best fit of

equation (6.1) to all the superimposed data for subjects LC and YC, respectively. The values of R^2 indicate how well all the threshold data were superimposed by spatial scaling.

6.3.2 2D scaling across orientation differences from 45-1.5 deg

For comparison with spatial scaling, 2D scaling, the simultaneous vertical and horizontal scaling, was used to superimpose the threshold data across eccentricities and orientation differences in this section. The foveal threshold data at 45 deg orientation difference (E=0, OD=45) was again chosen to be the basic condition, where all the threshold data were superimposed.

The vertical and horizontal scaling factors of 2D scaling, normalised Th_{min} and normalised H_c, obtained by fitting equation (6.1) to the data of Fig. 6.1 and dividing Th_{min} (E, OD) at eccentricity E and orientation difference OD by Th_{min} (E=0, OD=45) and H_c (E, C) by H_c (E=0, OD=45)}. Like the spatial scaling factor obtained in previous section, the 2D scaling factors are dependent on two variables, eccentricity (E) and orientation difference (OD). In Fig 6.6 (A, B, E, F), these experimentally obtained 2D scaling factors, i.e. normalized Th_{min} and H_c were plotted against E and OD. Equation (6.2) was again used to model how the 2D scaling factors changed with eccentricity and orientation difference with respect of the data at (E=0, OD=45).

During modelling the vertical scaling factor, i.e. normalised Th_{min}, constants k_1, k_4 and E'_2 were discarded because they were found either being redundant on the basis of R^2 or inaccurate for the fitting (see Appendix IV for the procedure of obtaining parameters). Equation (6.2) was thus reduced to equation (6.4):

$$F_t = 1 + E/E_2 + E \times (OD)^{-2}/k_2 + (OD^{-1} - 45)^{-1}/k_3 .$$

Equation 6.4

During modelling the horizontal scaling factor, i.e. normalised H_c, constants k_3 and E'_2 were discarded due to being either redundant on the basis of R^2 value or inaccurate for the fitting (see Appendix IV for the procedure of obtaining parameters). Equation (6.2) was reduced to equation (6.5), which is the same as equation (6.3) used for the sole spatial scaling factor:

$$F_t = 1 + E/E_2 + (OD^{-2} - 45^{-2})/k_1 + E \times (OD)^{-2}/k_2 + E \times (OD)^{-1}/k_4 .$$

Equation 6.5

In Fig 6.6 (C, D), the vertical scaling factors, i.e. normalised Th_{min}, were estimated by equation (6.4). In Fig 6.6 (G, H), the horizontal scaling factors, i.e. normalized H_c, were estimated by equation (6.5). The R^2s of the estimation of the 2D scaling factors ranged from 0.90 to 0.98, showing that equations (6.4) and (6.5) successfully modelled the 2D scaling factor across eccentricities and orientation differences. The modelling results are summarised in Table 6.2.

Fig 6.6 Empirical & modelled 2D scaling surfaces for the contrast threshold of Gaussian filtered line

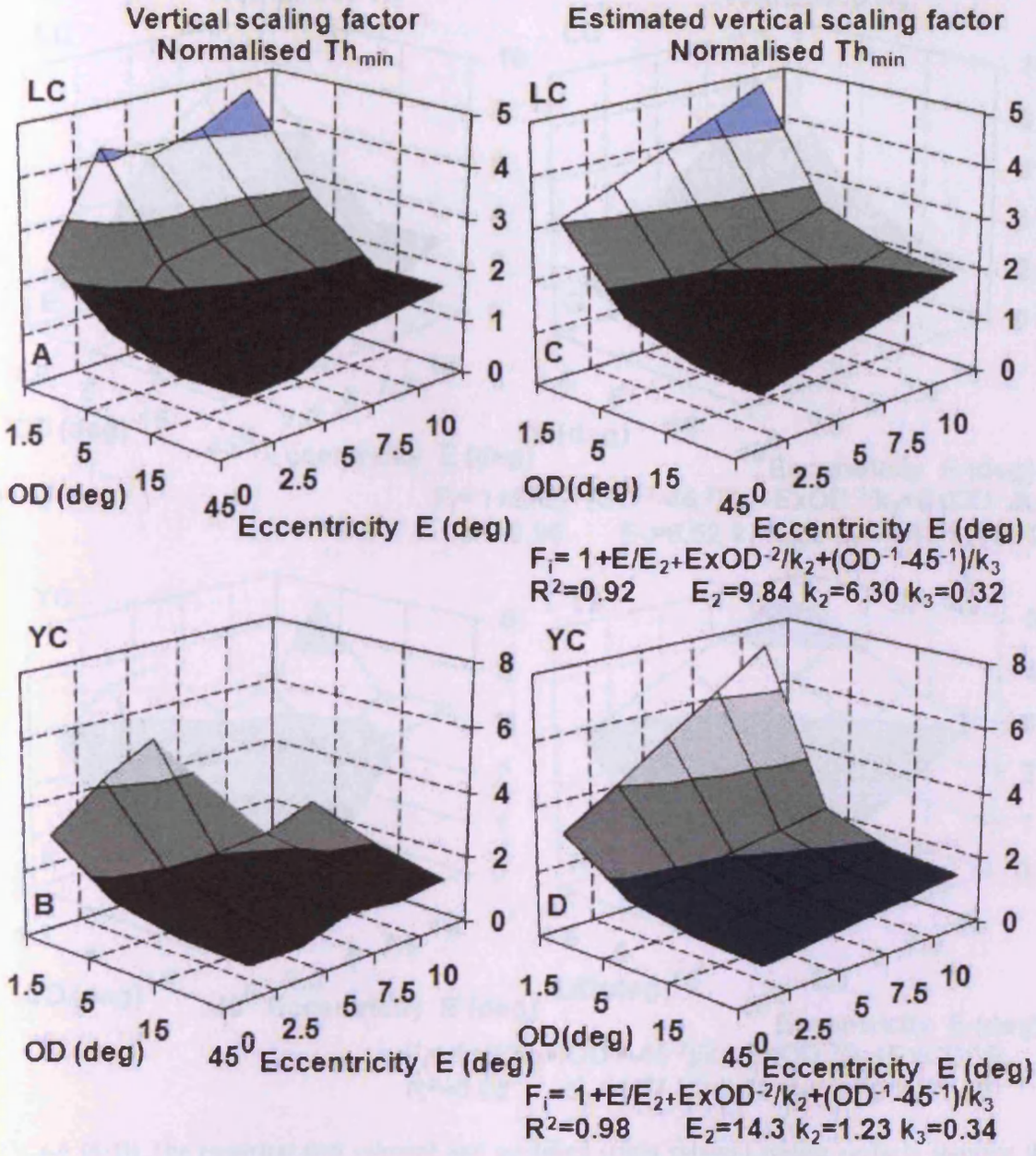

Fig 6.6(A-D) The Empirical (left column) and modelled (right column) scaling surfaces showing the vertical scaling factor, i.e. normalised Th_{min}, at all eccentricities (E) and orientation differences (OD) of the Gaussian filtered lines for subjects LC and YC. The left-hand column (A, B) shows the empirical scaling surfaces separately for LC and YC. The empirical surfaces were fitted with equation (6.4) which modelled the effects of eccentricity and orientation difference on normalised Th_{min}. The modelled scaling surfaces are shown in the right-hand column (C, D) along with the fitting equation (6.4), the values of the parameters used, and R^2.

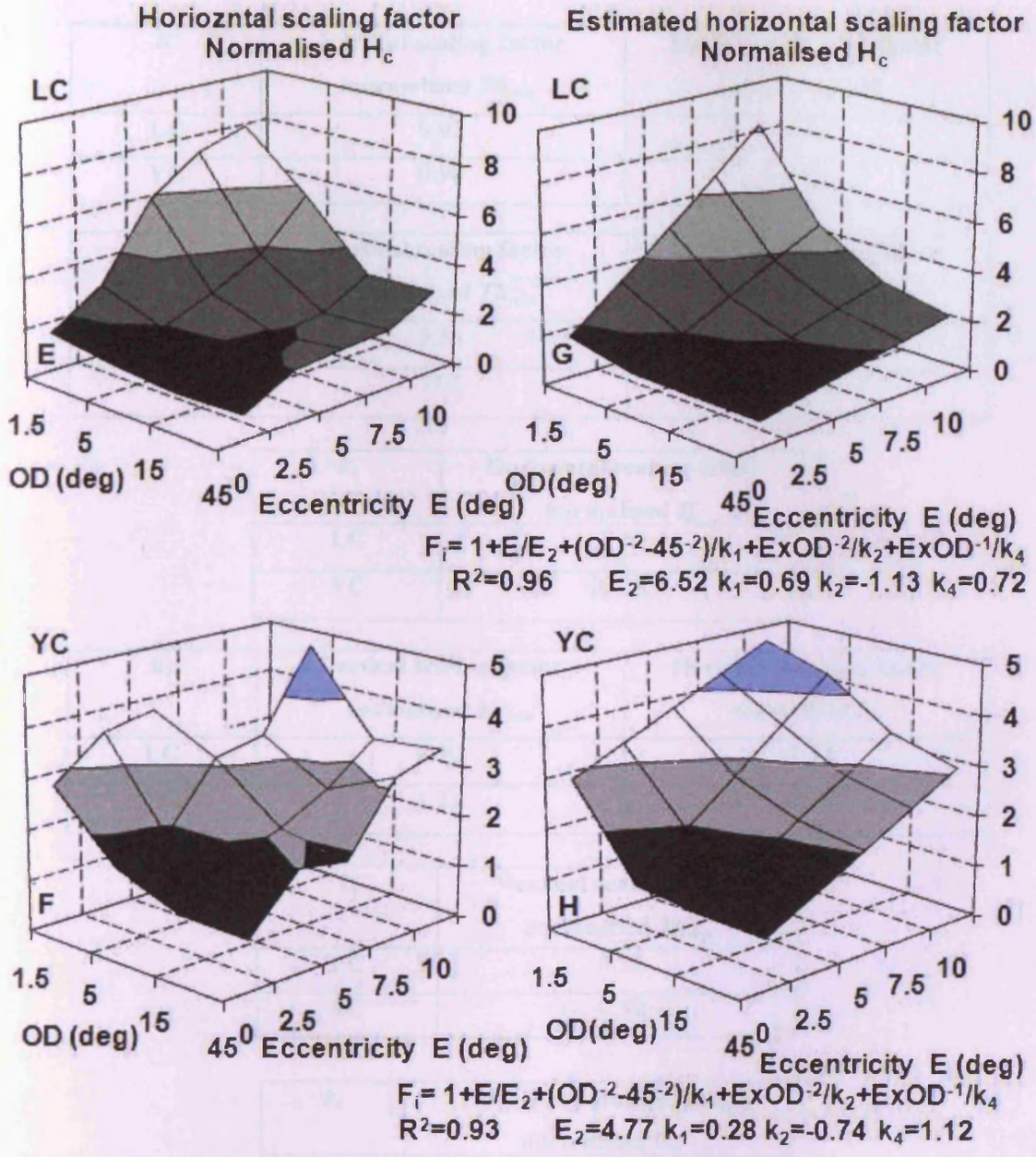

Fig 6.6 (E-H) The empirical (left column) and modelled (right column) scaling surfaces showing the horizontal scaling factors, i.e. normalised H_c, at all eccentricities (E) and orientation differences (OD) of the Gaussian filtered lines for LC and YC. The left-hand column (E, F) shows the empirical scaling surfaces separately for LC and YC. The empirical surfaces were fitted with equation (6.5) which modelled the effects of eccentricity and orientation difference on the normalised H_c. The modelled scaling surfaces are shown in the right-hand column (G, H) along with the fitting equation (6.5), the values of the parameters used, and R^2.

A

R^2	Vertical scaling factor normalised Th_{min}	Horizontal scaling factor normalised H_c
LC	0.92	0.96
YC	0.98	0.93

B

E_2	Vertical scaling factor normalised Th_{min}	Horizontal scaling factor normalised H_c
LC	9.84	6.52
YC	14.3	4.77

C

k_1	Horizontal scaling factor normalised H_c
LC	0.69
YC	0.28

D

k_2	Vertical scaling factor normalised Th_{min}	Horizontal scaling factor normalised H_c
LC	6.30	-1.13
YC	1.23	-0.74

E

k_3	Vertical scaling factor normalised Th_{min}
LC	0.32
YC	0.34

F

k_4	Horizontal scaling factor normalised H_c
LC	0.72
YC	1.12

Table 6.2 The R^2s and constants of modelling 2D scaling factors for subjects LC and YC

Then the unscaled experimental contrast threshold data at all eccentricities and orientation differences in Fig 6.3 were both vertically and horizontally scaled to the basic condition (E=0, OD=45) in Fig 6.7, by the estimated 2D scaling factors, i.e. estimated normalized Th_{min} and estimated normalized H_c (see Fig 6.6 (E, F, G, H)). The R^2s of the best fit of equation (6.1) to all the scaled data was 0.81 and 0.88 for subjects LC and YC, respectively. The 2D scaling successfully superimposed all the threshold data to (E=0, OD=45), indicating that the contrast threshold performance changes across all eccentricities and orientation differences studied were described quite accurately in quantitative terms.

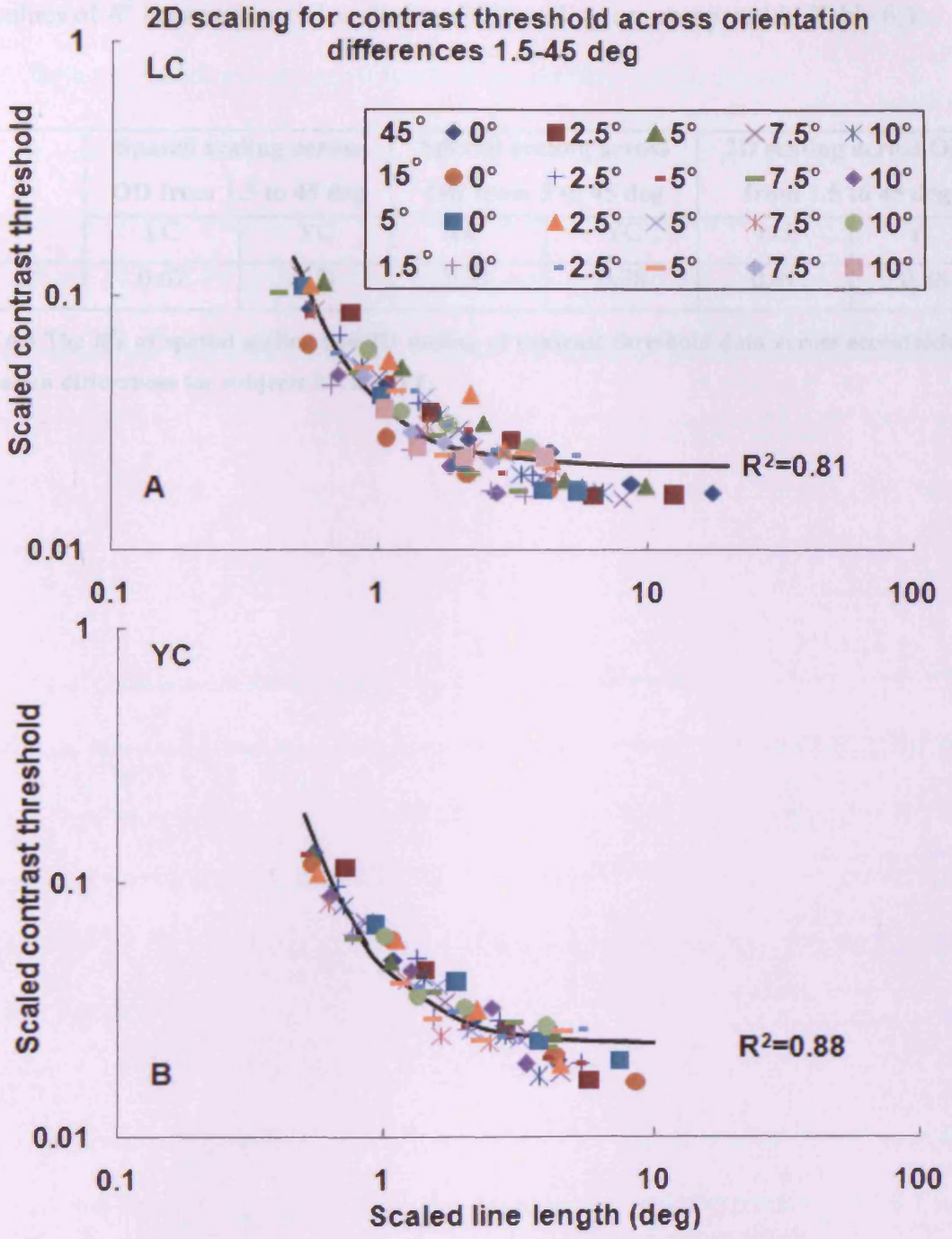

Fig 6.7 (A-B) The 2D scaled contrast thresholds for the Gaussian filtered lines

The original threshold data from Fig 6.3 (A, B) were both vertically and horizontally scaled by means of the modelled 2D scaling surfaces of Fig 6.6 (C, D, G, H). Data for the eccentricities of 0-10 deg and orientation differences of 45-1.5 deg collapsed onto the base condition (E=0, OD=45). The data for subjects LC and YC are as indicated. The smooth curve i.e. equation (6.1) was fitted to the scaled threshold data and R^2 indicates the accuracy of the fit for describing all the data after 2D scaling.

The values of R^2 between spatial scaling and 2D scaling are compared in Table 6.3.

	Spatial scaling across OD from 1.5 to 45 deg		**Spatial scaling across OD from 5 to 45 deg**		**2D scaling across OD from 1.5 to 45 deg**	
	LC	YC	LC	YC	LC	YC
R^2	0.67	0.71	0.71	0.78	0.81	0.88

Table 6.3 The R^2s of spatial scaling and 2D scaling of contrast threshold data across eccentricities and orientation differences for subjects LC and YC.

6.3.3 Spatial scaling at individual orientation difference

After the removal of the threshold data at 1.5 deg orientation difference, the data from 5-45 deg collapsed better, indicating by that the average of R^2s between subjects increased from 0.69 to 0.75. This could be caused by two reasons: (i) since the most offset threshold data were removed, the data superimposition should be better in theory. It applies for any case; (ii) the threshold data of 1.5 deg have a different feature, compared with those at other orientation difference. The removal of data at 1.5 deg meant that the difference was removed.

To clarify the reasons behind, spatial scaling were conducted and E_{2OD}s were obtained individually at each orientation difference. If the improvement of R_2 was caused by the first reason, the E_{2OD} at each orientation difference would found to be within the same range because the value of E_2 reflects how the performance in a visual task changes across visual field. Otherwise, E_2 at 1.5 deg orientation difference should fall in a different range from those at other differences.

In Fig 6.8, at each orientation difference, a preliminary spatial scaling factor was obtained at each eccentricity through the spatial scaling procedure previously described in Chapter 1 Section 1.3. Then at individual orientation difference, these scaling factors were fitted through (0, 1) against eccentricity by an optimal linear function with the corresponding best fit R^2, as shown in each sub figure. Final spatial scaling factors were determined by these linear functions.

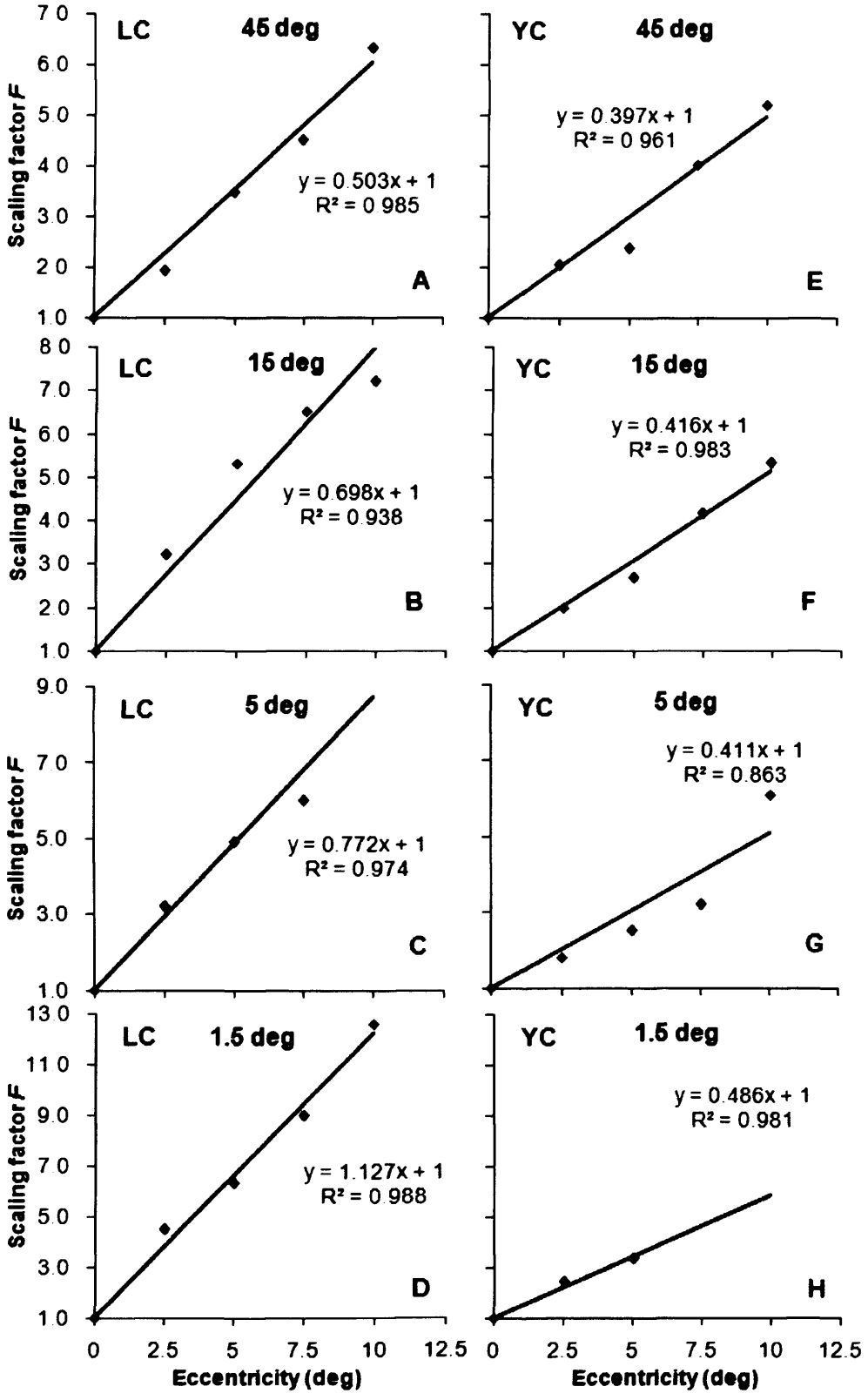

Fig 6.8 (A-H) Spatial scaling factors as a function of eccentricity at each orientation difference

At each eccentricity and orientation difference, a preliminary spatial scaling factor (■) was obtained through the spatial scaling procedure previously described in Chapter 1 Section 1.3. By individual orientation difference, the scaling factors were fitted through (0, 1) by an optimal linear function with its best fit R^2, shown in each graphs. Subjects LC and YC are as indicated.

As the inverse of the slope of the linear function of Fig 6.8, the spatial E_{2OD} at each orientation difference was calculated and shown in Table 6.4.

Table 6.4 Spatial E_{2OD} at each contrast

E_{2OD}	LC	YC	Average
45 deg	1.99	2.52	2.25
15 deg	1.43	2.40	1.92
5 deg	1.30	2.43	1.86
1.5 deg	0.89	2.06	1.47

Fig 6.9 shows E_{2OD} of each subjects and its average between subjects plotted as a function of orientation difference.

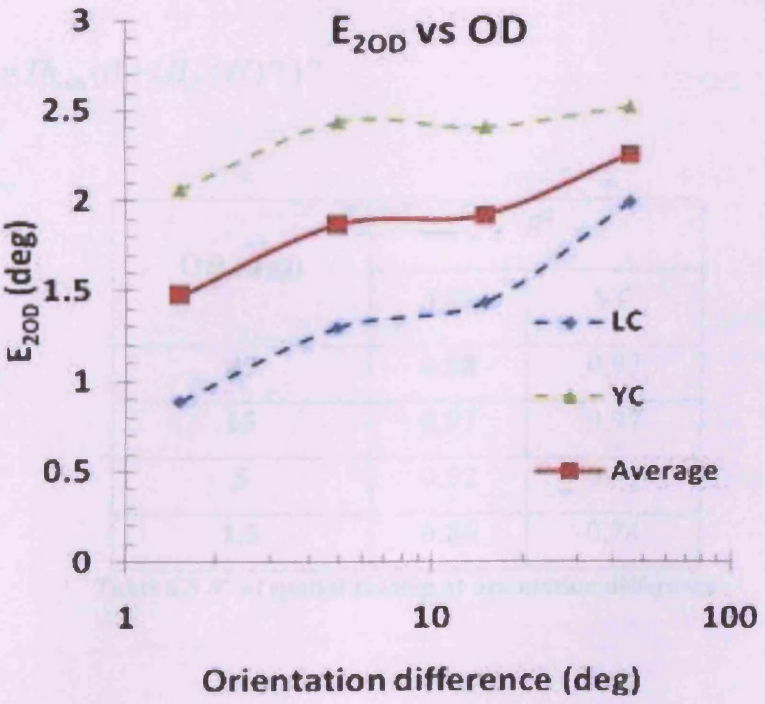

Fig 6.9 Spatial E_{2OD} is plotted as a function of orientation difference for subjects LC and YC.

The blue dash smooth curve is the function of E_{2OD} vs. orientation difference for subject LC. The green one is for YC. The average E_{2OD} between subjects is plotted against orientation difference with the red solid smooth curve.

By the final spatial scaling factors, the threshold data at each orientation difference (see Fig 6.1) were scaled horizontally to superimpose on to its corresponding fovea curve, as shown in Fig 6.10. The R^2 of the best fit to each superimposed threshold set by equation (6.6) (Makela *et al* 2001; Melmoth *et al.* 2000a, b; Sally *et al.* 2005) was calculated and displayed in each sub-figure. Generally, the threshold data collapsed well onto the corresponding foveal function at each orientation difference, shown by R^2 being greater than 0.85 (see Table 6.5). The R^2 of the threshold superimposition at 1.5 deg for subject YC was comparatively lower because of inaccurate spatial scaling caused by the lack of data at 7.5 and 10 deg eccentricities.

$$Th = Th_{\min}((1+(H_c / H)^{P_2})^{P_1}$$ **Equation 6.6**

OD (deg)	R^2	
	LC	YC
45	0.98	0.97
15	0.97	0.97
5	0.92	0.91
1.5	0.86	0.74

Table 6.5 R^2 of spatial scaling at orientation difference

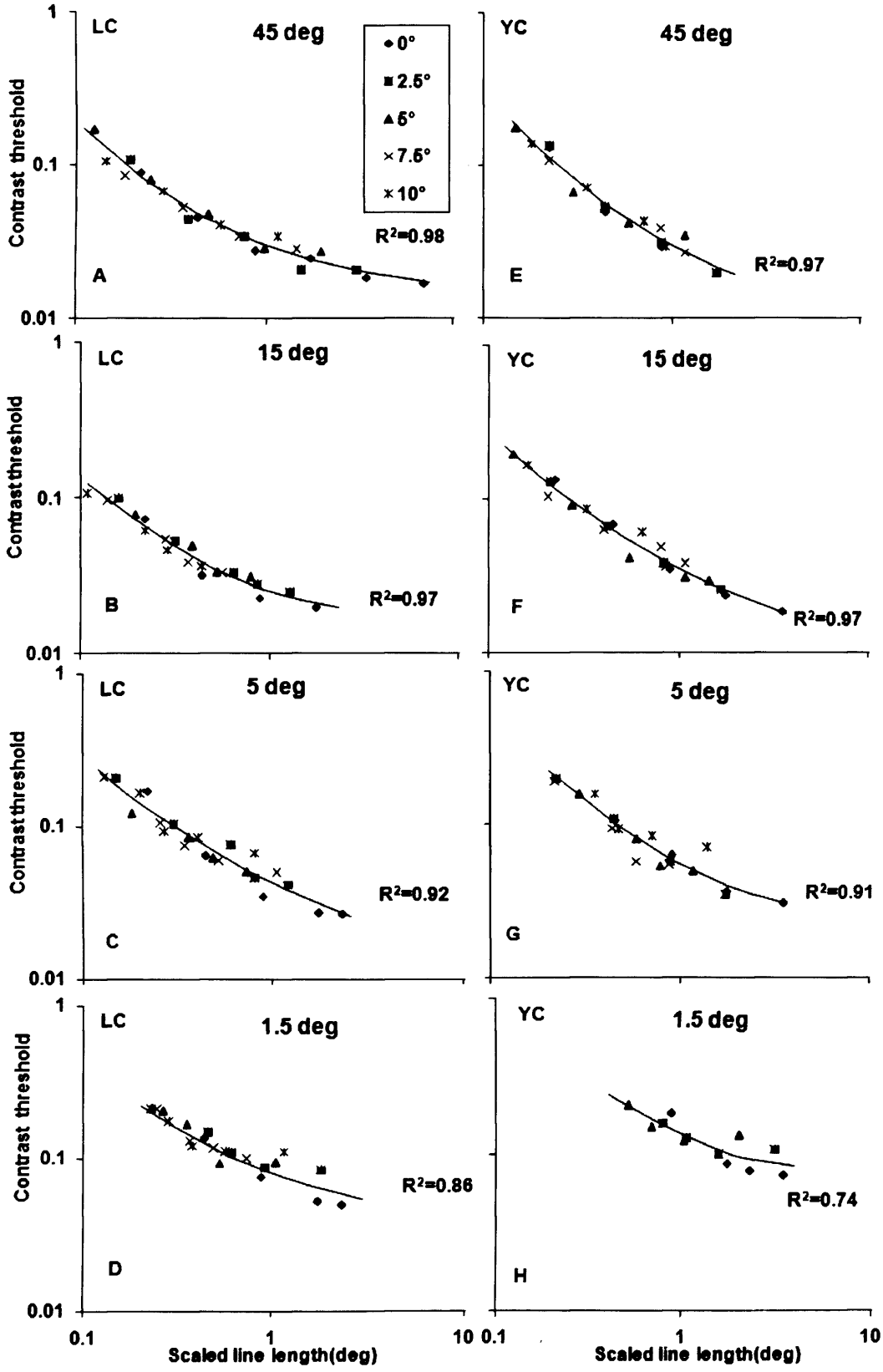

Fig 6.10 Spatial scaling of contrast threshold of orientation discrimination at 45-1.5 deg orientation

differences

At each orientation difference, the eccentric threshold curves (shown in Fig 6.1) were horizontally shifted to superimpose onto each fovea curve by spatial scaling factors calculated by using the corresponding linear functions in Fig 6.9. The smooth curve was the best fit to each superimposed threshold set at each difference by equation (6.6). Data collapsed well onto the foveal function at indicating by the high R^2 values. Subjects LC and YC are as indicated.

6.4 Discussion

The contrast threshold curves measured at various eccentricities and orientation differences were successfully fitted by using one equation, $Th = Th_{\min}(1+(H_c / H)^2)^{2.5}$. The format of the equation used is in agreement with, $S = S_{\max}(1+((w_0 / w)^p)^{-n}$, used for contrast sensitivity data of face identification by Makela *et al* (2001), Melmoth *et al.* (2000a, b) and Sally *et al.* (2005). However, the equation used differs slightly from the equation $Th = Th_{\min}(1+H_c / H)^5$ used for fitting the orientation discrimination threshold data in Chapters 3-5 and $Th = \theta_{\min}(1+L_{crit} / x)^n$ used for fitting the orientation discrimination threshold data of both broadband and narrow band line stimuli by Sally and Gurnsey (2003, 2004 and 2007). When comparing the shapes of data curves measured, the curve of contrast threshold vs. line length changes from decrease to plateau more abruptly than the curve of the orientation discrimination threshold.

The contrast threshold was found to decrease and asymptote with increasing line length which is in agreement with Makela *et al.* (2001), Melmoth *et al.* (2000a and 2000b), Melmoth and Rovamo (2003), Sullivan *et al.* (1972), and Vassilev (1973). At any orientation difference, foveal performance is noticeably superior to that of the periphery, which is consistent with Nasanen and O'Leary (1998) in contrast thresholds for recognizing low-frequency Fourier filtered numerals, Chung *et al.* (2002) in contrast thresholds for identifying Times-Roman letters, and Sally *et al.* (2005) in contrast thresholds allowing 1.5 deg orientation difference discrimination of line stimulus.

6.4.1 The theoretical minimum threshold Th_{min} and critical line length H_c

By fitting each eccentric threshold curve by equation (6.1), the theoretical minimum contrast threshold Th_{min} and the critical line length H_c were obtained. Both Th_{min} and H_c increase with eccentricity at each orientation difference (see Fig 6.6 (A, B, E, F)), which is in agreement with Rovamo *et al.* (1978), Rovamo *et al.* (1992), and Sally *et al.* (2005). On the other hand, Th_{min} first sharply decreased with increasing orientation difference from 1.5 deg to 15 deg and then became independent of orientation difference from 15 to 45 deg, as shown in Fig 6.11. In comparison with Th_{min}, the decrease of H_c with increasing orientation difference is much slower and tends to asymptote earlier about at 5 deg, as shown in Fig 6.12. To show these dependencies clearly, the averages of Th_{min} and H_c from all eccentricities at each orientation difference was calculated for each subject and plotted in the Figs 6.11 and 6.12.

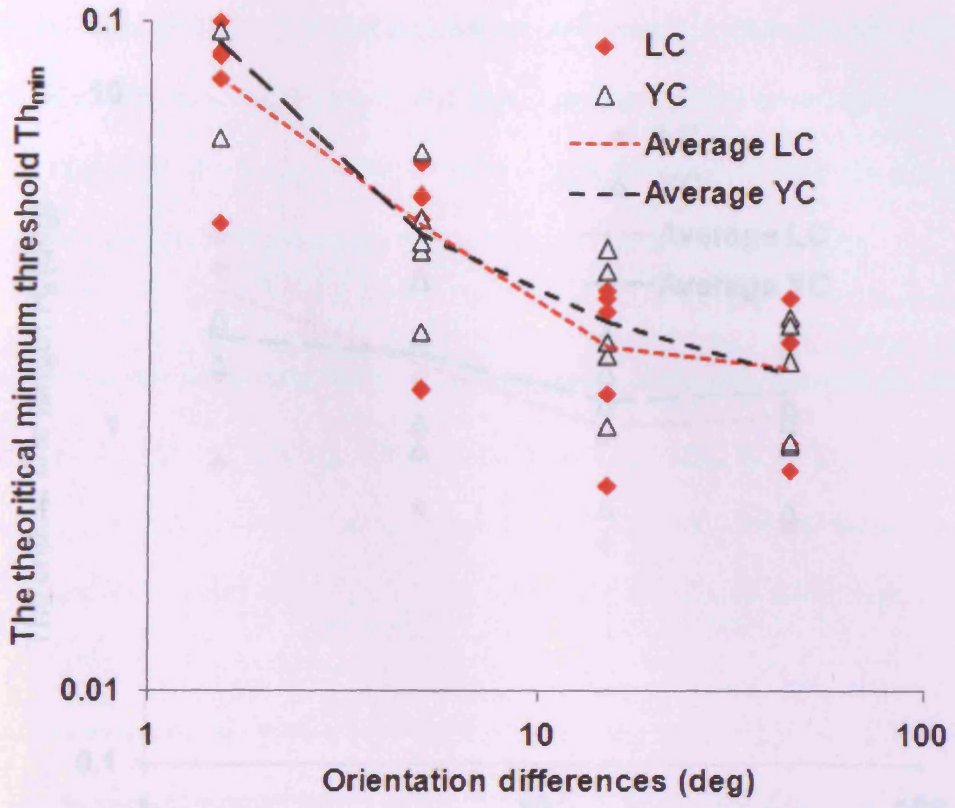

Fig 6.11 The theoretical minimum contrast threshold Th_{min} for orientation discrimination of 1.5-45 deg.

Th_{min} at 0-10 deg eccentricities was plotted against orientation difference for subjects LC and YC. The dotted curves connect the averages of Th_{min} from all eccentricities at each orientation difference. The data for LC were marked in red while in black for YC.

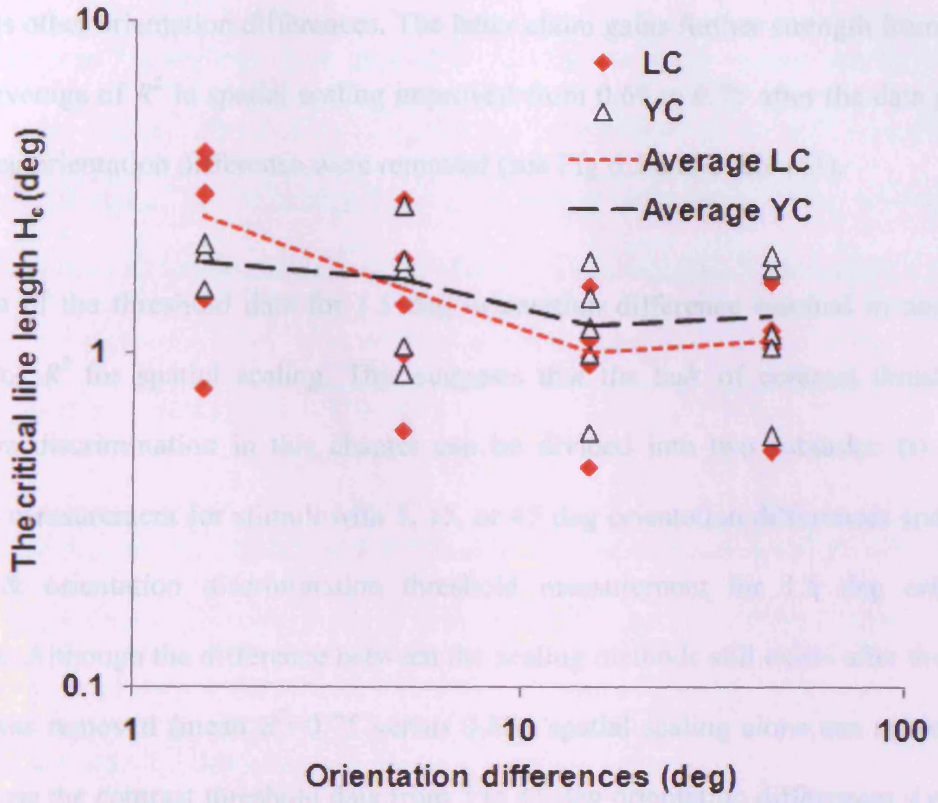

Fig 6.12 The critical line length H_c was plotted against orientation difference for subjects LC and YC. Other details are as in Fig 6.11.

6.4.2 Spatial scaling and 2D scaling

In order to equate the threshold performance, both spatial scaling and 2D scaling were used to superimpose all the threshold data to the same basic condition (E=0, OD=45). The superimposition of the threshold data by 2D scaling (with the average of R^2 being about 0.85 between subjects) was much better than that of spatial scaling (with the average of R^2 being 0.69 between subjects) (see Figs 6.4 and 6.7, and Table 6.3). The main reason for the 2D scaling being much better than the spatial scaling is that the foveal performance is noticeably superior to that of the periphery (see Fig 6.1 and 6.8). Another reason is the fact

that eccentric threshold at 1.5 deg orientation difference is considerably higher than thresholds other orientation differences. The latter claim gains further strength from the fact that the average of R^2 in spatial scaling improved from 0.69 to 0.75 after the data points at the 1.5 deg orientation difference were removed (see Fig 6.5 and Table 6.3).

Exclusion of the threshold data for 1.5 deg orientation difference resulted in about 10% increase of R^2 for spatial scaling. This suggests that the task of contrast threshold for orientation discrimination in this chapter can be divided into two subtasks: (i) contrast threshold measurement for stimuli with 5, 15, or 45 deg orientation differences and (ii) the contrast & orientation discrimination threshold measurement for 1.5 deg orientation difference. Although the difference between the scaling methods still exists after the data of 1.5 deg was removed (mean R^2=0.75 versus 0.85), spatial scaling alone can appropriately superimpose the contrast threshold data from 5 to 45 deg orientation differences, *i.e.* for the subtask (i). It suggests that the failure of the spatial scaling across 1.5 to 45 deg orientation difference could be due to the complexity of the task but not caused by the threshold performance between the fovea and periphery being qualitatively different, which is in agreement with Melmoth *et al.* (2001a).

Later the success of spatial scaling at each orientation difference (see Fig 6.10 and Table 6.5) further supports the above finding that the periphery threshold performance in this visual task could be quantitatively equated with that of the fovea.

6.4.3 Global E_2 found from the scaling across orientation differences

Both spatial and 2D scalings were applied to the threshold data across eccentricities and orientation differences. Hence, the scaling factors were dependent on both eccentricity and orientation difference. All the scaling factors, the spatial scaling factors, the vertical scaling factor and horizontal scaling factors of 2D scaling were successfully modelled by various versions of equation (6.2) with independent variables E and OD (see equations (6.3), (6.4) and (6.5)), with R^2 ranging from 0.92 to 0.98.

The global spatial scaling E_2s found during spatial scaling across orientation differences are quite similar between subjects, 3.49 for LC and 2.67 deg for YC (see Table 6.1). The average of E_2s between subjects is 3.1 deg and similar to 2.9 deg of Rovamo and Virsu (1979) and 2.4 deg of Vakrou *et al.* (2007).

The horizontal E_2s of the 2D scaling (4.77 and 5.62 deg, see Table 6.2) are larger than the global spatial E_2s due to the fact that vertical scaling was applied simultaneously. The vertical scaling E_{2v}, i.e. contrast E_2, averaged to 12.1 deg, which means that contrast scaling was rather small in comparison with size scaling. The average horizontal scaling E_{2h} in 2D scaling is 5.2 deg, which is close to 5.8 deg found by Sally *et al.* (2005) when they measured contrast threshold for discriminating a 1.5 deg tilted Gaussian filtered line stimulus from a vertical one.

6.4.4 Local E_{2OD} found from the spatial scaling at each orientation difference OD

From Fig 6.9, the local E_{2OD} found at each orientation difference first increases (from 1.5 to 5 deg) and becomes independent of orientation difference (from 5-45 deg). The difference of E_{2OD} between 1.5 and 5-45 deg orientation difference suggests that the discrimination at 1.5 deg is different (and more complicated) from those of 5-45 deg orientation difference. It further supports the the previous finding in Section 6.4.2, i.e., that the task of contrast threshold for orientation discrimination can be divided into two subtasks: (i) contrast threshold measurement at 5, 15, or 45 deg and (ii) the contrast & orientation discrimination threshold measurement at 1.5 deg orientation difference. This proves the hypothesis made in Chapter 1 Section 1.5.2: "the visual process mechanism of the visual task at large orientation difference was different from that at as small as orientation discrimination threshold."

The average of E_{2OD}s between subjects at 5-45 deg were found about 2 deg, which is similar to those of orientation discrimination in Chapters 3-5 and the previous finding in literature (e.g. 1.93 deg of Makela *et al.* 1993).

Chapter 7 Contrast threshold allowing fixed orientation difference discrimination for 4cpi grating

7.1 Introduction

Sinusoidal grating is the most common stimulus used in contrast threshold measurement (Banks, Geisler, and Bennett 1987; Campbell and Robson 1968; Dakin and Mareschal 2004; Foley and Legge 1981; Harris and Wink 2000; Luntinen and Nasanen 1993; Nachmias and Sansbury 1974; Rovamo, Rovamo and Virsu 1979; Tiippana and Nasanen 1999; Vakrou *et al.* 2007; Varadharajan and Farias 2007)

Campbell and Robson (1968) measured foveal contrast threshold of various grating patterns (sinusoidal, square, saw-tooth- and rectangular wave) at a wide range of spatial frequencies. The average luminance of a white screen was 500 cd/m^2. A white cardboard 30 cm in diameter with a central aperture either 10x10 or 2x2 cm^2 was placed in front of the screen. Subjects had to adjust the contrast of a grating with a given spatial frequency until it just disappeared from the screen. The results showed that the average minimum threshold was at 2-3 cpd. Contrast sensitivity (as the inverse of the contrast threshold) decreased at both higher and lower frequencies.

Nachmias and Sansbury (1974) measured foveal contrast discrimination thresholds for 3 and 9 cpd sinusoidal gratings. They found that (i) contrast discrimination threshold ΔC as a function of stimulus contrast C was u-shaped and ΔC was at the minimum around C=1%; and (ii) ΔC was much smaller than the contrast detection threshold of the stimulus.

Rovamo *et al.* (1978) measured contrast sensitivities of sinusoidal gratings at different spatial frequencies of 0.5 to 4 cpd at the fovea and eccentricities of 1.5, 4, 7.5, 14, and 30 deg. Grating stimuli were generated on a white CRT screen and were presented in a semi-circular frame with a 16 cm in diameter. The mean screen luminance was 11 cd/m^2. Subjects indicated in which one of two intervals the grating stimulus occurred. Contrast sensitivity was calculated as the inverse of stimulus threshold contrast. The threshold was estimated by a 4:1 staircase procedure. They found that (i) contrast sensitivity and visual acuity decreased with increasing eccentricity; (ii) 'the foveal contrast sensitivity function can be generated at any part of the visual field' by scaling the peripheral sensitivity function using the corresponding cortical magnification factor; and (iii) the best foveal contrast sensitivity was obtained with a 4 cpd grating.

Foley and Legge (1981) measured contrast detection and discrimination thresholds for 6x6 deg^2 vertical sinusoidal gratings against a background luminance 170 cd/m^2 by a 2AFC paradigm. Subjects had to judge in which interval the target grating was presented. They found that (i) the psychometric functions of contrast detection and discrimination were different in that the contrast discrimination threshold function was considerably steeper than that of contrast detection; and (ii) in agreement with Nachmias and Sansbury (1974), 'threshold discrimination was better than detection'.

Rovamo, Franssila and Nasanen (1992) measured *r.m.s.* contrast sensitivity as a function of eccentricity (from 0 to 40 deg) using a 2x2 deg^2 3 cpd sinusoidal gratings against a background luminance of 11 cd/m^2. The grating was viewed at 114 cm and had 36 cycles

per image. The found that (i) contrast sensitivity decreased with increasing eccentricity; (ii) and the sensitivity dropped faster at the further periphery (6-40 deg) compared to more central eccentricity (0-6 deg).

Reisbeck and Gegenfurtner (1998) measured foveal contrast detection thresholds of 1 cpd sinusoidal gratings within a 4 deg diameter circular aperture using a 2AFC paradigm. Stimulus was presented on a television monitor with an average luminance of 26.25 cd/m^2. Subjects reported in which of the two intervals a stimulus was presented. Using the same procedure, contrast threshold allowing discriminating the vertical and horizontal grating was measured, except that subjects had to indicate whether the presented grating was vertical or horizontal. They found that there was no significant difference between contrast detection thresholds and thresholds of discrimination orientation.

Vakrou *et al.* (2007) measured contrast sensitivity allowing discrimination of whether the target stimulus was tilted clockwise or counter-clockwise. Two types of stimuli were used: first-order stimulus (Gabor patches) and second-order stimulus (sinusoidal gratings whose luminance files were tilted-Gabor-modulated). The mean luminance of the background was 30 cd/m^2 and the viewing distance varied from 0.309 m to 13.59 m. Contrast threshold was measured as a function of spatial frequency (ranging from about 0.5 to 20 cpd) at the eccentricity of 0-20 deg. The study found that (i) for first-order Gabor stimuli, the sensitivity (as the reciprocal of the contrast threshold measured) decreased abruptly and almost linearly with increasing spatial frequency; (ii) for first-order Gabor stimuli spatial scaling successfully superimposed all the eccentric data, and the average E_2 was found to be 2.46 deg; (ii) for second-order stimuli, the sensitivity function was band-passed shaped

against spatial frequency, and the foveal sensitivity was found to be noticeably superior to that of the periphery, which made impossible equating the performance across eccentricities by spatial scaling; (iii) however, when the ratio between the spatial frequencies of the grating (the first order stimulus) and its Gabor envelope was a fixed number, the sensitivity function can be superimposed across eccentricities and an average E_2 was found be 1.88 deg. Vakrou *et al.* suggested that there was no qualitative difference in performance across visual field.

When previously studying contrast threshold allowing discrimination, researchers either used a single orientation difference between stimuli (e.g., 90 deg used by Reisbeck and Gegenfurtner (1998) to measure for discriminating between horizontal and vertical gratings, and 1.5 deg used by Sally and Gurnsey threshold 2005 to measure threshold for discriminating 1.5 deg vertically tilted line from the vertical one), or measuring contrast threshold for discriminating the direction of the stimulus tilt, clockwise or counter-clockwise (Vakrou *et al.* 2007). There was no such systematic study conducted for measuring threshold contrast allowing discriminating a ranged of fixed orientation differences from well-above orientation discrimination to discrimination threshold.

In order to continue with the investigation about orientation discrimination and contrast for 4cpi gratings in Chapter 5, *i.e.*, to further investigate the behaviour of orientation discrimination at lower contrast (near detection threshold), in this chapter, contrast thresholds allowing orientation discrimination are measured at four fixed orientation differences (45, 15, 5, and 1.5 deg) and the eccentricities of 0-10 deg.

The aims were to find out (i) whether the thresholds could be equated across eccentricities and orientation differences by spatial scaling, and (ii) whether the visual process of the task at great orientation difference was different from that at nearby orientation discrimination threshold for a grating stimulus.

7.2 Methods

7.2.1 Apparatus

Stimuli were displayed on the monitor as previously described in Chapter 2. For details see Section 2.2.1.

7.2.2 Stimuli

A series of magnified versions of a 4cpi vertical sinusoid grating and four series of magnified versions of 4cpi vertical grating stimuli with the tilt of 45, 15, 5 and 1.5 deg from vertical were generated separately at various contrast levels of 0.0005 to 1 using the software described in Chapter 2 and developed by Dr Risto Nasanen. The grating stimuli had the same configuration as the 4cpi gratings used in the orientation discrimination experiments in Chapter 4.

7.2.3 Subjects

Two highly trained subjects, LC and BU (aged 26 and 21 years, respectively), took part in the experiments. Both were corrected moderate myopes with no ocular abnormality (see Appendix I for the details of the subjects).

7.2.4 Procedure

The procedure was as in Chapter 6. Two grating stimuli of the same size, one vertical and the other tilted counter-clockwise 45, 15, 5 or 1.5 deg, were presented in random order in two intervals. Subjects had to indicate by means of the keyboard in which interval the grating tilted more counterclockwise was displayed. The viewing distances were 85.5, 114, 171 and 228 cm, resulting in stimuli with a range of 0.2513-10.69 deg of visual angle in the diameter of the circular grating. The smallest one (0.2513 deg) was achieved by presenting the smallest 10 mm diameter grating stimulus at the furthest viewing distance of 228 cm.

The threshold contrast were measured separately at orientation differences of 45, 15, 5 and 1.5 deg by using the 2AFC method described previously in Chapter 2. Data collection started with 45 deg orientation difference, and then continued with 15, 5 and 1.5 deg.

7.3 Results

In Fig 7.1, contrast sensitivity of orientation discrimination were plotted as a function of grating diameter (deg) in the visual field at orientation differences of 45, 15, 5 and 1.5 deg, and eccentricities of 0, 2.5, 5, 7.5 and 10 deg for each subject. Thresholds generally decrease and tend to reach a plateau as grating diameter increases. Threshold performance deteriorates with increasing eccentricity irrespective of orientation difference. Threshold functions move to the right along the horizontal axis with increasing eccentricity, thus implying a magnification of spatial scale. At any eccentricity the threshold functions for the orientation differences of 45, 15 and 5 deg are almost at the same vertical level whereas the functions for the orientation difference of 1.5 deg are noticeably shifted upwards.

As in Chapter 6, all the threshold (*Th*) data curves in Fig 7.1 were fitted with an equation, which was identical to equation (6.1), due to the similarity of the curves at all eccentricities and orientation differences:

$$Th = Th_{\min}(1+(H_c / H)^2)^{2.5}, \qquad \textbf{Equation 7.1}$$

(see equation (6.1) for the details of the equation and Appendix VI for the procedure of obtaining the optimal curve fitting equation). R^2 was calculated for the fit at each eccentricity and orientation difference to check the fitting accuracy of equation (7.1). R^2 values ranged within 0.86-0.99 with an average of 0.97 between subjects, indicating that equation (7.1) describes accurately all the threshold data curves (see the curve fitting results in Appendix VI Table 7).

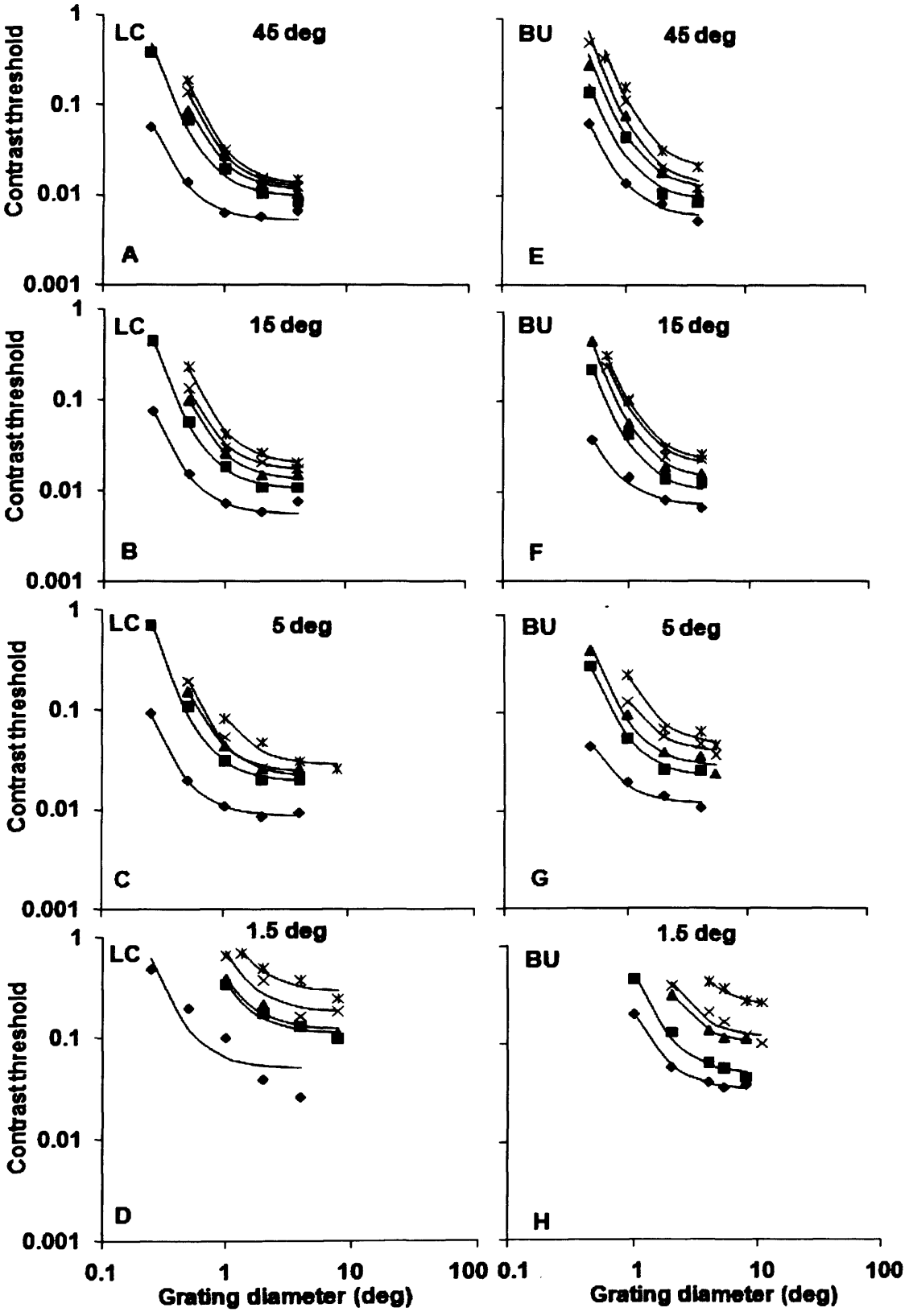

Fig 7.1 Contrast thresholds of orientation discrimination of the 4cpi grating at orientation differences of 1.5-45 deg

The contrast thresholds were plotted against grating diameter (deg) at eccentricities of 0, 2.5, 5, 7.5, and 10 deg and at orientation differences of 45, 15, 5 and 1.5 deg, for subjects LC and BU. Each data set was fitted with equation (7.1) (solid line) to model the decrease and plateau in threshold with increasing grating diameter.

7.3.1 Spatial scaling across orientation differences from 45-1.5 deg

In Chapter 6 Section 6.3.1 spatial scaling was applied to scale the contrast threshold curves of the Gaussian filtered line stimulus Here spatial scaling was used to superimpose all the contrast threshold data curves of the 4 cpi grating stimulus from 0-10 deg eccentricities and 1.5 to 45 deg orientation differences (shown in Fig 7.1) to the basic condition, the fovea and 45 deg orientation difference data (E=0, OD=45). As spatial scaling was applied to the threshold data across eccentricities and orientation differences, the scaling factors had two independent variables, eccentricity (E) and orientation difference (OD). The scaling factors increase with increasing eccentricity and decreasing orientation difference, as shown in Fig 7.2 (A, B).

Equation (7.2) was used to model the scaling factors as a function of E and OD, including all the 2nd order polynomial parameters involving eccentricity (E) and orientation difference $(OD)^{-1}$, as in equation (6.2) (for more details of the equation, see Chapter 6 Section 6.3.1).

$$F_i = 1 + E/E_2 + (OD^{-2} - 45^{-2})/k_1 + E \times (OD)^{-2}/k_2 + (OD^{-1} - 45)^{-1}/k_3 + E \times (OD)^{-1}/k_4 + E^2/E_2'$$

Equation 7.2

According to R^2 values and the accuracy of the constants (see Appendix IV for the procedure of choosing parameters), the parameters k_3 and E'_2 were discarded, and equation (7.2) was reduced to equations (7.3):

$$F_s = 1 + E/E_2 + (OD^{-2} - 45^{-2})/k_1 + E \times (OD)^{-2}/k_2 + E \times (OD)^{-1}/k_4,$$

Equation 7.3

where F_s represent spatial scaling factor.

By using equation (7.3) fitted separately to the scaling surfaces of Fig. 7.2(A, B) for subject LC and AS, the spatial scaling factors were estimated and plotted in Fig 7.2 (C, D). The resulting constants and R^2 values are summarised in Table 7.1. The high R^2s show that equation (7.3) successfully estimated spatial scaling factors depending on E and OD.

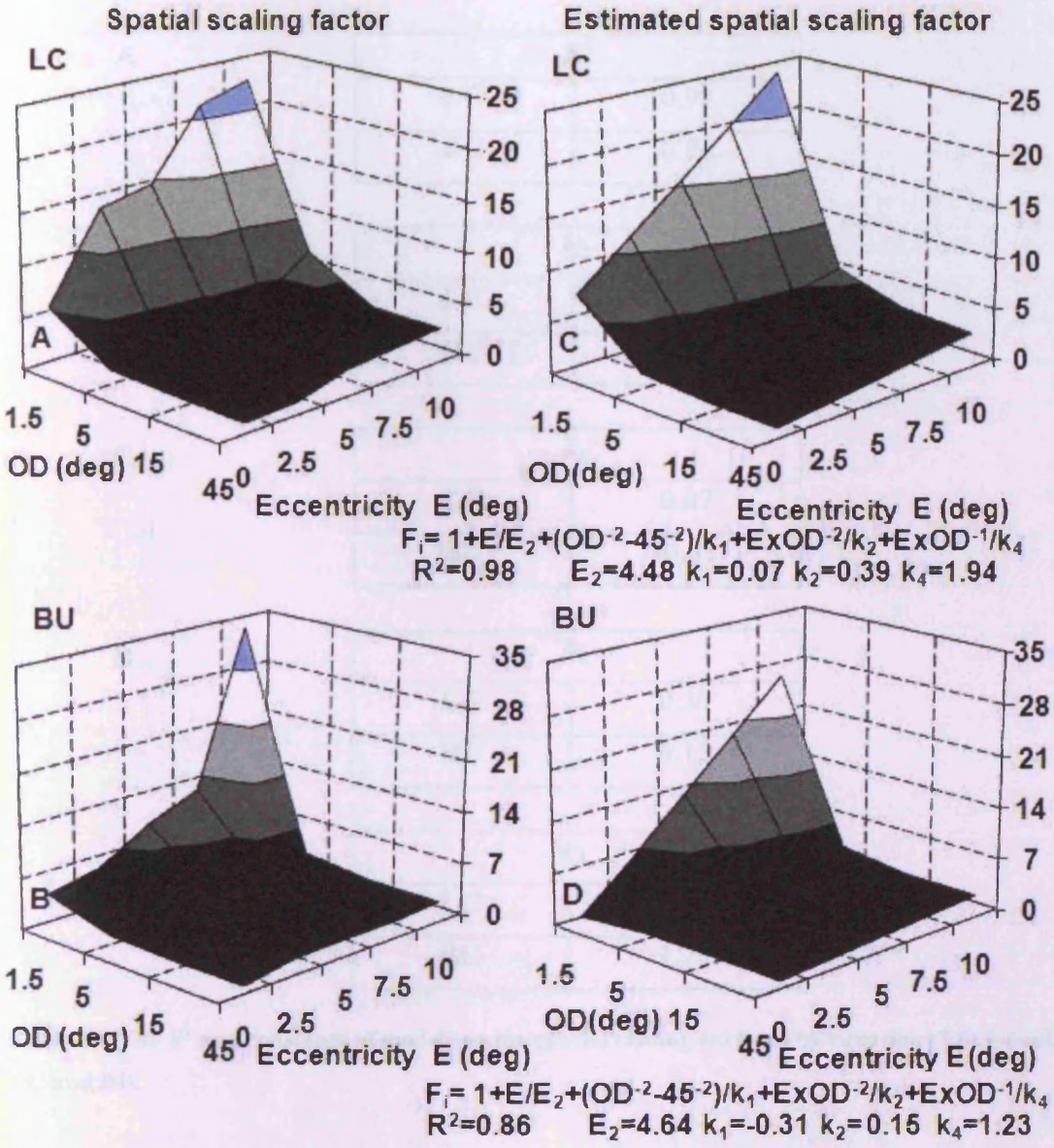

Fig 7.2 (A-D) Empirical and modelled spatial scaling surfaces for the 4cpi gratings

The empirical (left column) and modelled (right column) spatial scaling surfaces at all eccentricities (*E*) and orientation differences (*OD*) of the 4cpi gratings for subjects LC and BU. The left-hand column (A, B) shows the empirical scaling surfaces separately for LC and BU. The empirical surfaces were fitted with equation (7.3) which modelled the effects of eccentricity and orientation difference on the scaling factor F_i. The modelled scaling surfaces are shown in the right-hand column (C, D) along with the fitting equation (7.3), the corresponding parameter values used and R^2.

A

R^2	
LC	0.98
BU	0.86

B

E_2	
LC	4.48
BU	4.64

C

k_1	
LC	0.07
BU	-0.31

D

k_2	
LC	0.39
BU	0.15

E

k_4	
LC	1.94
BU	1.23

Table 7.1 The R^2 and constants of modelling the spatial scaling surfaces by equation (7.3) for subjects LC and BU.

Before spatial scaling, the unscaled experimental threshold data at all eccentricities and orientation differences were plotted against grating diameter in Fig 7.3 for subjects LC and BU.

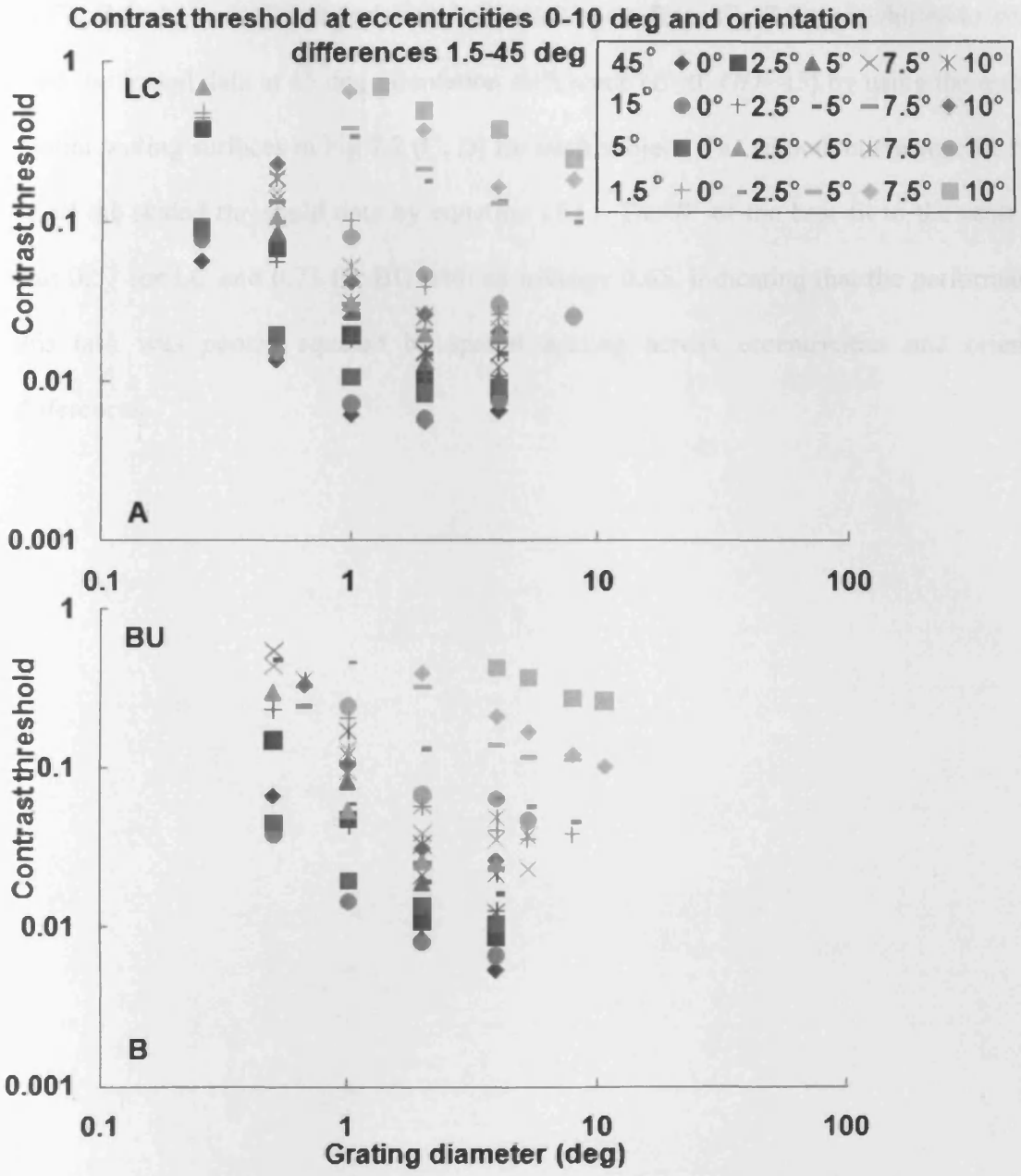

Fig 7.3 The unscaled experimental contrast threshold data of the 4cpi gratings

The unscaled threshold were plotted against grating diameter (deg) at the eccentricities of 0-10 deg and orientation differences of 1.5-45 deg for subjects LC and BU.

In Fig 7.4, the unscaled experimental threshold data from Fig 7.3 were shifted to collapse onto the foveal data at 45 deg orientation difference (E=0, OD=45) by using the estimated spatial scaling surfaces in Fig 7.2 (C, D) for each subject. The smooth curve was the best fit to all the scaled threshold data by equation (7.1). The R^2 of the best fit to the scaled data was 0.57 for LC and 0.73 for BU with an average 0.65, indicating that the performance of this task was poorly equated by spatial scaling across eccentricities and orientation differences.

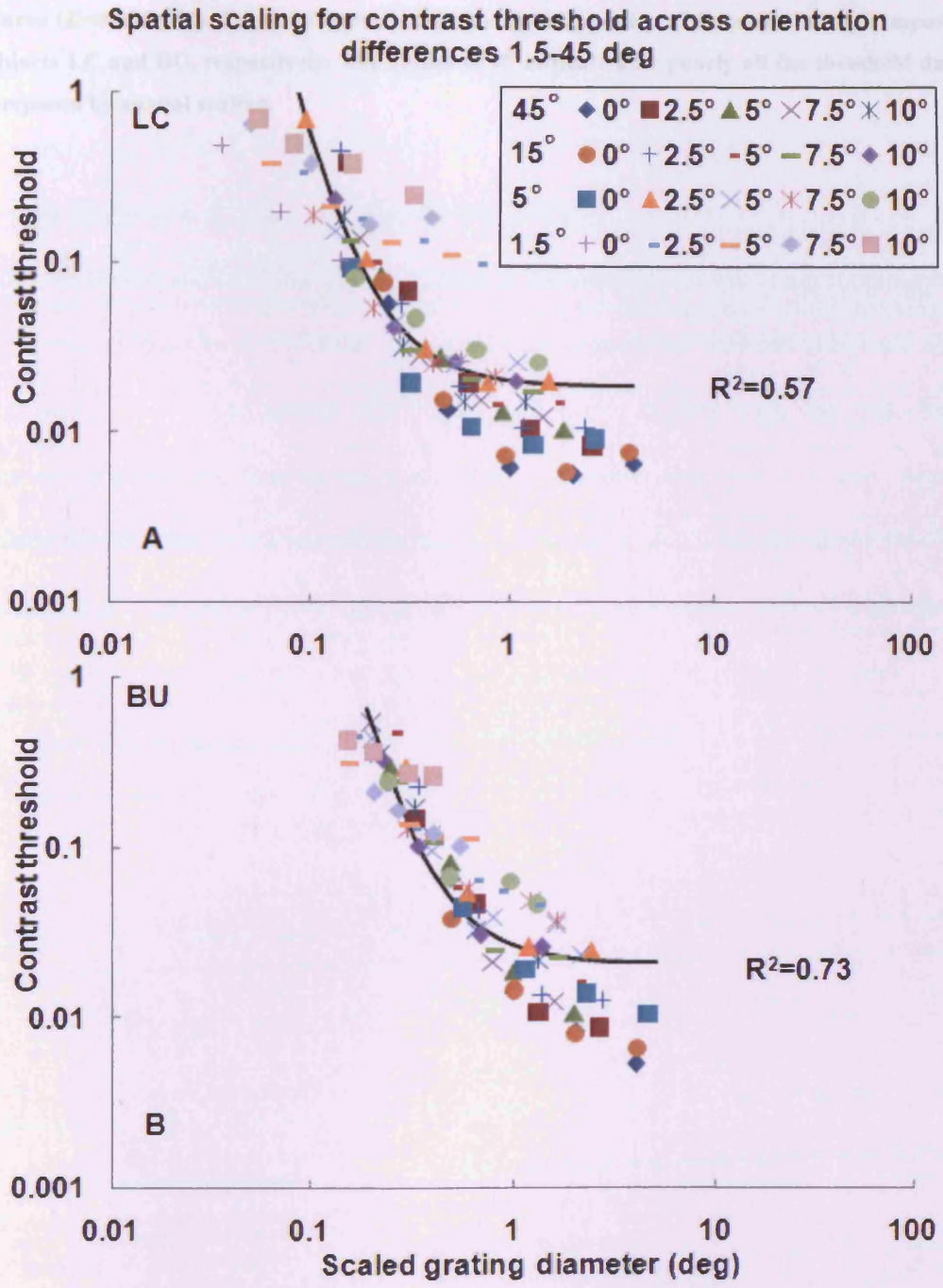

Fig 7.4 Contrast threshold data of the 4cpi gratings at 1.5-45 deg orientation difference and 0-10 deg eccentricity superimposed by spatial scaling.

The unscaled experimental contrast threshold data from Fig 7.3 (A, B) were horizontally scaled by using the estimated spatial scaling surfaces in Fig 7.2 (C, D). Data from the eccentricities of 0-10 deg and orientation differences of 1.5-45 deg collapsed onto the foveal and 45 deg orientation difference

data curve (E=0, OD=45). The solid curve is the best fit of equation (7.1) to all the superimposed data for subjects LC and BU, respectively. The values of R^2 indicate how poorly all the threshold data were superimposed by spatial scaling.

One reason of the poor R^2s is the fact that the scaled threshold data at 1.5 deg deviated from other scaled data for both subjects, as was the case with the Gaussian filtered line stimulus in Chapter 6. According to the previous orientation discrimination experiments in Chapters 3-5, the orientation difference 1.5 deg is close to the orientation discrimination threshold at 10% contrast. Thus, the complexity of the task for measuring contrast threshold allowing discrimination of 1.5 orientation difference was much higher than the task for other orientation differences. For comparison, the threshold data for 1.5 deg orientation difference was excluded and spatial scaling was applied only to the threshold data of 5-45 deg orientation differences were scaled for superposition at (E=0, OD=45), shown in Fig 7.5. The average R^2s of the best fit to the scaled data increased from 0.65 to 0.85.

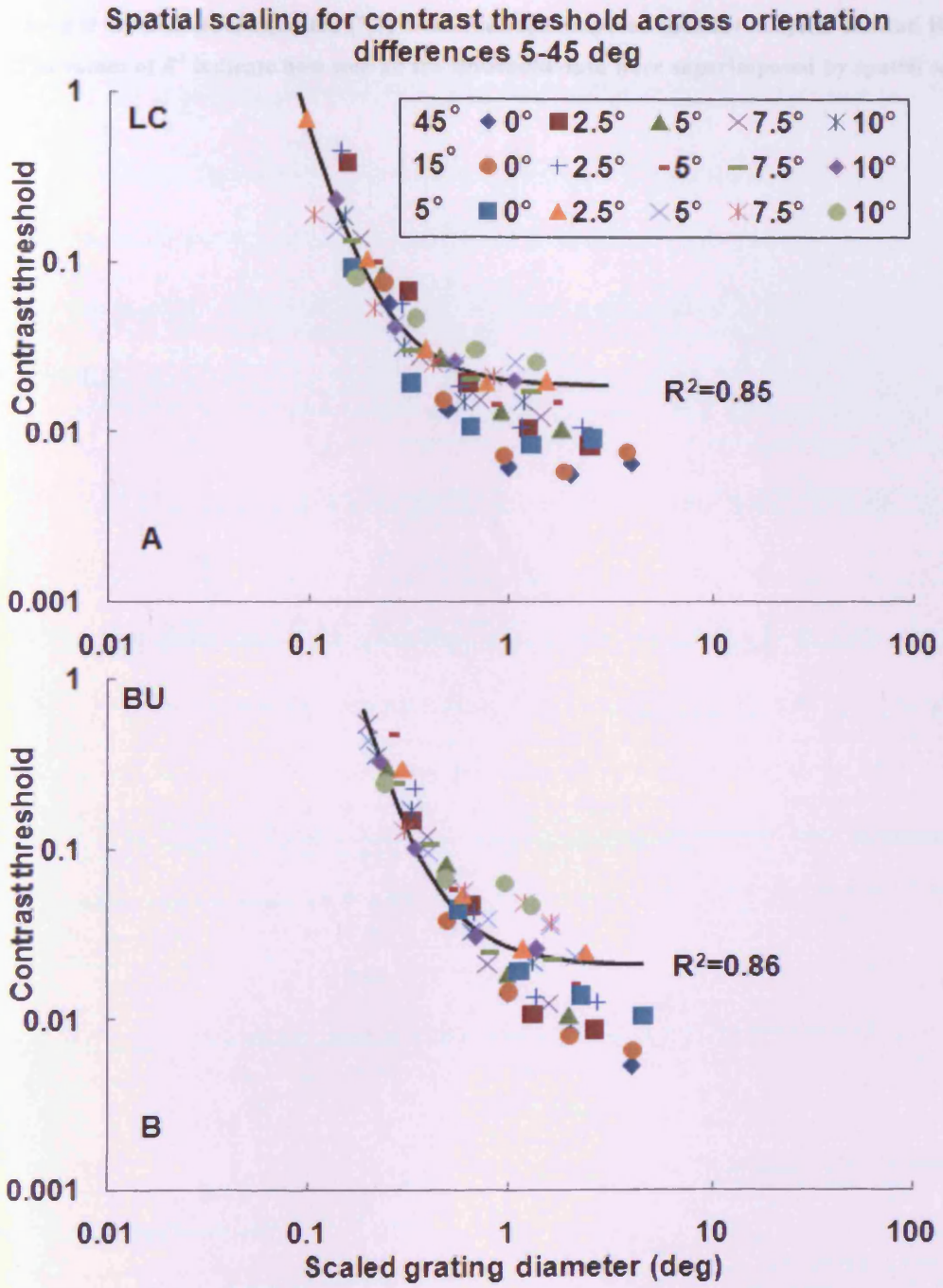

Fig 7.5 Contrast threshold data of the 4cpi gratings at 5-45 deg orientation difference and 0-10 deg eccentricity superimposed by spatial scaling.

A part of the original contrast threshold data from Fig 7.3 were scaled by using the estimated spatial scaling surfaces in Fig 7.2 (C, D). Data from the eccentricities of 0-10 deg and orientation differences of 5-45 deg collapsed onto the foveal and 45 deg orientation difference data curve (*E*=0, *OD*=45). The solid

curve is the best fit of equation (7.1) to all the superimposed data for subjects LC and BU, respectively. The values of R^2 indicate how well all the threshold data were superimposed by spatial scaling.

7.3.2 2D scaling across orientation differences from 45-1.5 deg

In this section, 2D scaling was used to superimpose the threshold data across eccentricities and orientation differences, as in Chapter 6 Section 6.3.2. The foveal threshold data at 45 deg orientation difference (E=0, OD=45) was again chosen to be the basic condition of the scaling.

Th_{min} and H_c were obtained through the curve fitting of the threshold data curves of Fig. 7.1 by equation (7.1). To obtain the 2D scaling factors, $Th_{\min}$ and H_c at each eccentricity and orientation difference were separately normalised by $Th_{\min}$ (E=0, OD=45) and H_c (E=0, OD=45). The resulting experimental 2D scaling factors, i.e. normalised $Th_{\min}$ and normalised H_c, were plotted against eccentricity and orientation difference in Fig 7.6(A, B, E, F). The scaling factors increase as eccentricity increases and orientation difference decreases. The increase with eccentricity is steeper at smaller orientation differences while the increase with decreasing orientation difference is steeper at larger eccentricities. Equation (7.2) was again used to model the dependency of the scaling factors on E and OD.

According to R^2 and the accuracy of the constants (see Appendix IV for the procedure of selecting parameters), equation (7.2) was reduced to equation (7.4) for estimating the vertical scaling factor, i.e. normalised $Th_{\min}$ and to equation (7.5) for estimating the horizontal scaling factor, i.e. normalised H_c:

$$F_t = 1 + E/E_2 + E \times (OD)^{-2}/k_2 + (OD^{-1} - 45)^{-1}/k_3 .$$

Equation 7.4

$$F_i = 1 + E/E_2 + (OD^{-2} - 45^{-2})/k_1 + E \times (OD)^{-2}/k_2 + E \times (OD)^{-1}/k_4 .$$

Equation 7.5

The 2D scaling factors of Fig 7.6 (A, B, E, F) were estimated by equations (7.4) and (7.5) in Fig 7.6 (C, D, G, H). The R^2s of the estimation ranged from 0.87 to 0.97, indicating that equations (7.4) and (7.5) successfully modelled the 2D scaling factors across eccentricities and orientation differences.

Fig 7.6 Empirical & modelled 2D scaling factors for the contrast threshold of the 4cpi gratings

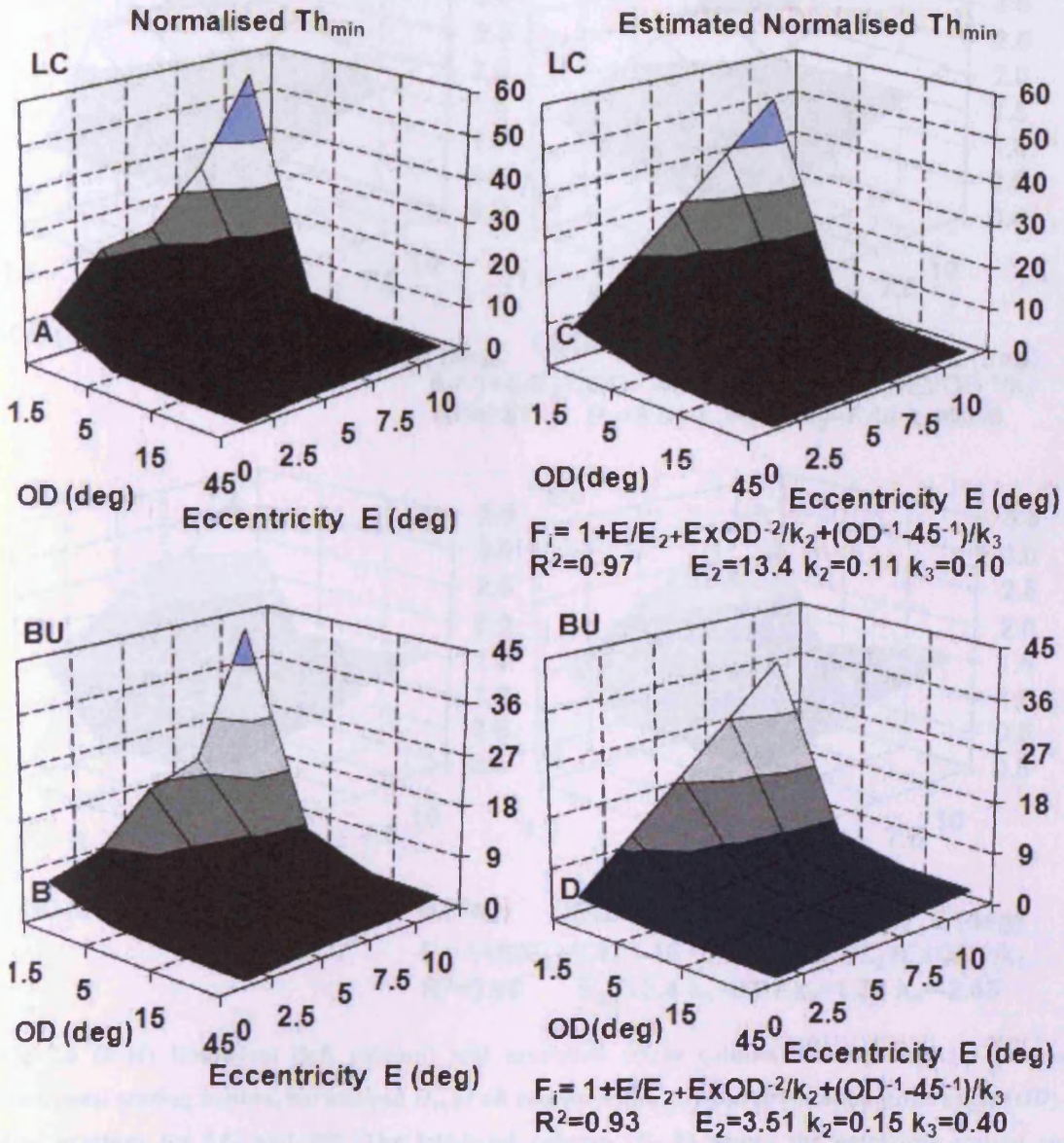

Fig 7.6 (A-D) Empirical (left column) and modelled (right column) scaling surfaces showing the vertical scaling factor, normalised Th_{min}, at all eccentricities (E) and orientation differences (OD) of the 4cpi grating for subjects LC and BU. The left-hand column (A, B) shows the empirical scaling surfaces separately for LC and BU. The empirical surfaces were fitted with equation (7.4) which modelled the effects of eccentricity and orientation difference on normalised Th_{min}. The modelled scaling surfaces are shown in the right-hand column (C, D) along with the fitting equation (7.4), the corresponding parameter values and R^2.

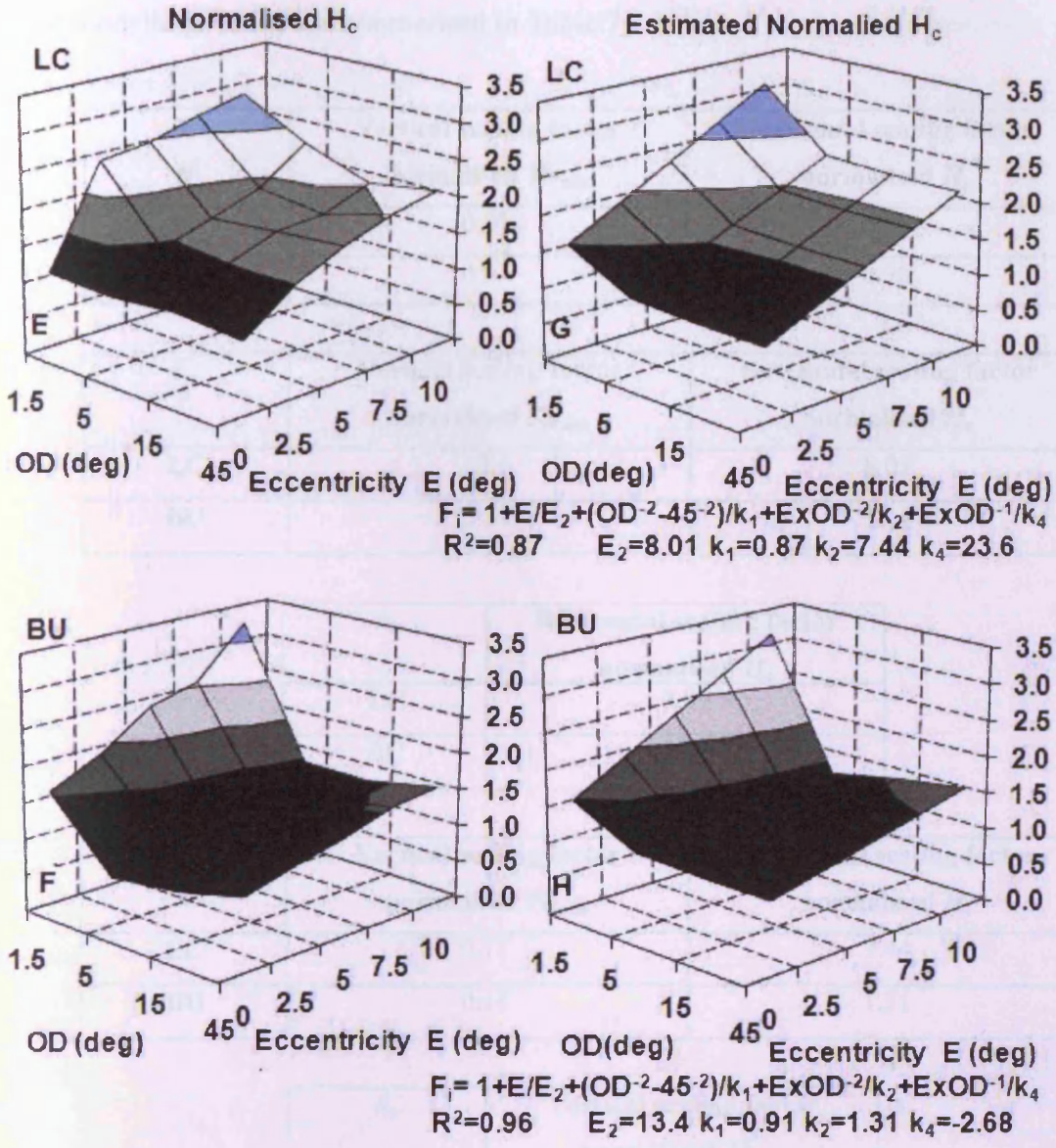

Fig 7.6 (E-H) Empirical (left column) and modelled (right column) scaling surfaces showing the horizontal scaling factors, normalised H_c, at all eccentricities (E) and orientation differences (OD) of the 4cpi gratings for LC and BU. The left-hand column (E, F) shows the empirical scaling surfaces separately for LC and BU. The empirical surfaces were fitted with equation (7.5) which modelled the effects of eccentricity and orientation difference on the normalised H_c. The modelled scaling surfaces are shown in the right-hand column (G, H) along with the fitting equation (7.5), the corresponding parameter values and R^2.

The modelling results are summarised in Table 7.2 below.

A

R^2	Vertical scaling factor normalised Th_{min}	Horizontal scaling factor normalised H_c
LC	0.97	0.87
BU	0.93	0.96

B

E_2	Vertical scaling factor normalised Th_{min}	Horizontal scaling factor normalised H_c
LC	13.4	8.01
BU	3.51	13.4

C

k_1	Horizontal scaling factor normalised H_c
LC	0.87
BU	0.91

D

k_2	Vertical scaling factor normalised Th_{min}	Horizontal scaling factor normalised H_c
LC	0.11	7.44
BU	0.15	1.31

E

k_3	Vertical scaling factor normalised Th_{min}
LC	0.10
BU	0.40

F

k_4	Horizontal scaling factor normalised H_c
LC	23.6
BU	-2.68

Table 7.2 The R^2s and constants of modelling of 2D scaling factors, normalised Th_{min} and H_c for subjects LC and BU.

In Fig 7.7, the unscaled experimental contrast threshold data at all eccentricities and orientation differences from Fig 7.3 were shifted to the basic condition (E=0,OD=45) by the estimated 2D scaling factors, i.e. the estimated normalised Th_{min} and estimated normalised H_c from Fig 7.6 (E, F, G, H). The R^2s of the best fit of equation (7.1) to all the scaled data was 0.86 and 0.92 for subjects LC and BU, respectively, showing that the threshold performance changes across all eccentricities and orientation differences can be described quite accurately in quantitative terms.

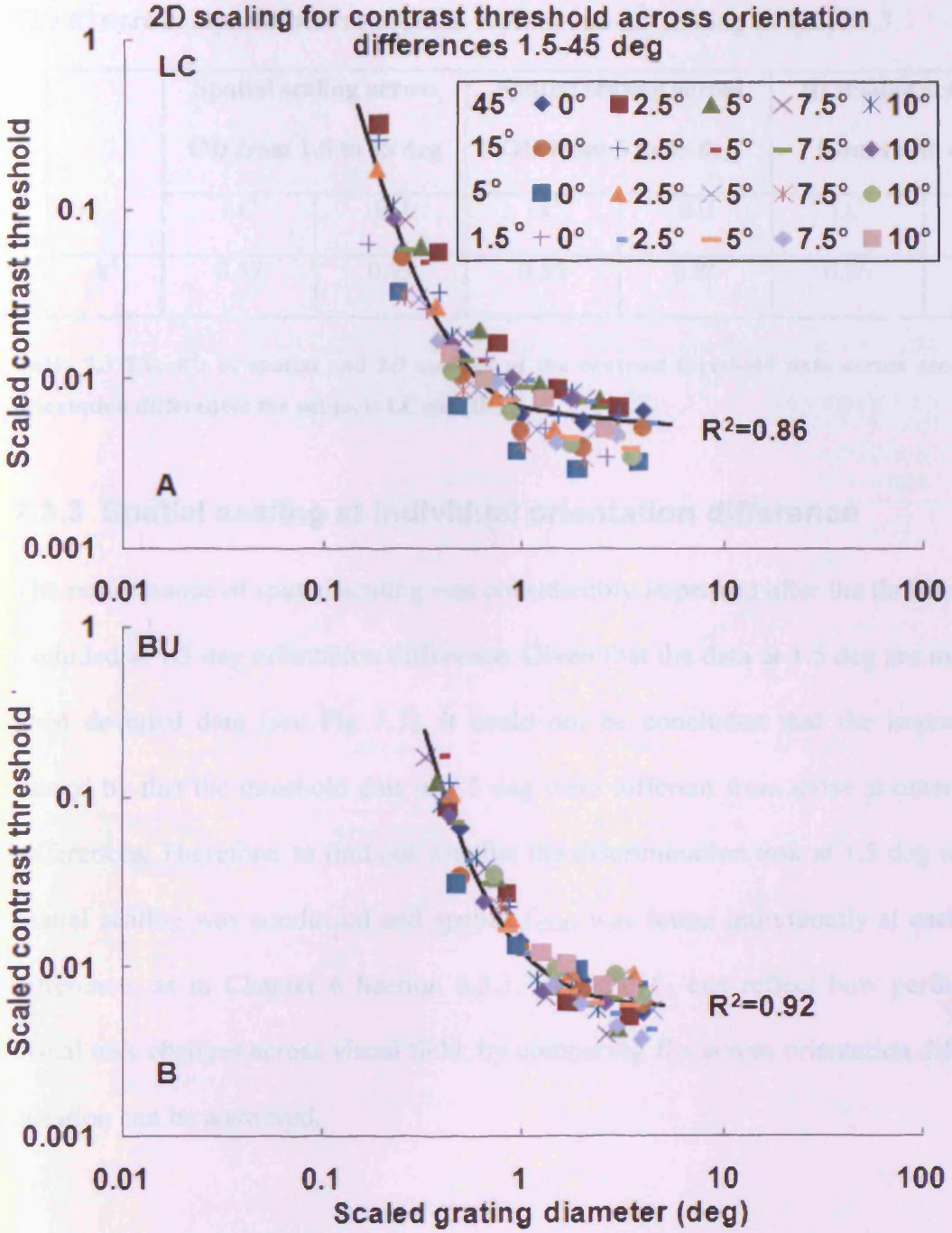

Fig 7.7 (A-B) The 2D scaled contrast thresholds for the 4cpi gratings at 0-10 deg eccentricity and 1.5-45 deg orientation difference

The original threshold data from Fig 7.3 (A, B) were both vertically and horizontally scaled by means of the modelled 2D scaling surfaces of Fig 7.6 (C, D, G, H). Data for the eccentricities of 0-10 deg and orientation differences of 45-1.5 deg collapsed onto the base condition (E=0, OD=45). The data for subjects LC and BU are as indicated. The smooth curve i.e. equation (7.1) was fitted to the scaled threshold data and R^2 indicates the accuracy of the fit for describing all the data after 2D scaling.

The R^2 s are compared between spatial scaling and 2D scaling in Table 7.3.

	Spatial scaling across OD from 1.5 to 45 deg		**Spatial scaling across OD from 5 to 45 deg**		**2D scaling across OD from 1.5 to 45 deg**	
	LC	BU	LC	BU	LC	BU
R^2	0.57	0.73	0.85	0.86	0.86	0.92

Table 7.3 The R^2s of spatial and 2D scalings of the contrast threshold data across eccentricities and orientation differences for subjects LC and BU

7.3.3 Spatial scaling at individual orientation difference

The performance of spatial scaling was considerably improved after the threshold data were excluded at 1.5 deg orientation difference. Given that the data at 1.5 deg are meanwhile the most deviated data (see Fig 7.3), it could not be concluded that the improvement was caused by that the threshold data at 1.5 deg were different from those at others orientation differences. Therefore, to find out whether the discrimination task at 1.5 deg was different, spatial scaling was conducted and spatial E_{2OD} was found individually at each orientation difference, as in Chapter 6 Section 6.3.3. Because E_2 can reflect how performance of a visual task changes across visual field, by comparing E_2s across orientation differences, the question can be answered.

In Fig 7.8, at each orientation difference, a preliminary spatial scaling factor was found at each eccentricity through the spatial scaling procedure described in Chapter 1 Section 1.3. At individual orientation difference, the preliminary scaling factors were fitted through (0, 1) against eccentricity by an optimal linear function with the corresponding best fit R^2. Final spatial scaling factors were calculated by these linear functions.

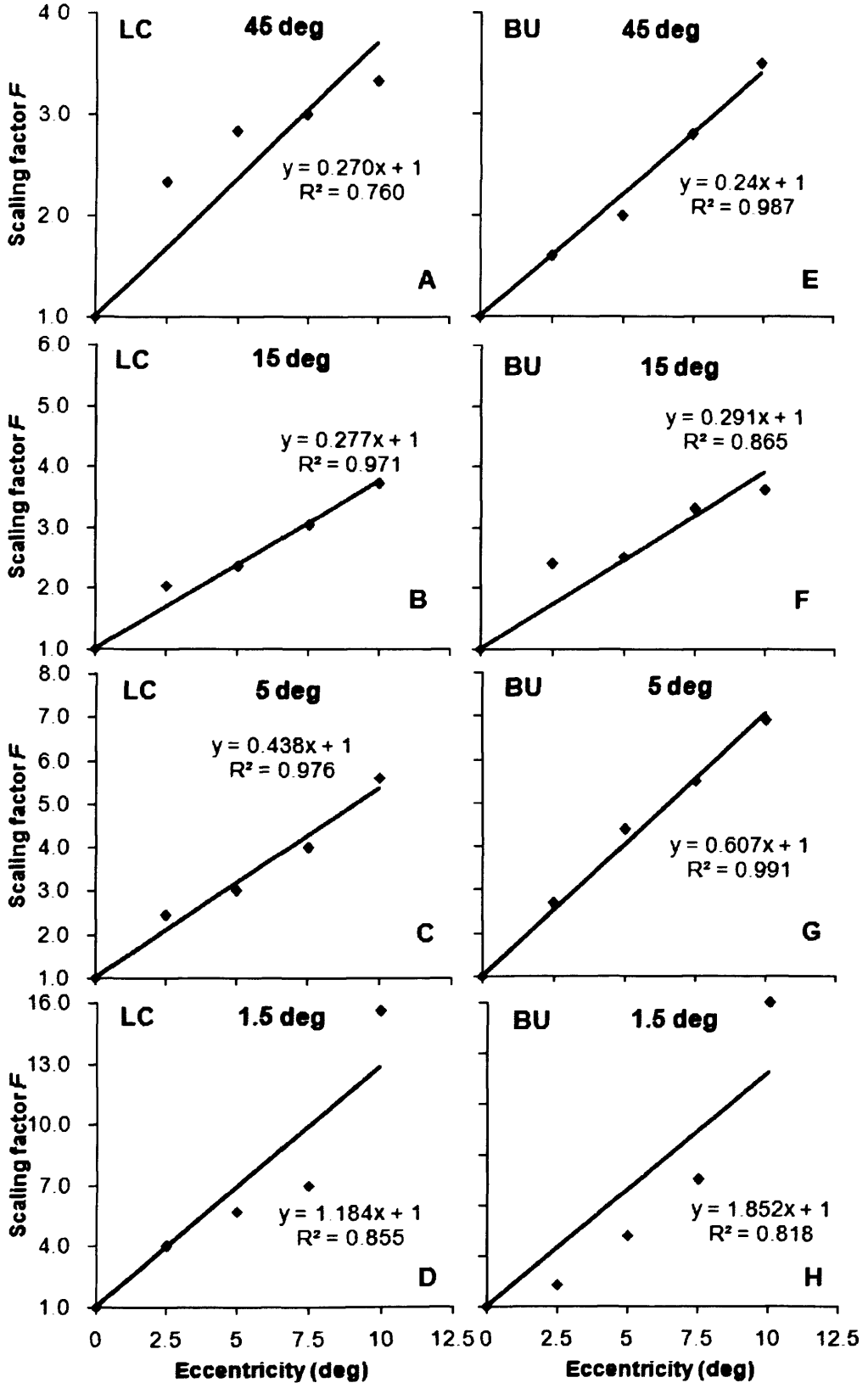

Fig 7.8 (A-H) Spatial scaling factors as a function of eccentricity at each orientation difference

At each eccentricity and orientation difference, a preliminary spatial scaling factor (■) was obtained through the spatial scaling procedure previously described in Chapter 1 Section 1.3. By individual orientation difference, the scaling factors were fitted through (0, 1) by an optimal linear function with its best fit R^2, shown in each graphs. Subjects LC and BU are as indicated.

The spatial E_{2OD} at each orientation difference was calculated as the inverse of the slope of each linear function and shown in Table 7.4.

Table 7.4 Spatial E_{2OD} at each orientation difference

E_{2OD}	LC	BU	Average
45 deg	4.03	3.69	3.86
15 deg	3.66	3.60	3.63
5 deg	2.17	2.28	2.23
1.5 deg	1.06	0.84	0.95

The E_{2OD} of each subjects and its average between subjects are plotted as a function of orientation difference in Fig 7.9.

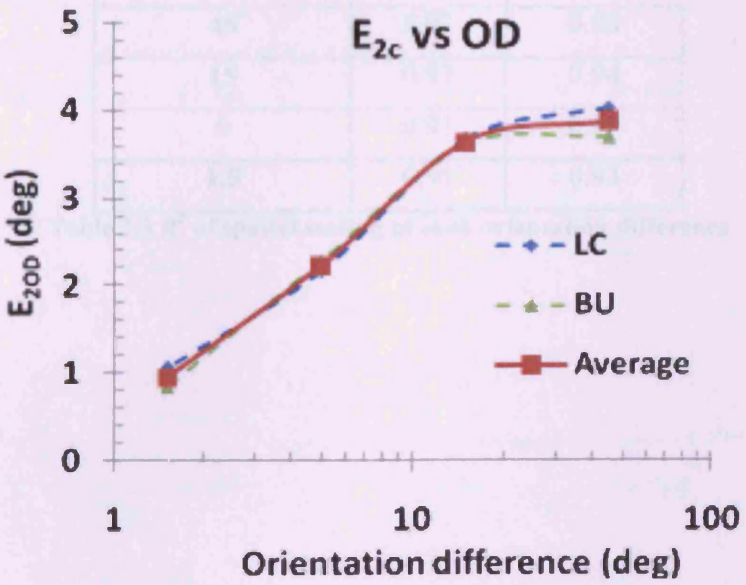

Fig 7.9 Spatial E_{2OD} is plotted as a function of orientation difference for subjects LC and BU.

The blue dash smooth curve is the function of E_{2OD} vs. orientation difference for subject LC. The green one is for BU. The average of E_{2OD}s between subjects is plotted against orientation difference with the red solid smooth curve.

Thus, the eccentric threshold data at each orientation difference (see Fig 7.1) were

horizontally shifted to superimpose on to its corresponding fovea curve by their final scaling factors in Fig 7.10. The R^2 of the best fit to each scaled threshold set by equation (7.6) (Makela *et al* 2001; Melmoth *et al.* 2000a, b; Sally *et al.* 2005) was calculated. The threshold data superimposed well at the fovea at each orientation difference, with R^2s being greater than 0.85 (see Table 7.5).

$$Th = Th_{\min}((1+(H_c / H)^{p_2})^{p_1}$$ **Equation 7.6**

OD (deg)	R^2	
	LC	BU
45	0.97	0.98
15	0.93	0.94
5	0.91	0.89
1.5	0.91	0.93

Table 7.5 R^2 of spatial scaling at each orientation difference

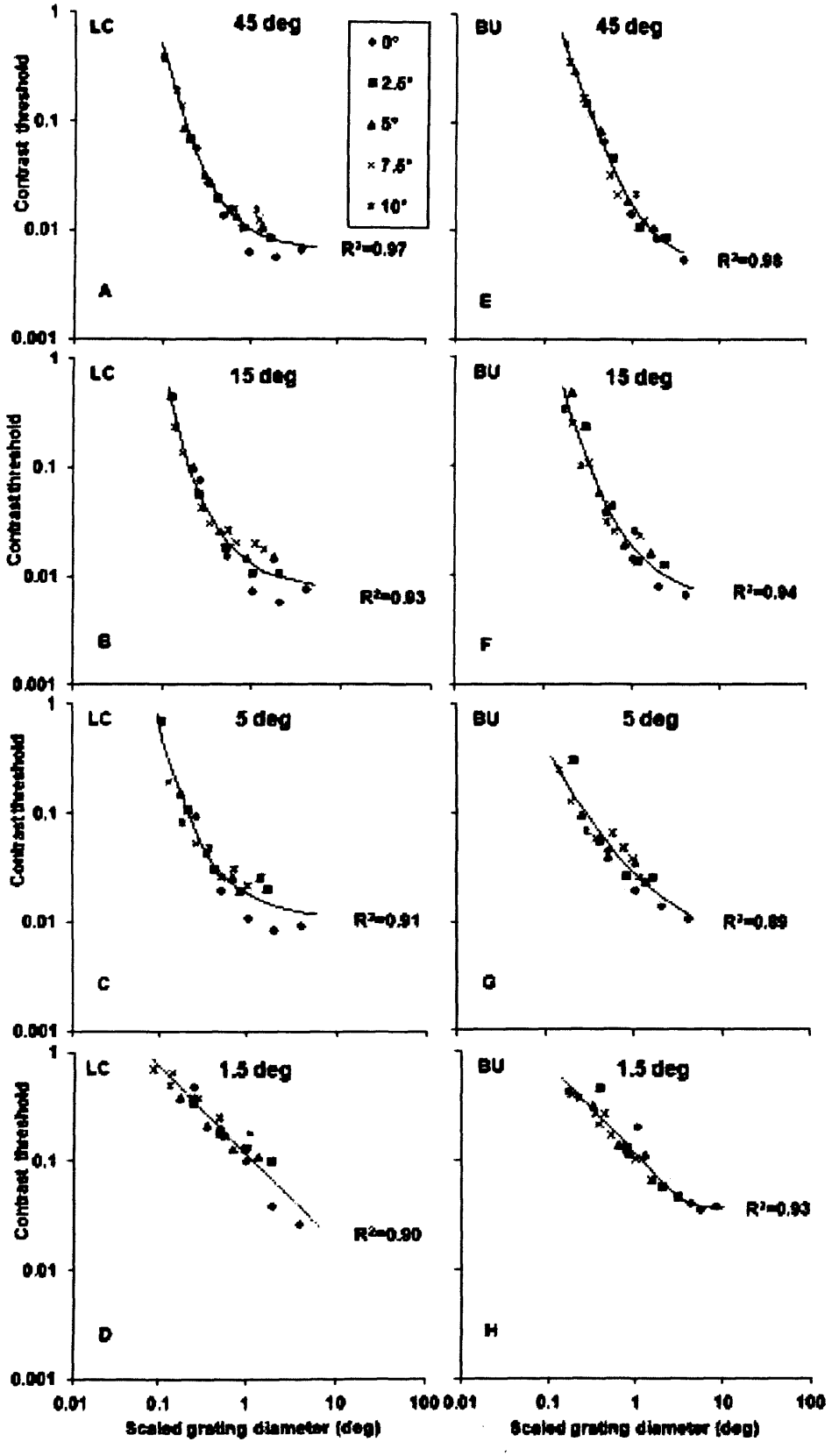

Fig 7.10 Spatial scaling of contrast threshold of orientation discrimination at 45-1.5 deg orientation

differences

At each orientation difference, the eccentric threshold curves (shown in Fig 7.1) were horizontally shifted to superimpose onto each fovea curve by spatial scaling factors calculated by using the corresponding linear function in Fig 7.9. The smooth curve was the best fit to each superimposed threshold set at each difference by equation (7.6). Data collapsed well onto the foveal function at indicating by the high R^2 values. Subjects LC and BU are as indicated.

7.4 Discussion

Equation $Th = Th_{\min}(1+(H_c / H)^2)^{2.5}$ accurately described contrast threshold as a function of grating diameter at all eccentricities of 0-10 deg and orientation differences of 1.5-45 deg (see Fig 7.1). This is in agreement with the Gaussian filtered line stimulus in Chapter 6 and with the model $S = S_{\max}(1+(w_0 / w)^p)^{-n}$ used for contrast sensitivity data of face identification by Makela *et al.* (2001), Melmoth *et al.* (2000a, b), and for contrast threshold of orientation discrimination at 1.5 deg orientation difference by Sally *et al.* 2005. However, it differs from the model $Th = \theta_{\min}(1+L_{crit} / x)^n$ used for fitting the orientation discrimination threshold data in Chapters 3-5 and Sally and Gurnsey (2003, 2004 and 2007)

The contrast threshold was first found to decrease and then to approach a plateau with increasing stimulus size, in agreement with Gaussian filtered lines in Chapter 6 as well as with Melmoth and Rovamo (2003), and Sally *et al.* (2005).

7.4.1 The theoretical minimum threshold Th_{min} and critical grating diameter H_c

The theoretical minimum contrast thresholds Th_{min}, obtained by fitting equation (7.1) to the data curves of Fig 7.1, increase with eccentricity at each orientation difference (see Fig 7.6 (A,B)), in agreement with Rovamo *et al.* (1978), Rovamo *et al.* (1992), and Sally *et al.* (2005). With increasing orientation difference, Th_{min} firstly decreased from 1.5 deg to 15 deg and then remained almost independent of orientation difference from 15 to 45 deg (see Fig 7.11 below), in agreement with $Th_{\min}$ for the contrast threshold curves of Gaussian

filtered lines in Chapter 6. The averages of Th_{min} and H_c from all eccentricities at each orientation difference was calculated for each subject and plotted in the Figs 7.11 and 7.12 to show these dependencies clearly.

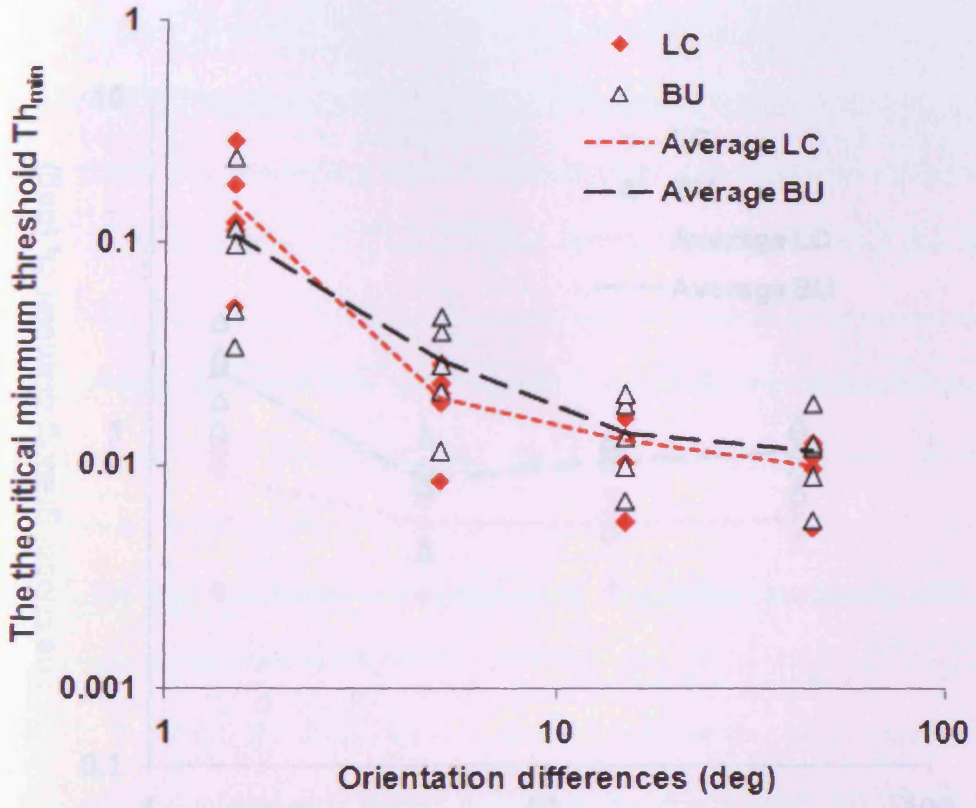

Fig 7.11 The theoretical minimum contrast threshold Th_{min} for orientation discrimination of 1.5-45 deg. Th_{min} at 0-10 deg eccentricities was plotted against orientation difference for subjects LC and BU. The dotted curves connect the averages of Th_{min} from all eccentricities at each orientation difference. The data for LC were marked in red while the colour was black for BU.

The critical stimulus size H_c increases with eccentricity at each orientation difference in Fig 7.6 (E, F). However, H_c was almost independent of orientation difference at 5-45 deg in Fig 7.12. This independence is in agreement with the H_c of Gaussian filtered line stimulus in Fig 6.12 of Chapter 6.

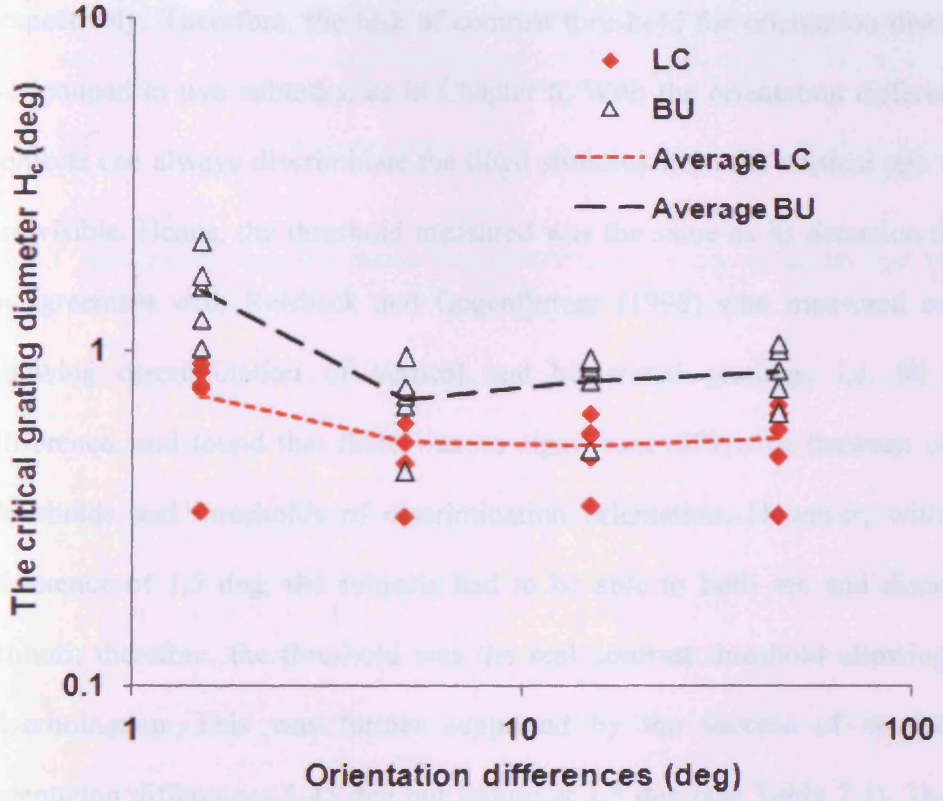

Fig 7.12 The critical grating diameter H_c was plotted against orientation difference for subjects LC and BU.

Other details are as in Fig 7.11.

7.4.2 Spatial scaling and 2D scaling

In orientation discrimination experiments of Chapter 4, the minimum orientation discrimination thresholds found ranged from 0.6 to 2.7 deg at eccentricities of 0-10 deg and 10% contrast and were 1.5 and 2.7 deg at the eccentricity of 10 deg for LC and BU, respectively. Therefore, the task of contrast threshold for orientation discrimination could be grouped in two subtasks, as in Chapter 6. With the orientation difference of 5-45 deg, subjects can always discriminate the tilted stimulus from the vertical one when the stimuli are visible. Hence, the threshold measured was the same as its detection threshold. This is in agreement with Reisbeck and Gegenfurtner (1998) who measured contrast threshold allowing discrimination of vertical and horizontal gratings, i.e. 90 deg orientation difference, and found that there was no significant difference between contrast detection thresholds and thresholds of discrimination orientation. However, with the orientation difference of 1.5 deg, the subjects had to be able to both see and discriminate the two stimuli; therefore, the threshold was the real contrast threshold allowing the orientation discrimination. This was further supported by the success of spatial scaling across orientation differences 5-45 deg but failure at 1.5 deg (see Table 7.3). The average of R^2s between subjects increased from 0.65 to 0.85 after excluding the contrast threshold data at 1.5 deg orientation difference, which almost reaches the performance level of 2D scaling with the average R^2 of 0.89. It confirms that the peripheral performance in this visual task is only quantitatively different from that of the fovea.

Both spatial and 2D scalings were applied to the threshold data across eccentricities and orientation differences. Therefore, the scaling factors were dependent on both eccentricity

and orientation difference. The variants, i.e. equations (7.3–7.5), of equation (7.2) successfully modelled all the scaling factors with R^2 ranging from 0.86 to 0.98. The same variants were used for the Gaussian filtered line stimulus in Chapter 6.

Furthermore, the success of spatial scaling (with R^2>0.85, see Table 7.5) at each orientation difference further supports that the difference of threshold performance between the fovea and periphery is quantitative but not qualitative (see Fig 7.10).

7.4.3 Global E_2 found from the scaling across orientation differences

The global spatial E_2s found during spatial scaling across orientation differences (4.48 deg for LC and 4.68 deg for BU) are much smaller than the horizontal E_2s of the 2D scaling (8.01 deg for LC and 13.4 deg for BU). This difference was caused by the simultaneous application of the vertical scaling in 2D scaling. TheE_2s are also close to 3.1 deg found in Chapter 6 for the Gaussian filtered lines and to 5.8 deg found by Sally *et al.* (2005) who measured contrast threshold for discriminating 1.5 deg orientation difference between tilted and vertical line stimuli.

7.4.4 Local E_{2OD} found from the spatial scaling at each orientation difference OD

As shown in Fig 7.9, the local E_{2OD} at each orientation difference first increases (from 1.5 to 5 deg) and becomes independent of orientation difference (from 5-45 deg). The average of E_{2OD} at 1.5 deg is about 1 deg and much smaller than those of other differences ranging

from 2.3 to 3.9 deg. This supports that the finding in Section 7.4.2, *i.e.*, that the visual task at 1.5 deg is different from (and more complicated than) those of 5-45 deg orientation differences. It is also consistent with the conclusion in Chapter 6 and confirms the hypothesis (in Chapter 1 Section 1.5.2: "the visual process mechanism of the visual task at large orientation difference was different from that at as small as orientation discrimination threshold.").

Chapter 8 The effects of eccentricity, orientation difference and cpi on contrast threshold of orientation discrimination

8.1 Introduction

Some early studies investigated the effect of the number of cycles (*i.e.* cpi) or grating area on contrast sensitivity using sinusoidal gratings (Banks *et al.* 1987; Hoekstra *et al.* 1974; Jamar and Koenderink 1985; McCann, Savoy and Hall Jr 1978; Rovamo *et al.* 1993 Savoy and McCann 1975; Virsu and Rovamo 1979). Contrast sensitivity was found to increase and saturate with increasing grating area or the number of cycles for gratings at low spatial frequencies (Luntinen, Rovamo and Nasanen 1995; McCann *et al.* 1978; Savoy and McCann 1975; Virsu and Rovamo 1979). Especially, for the sinusoidal gratings with less than 16 cycles, spatial frequency has no essential effect on the threshold contrast (Howell and Hess 1978; McCann *et al.* 1978; Savoy and McCann 1975) whereas the number of cycles has a stronger effect on grating contrast detection threshold (Hoekstra *et al.* 1974; Jamar and Koenderink 1983; Savoy and McCann 1975).

Hoekstra *et al.* (1974) measured contrast modulation thresholds using sinusoidal gratings as a function of the number of cycles in stimulus image. They found that (i) contrast threshold decreased and reached a plateau with increasing number of cycles; (ii) the critical number of cycles, in which the threshold became independent of the number of cycles, increased with increasing background luminance, and (iii) threshold data plotted as a function of the number of cycles collapsed together at different spatial frequencies for each luminance

level studied. Therefore, Hoekstra *et al.* suggested that the number of cycles but not spatial frequency determined the contrast modulation threshold when low-frequency (1-7 cpd) stimulus was used.

Savoy and McCann (1975) measured contrast sensitivity of a sinusoidal grating as a function of the number of cycles. The stimulus had a range of cycles from 0.5 to 80. The mean background luminance was 9.3 cd/m^2. The viewing distance ranged from 41 to 290 cm so that the sinusoidal grating subtended from 7.6 to 0.83 deg in visual field. Subjects had to adjust the stimulus contrast until it was just visible. They found that when the number of cycles was less than about 4, the contrast sensitivity of the target stimulus at different frequencies was almost the same and suggested that the number of cycles plays an essential role rather than spatial frequency for the visibility of the low-number-of-cycle sinusoidal gratings.

Howell and Hess (1978) conducted two experiments to separately measure contrast sensitivity as a function of grating-bar length and the number of grating cycles. Their results showed that contrast sensitivity improved and approached a plateau (i) with increasing grating-bar length when using a 5cpi grating at spatial frequencies of 0.1 to 20 cpd and (ii) with increasing cpi at spatial frequencies of 0.1 to 10 cpd.

Jamar and Koenderink (1983) investigated how the number of cycles of sinusoidal gratings influenced visual performance in a suprathreshold contrast situation. Contrast thresholds for detecting contrast and spatial frequency differences were measured as a function of the number of grating cycles. The study showed that thresholds decreased with increasing

number of grating cycles up to 16 and became independent thereafter, in agreement with Hoekstra *et al.* (1974).

Banks *et al.* (1987) measured foveal contrast sensitivity for 7.5 cpi sinusoidal gratings at spatial frequencies of 5, 7, 10, 14, 20, 28, and 40 cpd. They found that human contrast sensitivity was 1/20 of the ideal discriminator (Geisler 1984)[2], but the shapes of the two contrast sensitivity functions were quite similar at spatial frequencies of 5 to 40 cpd, which implied that the high-frequency roll-off of contrast sensitivity function for the gratings with a fixed number of cycles was due to the pre-neural factors alone.

Rovamo *et al.* (1993) measured contrast sensitivity as a function of grating area at spatial frequencies of 0.125 to 32 cpd and found that (i) contrast sensitivity at all spatial frequencies improved with increasing grating area for small gratings but the improvement ceased when the grating area exceeded a critical value and contrast sensitivity became independent of area; and (ii) when the critical area was expressed in terms of the number of cycles, the critical number of cycles increased and approached a plateau with increasing spatial frequency.

Luntinen *et al.* (1995) investigated how grating area and spatial frequency affected *r.m.s* contrast sensitivity. The sensitivity first increased and then saturated with increasing grating area. The critical area, where the increase of contrast sensitivity saturated, decreased with

---

[2] Geisler (1984) derived an ideal discriminator with a 2AFC paradigm, which was created by combining the effect of the pre-neural factors including the quantal fluctuations, the optical transfer function, and the spatial distribution of the receptors in the retina.

increasing spatial frequency, in agreement with Virsu and Rovamo (1979) and Rovamo *et al.* (1993).

The previous studies generally suggested that the number of grating cycles had a much stronger influence on the contrast threshold than spatial frequency when the number was lower than 16 cycles and a critical grating area existed where the threshold became independent. Therefore, in addition to eccentricity and orientation difference, cpi was examined as another variable, on which the threshold performance was dependent.

In details, first, another two experiments of measuring contrast thresholds allowing orientation discrimination were conducted by using 2 and 16cpi sinusoidal gratings at orientation differences of 45, 15, 5, and 1.5 deg and at the eccentricities of 0-10 deg, as for the 4cpi gratings in Chapter 7. The threshold data for the 2 and 16cpi gratings are presented, analyzed and modelled, as for the 4cpi gratings in Chapter 7. Secondly, all the contrast threshold data allowing orientation discrimination obtained by using the Gaussian filtered line and gratings with different cycle numbers are pooled together to investigate the relation of the number of cycles, eccentricity, orientation difference, grating area, and contrast.

We aimed to test the 2nd and 3rd hypothesis[3], made in Chapter 1 Section 1.5.2

[3] The 2nd hypothesis: for low-cycle-number grating stimulus, the number of cycles plays a crucial role on the visual performance across visual field.

The 3rd hypothesis: the visual process mechanism of the visual task at large orientation difference is different from that at as small as orientation discrimination threshold.

8.2 Methods

8.2.1 Apparatus

Apparatus used in this experiment has been previously described in Chapter 2.

8.2.2 Stimuli

The 2 and 16cpi sinusoidal grating series were created as the 4cpi grating series in Chapter 7. The configurations of the 2 and 16cpi gratings were the same as the 2 and 16cpi gratings used in the orientation discrimination experiments in Chapter 5.

8.2.3 Subjects

Subjects were LC and BU, as in Chapter 7.

8.2.4 Procedure

The procedure of thresholds measured was as in Chapter 7. Subjects indicated which one of two successive intervals contained the grating tilted more counterclockwise via the keyboard. The viewing distances for the 2cpi gratings were 57, 114, 171 and 228 cm, resulting in grating stimulus size ranging from 0.2513 to 15.98 deg of visual angle in grating diameter. The smallest size 0.2513 deg was achieved by presenting the smallest grating, 10 mm in diameter, at the furthest viewing distance of 228 cm. The viewing

distances for the 16cpi gratings were 57, 114, 171, 228 and 456 cm, resulting in gratings with a range of from 0.5026 to 15.98 deg of visual angle in grating diameter. The smallest size 0.5026 deg was achieved by presenting the smallest grating 40 mm (or 20 mm) in diameter stimulus at the furthest viewing distance of 456 cm (or 228 cm) for LC (or for BU).

8.3 Results

Figs 8.1 and 8.2 show contrast thresholds allowing orientation discrimination plotted as a function of grating diameter (deg) in the visual field at orientation differences of 45, 15, 5, and 1.5 deg, and eccentricities of 0, 2.5, 5, 7.5 and 10 deg for the 2 and 16 cpi gratings, respectively. Thresholds generally decrease and reach a plateau with increasing grating diameter. As in Figs 6.1 and 7.1, the threshold data at orientation differences of 5-45 deg are at the similar vertical level at each eccentricity while the thresholds at the orientation difference of 1.5 deg are noticeably higher. Subject BU was not able to discriminate the grating tilted 1.5 deg from the vertical grating at the eccentricities of both 7.5 and 10 deg for the 2cpi gratings.

As in Chapters 6 and 7, each threshold (*Th*) data set for the 2 and 16cpi gratings was in Fig 8.1 fitted with equation (8.1) (which is the same as equations (6.1) and (7.1)):

$$Th = Th_{\min}(1+(H_c / H)^2)^{2.5}. \qquad \textbf{Equation 8.1}$$

For details of equation (8.1), see equation (6.1) in Chapter 6 and Appendix VI. The R^2 of the fits of equation (8.1) to each threshold data set ranged from 0.91 to 0.99 with an average of 0.97 for the 2 cpi gratings (see Appendix VI Table 6), and from 0.91-0.99 with an average of 0.98 for the 16 cpi gratings (see Appendix VI Table 8). Thus, equation (8.1) accurately described each threshold data set for the 2 and 16cpi gratings.

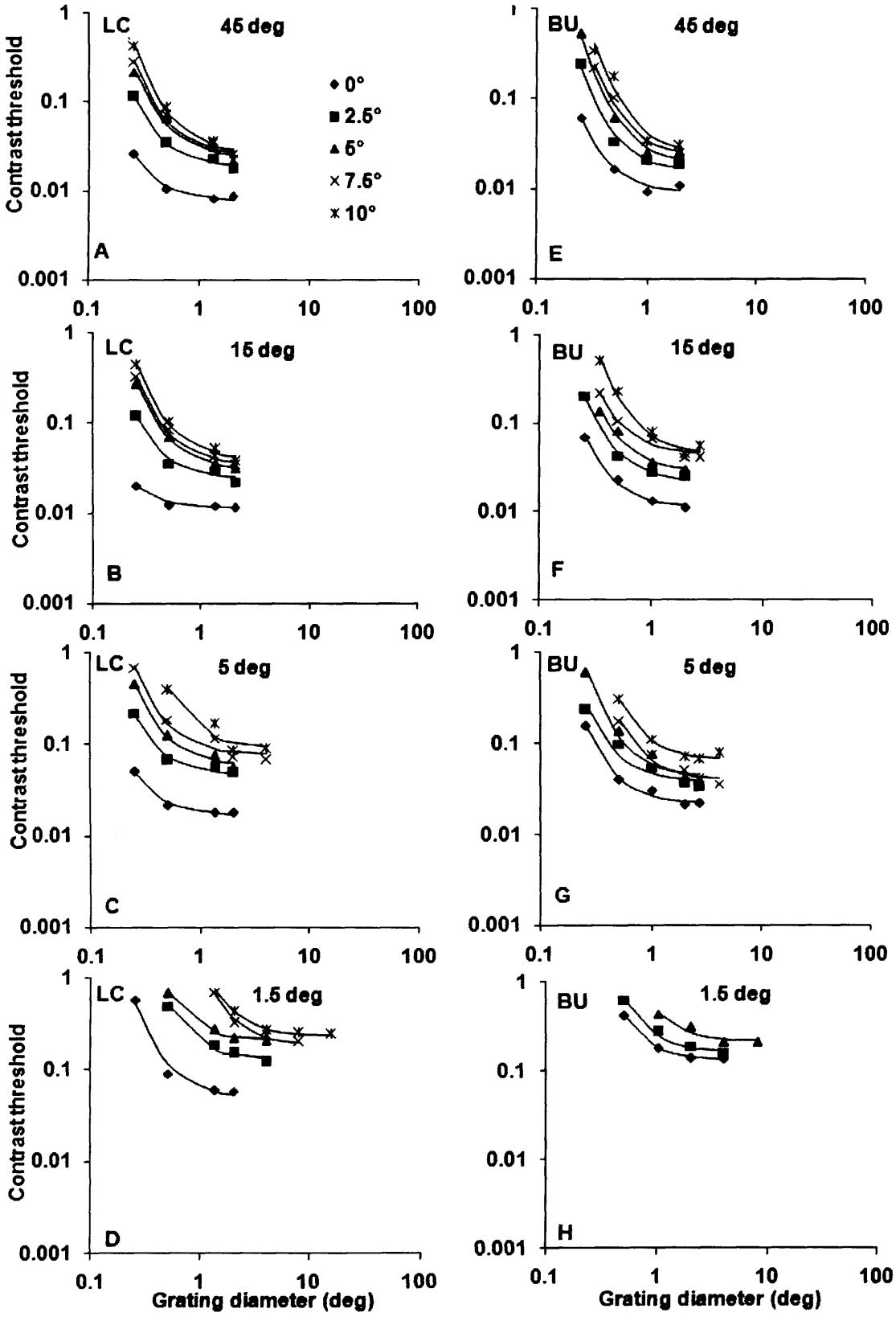

Fig 8.1 Contrast thresholds of orientation discrimination of the 2cpi grating at 1.5-45 deg orientation

differences and 0-10 deg eccentricities.

The contrast thresholds at orientation differences of 45, 15, 5, and 1.5 deg were plotted against grating diameter (deg) at eccentricities of 0, 2.5, 5, 7.5, and 10 deg for subjects LC and BU. Each data set was fitted with equation (8.1) (solid line) to model the decrease and plateau in threshold with increasing grating diameter.

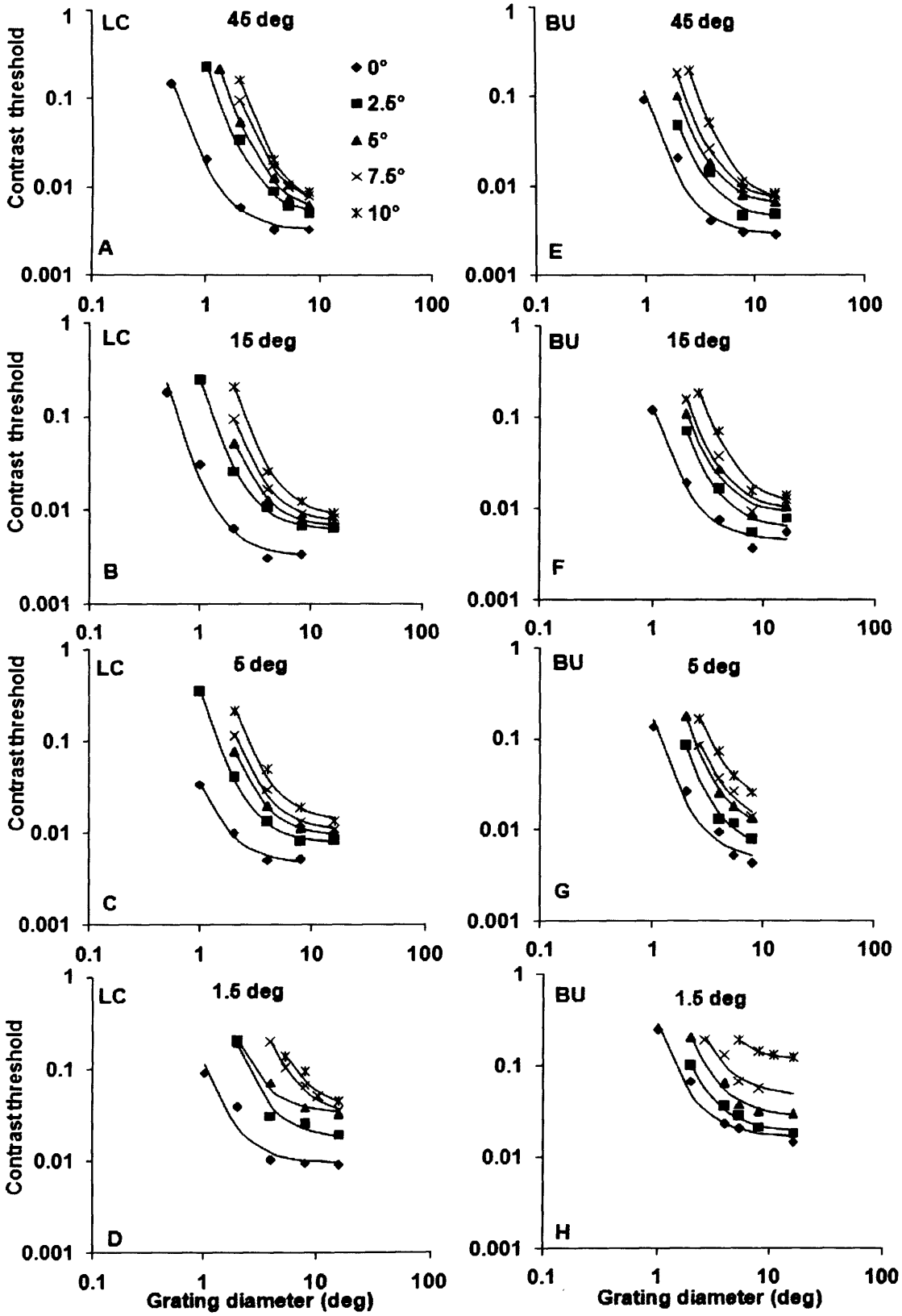

Fig 8.2 Contrast thresholds of orientation discrimination of the 16cpi gratings at 1.5-45 deg orientation differences and 0-10 deg eccentricities. Other details are as in Fig 8.1.

8.3.1 Spatial scaling across orientation differences from 45-1.5 deg

In this section spatial scaling was used to superimpose the contrast threshold data from different eccentricities and orientation differences to the basic condition, the fovea and 45 deg orientation difference data (E=0, OD=45), separately for the 2 and 16 cpi gratings .

As spatial scaling was applied to the threshold data across eccentricities and orientation differences, the scaling factors had two independent variables, eccentricity (E) and orientation difference (OD), as in Chapters 6 and 7. In Figs 8.3 (A,B) and 8.4 (A,B), the factors obtained through the spatial scaling procedure (See Chapter 1 Section 1.3.3) were plotted against eccentricity and orientation difference, for the 2 and 16cpi gratings, respectively. As shown in the figures, the spatial scaling factor increases with increasing eccentricity and decreasing orientation difference. Equation (8.2), used to model the dependency of the scaling factor on E and OD, included all the 2nd order polynomial parameters involving E and OD^{-1}, as in equations (6.2) and (7.2) (for more details of the equation, see Chapter 6 Section 6.3.1).

$$F_i = 1 + E/E_2 + (OD^{-2} - 45^{-2})/k_1 + E \times (OD)^{-2}/k_2 + (OD^{-1} - 45)^{-1}/k_3 + E \times (OD)^{-1}/k_4 + E^2/E_2'$$

Equation 8.2

The parameters k_3 and E'_2 were discarded according to R^2 and the accuracy of the constants (see Appendix IV for the procedure of selecting parameters and obtaining the optimal equation for modelling), and equation (8.2) was reduced to equation (8.3):

$$F_s = 1 + E/E_2 + (OD^{-2} - 45^{-2})/k_1 + E \times (OD)^{-2}/k_2 + E \times (OD)^{-1}/k_4 .$$

Equation 8.3

By using equation (8.3) fitted separately to the spatial scaling factors of Fig. 8.3(A, B) and 8.4(A, B), the spatial scaling factors were estimated and plotted in Figs 8.3 (C, D) and 8.4 (C, D) for the 2 and 16cpi gratings, respectively.

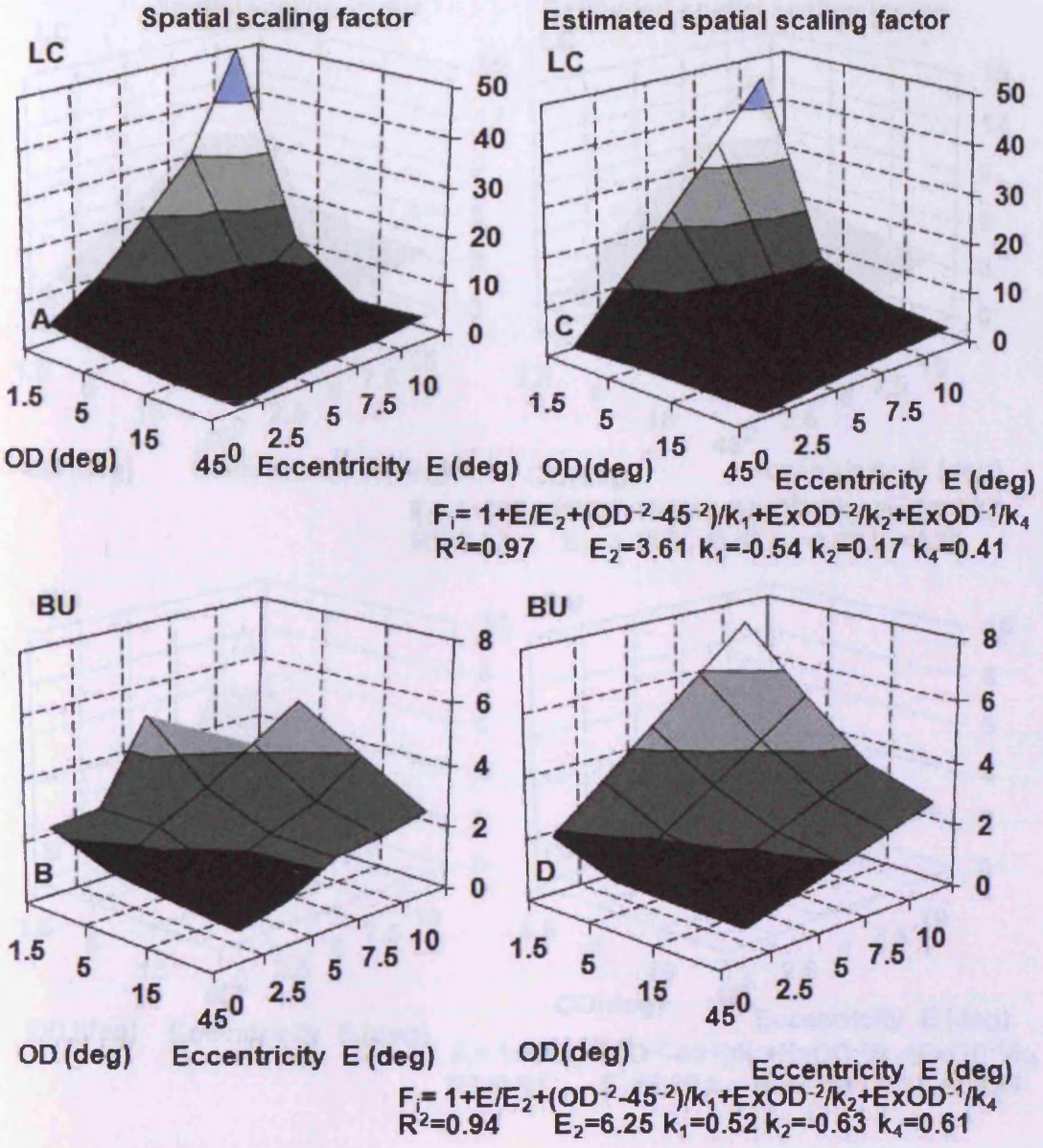

Fig 8.3 (A-D) Empirical and modelled spatial scaling surfaces for the 2cpi gratings

The empirical (left column) and modelled (right column) spatial scaling surfaces at all eccentricities (*E*) and orientation differences (*OD*) of the 2cpi gratings for subjects LC and BU. The left-hand column (A, B) shows the empirical scaling surfaces separately for LC and BU. The empirical surfaces were fitted with equation (8.3) which modelled the effects of *E* and *OD* on the spatial scaling factor F_i. The modelled scaling surfaces are shown in the right-hand column (C, D) along with the fitting equation (8.3), the corresponding parameters values and R^2.

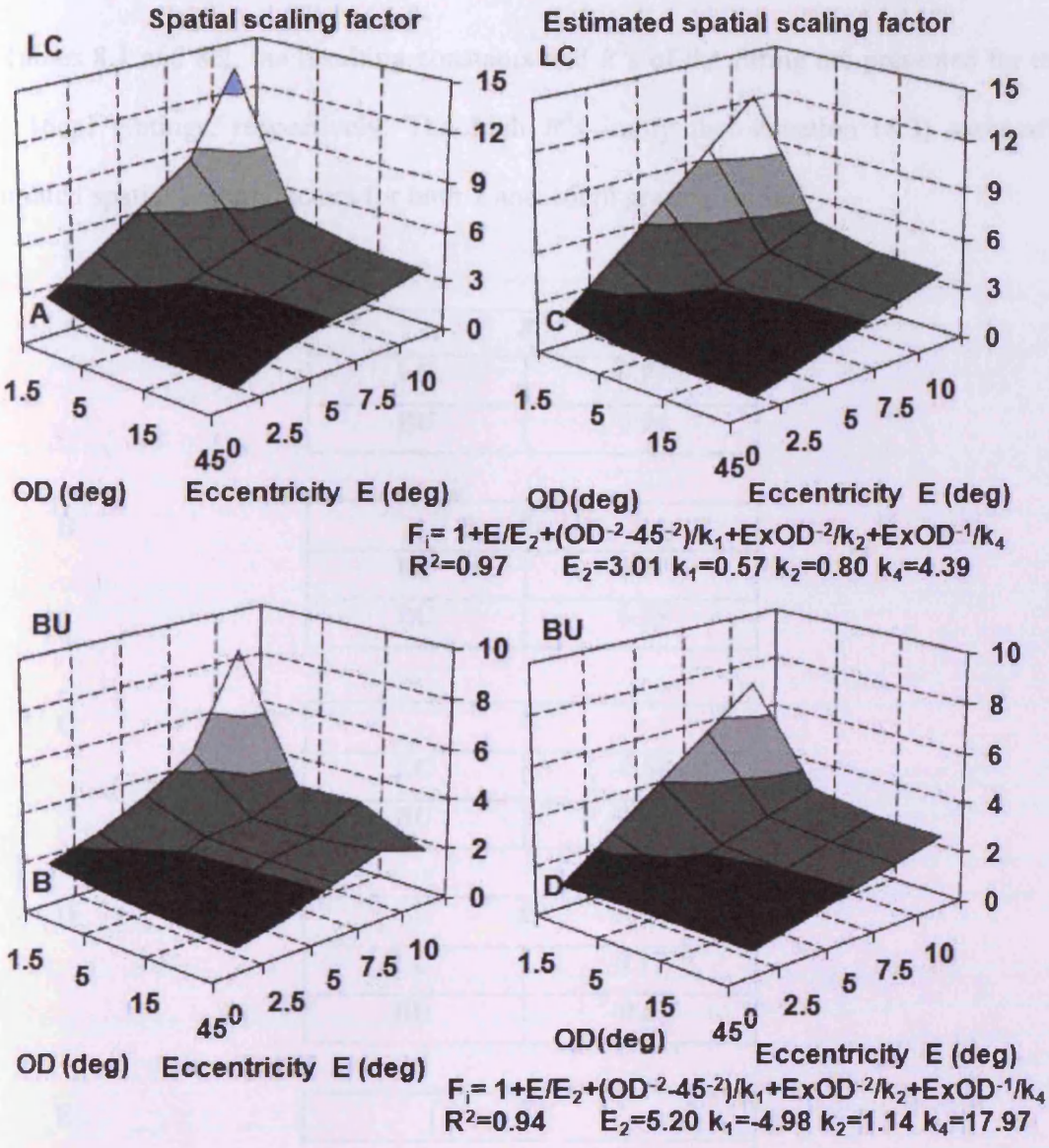

Fig 8.4 (A-D) Empirical and modelled spatial scaling surfaces for the 16cpi gratings

The empirical (left column) and modelled (right column) spatial scaling surfaces at all eccentricities (*E*) and orientation differences (*OD*) of the 16cpi gratings for subjects LC and BU. The left-hand column (A, B) shows the empirical scaling surfaces separately for LC and BU. The empirical surfaces were equation (8.3) which modelled the effects of *E* and *OD* on the spatial scaling factor F_i. The modelled scaling surfaces are shown in the right-hand column (C, D) along with the fitting equation (8.3), the corresponding parameters values and R^2.

In Tables 8.1 and 8.2, the resulting constants and R^2s of the fitting are presented for the 2 and 16cpi gratings, respectively. The high R^2s imply that equation (8.3) successfully estimated spatial scaling factors for both 2 and 16cpi grating stimuli.

A

R^2	
LC	0.97
BU	0.94

B

E_2	
LC	3.61
BU	6.25

C

k_1	
LC	-0.54
BU	0.52

D

k_2	
LC	0.17
BU	-0.63

E

k_4	
LC	0.41
BU	0.61

Table 8.1 The R^2 and constants for modelling spatial scaling surfaces of the 2cpi gratings by equation (8.3) for subjects LC and BU.

A

R^2	
LC	0.97
BU	0.94

B

E_2	
LC	3.01
BU	5.20

C

k_1	
LC	0.57
BU	-4.98

D

k_2	
LC	0.80
BU	1.14

E

k_4	
LC	4.39
BU	17.97

Table 8.2 The R^2 and constants for modelling spatial scaling surfaces of the 16cpi gratings by equation (8.3) for subjects LC and BU.

In Figs 8.5 and 8.6, the unscaled experimental threshold data at all eccentricities and orientation differences for subjects LC and BU were plotted against grating diameter for the 2 and 16cpi gratings.

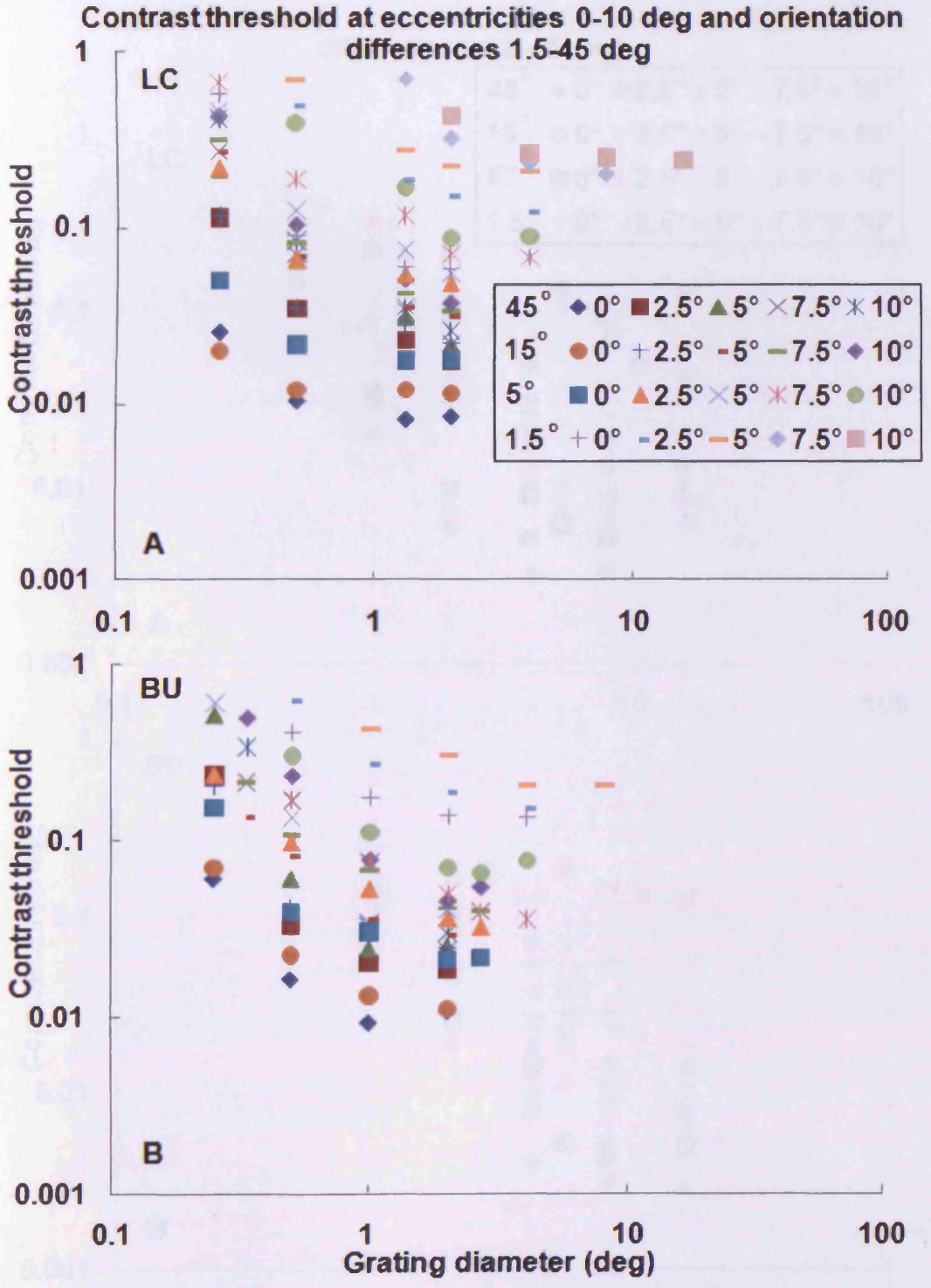

Fig 8.5 The unscaled experimental contrast threshold data of the 2cpi gratings

The unscaled threshold data of the 2cpi gratings were plotted against grating diameter (deg) at the eccentricities of 0-10 deg, and orientation differences of 1.5-45 deg for subjects LC and BU.

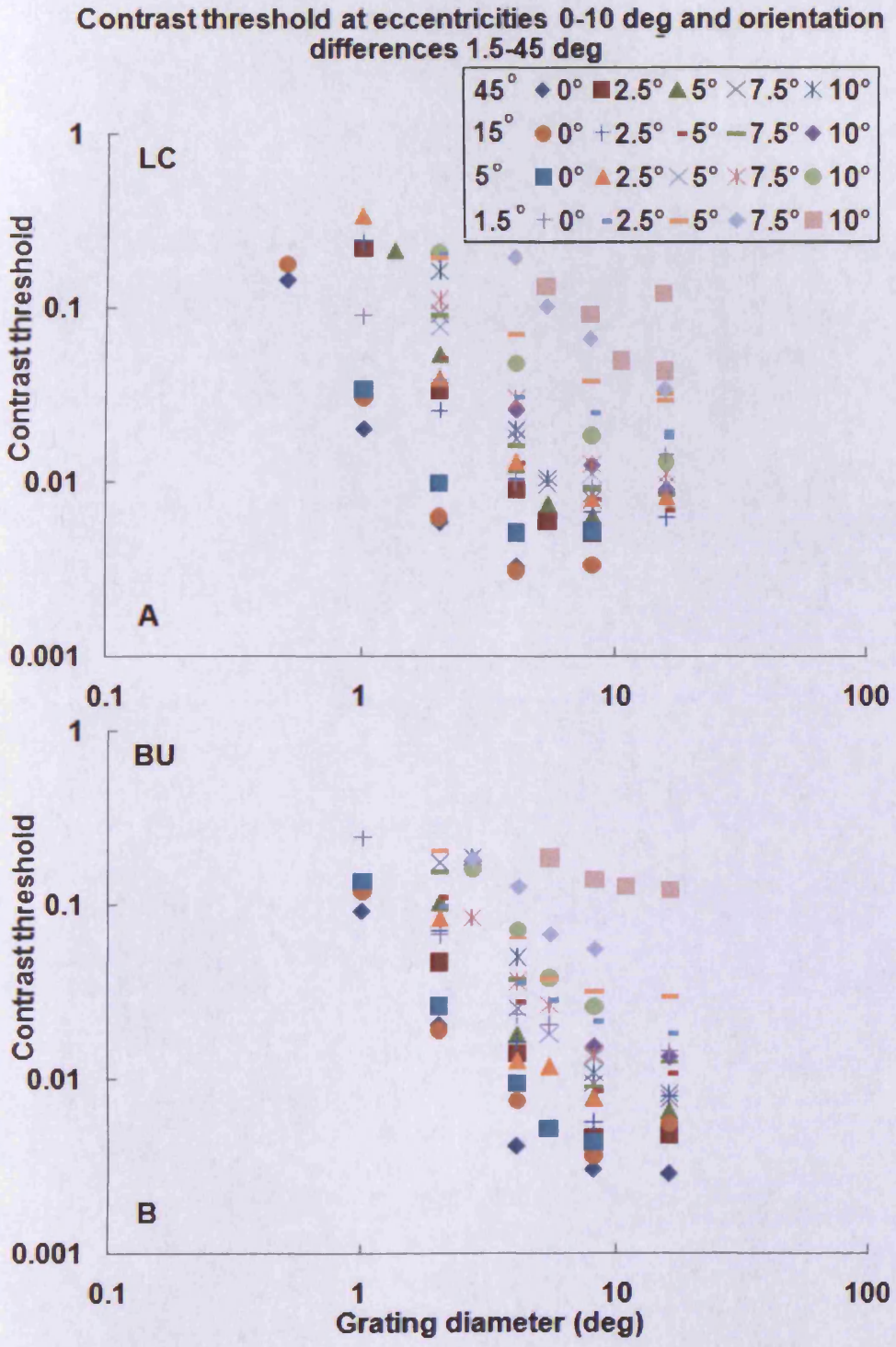

Fig 8.6 The unscaled experimental contrast threshold data of the 16cpi gratings

The unscaled threshold data of the 16cpi gratings were plotted against grating diameter (deg) at the eccentricities of 0-10 deg, and orientation differences of 1.5-45 deg for subjects LC and BU.

To superimpose the experimental threshold data in Figs 8.5 (for the 2cpi gratings) and 8.6 (for the 16cpi gratings), the estimated spatial surfaces in Figs 8.3 (C, D) (for the 2cpi gratings) and 8.4 (C, D) (for the 16cpi gratings) were used to horizontally shift the original threshold data to the basic condition (E=0, OD=45) for the 2 and 16cpi gratings, respectively. The results of spatial scaling are shown in Figs 8.7 and 8.8, for the 2 and 16cpi gratings, respectively. The R^2s of the best fit of equation (8.1) to the scaled data are shown in the figures.

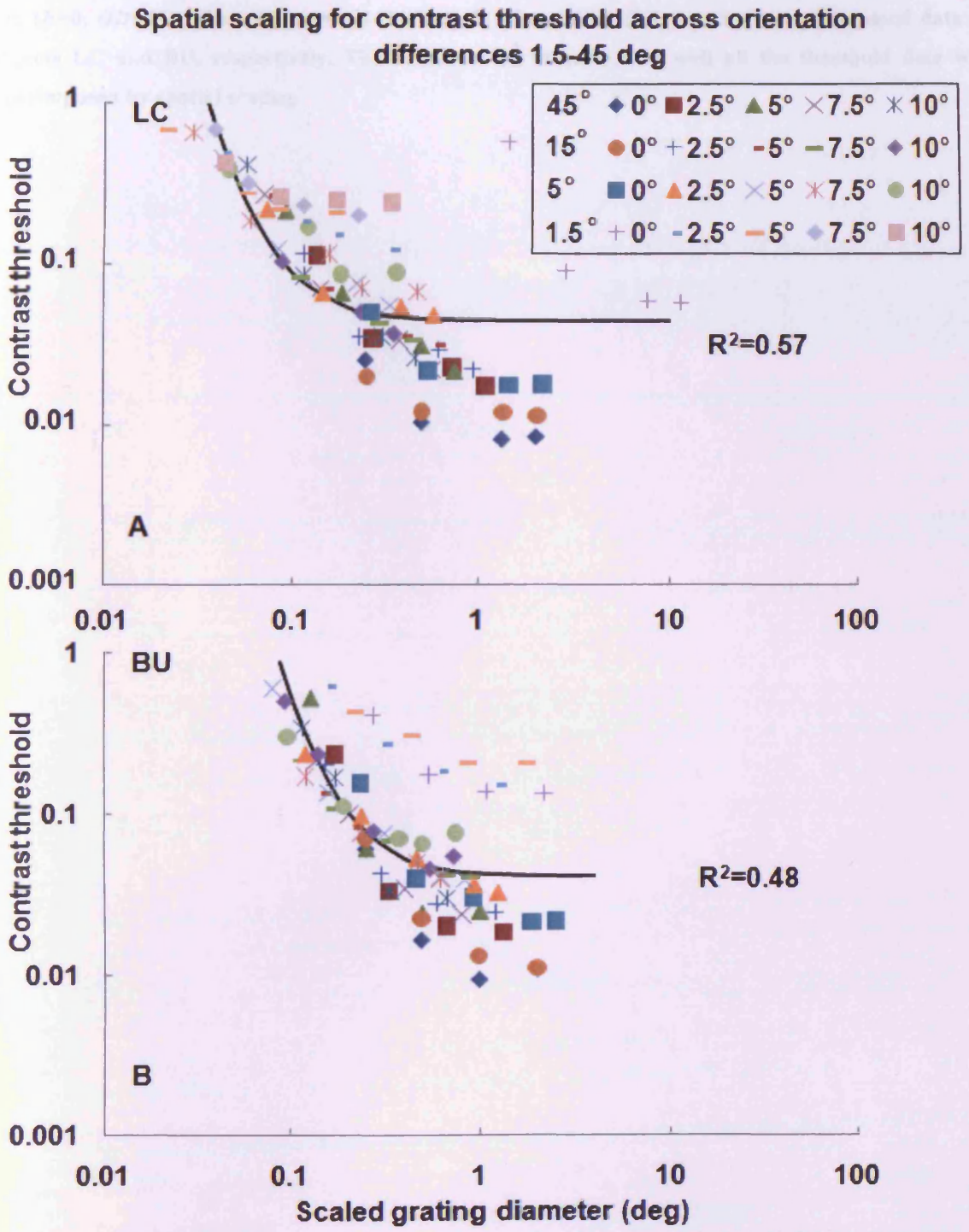

Fig 8.7 Contrast threshold data of the 2cpi gratings at 1.5-45 deg orientation difference and 0-10 deg eccentricity superimposed by spatial scaling.

The unscaled contrast threshold data of the 2cpi gratings in Fig 8.5 (A, B) were horizontally shifted by using the estimated spatial scaling surfaces in Fig 8.3 (C, D). Data from the eccentricities of 0-10 deg and orientation differences of 1.5-45 deg collapsed onto the foveal and 45 deg orientation difference

data (E=0, OD=45). The solid curve is the best fit of equation (8.1) to all the superimposed data for subjects LC and BU, respectively. The values of R^2 indicate how well all the threshold data were superimposed by spatial scaling.

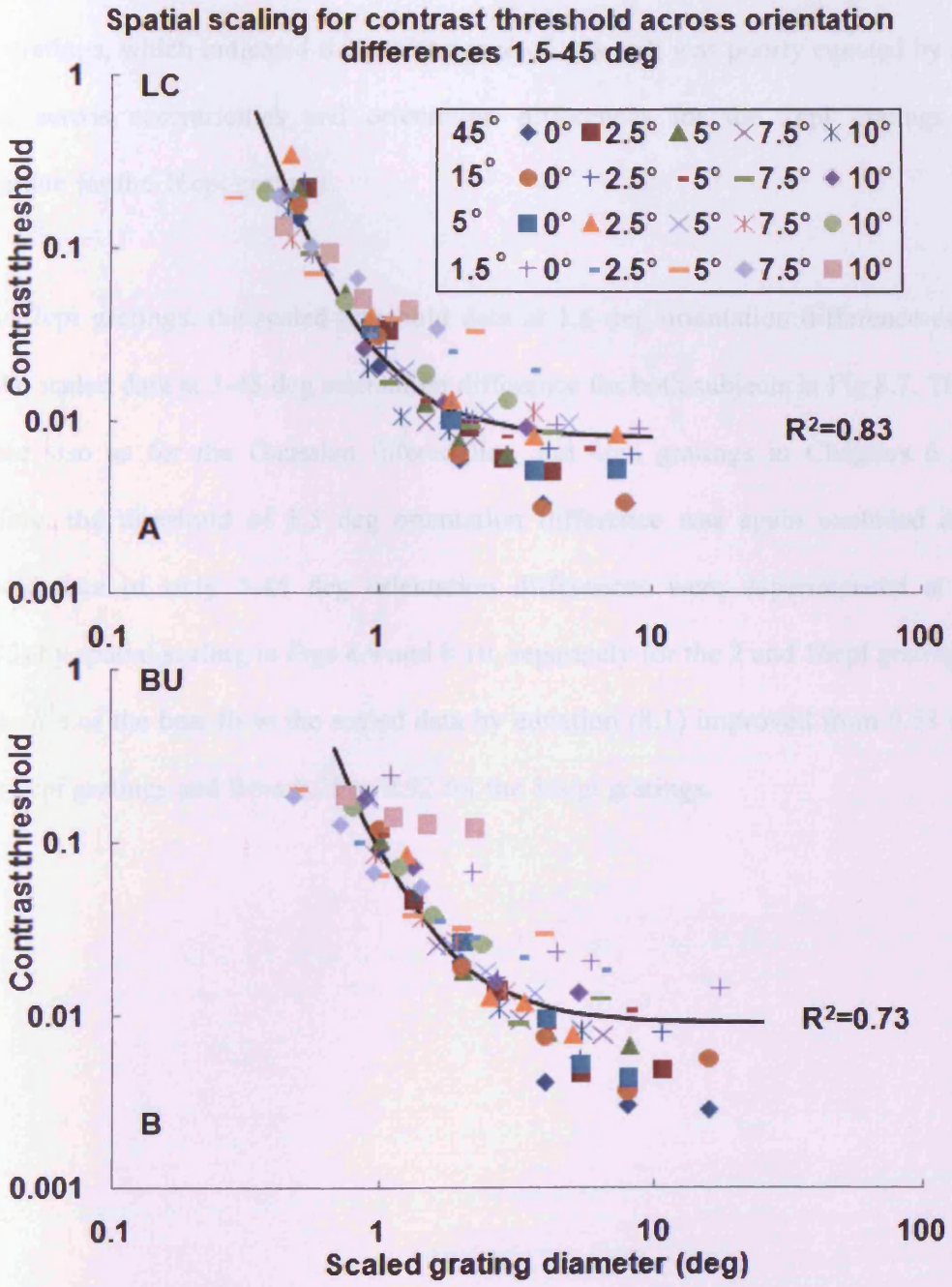

Fig 8.8 Contrast threshold data of the 16cpi gratings at 1.5-45 deg orientation difference and 0-10 deg eccentricity superimposed by spatial scaling.

The experimental threshold data of the 16cpi gratings in Fig 8.6 (A, B) were horizontally scaled by using the estimated spatial scaling surfaces in Fig 8.4 (C, D). Other details as in Fig 8.7

The averages of the R^2s between subjects were 0.53 for the 2cpi gratings and 0.78 for the 16cpi gratings, which indicated the performance of this task was poorly equated by spatial scaling across eccentricities and orientation differences for the 2cpi gratings while appropriate for the 16cpi gratings.

For the 2cpi gratings, the scaled threshold data at 1.5 deg orientation difference deviated from the scaled data at 5-45 deg orientation difference for both subjects in Fig 8.7. This was the case also as for the Gaussian filtered line and 4cpi gratings in Chapters 6 and 7. Therefore, the threshold of 1.5 deg orientation difference was again excluded and the threshold data of only 5-45 deg orientation differences were superimposed at (E=0, OD=45) by spatial scaling in Figs 8.9 and 8.10, separately for the 2 and 16cpi gratings. The average R^2s of the best fit to the scaled data by equation (8.1) improved from 0.53 to 0.75 for the 2cpi gratings and from 0.78 to 0.92 for the 16cpi gratings.

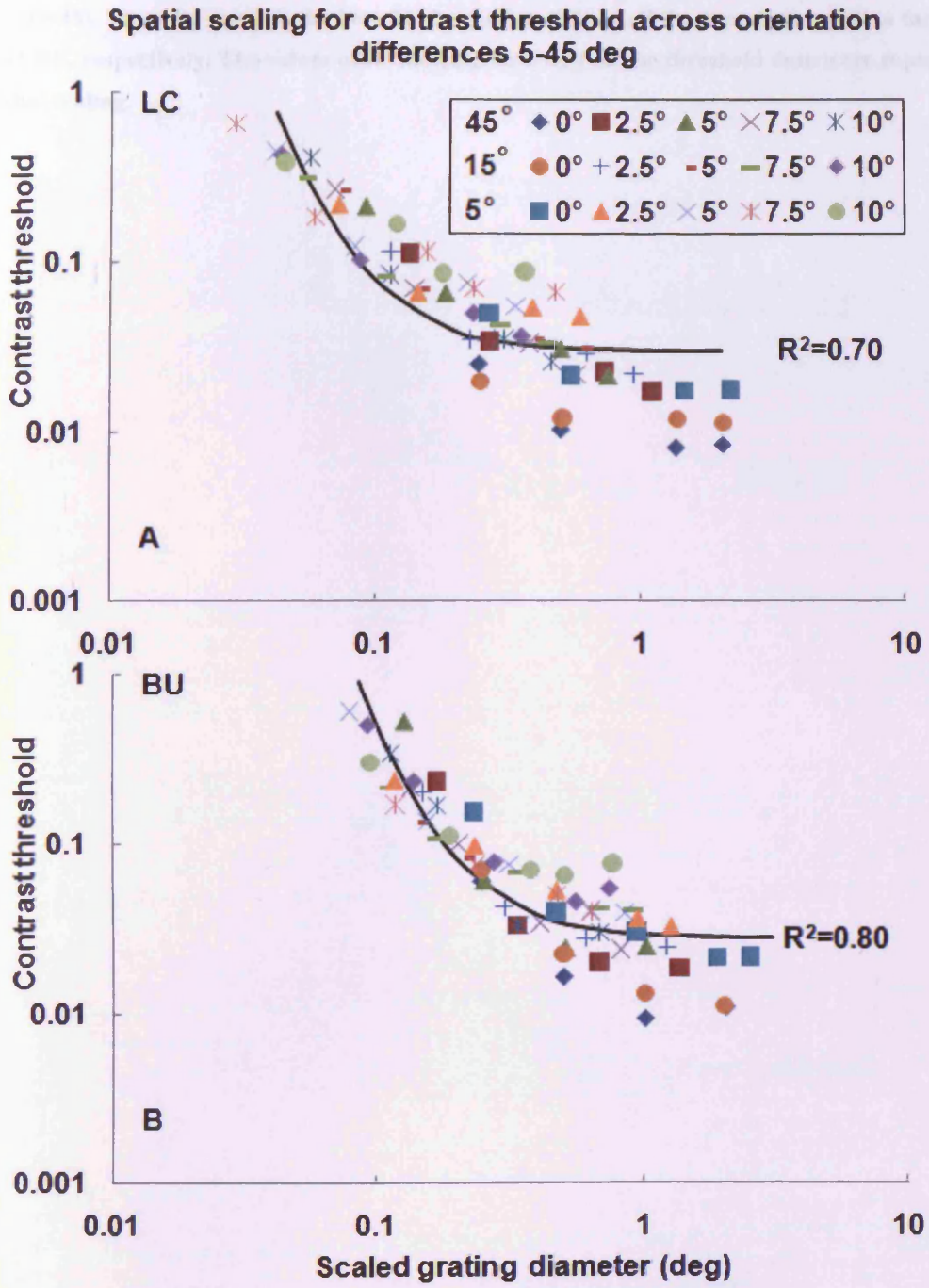

Fig 8.9 Contrast threshold data of the 2cpi gratings at 5-45 deg orientation difference and 0-10 deg eccentricity superimposed by spatial scaling.

The original contrast threshold data of the 2cpi gratings were horizontally scaled by using the estimated spatial scaling surfaces in Fig 8.3 (C, D). Data from the eccentricities of 0-10 deg and orientation differences of 5-45 deg collapsed onto the foveal and 45 deg orientation difference data

(E=0, OD=45). The solid curve is the best fit of equation (8.1) to all the superimposed data for subjects LC and BU, respectively. The values of R^2 indicate how well all the threshold data were superimposed by spatial scaling.

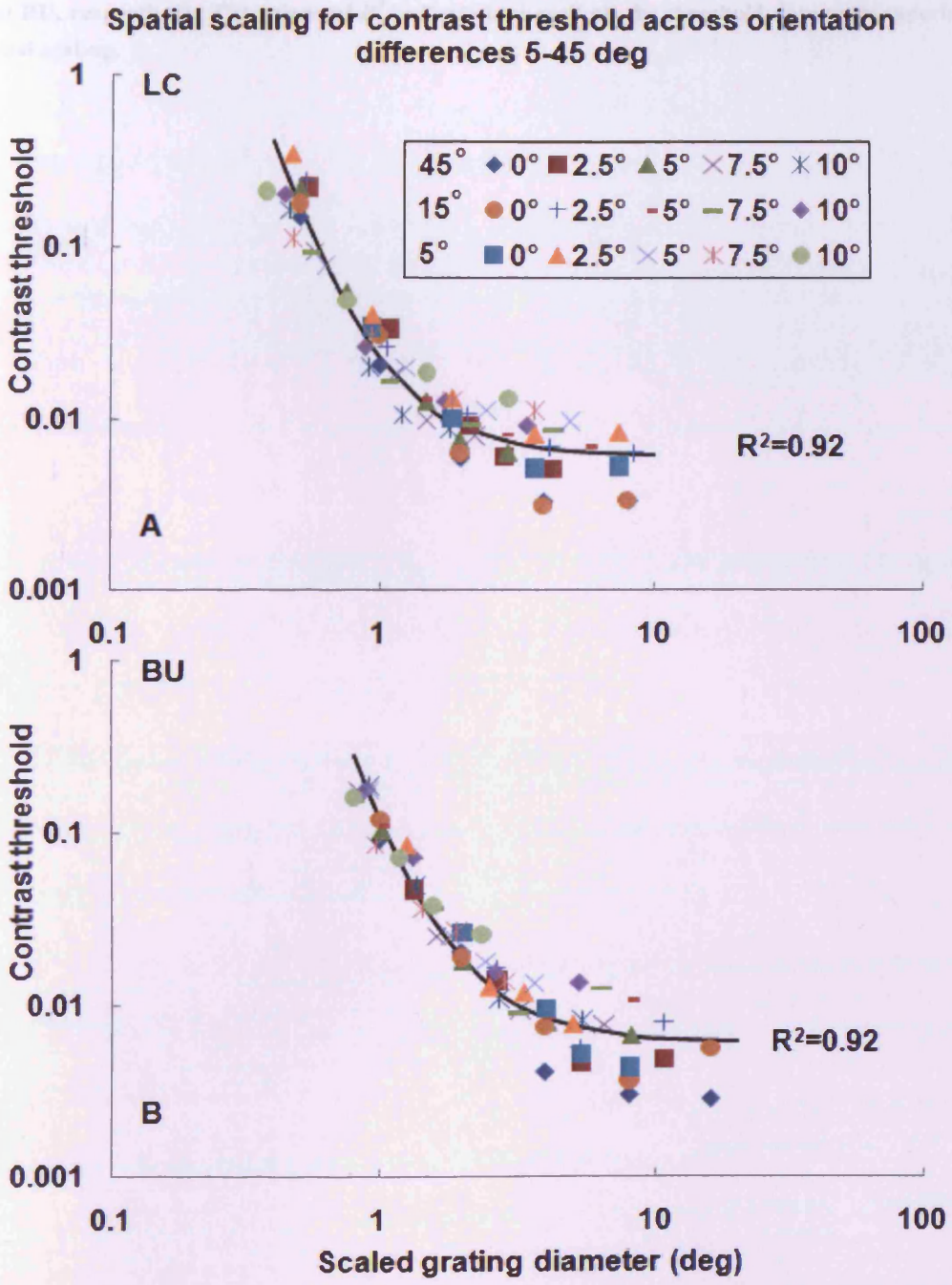

Fig 8.10 Contrast threshold data of the 16cpi gratings at 5-45 deg orientation difference and 0-10 deg eccentricity superimposed by spatial scaling.

The experimental unscaled threshold data of the 16cpi gratings were horizontally scaled by using the estimated spatial scaling surfaces in Fig 8.4 (C, D). Data from the eccentricities of 0-10 deg and orientation differences of 5-45 deg collapsed onto the foveal and 45 deg orientation difference data

(E=0, OD=45). The solid curve is the best fit of equation (8.1) to all the superimposed data for subjects LC and BU, respectively. The values of R^2 indicate how well all the threshold data were superimposed by spatial scaling.

8.3.2 2D scaling across orientation differences of 45-1.5 deg

2D scaling was separately used for the 2 and 16cpi gratings to superimpose the threshold data of across eccentricities and orientation differences, as in Chapters 6 and 7 for the Gaussian filtered lines and 4cpi gratings. For each stimulus, the foveal threshold data at 45 deg orientation difference (E=0, OD=45) was chosen to be the basic condition of the scaling as before.

The 2D scaling factors, normalized Th_{min} (vertical factor) and normalized H_c (horizontal factor), were obtained as for the Gaussian filtered lines and 4cpi gratings. Firstly, Th_{min} and H_c at each eccentricity and orientation difference, previously obtained through fitting of the threshold data curves of Fig. 8.1 and 8.2 by equation (8.1), were separately normalised by Th_{min} (E=0, OD=45) and H_c (E=0, OD=45). The normalised Th_{min} and H_c, i.e. the experimental 2D scaling factors, were plotted against eccentricity and orientation difference in Figs 8.11 (A, B, E, F) for the 2cpi gratings and Figs 8.12 (A, B, E, F) for the 16cpi gratings. The factors increase as eccentricity increases and orientation difference decreases. As Figs show, increase with eccentricity is faster when orientation difference is smaller while increase with decreasing orientation difference is faster at large eccentricities.

As the spatial scaling factors, the 2D scaling factors also have two independent variables, E and OD. Therefore, equation (8.2), used for modeling spatial scaling factors in Section 8.3.1, was used here to model the dependency of the 2D scaling factors, i.e. normalized Th_{min} (vertical) and normalised H_c (horizontal), on E and OD. Based on R^2 and the accuracy

of the constants (see the procedure of selecting parameters in Appendix IV), equation (8.2) was reduced to equation (8.4) for estimating the vertical scaling factor, normalised Th_{min} and to equation (8.5) for estimating the horizontal scaling factor, normalised H_c:

$$F_i = 1 + E/E_2 + E \times (OD)^{-2}/k_2 + (OD^{-1} - 45)^{-1}/k_3 ,$$

Equation 8.4

$$F_i = 1 + E/E_2 + (OD^{-2} - 45^{-2})/k_1 + E \times (OD)^{-2}/k_2 + E \times (OD)^{-1}/k_4 .$$

Equation 8.5

The experimental 2D scaling factors of Fig 8.11 (A, B, E, F) for the 2cpi gratings and 8.12 (A, B, E, F) for the 16cpi gratings were estimated by equations (8.4) and (8.5) in Figs 8.11 (C, D, G, H) for the 2cpi gratings and 8.12 (C, D, G, H) for the 16cpi gratings. The R^2s of the estimation ranged from 0.86 to 0.97, indicating that equations (8.4) and (8.5) successfully modelled the 2D scaling factors across eccentricities and orientation differences.

Fig 8.11 Empirical & modelled 2D scaling factors for the contrast threshold of the 2cpi gratings

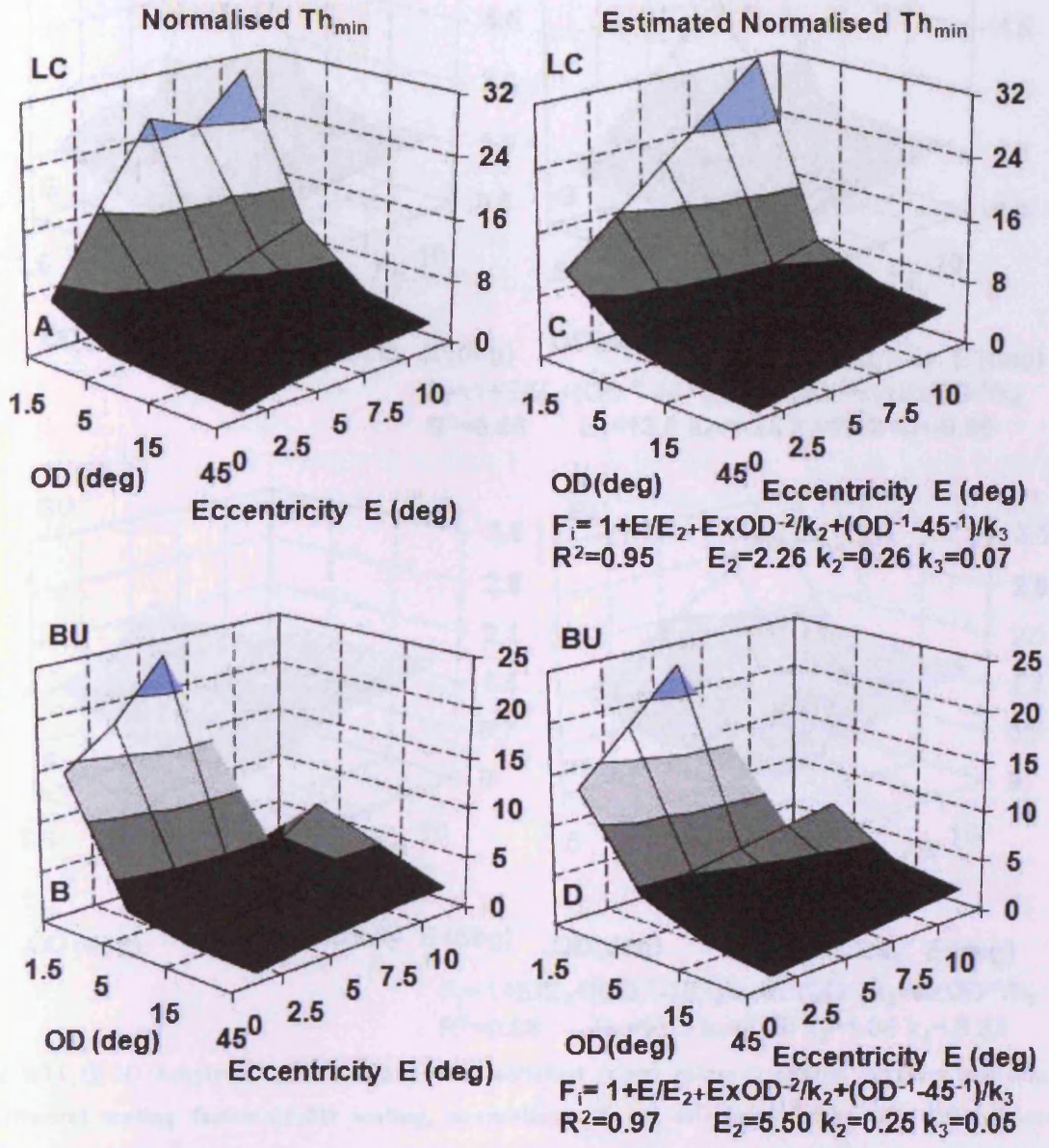

Fig 8.11 (A-D) Empirical (left column) and modelled (right column) scaling surfaces showing the vertical scaling factor of 2D scaling, normalised Th_{min}, at all eccentricities (E) and orientation differences (OD) of the 2cpi grating for subjects LC and BU. The left-hand column (A, B) shows the empirical scaling surfaces separately for LC and BU. The empirical surfaces were fitted with equation (8.4) which modelled the effects of eccentricity and orientation difference on normalised Th_{min}. The modelled scaling surfaces are shown in the right-hand column (C, D) along with the fitting equation (8.4), the corresponding parameter values and R^2.

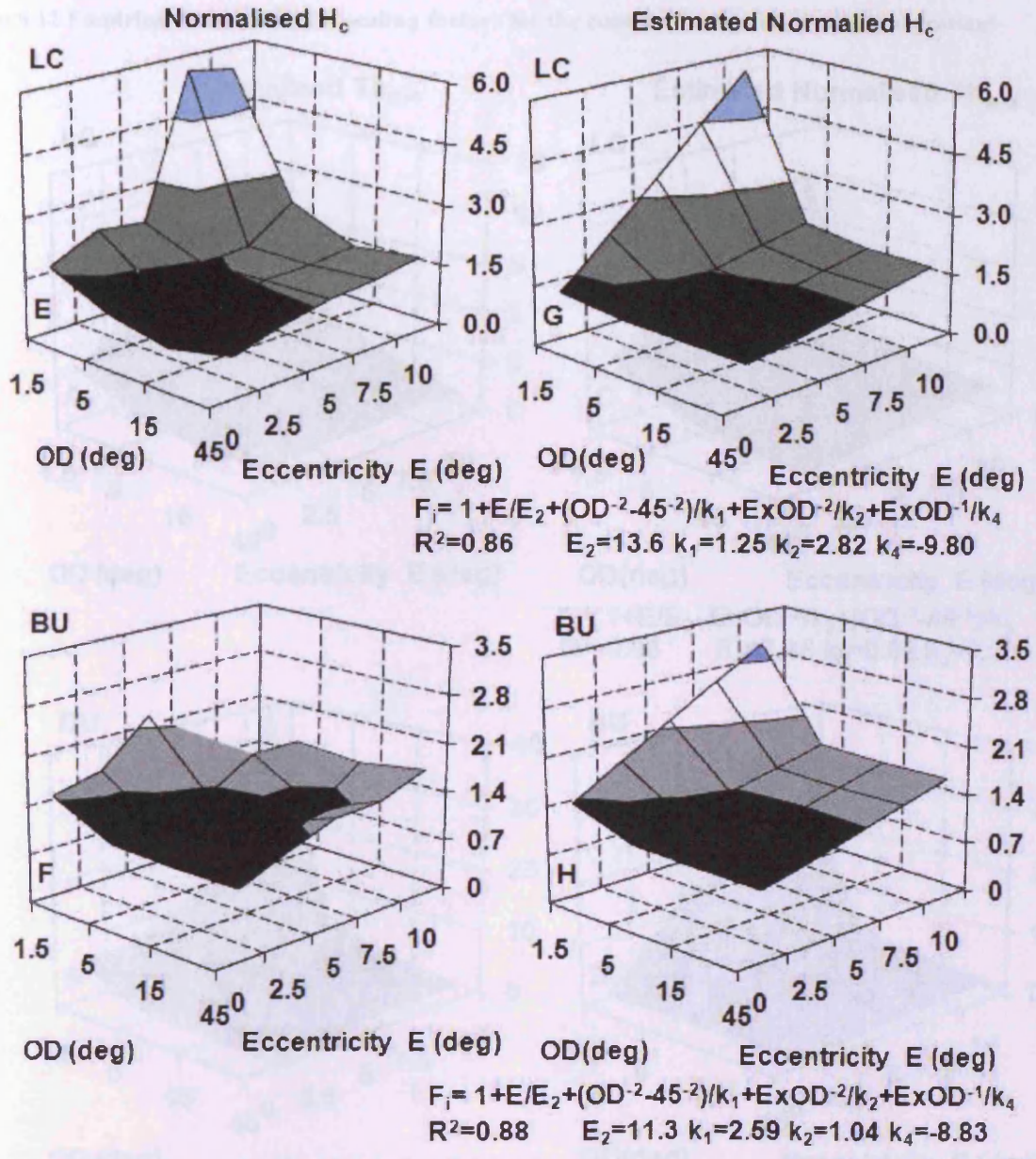

Fig 8.11 (E-H) Empirical (left column) and modelled (right column) scaling surfaces showing the horizontal scaling factor of 2D scaling, normalised H_c, at all eccentricities (E) and orientation differences (OD) of the 2cpi gratings for LC and BU. The left-hand column (E, F) shows the empirical scaling surfaces separately for LC and BU. The empirical surfaces were fitted with equation (8.5) which modelled the effects of eccentricity and orientation difference on the normalised H_c. The modelled scaling surfaces are shown in the right-hand column (G, H) along with the fitting equation (8.5), the corresponding parameter values and R^2.

Fig 8.12 Empirical & modelled 2D scaling factors for the contrast threshold of the 16cpi gratings

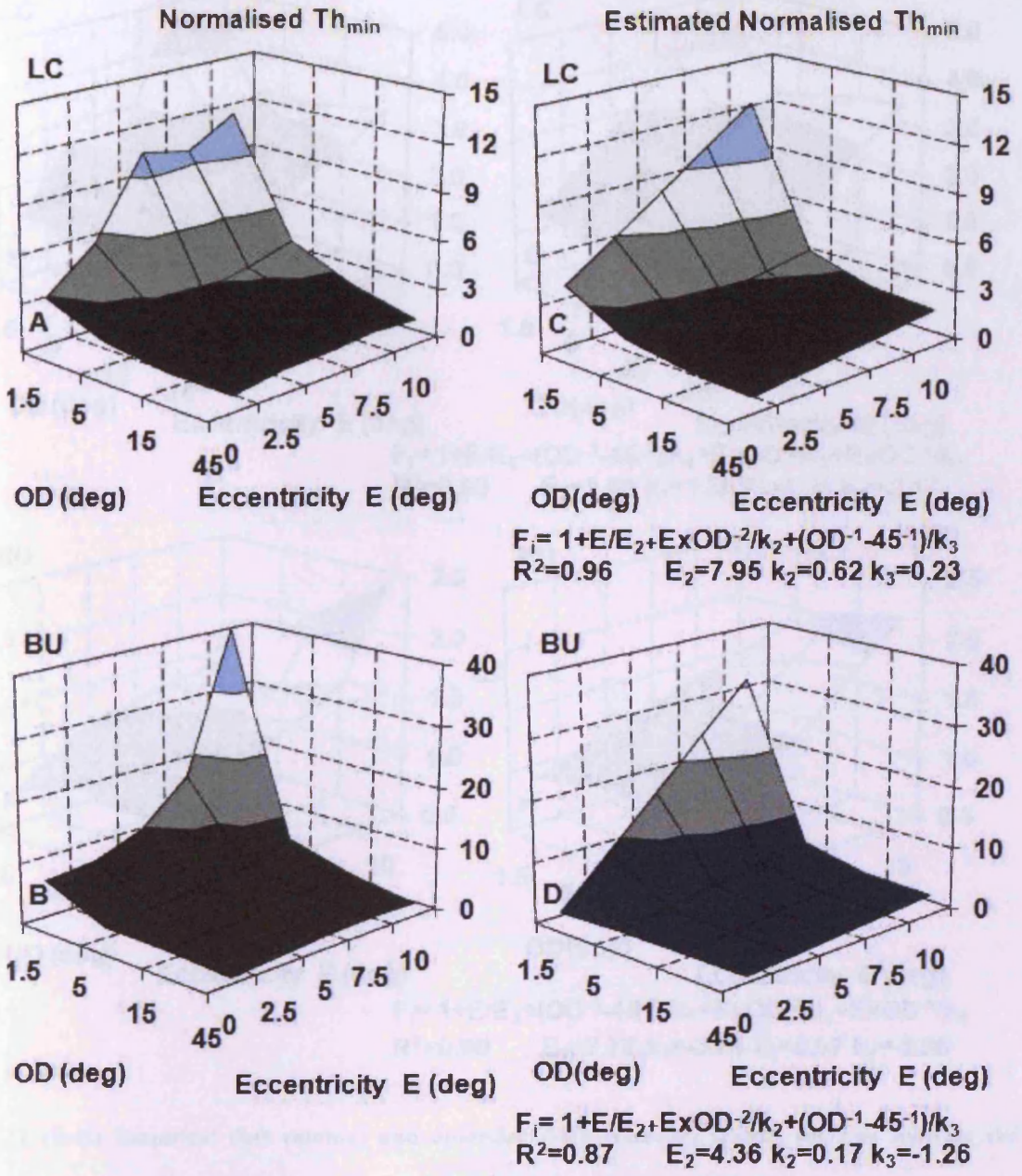

Fig 8.12 (A-D) Empirical (left column) and modelled (right column) scaling surfaces showing the vertical scaling factor of 2D scaling, normalised Th_{min}, at all eccentricities (E) and orientation differences (OD) of the 16cpi grating for subjects LC and BU. Other details are as in Fig 8.11 (A-D).

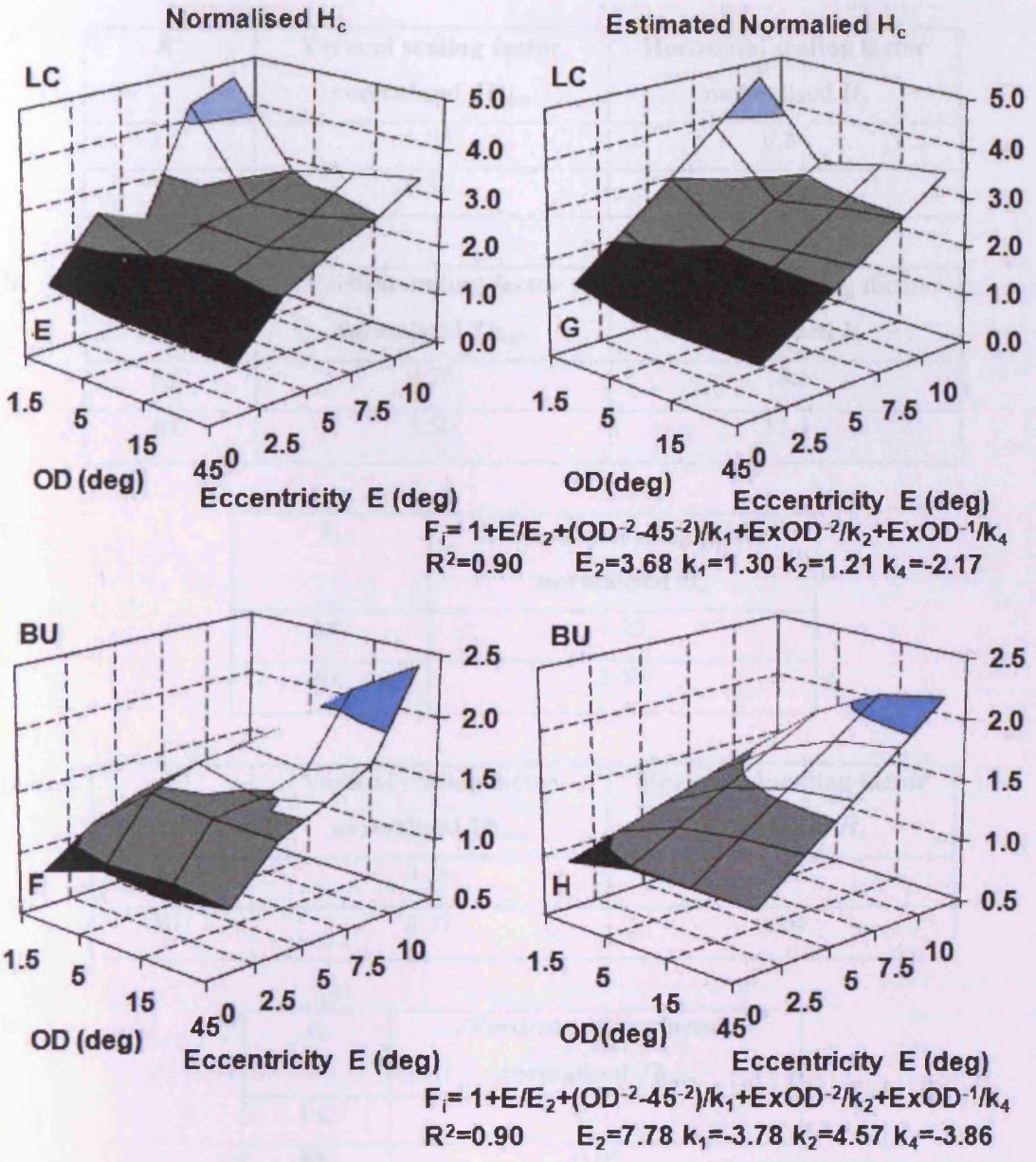

Fig 8.12 (E-H) Empirical (left column) and modelled (right column) scaling surfaces showing the horizontal scaling factor of 2D scaling, normalised H_c, at all eccentricities (E) and orientation differences (OD) of the 16cpi gratings for LC and BU. Other details are as in Fig 8.11 (E-H).

The results for estimating the 2D scaling factors are summarised in Tables 8.3 for the 2cpi gratings and 8.4 for the 16cpi gratings.

A

R^2	Vertical scaling factor normalised Th_{min}	Horizontal scaling factor normalised H_c
LC	0.95	0.86
BU	0.97	0.88

B

E_2	Vertical scaling factor normalised Th_{min}	Horizontal scaling factor normalised H_c
LC	2.26	13.6
BU	5.50	11.3

C

k_1	Horizontal scaling factor normalised H_c
LC	1.25
BU	2.59

D

k_2	Vertical scaling factor normalised Th_{min}	Horizontal scaling factor normalised H_c
LC	0.26	2.82
BU	0.25	1.04

E

k_3	Vertical scaling factor normalised Th_{min}
LC	0.07
BU	0.05

F

k_4	Horizontal scaling factor normalised H_c
LC	-9.80
BU	-8.83

Table 8.3 The R^2s and constants of modelling of 2D scaling factors, i.e. normalised Th_{min} and H_c of the 2cpi gratings for subjects LC and BU.

A

R^2	Vertical scaling factor normalised Th_{min}	Horizontal scaling factor normalised H_c
LC	0.96	0.90
BU	0.87	0.90

B

E_2	Vertical scaling factor normalised Th_{min}	Horizontal scaling factor normalised H_c
LC	7.95	3.68
BU	4.36	7.78

C

k_1	Horizontal scaling factor normalised H_c
LC	1.30
BU	-3.78

D

k_2	Vertical scaling factor normalised Th_{min}	Horizontal scaling factor normalised H_c
LC	0.62	1.21
BU	0.17	4.57

E

k_3	Vertical scaling factor normalised Th_{min}
LC	0.23
BU	-1.26

F

k_4	Horizontal scaling factor normalised H_c
LC	-2.17
BU	-3.86

Table 8.4 The R^2s and constants of modelling of 2D scaling factors, i.e. normalised Th_{min} and H_c of the 16cpi gratings for subjects LC and BU.

For each stimulus, the unscaled contrast threshold data from Figs 8.5 and 8.6 were scaled to the basic condition (E=0, OD=45) by the corresponding estimated 2D scaling factors, the estimated normalized Th_{min} and H_c in Figs 8.11 and 8.12 (E, F, G, H). The results of the 2D scaling for the 2cpi gratings are shown in Fig 8.13 and for the 16cpi gratings in Fig 8.14. The R^2s of the best fit by equation (8.1) to the superimposed data was calculated and is shown in the corresponding figures for each stimulus. The averages of R^2s between subjects are 0.87 and 0.91 for the 2 and 16cpi grating, respectively, which indicates that 2D scaling successfully equated the contrast threshold performance across all eccentricities and orientation differences.

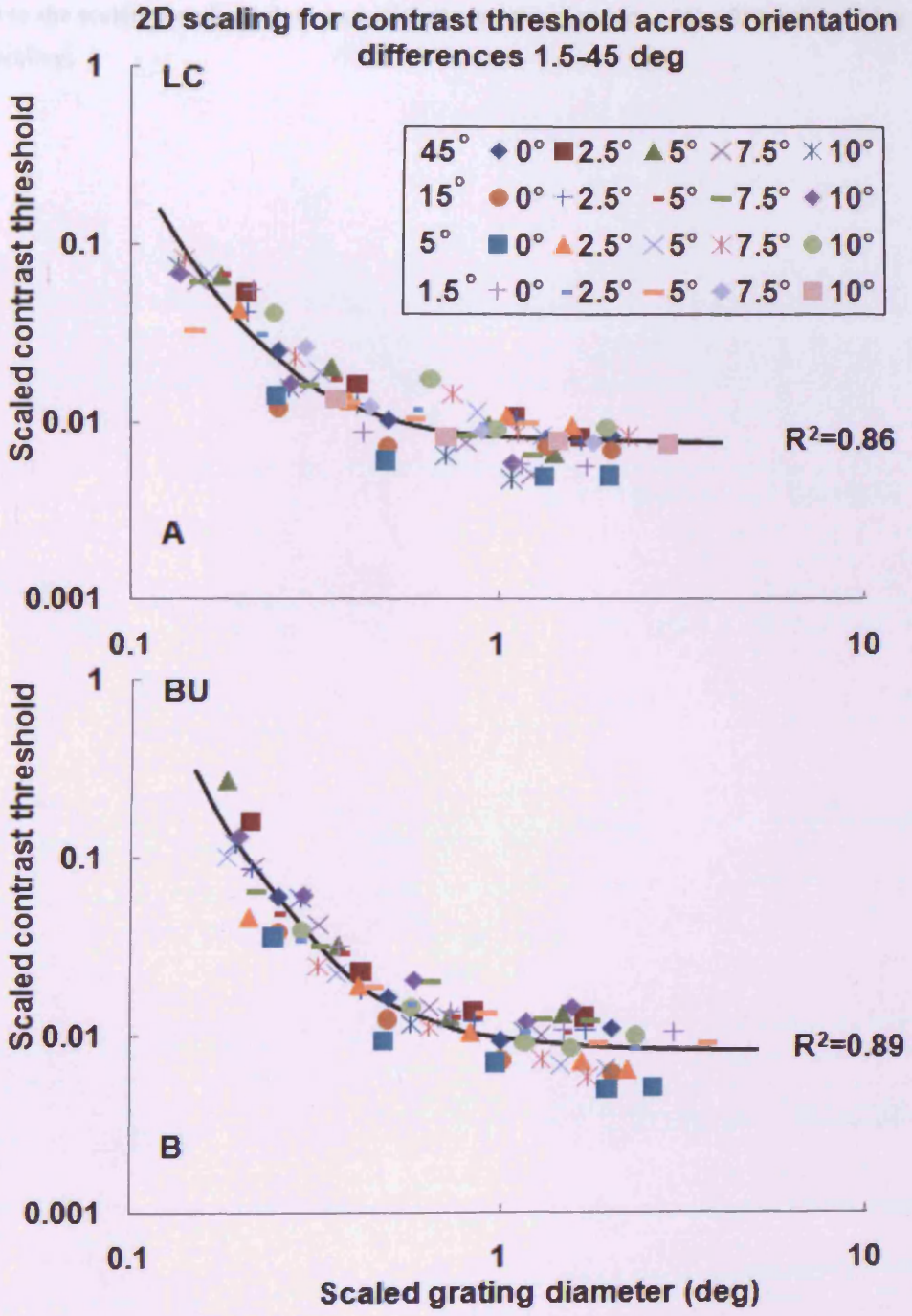

Fig 8.13 (A-B) The 2D scaled contrast thresholds for the 2cpi gratings at 0-10 deg eccentricity and 1.5-45 deg orientation difference

The unscaled threshold data of the 2cpi gratings from Fig 8.5 (A-B) were both vertically and horizontally scaled by means of the estimated 2D scaling surfaces of Fig 8.11 (C, D, G, H). Data for the eccentricities of 0-10 deg and orientation differences of 45-1.5 deg collapsed onto the base condition (*E*=0, *OD*=45). The data for subjects LC and BU are as indicated. The smooth curve i.e. equation (8.1)

was fitted to the scaled threshold data and R^2 indicates the accuracy of the fit for describing all the data after 2D scaling.

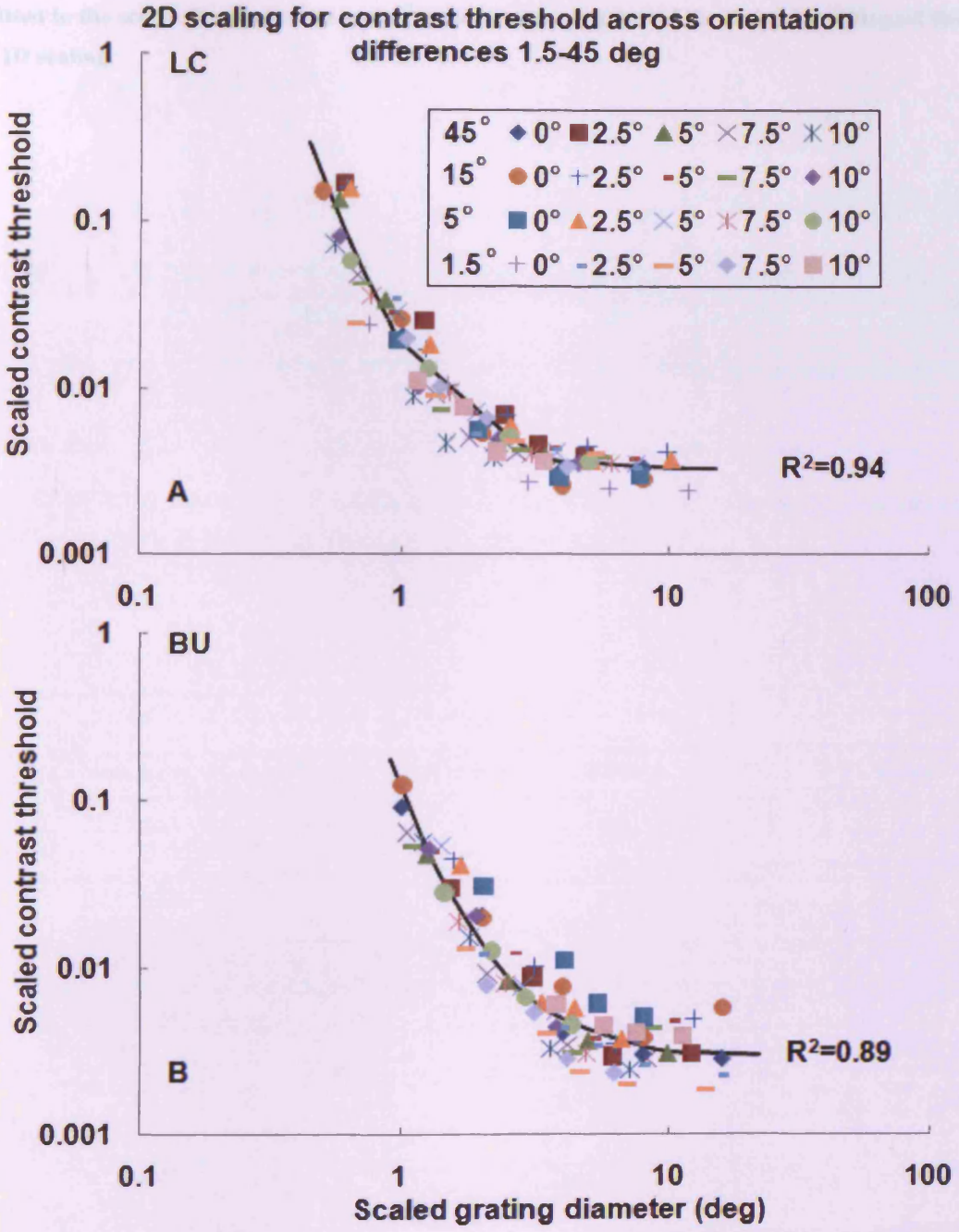

Fig 8.14 (A-B) The 2D scaled contrast thresholds for the 16cpi gratings at 0-10 deg eccentricity and 1.5-45 deg orientation difference

The unscaled threshold data of the 16cpi gratings from Fig 8.6 (A-B) were both vertically and horizontally scaled by means of the estimated 2D scaling surfaces of Fig 8.12 (C, D, G, H). Data for the eccentricities of 0-10 deg and orientation differences of 45-1.5 deg collapsed onto the base condition (*E*=0, *OD*=45). The data for subjects LC and BU are as indicated. The smooth curve i.e. equation (8.1)

was fitted to the scaled threshold data and R^2 indicates the accuracy of the fit for describing all the data after 2D scaling.

The values of R^2 are compared between spatial scaling and 2D scaling in Table 8.5 for the 2cpi gratings and Table 8.6 for the 16cpi gratings.

2cpi	Spatial scaling across OD from 1.5 to 45 deg		Spatial scaling across OD from 5 to 45 deg		2D scaling across OD from 1.5 to 45 deg	
	LC	BU	LC	BU	LC	BU
R^2	0.57	0.48	0.70	0.80	0.86	0.89

Table 8.5 The R^2s of spatial and 2D scaling applied to the contrast threshold data of the 2cpi gratings across eccentricities and orientation differences for subjects LC and BU

16cpi	Spatial scaling across OD from 1.5 to 45 deg		Spatial scaling across OD from 5 to 45 deg		2D scaling across OD from 1.5 to 45 deg	
	LC	BU	LC	BU	LC	BU
R^2	0.83	0.73	0.92	0.92	0.94	0.89

Table 8.6 The R^2s of spatial and 2D scaling applied to the contrast threshold data of the 16cpi gratings across eccentricities and orientation differences for subjects LC and BU

8.3.3 The Wilcoxon test for R^2s from spatial and 2D scaling

The R^2s of spatial and 2D scaling for the contrast thresholds of orientation discrimination of various stimuli were summarised in Table 8.7. The averages of each method are 0.66 for spatial scaling and 0.88 for 2D scaling across 1.5 to 45 deg orientation differences. As Table 8.7 shows R^2 of spatial scaling was worse than 2D scaling for each stimulus and subject (see the data of 2nd and 3rd columns from the left in the table). The result of

Wilcoxon test shows that the difference of R^2s between spatial and 2D scaling for superimposing threshold data across 1.5-45 deg is statistically significant at the level 0.008. Therefore, performance of 2D scaling is significantly better than that of spatial scaling at the level 0.05.

Compared with R^2 obtained by spatial scaling across 1.5-45 deg, it improved in each case and its average increased from 0.66 to 0.82 when the scaling was only applied to the threshold data of 5-45 deg orientation differences (see the 4th column from the left in Table 8.7). Wilcoxon test revealed that the difference (between the 3rd and 4th columns from the left in the table) is statistically significant at the level 0.008.

Subject & Stimulus	**2D scaling across 1.5 to 45 deg**	**Spatial scaling across 1.5 to 45 deg**	**Spatial scaling across 5 to 45 deg**
LC&Gaussian line	0.81	0.67	0.71
LC&2cpi	0.86	0.57	0.70
LC&4cpi	0.86	0.57	0.85
LC&16cpi	0.94	0.83	0.92
YC&Gaussian line	0.88	0.71	0.78
BU&2cpi	0.89	0.48	0.80
BU&4cpi	0.92	0.73	0.86
BU&16cpi	0.89	0.73	0.92
Average	**0.88**	**0.66**	**0.82**

Table 8.7 The R^2s of spatial and 2D scaling at each cpi for different subjects

8.3.4 Cpi and global spatial scaling E_2 during spatial scaling across orientation differences

In Table 8.8 are summarised the global spatial scaling E_2 obtained during spatial scaling across orientation differences for different subjects and stimuli. There is a tendency that the E_2 increases with increasing cpi, which suggesting less size scaling needed for larger cpi grating (Nasanen *et al.* 1993). Averaging across subjects makes it clearer by reducing scatter.

In Fig 8.15 are shown the global spatial E_2 and its average between subjects as a function of cpi.

Stimulus	LC (deg)	YC&BU (deg)	Average E_2 between subjects (deg)
Gaussian line	3.49	2.67	**3.08**
2cpi	3.01	5.2	**4.11**
4cpi	4.48	4.64	**4.56**
16cpi	3.61	6.25	**4.93**
Average across subjects and stimuli (deg)			**4.17**

Table 8.8 The global spatial E_2 at each cpi for different subjects and its average between subjects

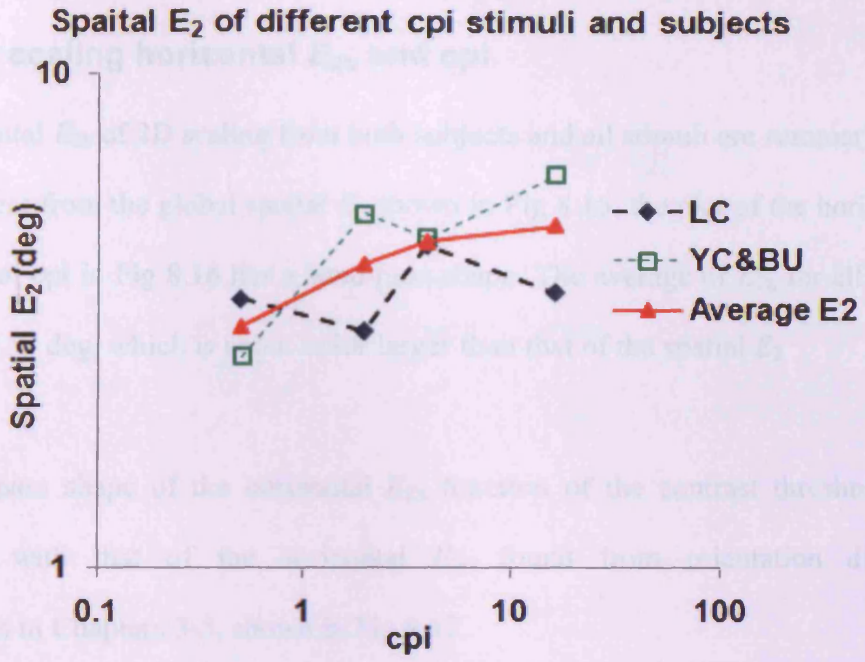

Fig 8.15 The global spatial E_2 and its average between subjects plotted as function of cpi.

The E_2 was found during spatial scaling across orientation differences from 1.5 to 45 deg. Different data curves are as indicated by the different symbols and curve types in the figure.

8.3.5 2D scaling horizontal E_{2h} and cpi

The horizontal E_{2h} of 2D scaling from both subjects and all stimuli are summarised in Table 8.9. Different from the global spatial E_2 shown in Fig 8.15, the plot of the horizontal E_{2h} as a function of cpi in Fig 8.16 has a band-pass shape. The average of E_{2h} for all subjects and stimuli is 8.52 deg, which is about twice larger than that of the spatial E_2.

The band pass shape of the horizontal E_{2h} function of the contrast threshold data is in agreement with that of the horizontal E_{2h} found from orientation discrimination experiments in Chapters 3-5, shown in Fig 8.17.

Stimulus	LC (deg)	YC&BU (deg)	Average E_2 between subjects (deg)
Gaussian line	4.77	5.62	**5.20**
2cpi	13.6	11.3	**12.45**
4cpi	8.01	13.4	**10.71**
16cpi	3.68	7.78	**5.73**
Average across all subjects and stimuli (deg)			**8.52**

Table 8.9 The horizontal E_{2h} of at each cpi for different subjects and its average between subjects

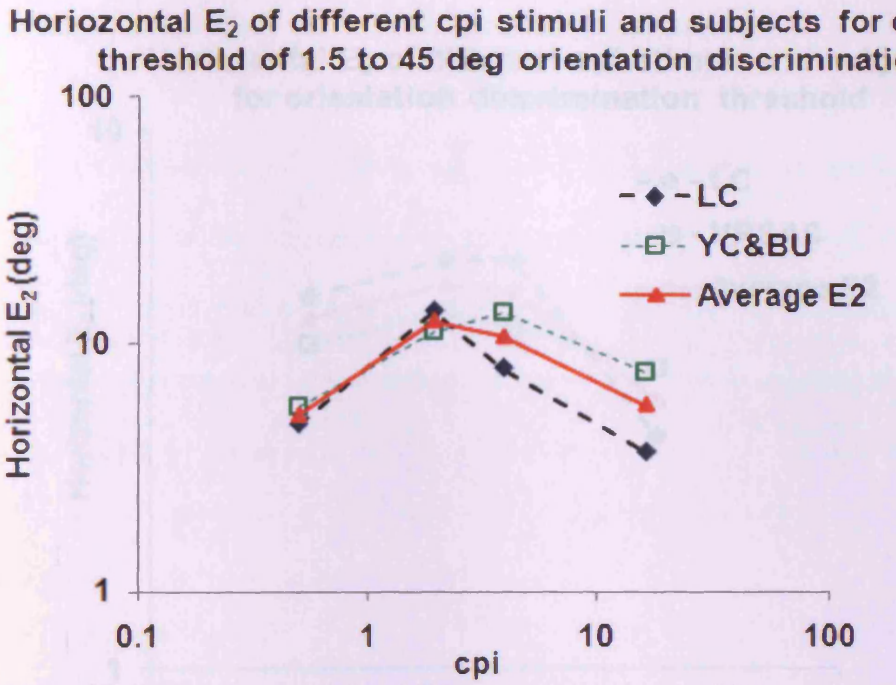

Fig 8.16 The 2D scaling horizontal E_{2h} and its average between subjects as function of cpi for the contrast threshold data for subjects LC, YC and BU.

Different data curves are as indicated by the different symbols and curve types in the figure.

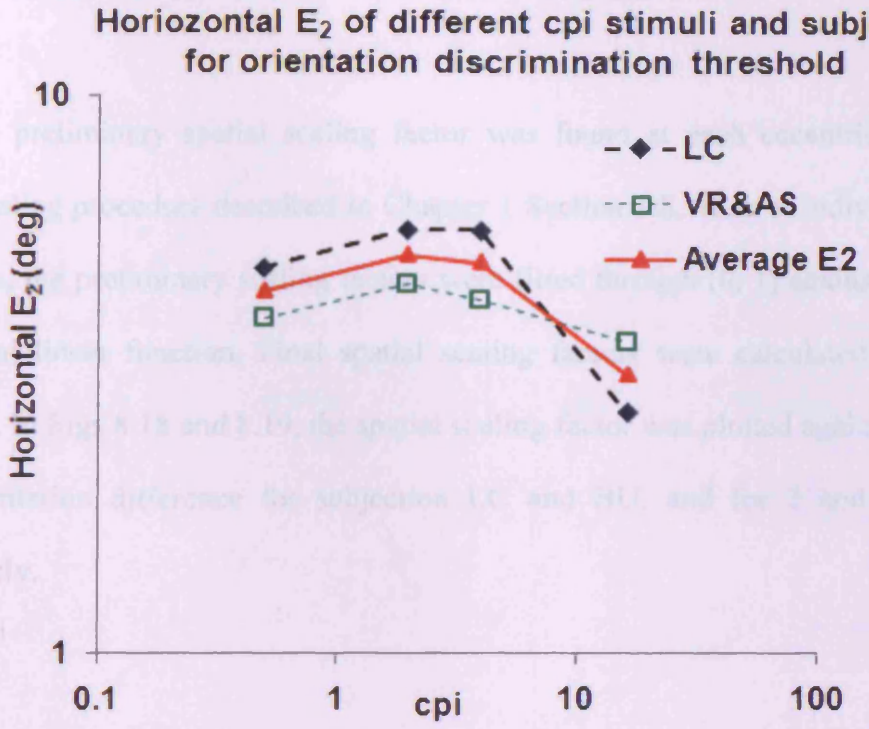

Fig 8.17 The 2D scaling horizontal E_{2h} and its average between subjects as function of cpi for the orientation discrimination threshold data for subjects LC, VR&AS from Chapters 3-5

Different data curves are as indicated by the different symbols and curve types in the figure.

8.3.6 Spatial scaling at individual orientation difference

Because the thresholds at 1.5 deg orientation difference are the most offset data (Figs 8.5 and 8.6), it could not be determined that the improvement of performance of spatial scaling after excluding the data at 1.5 deg was due to the 1.5 deg data being different from other data. Therefore, in this section, as in Chapters 6 and 7, spatial scaling was separately applied to the threshold data of 2 and 16cpi stimuli at each orientation difference. The local spatial E_{2OD} was obtained at each orientation difference. By comparing E_{2OD}s found at each orientation difference, it can be found out whether the discrimination task at 1.5 deg

orientation difference was different from those at other differences.

Firstly, a preliminary spatial scaling factor was found at each eccentricity through the spatial scaling procedure described in Chapter 1 Section 1.3. Then at individual orientation difference, the preliminary scaling factors were fitted through (0, 1) against eccentricity by an optimal linear function. Final spatial scaling factors were calculated by these linear functions. In Figs 8.18 and 8.19, the spatial scaling factor was plotted against eccentricity at each orientation difference for subjection LC and BU, and for 2 and 16cpi gratings, respectively.

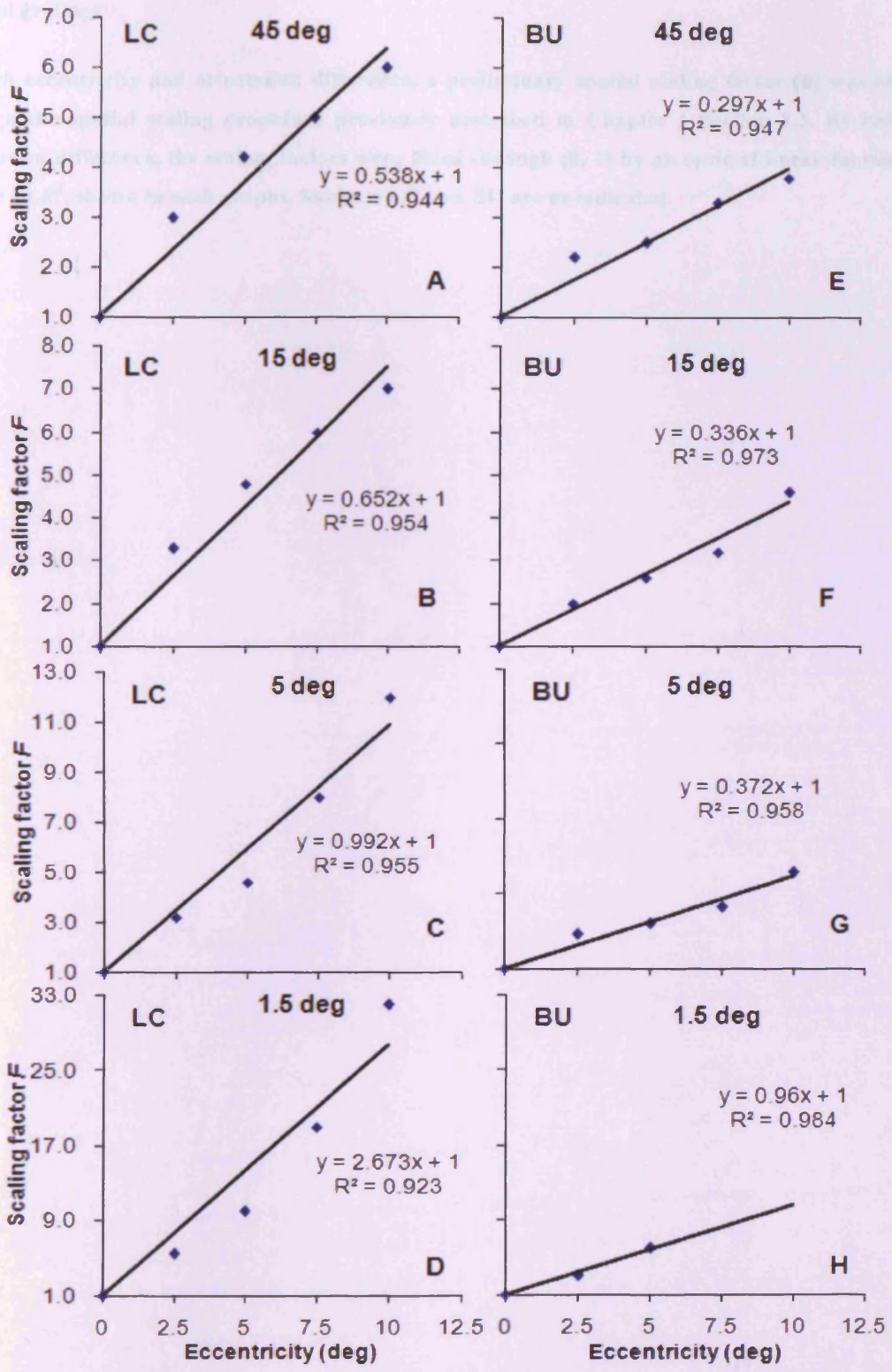

Fig 8.18 (A-H) Spatial scaling factors plotted as a function of eccentricity at each orientation difference

for 2cpi gratings

At each eccentricity and orientation difference, a preliminary spatial scaling factor (■) was obtained through the spatial scaling procedure previously described in Chapter 1 Section 1.3. By individual orientation difference, the scaling factors were fitted through (0, 1) by an optimal linear function with its best fit R^2, shown in each graphs. Subjects LC and BU are as indicated.

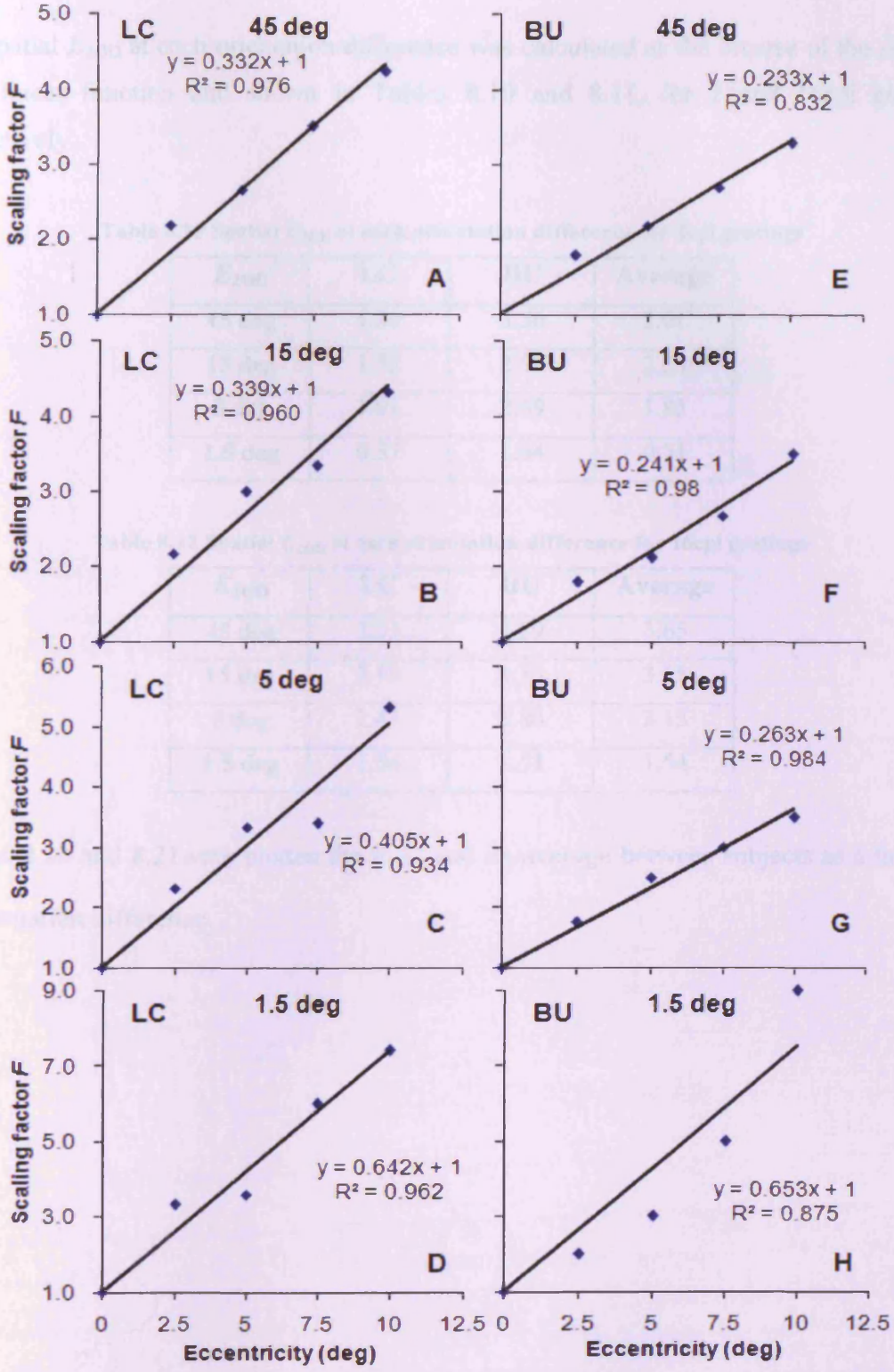

Fig 8.19 (A-H) Spatial scaling factors plotted as a function of eccentricity at each orientation difference for 16cpi gratings. Other details are as Fig 8.18.

The spatial E_{2OD} at each orientation difference was calculated as the inverse of the slope of each linear function and shown in Tables 8.10 and 8.11, for 2 and 16cpi gratings, respectively.

Table 8.10 Spatial E_{2OD} at each orientation difference for 2cpi gratings

E_{2OD}	LC	BU	Average
45 deg	1.86	3.36	2.61
15 deg	1.53	2.98	2.25
5 deg	1.01	2.69	1.85
1.5 deg	0.37	1.04	0.71

Table 8.11 Spatial E_{2OD} at each orientation difference for 16cpi gratings

E_{2OD}	LC	BU	Average
45 deg	3.01	4.29	3.65
15 deg	2.95	4.15	3.55
5 deg	2.47	3.80	3.13
1.5 deg	1.56	1.53	1.54

In Figs 8.20 and 8.21were plotted the E_{2OD} and its average between subjects as a function of orientation difference.

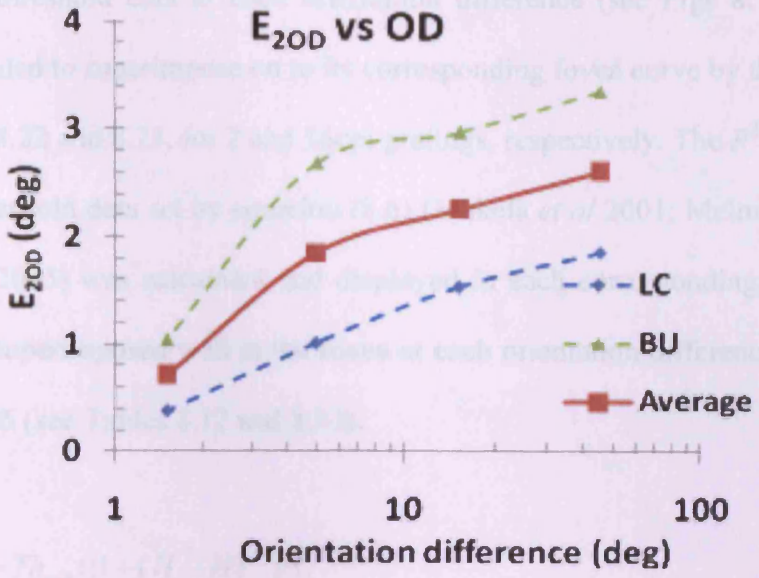

Fig 8.20 Spatial E_{2OD} plotted as a function of orientation difference for 2cpi gratings.

The blue dash smooth curve is the function of E_{2OD} vs. orientation difference for subject LC. The green one is for BU. The average of E_{2OD}s between subjects is plotted against orientation difference with the red solid smooth curve.

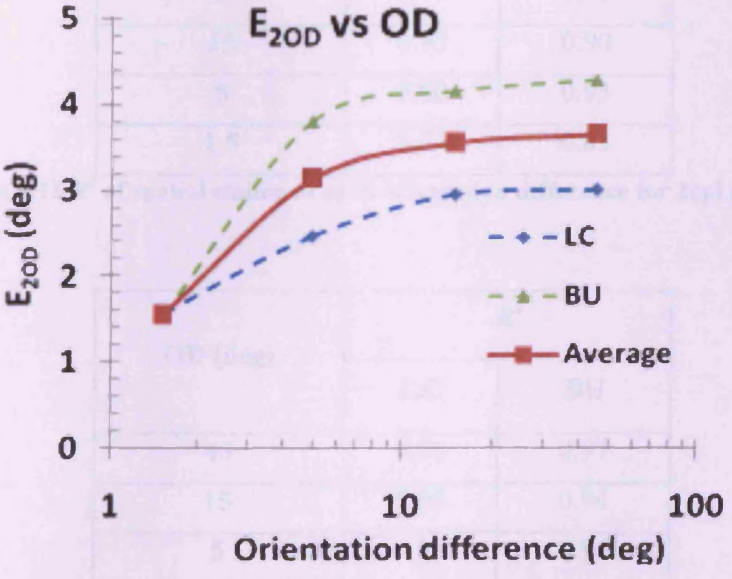

Fig 8.21 Spatial E_{2OD} is plotted as a function of orientation difference for 16cpi gratings.

The blue dash smooth curve is the function of E_{2OD} vs. orientation difference for subject LC. The green one is for BU. The average of E_{2OD}s between subjects is plotted against orientation difference with the red solid smooth curve.

The eccentric threshold data at each orientation difference (see Figs 8.1 and 8.2) were horizontally scaled to superimpose on to its corresponding fovea curve by their final scaling factors in Figs 8.22 and 8.23, for 2 and 16cpi gratings, respectively. The R^2 of the best fit to each scaled threshold data set by equation (8.6) (Makela *et al* 2001; Melmoth *et al.* 2000a, b; Sally *et al.* 2005) was calculated and displayed in each corresponding sub figure. The threshold data superimposed well at the fovea at each orientation difference, with R^2 being greater than 0.85 (see Tables 8.12 and 8.13).

$$Th = Th_{\min}((1+(H_c / H)^{p_2})^{p_1}$$ **Equation 8.6**

OD (deg)	R^2	
	LC	BU
45	0.95	0.93
15	0.93	0.90
5	0.90	0.93
1.5	0.75	0.83

Table 8.12 R^2 of spatial scaling at each orientation difference for 2cpi gratings

OD (deg)	R^2	
	LC	BU
45	0.96	0.97
15	0.95	0.94
5	0.94	0.96
1.5	0.91	0.73

Table 8.13 R^2 of spatial scaling at each orientation difference for 16cpi gratings

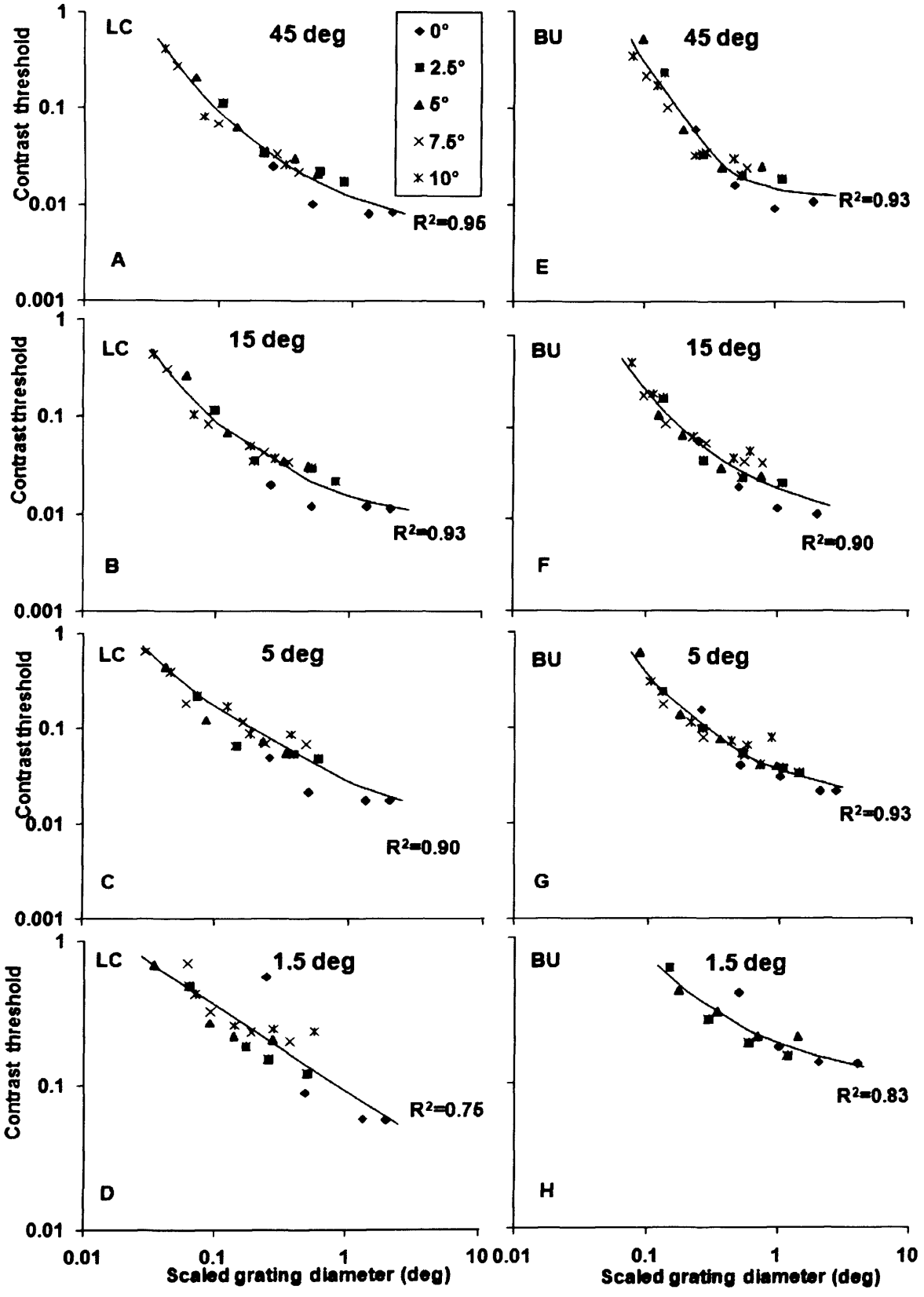

Fig 8.22 Spatial scaling of contrast threshold of orientation discrimination at 45-1.5 deg orientation

differences for 2cpi gratings.

At each orientation difference, the eccentric threshold curves (shown in Fig 8.1) were horizontally shifted to superimpose onto each fovea curve by spatial scaling factors calculated by using the corresponding linear function in Fig 8.18. The smooth curve was the best fit to each superimposed threshold set at each difference by equation (8.6). Data collapsed well onto the foveal function at indicating by the high R^2 values. Subjects LC and BU are as indicated.

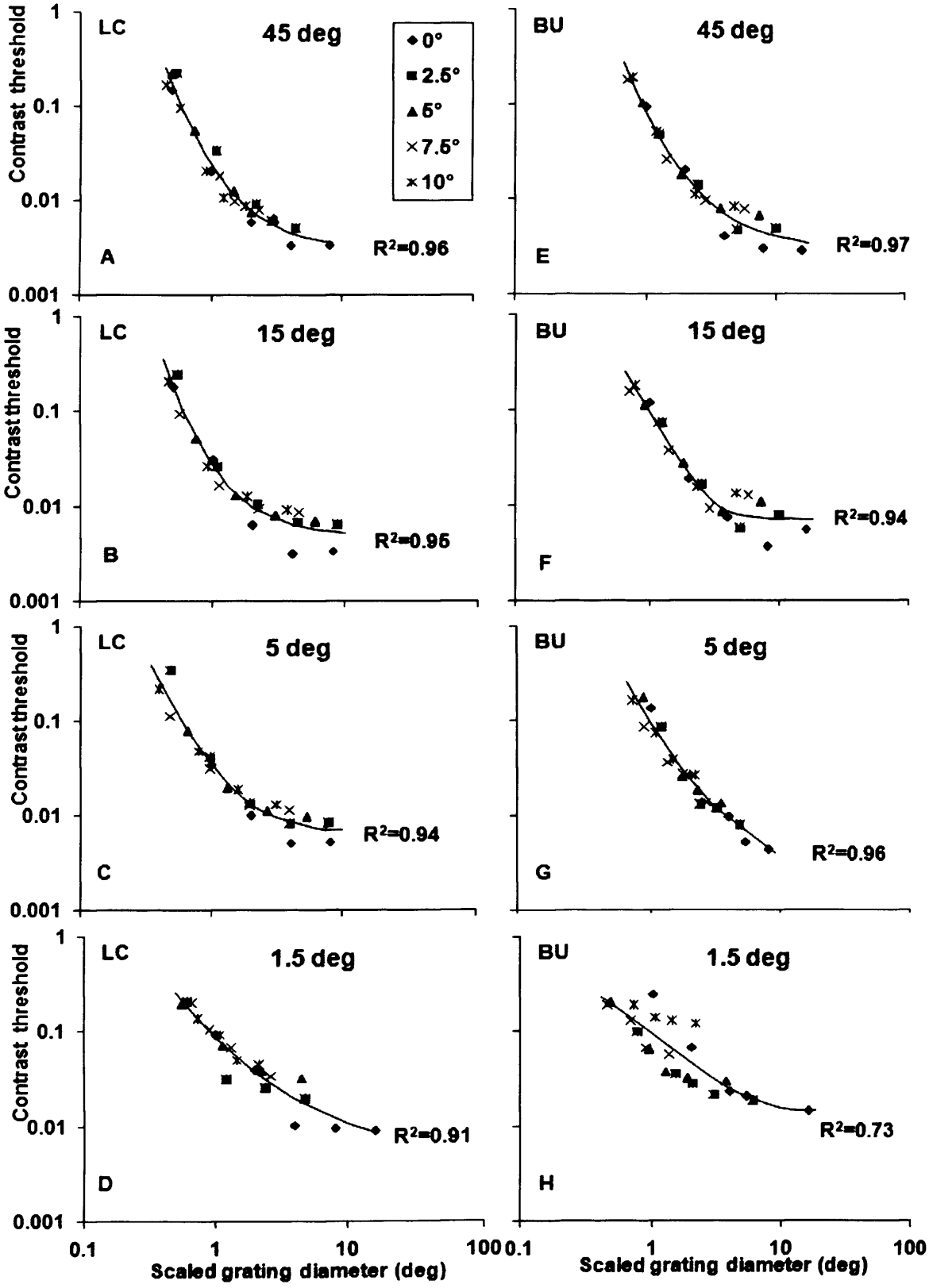

Fig 8.23 Spatial scaling of contrast threshold of orientation discrimination at 45-1.5 deg orientation

differences for 16cpi gratings.

At each orientation difference, the eccentric threshold curves (shown in Fig 8.2) were horizontally shifted to superimpose onto each fovea curve by spatial scaling factors calculated by using the corresponding linear function in Fig 8.19. The smooth curve was the best fit to each superimposed threshold set at each difference by equation (8.6). Data collapsed well onto the foveal function at indicating by the high R^2 values. Subjects LC and BU are as indicated.

The R^2 of the threshold superimposition at 1.5 deg for subject BU was comparatively lower (<0.75) due to the inaccurate spatial scaling caused by the lack of data at 7.5 and 10 deg eccentricities.

8.4 Discussion

As in Chapters 6 and 7, contrast threshold data of each subject were measured at all orientation differences and eccentricities and were superimposed at the basic condition (E=0, OD=45) by spatial and 2D scaling, separately for the 2 and 16 cpi gratings.

Irrespective of stimulus, contrast threshold allowing orientation discrimination first decreased and then saturated with increasing grating diameter, which is consistent with Howell and Hess (1978), Luntinen *et al.* 1993, Makela *et al.* (1995), Sally *et al.* (2005).and Virsu and Rovamo (1979),

The theoretical minimum contrast threshold of orientation discrimination $Th_{\min}$ and the critical stimulus size H_c where the threshold saturated were obtained by fitting one equation $Th = Th_{\min}(1+(H_c / H)^2)^{2.5}$ to the contrast threshold (Th) measured as a function of grating diameter (H) at each orientation difference and eccentricity separately for the 2 and 16cpi gratings. The equation format is consistent with equations used for modelling contrast threshold measurements in Chapters 6-7 and Makela *et al.* (2001), Melmoth *et al.* (2000a, b) and Sally *et al* (2005).

8.4.1 2cpi grating

The theoretical minimum contrast threshold $Th_{\min}$ were obtained by fitting equation (8.1) to the data curves of contrast threshold versus grating diameter. $Th_{\min}$ depends on two variables, i.e. eccentricity and orientation difference. $Th_{\min}$ increases with eccentricity at

each orientation difference (see Fig 8.11) which is in agreement with Rovamo *et al.* (1978), Rovamo *et al.* (1992), and Sally *et al.* (2005). Unlike the Th_{min} of the Gaussian filtered lines and 4cpi gratings (see Figs 6.8 and 7.8 in Chapters 6 and 7, respectively) that increase and become independent of cpi, the Th_{min} of the 2cpi gratings almost linearly decreased with increasing orientation difference, as shown in Fig 8.24 below.

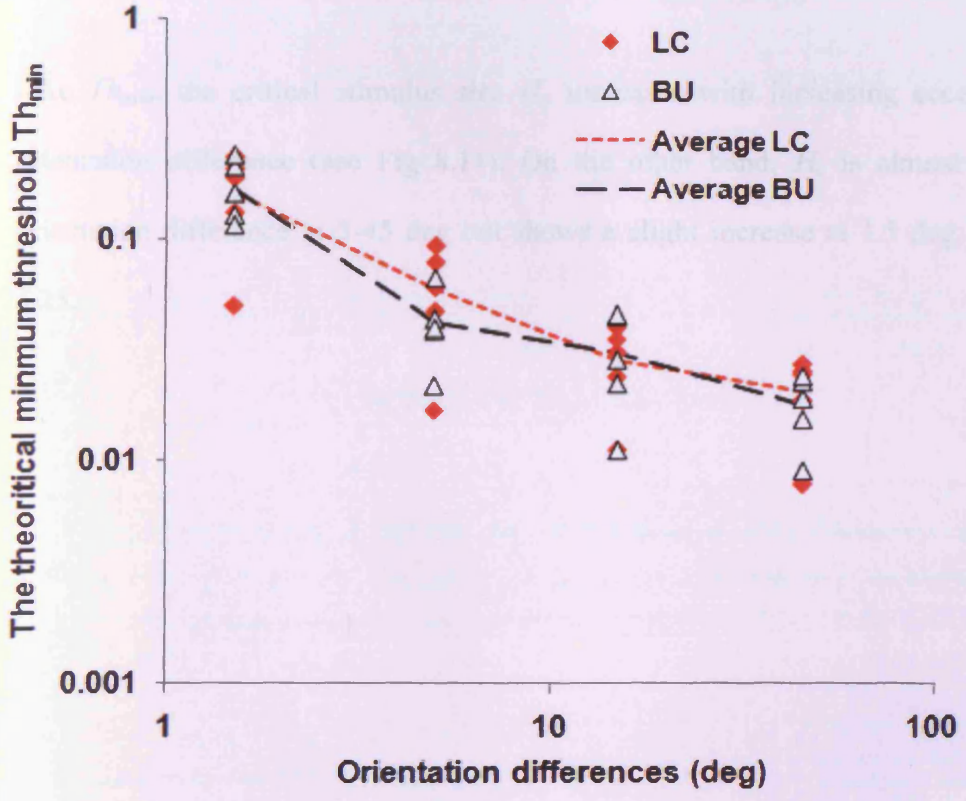

Fig 8.24 The theoretical minimum contrast threshold Th_{min} for the 2cpi gratings

Th_{min} *i.e.* the theoretical minimum contrast threshold allowing orientation discrimination was plotted as a function of orientation difference for subjects LC and BU. The red and black dashed curves are the averages of Th_{min} across eccentricities (0-10deg) at different orientation differences of 1.5, 5, 15 and 45 deg for LC and BU, respectively.

In the orientation discrimination experiments of Chapter 5, the average orientation

discrimination threshold across subjects was found to be 2.3 deg for 2cpi grating at the eccentricity of 10 deg and contrast of 10%. Thus, the measurements of the contrast threshold of orientation discrimination at orientation difference of 1.5 deg are more difficult than at 5-45 deg. The visual task at 1.5 deg actually measured the contrast threshold influenced by orientation discrimination threshold while the measurement at 5-45 deg was not affected by the orientation discrimination threshold.

Like Th_{min}, the critical stimulus size H_c increases with increasing eccentricity at each orientation difference (see Fig 8.11). On the other hand, H_c is almost independent of orientation difference at 5-45 deg but shows a slight increase at 1.5 deg, showing in Fig 8.25.

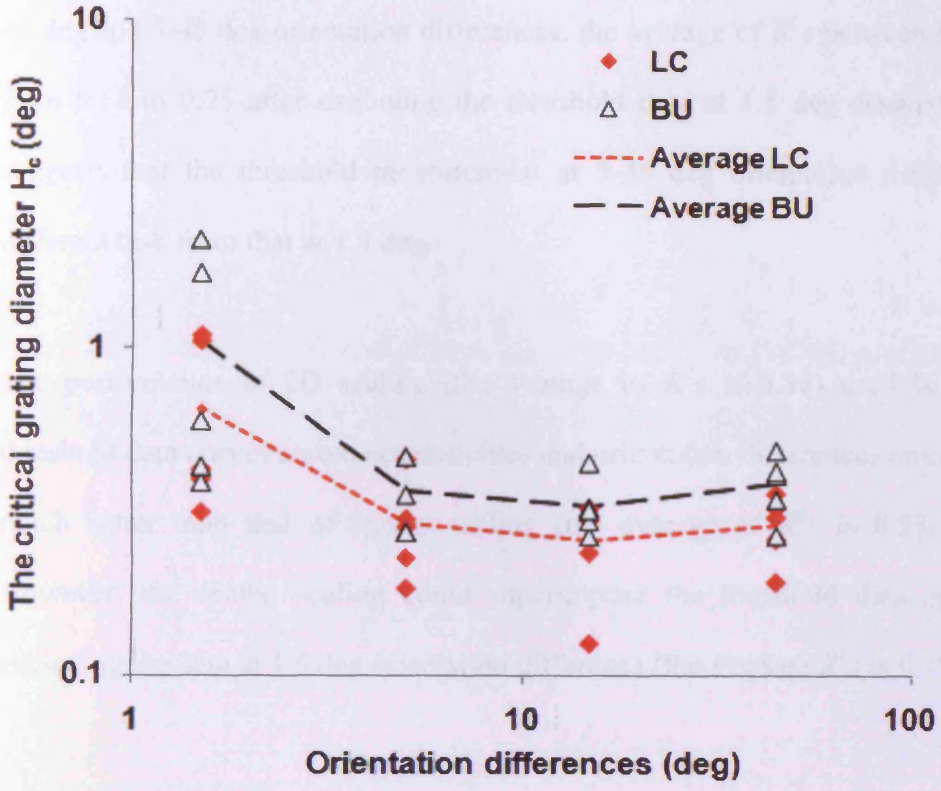

Fig 8.25 The theoretical critical size H_c for the 2cpi gratings

The theoretical critical size H_c for the contrast threshold allowing orientation discrimination was plotted as a function of orientation difference for subjects LC and BU. The red and black dashed curves are the averages of H_c across eccentricities (0-10 deg) at different orientation differences of 1.5, 5, 15 and 45 deg, for LC and BU, respectively.

As discussed in Section 8.3, both spatial and 2D scaling were across eccentricities and orientation differences. Therefore, all the scaling factors, i.e. spatial scaling factor and the vertical and horizontal factors of the 2D scaling, were dependent on two variables, eccentricity and orientation difference. The variants of equation (8.2), *i.e.* (8.3), (8.4) and (8.5) successfully estimated all the scaling factors: R^2 ranged from 0.86 to 0.97 in Tables 8.1(A) and 8.3(A).

When spatial scaling was separately applied to superimpose the threshold data across 1.5-45 deg and 5-45 deg orientation differences, the average of R^2s between subjects increased from 0.53 to 0.75 after excluding the threshold data at 1.5 deg orientation difference. It suggests that the threshold measurement at 5-45 deg orientation differences may be a different task from that at 1.5 deg.

The performance of 2D scaling (the average of R^2s is 0.88) used to superimpose the threshold data curves across eccentricities and orientation differences onto (E=0, OD=45) is much better than that of spatial scaling (the average of R^2s is 0.53) (see Table 8.5). However, the spatial scaling could superimpose the threshold data appropriately after excluding the data at 1.5 deg orientation difference (the average R^2s is 0.75).

The global spatial E_2s found by spatial scaling across orientation differences are 3.01 deg for LC and 5.20 deg for BU, which are smaller than the horizontal E_{2h}s of the 2D scaling (13.6 deg for LC and 11.3 deg for BU). This was caused by the application of the simultaneous vertical scaling of 2D, as was the case for the Gaussian filtered lines and 4cpi gratings. The average of the global spatial E_2s between subjects is 4.11 deg and really close to 4.56 deg found in Chapter 7 for the 4cpi gratings.

Further, at each orientation difference, spatial scaling successfully superimposed the eccentric threshold data to the fovea data curve (see Table 8.12 and Fig 8.22). The local E_{2OD} found increases as orientation difference increases (see Fig 8.20), which is different from those of Gaussian filtered lines (Chapter 6 Section 6.3.3 Fig 6.9) and 4cpi gratings (Chapter 7 Section 7.33 Fig 7.9). However, the increase is much sharper at 1.5 to 5 deg than

that at 5-15 deg, as shown in Fig 8.20.The average of E_{2OD} between subjects at 1.5 deg is about 0.7 deg and much smaller than those of other differences ranging from 1.9 to 2.6 deg. Therefore, the visual task at 1.5 deg has a different (and more complicated) feature, compared with those of 5-45 deg orientation differences. It mainly caused the failure of spatial scaling across orientation differences from 1.5 to 45 deg (the average of R^2s is 0.53), as discussed previously.

In summary, for this task, it can be concluded that the peripheral performance in the task is not qualitatively different from that of the fovea, and the failure of spatial scaling across orientation differences was caused by the complexity of the task, in agreement with Melmoth *et al.* (2001a, b).

8.4.2 16cpi grating

In Fig 8.26, the theoretical minimum contrast threshold Th_{min} was plotted against orientation difference. It decreases sharply with increasing orientation difference from 1.5 to 5 deg but tends to reach a plateau from 5 to 45 deg.

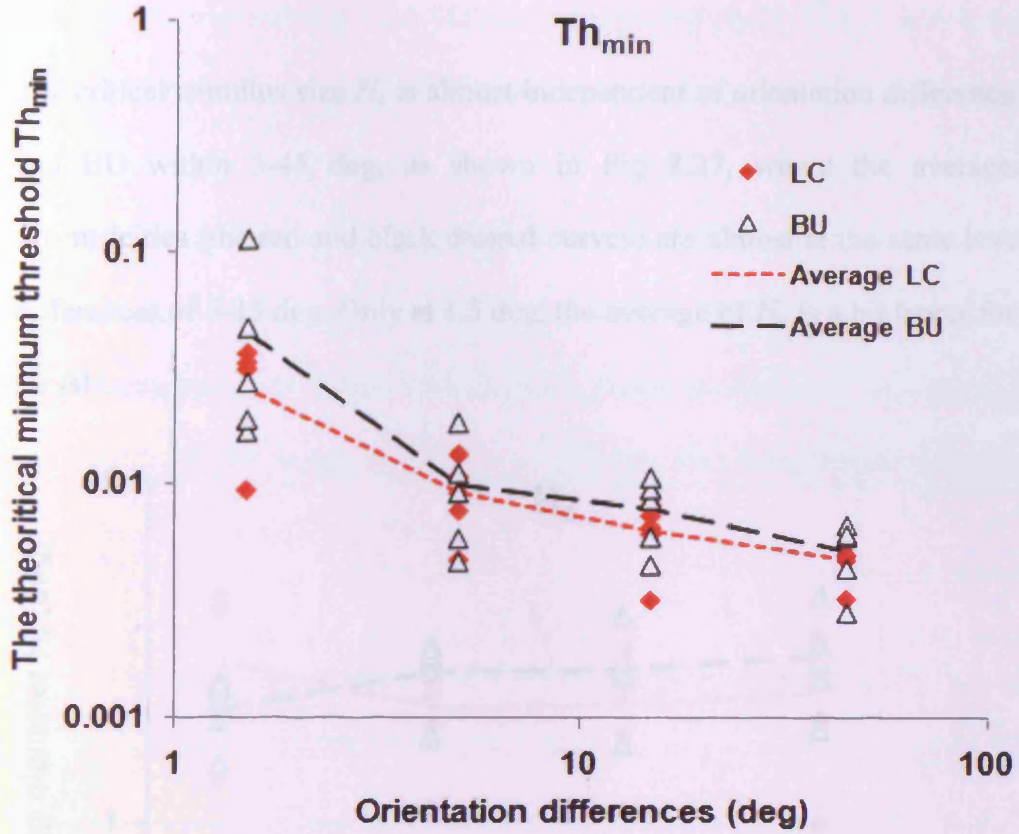

Fig 8.26 The theoretical minimum contrast threshold Th_{min} for the 16cpi gratings

Th_{min} *i.e.* the theoretical minimum contrast threshold allowing orientation discrimination was plotted as a function of orientation difference for subjects LC and BU. The red and black dashed curves are the averages of Th_{min} across eccentricities (0-10deg) at orientation differences of 1.5, 5, 15 and 45 deg for LC and BU, respectively.

In the orientation discrimination experiments of the 16cpi gratings in Chapter 5, the average orientation discrimination thresholds between subjects were 2.1 deg at the eccentricity of 10 deg and 10% contrast. Therefore, as for all other stimuli (the Gaussian filtered lines, and 2 and 4cpi gratings), the measurement of the contrast threshold of orientation discrimination at the orientation difference of 1.5 deg is a different visual task than at 5-45 deg. This is the reason why the R^2 of superimposing threshold data by spatial scaling improved from 0.78 to 0.92 after excluding the data at 1.5 deg.

The critical stimulus size H_c is almost independent of orientation difference for subjects LC and BU within 5-45 deg, as shown in Fig 8.27, where the averages of H_c across eccentricities (the red and black dashed curves) are almost at the same level for orientation differences of 5-45 deg. Only at 1.5 deg, the average of H_c is a bit larger for LC and smaller for BU.

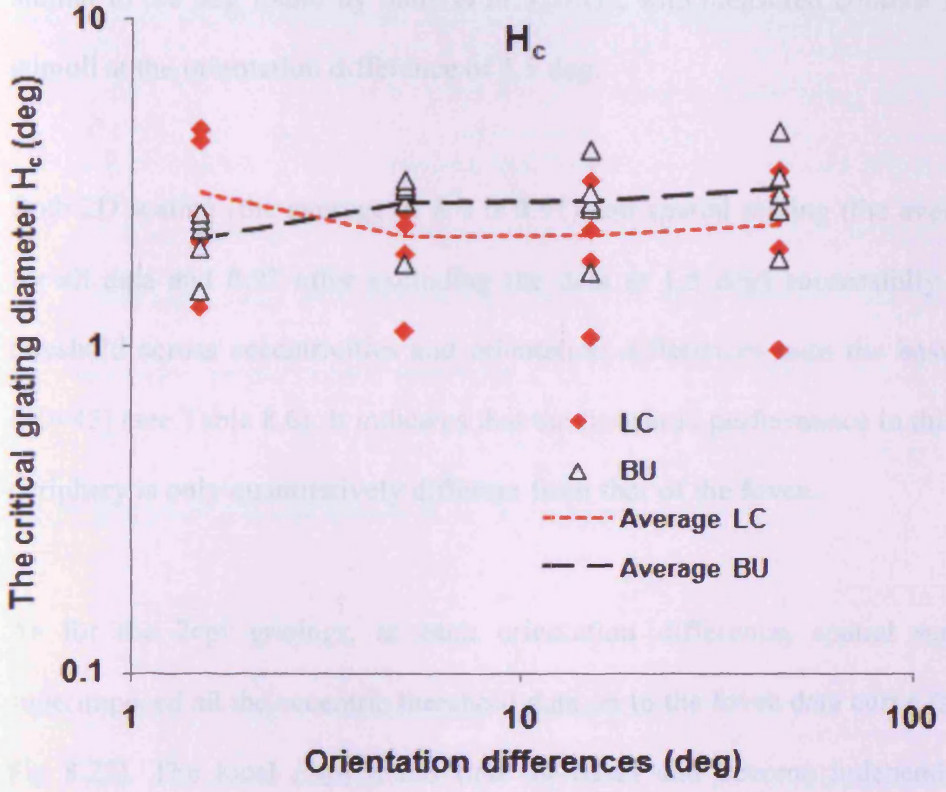

Fig 8.27 The theoretical critical size H_c for the 16cpi gratings

The theoretical critical size H_c for the contrast threshold allowing orientation discrimination was plotted as a function of orientation difference for subjects LC and BU. The red and black dashed curves are the averages of H_c across eccentricities (0-10deg) at orientation differences of 1.5, 5, 15 and 45 deg, for LC and BU, respectively.

The spatial scaling factor and the vertical and horizontal factors of 2D scaling were

successfully estimated by the variants of equation (8.2) .The R^2s of the estimates ranged from 0.87 to 0.97 (see Tables 8.2(A) and 8.4(A)).

The global spatial E_2s obtained during spatial scaling across orientation differences were found to be 3.61 deg for LC and 6.25 deg for BU. The average of the E_2s between subjects is 4.93 deg, which is similar to 4.11 and 4.56 deg for the 2 and 4cpi gratings. It is also quite similar to 5.8 deg found by Sally *et al.* (2005), who measured contrast thresholds of line stimuli at the orientation difference of 1.5 deg.

Both 2D scaling (the average of R^2s is 0.91) and spatial scaling (the average of R^2s is 0.78 for all data and 0.92 after excluding the data at 1.5 deg) successfully superimposed the threshold across eccentricities and orientation differences onto the basic condition (E=0, OD=45) (see Table 8.6). It indicates that the threshold performance in this visual task in the periphery is only quantitatively different from that of the fovea.

As for the 2cpi gratings, at each orientation difference, spatial scaling successfully superimposed all the eccentric threshold data on to the fovea data curve (see Table 8.13 and Fig 8.23). The local E_{2OD} found first increases and become independent of orientation difference (see Fig 8.21), which is in agreement those of Gaussian filtered lines (Chapter 6 Section 6.3.3 Fig 6.9) and 4cpi gratings (Chapter 7 Section 7.33 Fig 7.9). The average of E_{2OD} between subjects at 1.5 deg is about 1.5 deg and much smaller than those of other differences ranging from 3.1 to 3.7 deg. It further confirms the previous finding, *i.e.*, the visual task at 1.5 deg is different (and more complicated than) from those of 5-45 deg orientation differences.

Therefore, the failure of spatial scaling across orientation differences from 1.5 to 45 deg was caused by the scaling method being applied to the data which had a complicated feature but not the peripheral performance being qualitatively different from that of fovea in the task (Melmoth *et al.* 2001a, b)

8.4.3 The comparison of spatial and 2D scaling for all stimuli

In Section 8.3.3, Table 8.7 shows the R^2s of 2D and spatial scaling applied to all the stimuli for all the subjects. The 2D scaling was generally good and its R^2s ranged from 0.81 to 0.93, with an average 0.88. Spatial scaling across 1.5 to 45 deg orientation differences was poor, with the lowest of 0.48 and an average of 0.66. However, the R^2 was considerably improved after excluding the threshold data at 1.5 deg, with an average of 0.82, which is really close to that of 2D scaling. The Wilcoxon test further confirmed that the increase of the R^2 is statistically significant at the level of p=0.008.

All the results of the threshold data analysis in Chapters 6-7 and the present chapter show that the measurement of the contrast threshold data from 1.5 to 45 orientation differences can be divided into two subtasks for each stimulus: (i) the contrast threshold of stimuli at 5-45 deg orientation differences, and (ii) the contrast threshold for discriminating 1.5 deg orientation difference between stimuli. The threshold measurement was affected by the observers' orientation discrimination threshold, which was found to be from 0.6 to 3.2 deg for different stimuli in the orientation discrimination experiments (Chapters 3-5).

Therefore, the failure of spatial scaling for superimposing the threshold data across

orientation differences of 1.5 to 45 deg could be caused by the fact that the scaling was applied to the threshold data with various task requirements. This is consistent with Melmoth *et al.* (2001a) who suggested that it was the complexity of the visual task that made contrast scaling necessary and sole spatial scaling failed.

8.4.4 Global spatial E_2 across orientation differences and cpi

By comparing the global spatial E_2 of the spatial scaling with horizontal E_{2h} of the horizontal scaling of 2D scaling, it is found that the spatial E_2 is generally smaller than horizontal E_{2h}, and the average of the global spatial E_2 is 4.17 deg across subjects and stimuli (see Table 8.8), which is the half of the average of horizontal E_{2h} (8.52 deg see Table 8.9). This was caused by the simultaneous vertical scaling applied in 2D scaling. The average of the spatial E_2 is similar to 5.8 deg found by Sally and Gurnsey (2007) who measured contrast threshold for discriminating the 1.5 deg orientation difference between bar stimuli.

Fig 8.15 shows the global spatial E_2 for each subject has a rather complicated relationship with the number of grating cycles per image (cpi). However, its average between subjects increases and reaches a plateau as cpi increases. The result suggests that more size scaling is needed for achieving foveal levels of performance for smaller cpi stimulus.

8.4.5 Local E_{2OD} found from the spatial scaling at each orientation difference OD for all cpi

To clearly show how orientation difference *OD* and the cycle number *cpi* affect local spatial E_{2OD}, E_{2OD} is plotted against *OD* and *cpi* separately in Figs 8.28 and 8.29.

As shown in Fig 8.28, the local E_{2OD} first increases (from 1.5 to 5 deg) and becomes (or tends to become) independent of orientation difference (from 5-45 deg). The E_{2OD} at 1.5 deg is much smaller than those of other differences. In Fig 8.29, the curves of E_{2OD} as a function of cpi at 5-45 deg are noticeably higher than that of 1.5 deg. However, the curves at 1.5 and 5 deg are similar and are v-shaped, while invert v-shaped at 15 and 45 deg.

These figures support the common finding from the data analysis of the threshold data of Gaussian filtered lines (Chapter 6), 4cpi gratings (Chapter 7), 2 and 16cpi gratings (the present Chapter): the visual process mechanism of the visual task at large orientation difference is different from that at as small as orientation discrimination threshold

Therefore, the 3rd hypothesis is proved.

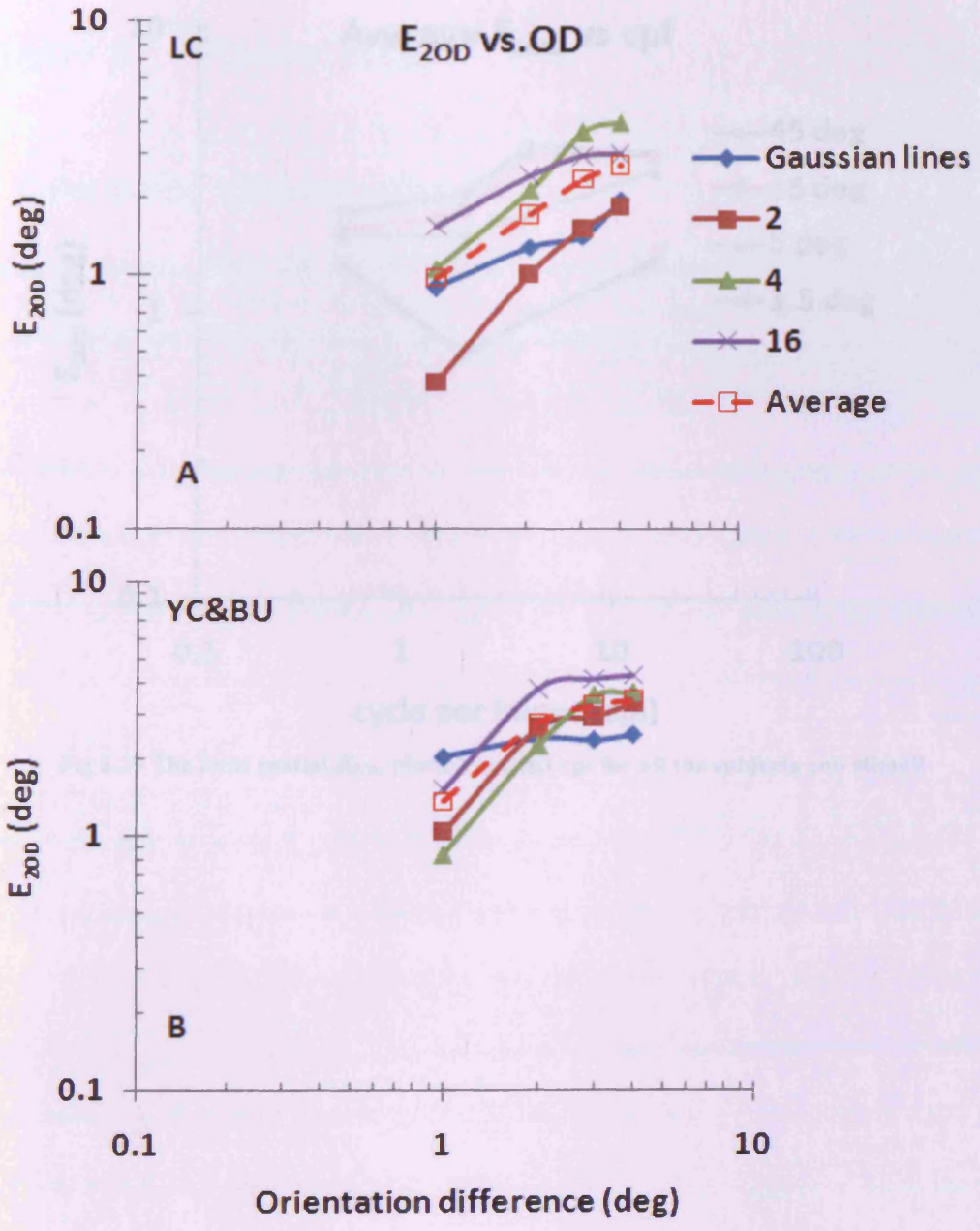

Fig 8.28 The local spatial E_{2OD} plotted against orientation difference for all the subjects and stimuli

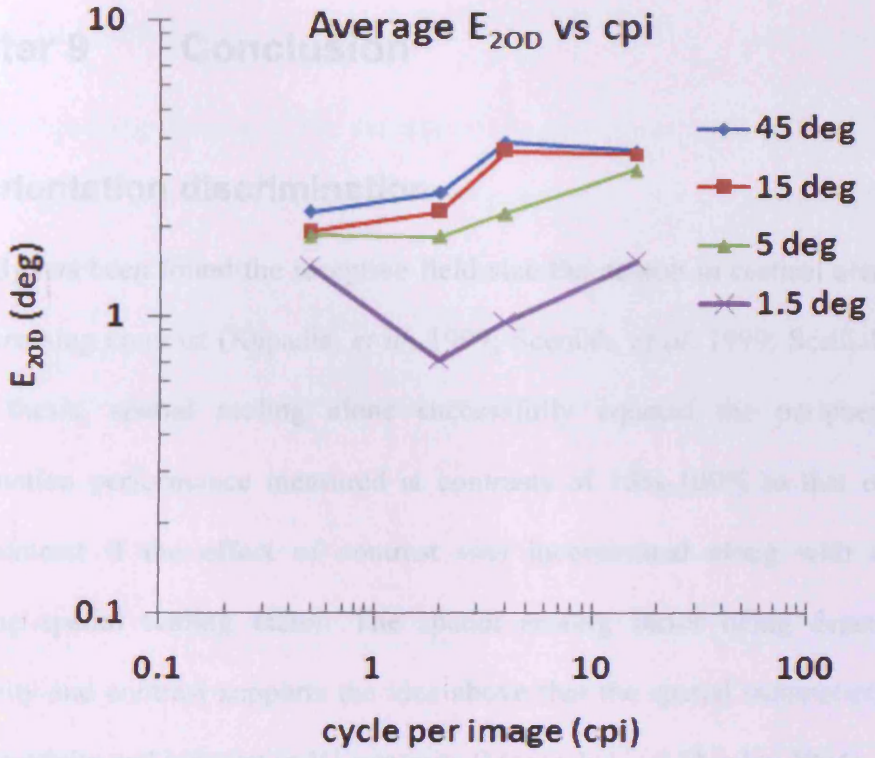

Fig 8.29 The local spatial E_{2OD} plotted against cpi for all the subjects and stimuli

Chapter 9 Conclusion

9.1 Orientation discrimination

It recently has been found the receptive field size the neuron in cortical area V1 increases with decreasing contrast (Kapadia, *et al.* 1999; Sceniak, *et al.* 1999; Sceniak, *et al.* 2002). In this thesis, spatial scaling alone successfully equated the peripheral orientation discrimination performance measured at contrasts of 10%-100% to that of the fovea at 100% contrast if the effect of contrast was incorporated along with eccentricity in estimating spatial scaling factor. The spatial scaling factor being dependent on both eccentricity and contrast supports the idea above that the spatial summation changes with both eccentricity and contrast in V1 neutrons (Mareschal and Shapley 2004).

Although 2D scaling generally performed better than spatial scaling on the basis of the R^2 of the superimposed thresholds obtained by scaling, the Wilcoxon test (see Chapter 5 Section 5.3.3) showed that the difference between spatial scaling and 2D scaling is not statistically significant. Therefore, the conclusion is made that the difference of orientation discrimination performance between fovea and periphery in this visual task is not qualitative, which is in agreement with Whitaker *et al.* (1992), Makela *et al.* (1993), Sally and Gurnsey (2003), etc. The peripheral orientation discrimination performance was successfully equated with that of the fovea by spatial scaling separately at each contrast, further proving that the peripheral performance is only quantitatively different from that of fovea in this visual task.

Based on the equation $F = 1 + E/E_2 + (\log C)^2/k_1 + E \times \log C/k_3$ used to model the spatial scaling factors across contrasts, the average of the global spatial E_2 between subjects ranged from 4.41 to 1.49 deg (see Table 5.7 in Chapter 5 Section 5.3.4). E_2 first sharply decreased and then reached a plateau at 16cpi as cpi increased (see Fig 5.12 in Chapter 5 Section 5.3.4). This suggests that the numbers of grating cycles plays an essential role in spatial scaling when the grating cycles are smaller than 16 cycles per image.

The theoretical minimum of orientation discrimination thresholds Th_{min} at 0 and 10 deg eccentricities and 100 and 10% contrasts are shown for all stimuli and subjects in Fig 9.1. The amount of the increase of $Th_{\min}$ as contrast decreases from 100% (black bar) to 10% (grey bar) is similar at the fovea and the eccentricity of 10 deg. This suggests that the deterioration of the foveal performance is not faster than that of the periphery with contrast reduction.

Fig 9.1 Th_{min} at 0&10 deg eccentricities and 100&10% contrasts

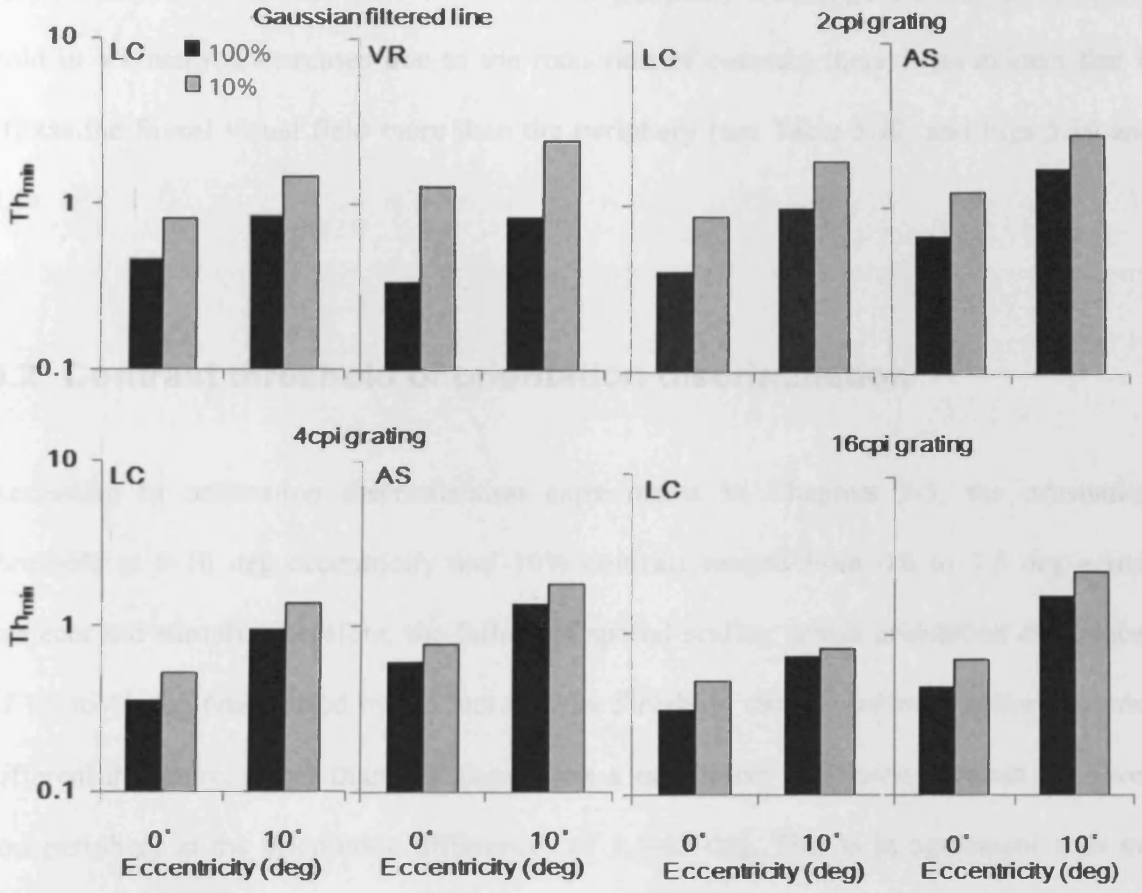

The theoretical minimum orientation discrimination threshold Th_{min} at 0 and 10 deg eccentricities and 100 and 10% were plotted for all types of stimuli and all subjects. Black bars refer to 100% while grey bars refer to 10%. Subjects as indicated.

Later, through spatial scaling at each contrast, spatial E_{2c} was found to be around 2 deg and almost independent of contrast (see Table 5.12 and Fig 5.19). It is different from the finding of Sally and Gurnsey in 2007, who found larger E_2 at lower contrast and claimed that the reduction of contrast had more effect on fovea than periphery. As their E_2s were determined by spatial scaling applied to the orientation discrimination thresholds only measured at fovea and 10 deg eccentricity and at 3-48% contrast, the limited data, the lack of eccentricities and high contrasts (e.g., full contrast) could result in inaccurate E_2.

Thus, based on the results in the thesis, it can be concluded that contrast reduction has no considerably different influence on fovea and periphery. Although the size of receptive field in V1 neutron increases due to the reduction of contrast, there is no evident that it affects the foveal visual field more than the periphery (see Table 5.12, and Figs 5.19 and 9.1).

9.2 Contrast threshold of orientation discrimination

According to orientation discrimination experiments in Chapters 3-5, the orientation threshold at 0-10 deg eccentricity and 10% contrast ranged from 0.6 to 3.5 deg across subjects and stimuli. Therefore, the failure of spatial scaling across orientation differences of 1.5 to 45 deg was caused by the fact that the threshold data scaled were collected under different difficulty, rather than that there were a qualitative difference between the fovea and periphery at the orientation differences of 1.5-45 deg. This is in agreement with the orientation discrimination results of Chapters 3-5 and with Melmoth *et al.* (2001a) who suggested that it is the complexity of the visual task that makes contrast scaling necessary and results in the failure of the sole spatial scaling. In this thesis, it was proved by (i) the success of spatial scaling applied across 5-45 deg orientation differences (see Table 8.7 in Chapter 8 Section 8.3.3) (ii) local spatial E_{2OD} obtained at 1.5 deg orientation difference being noticeably different from those of other differences (see Figs 8.28 and 8.29 in Chapter 8 Section 8.4.5).

We therefore suggest that contrast thresholds allowing orientation discrimination of the line

or grating stimulus task can be divided two subgroups, (i) the contrast thresholds for the orientation difference of 5-45 deg and (ii) the threshold contrast allowing 1.5 deg orientation discrimination.

The difference between the two groups is also reflected on the theoretical minimum threshold found at each orientation difference. In Fig 9.2 the theoretical minimum threshold Th_{min} is plotted as a function of cpi at each eccentricity and orientation difference. (For the convenience of data presentation, the Gaussian filtered line stimulus is regarded as 0.5 cpi grating according to its configuration.). Irrespective of eccentricity, Th_{min} at the orientation difference of 5-45 deg are roughly at the similar vertical level while Th_{min} at the orientation difference of 1.5 deg is at a much higher level. Also irrespective of eccentricity, $Th_{\min}$ plotted against cpi has a band-pass shape at the orientation difference of 1.5 deg but a low-pass shape at 5-45 deg,

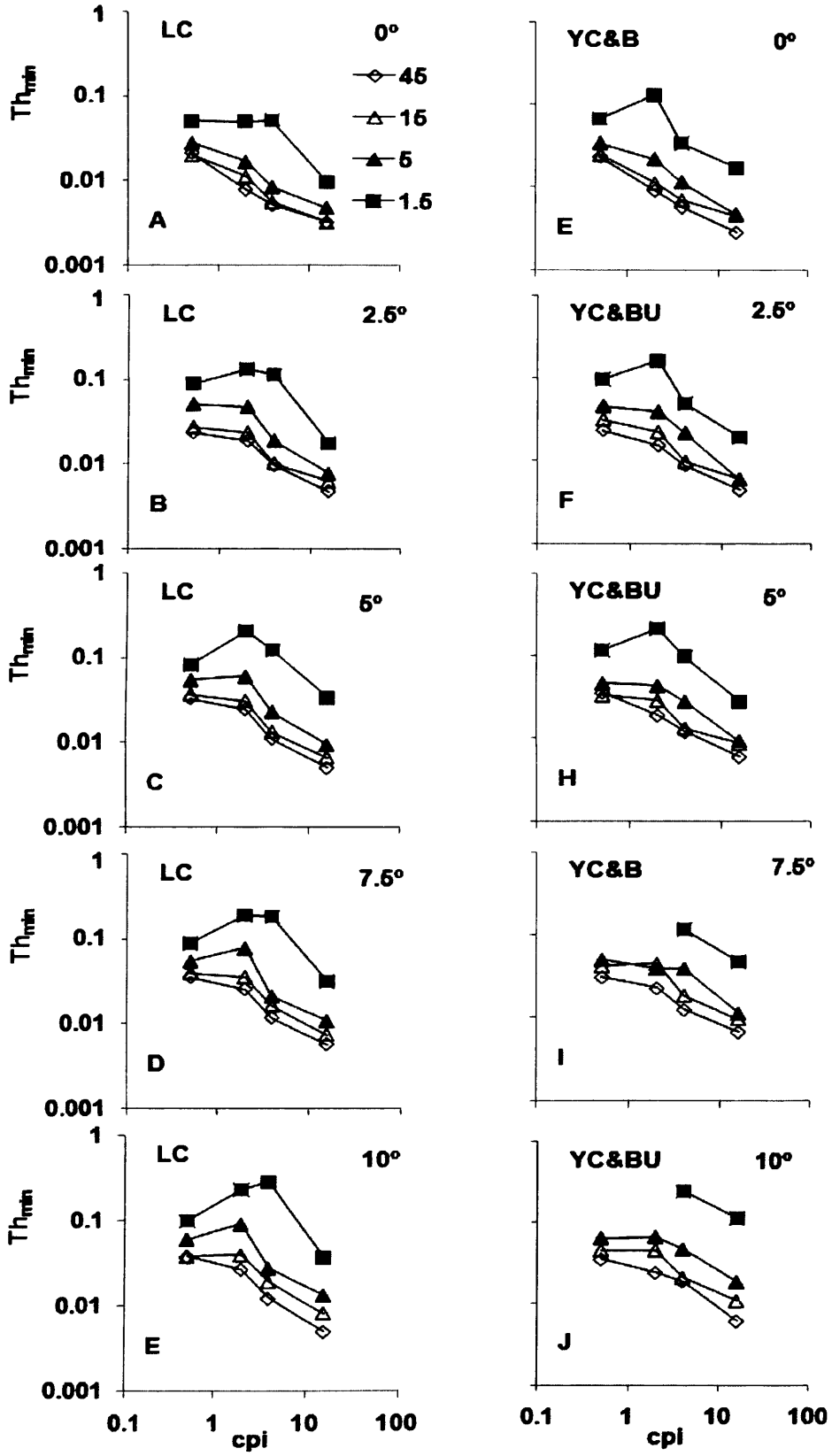

Fig 9.2 Th_{min} at each orientation difference of 45, 15, 5, and 1.5 deg was plotted as a function of cpi at each eccentricity of 0, 2.5, 5, 7.5 and 10 deg for subjects LC and BU.

Note that the Gaussian filtered line was regarded as 0.5cpi grating.

The maximum of Th_{min} occurs at about 3-4 cpi. Th_{min} was quite similar from 0.5 to 4 cpi at each eccentricity, which is in agreement with Savoy and McCann (1975) who measured contrast sensitivity of a sinusoidal grating as a function of the number of cycles.

The critical size H_c, marking the saturation of threshold was found to be almost independent of orientation difference at each cpi. This is shown in Fig 9.3 where H_c plotted as a function of cpi at each eccentricity collapsed together at all orientation differences. It support the 2nd hypothesis (made in Chapter 1 Section 1.5.2) that the number of the grating cycles per stimulus image has an essential effect on the size of threshold saturation for the low-cycle-number gratings ($\leq$16) (Jamar and Koenderink 1983). At all eccentricities and orientation differences, H_c as a function of cpi curve has a u-shape with the minimum at 2cpi. The critical size of the 0.5cpi grating (*i.e.* Gaussian filtered line) is almost the same as that of the 16cpi.

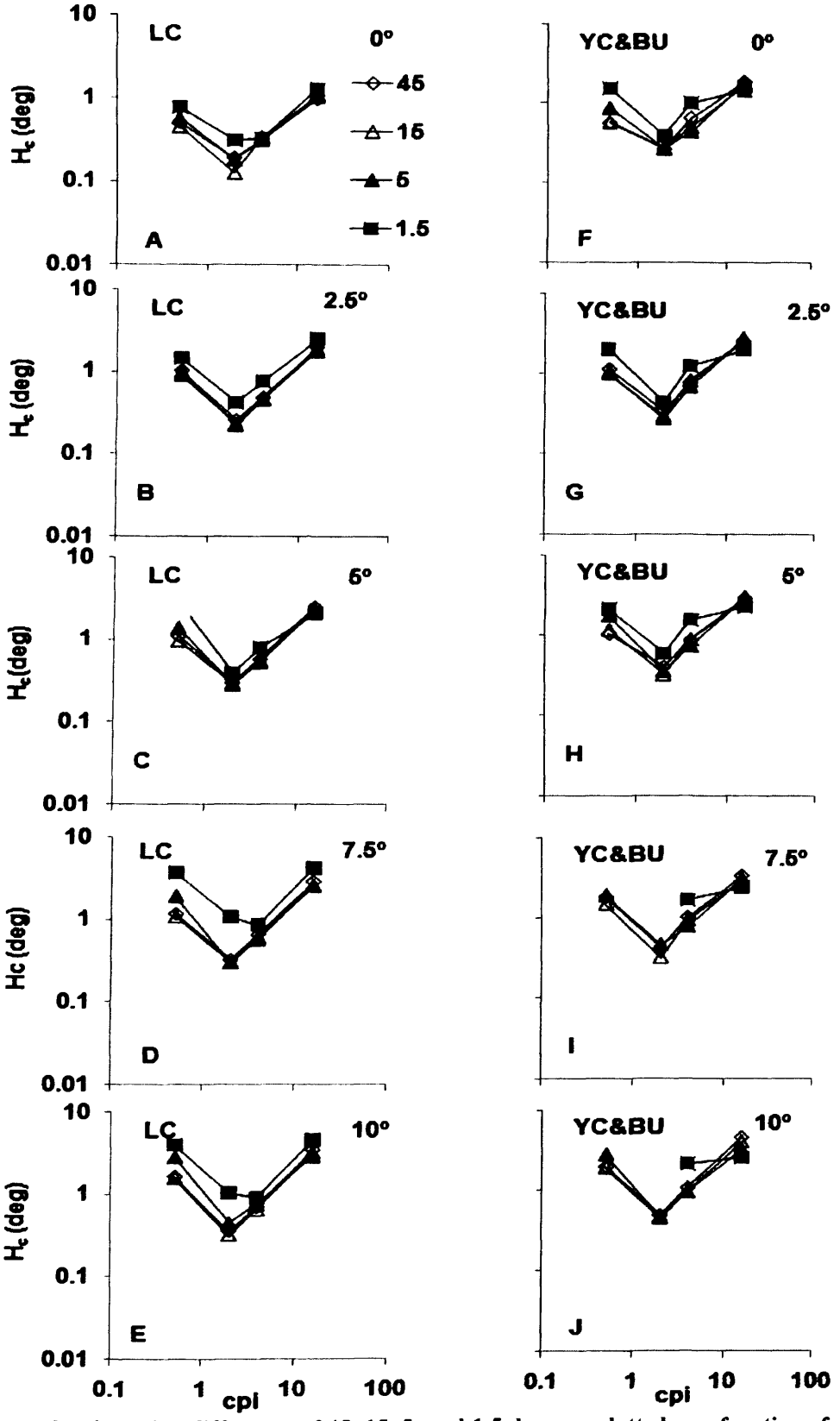

Fig 9.3 H_c **at each orientation difference of 45, 15, 5, and 1.5 deg was plotted as a function of cpi at each eccentricity of 0, 2.5, 5, 7.5 and 10 deg for subjects LC and BU.**

Note that the Gaussian filtered line was regarded as 0.5cpi grating.

9.3 Future work

Gaussian filtered lines were regarded as 0.5cpi grating when investigating the effect of cpi. The edge of the line stimulus weighed by the Gaussian window was less sharp than the 2-16cpi unfiltered grating stimuli. The sharp-edged line stimulus was not used in the experiments due to the resolution limit of the monitor used. When this problem is sorted in the future, it would be interesting to see how sharp-edged line stimulus would affect the results.

Further, the use of Gaussian filter on line stimulus also caused another problem, the difficulty of determining the perceived stimulus size, *i.e.* the length of the Gaussian-lengthened line. In the thesis, the filtered length was decided in the preliminary experiments. The filtered stimuli with different lengths at different contrasts were randomly presented and observers were asked to indicate where those lines ended in the screen. Then the visible sizes of the stimuli were measured. The perceived length was calculated as 2.5 times of the actual length (before filtering), which was roughly the average of the visible lengths reported. However, this compromised the accuracy of the actually perceived stimulus size, because the visible length after Gaussian filtering also depended on the stimulus contrast, e.g., the Gaussian filtered lines at 100% should looks longer than that of 10% contrast. And therefore, it affected the accuracy of the spatial scaling applied across contrasts, because the line stimulus size at 10% contrast was 'over-lengthened' and so over-shifted along size axis to superimpose on to 100% contrast data. To solve this problem, the

filtered line stimulus size needs to be re-measured separately at each contrast and determined contrast-based. The grating stimuli used in the thesis were all sharp-edged so that their scalings were not influenced by this problem.

Sally and Gurnsey (2003, 2004) used both broad- and narrow-band line stimuli to investigate the effect of contrast on orientation discrimination. The E_2s obtained were not identical. The effect of the bandwidth of stimulus on orientation discrimination is another interested topic for future research.

Since the results shows the contrast threshold for discriminating orientation differences of 1.5-5 deg and 5-45 deg are different, the next set of the experiments is going to be conducted to measure the threshold at lower than 5 deg orientation difference, e.g. 3 deg, due to the finding of the orientation discrimination thresholds found at 10% contrast being less than 3 deg at no more than 10 deg eccentricity. It would be interested see whether spatial scaling can successfully superimpose the contrast threshold data at orientation discrimination levels. Spatial E_2 would be measured to compare with that of the present findings.

The effect of contrast in other hyperacuity tasks related to spatial summation (for example, bisection acuity, spatial interval acuity) is also worth for investigating in the future.

References

Adams, D.L., & Horton, J.C. (2003). A precise retinotopic map of primate striate cortex generated from the representation of angioscotomas. *Journal of Neuroscience, 23* (9), 3771-3789.

Anderson, A.J., Mullen, K.T., & Hess, R.F. (1991). Human peripheral spatial resolution for achromatic and chromatic stimuli: limits imposed by optical and retinal factors. *Journal of Physiology, 442*, 47-64.

Andrews, D.P. (1967). Perception of contour orientation in the central fovea, Part II: spatial integration. *Vision Research, 7*, 998-1013.

Andrews, D.P., Butcher, A.K., & Buckley, B.R. (1973). Acuities for spatial arrangement in line figures: human and ideal observers compared. *Vision Research, 13*, 599-620.

Banks, M.S., Geisler, W.S., & Bennett, P.J. (1987). The physical limits of grating visibility. *Vision Research, 27* (11), 1915-1924.

Barrett, B.T., & Whitaker, D. (2004). A comparison of vernier acuity for narrowband and broadband stimuli. *Spatial Vision, 17* (1-2), 111-126.

Bearse Jr, M.A., & Freeman, R.D. (1994). Binocular summation in orientation discrimination depends on stimulus contrast and duration. *Vision Research, 34* (1), 19-29.

Beaudot, W.H.A., & Mullen, K.T. (2006). Orientation discrimination in human vision: Psychophysics and modeling. *Vision Research, 46* (1-2), 26-46.

Beck, J., & Halloran, T. (1985). Effects of spatial separation and retinal eccentricity on two-dot vernier acuity. *Vision Research, 25*, 1105-1111.

Berry, R.N. (1948). Quantitative relations among vernier, real depth, and stereoscopic depth acuities. *Journal of Experimental Psychology, 38*, 708-721.

Betts, L.R., Sekuler, A.B., & Bennett, P.J. (2007). The effects of aging on orientation discrimination. *Vision Research, 47* (13), 1769-1780.

Bockisch, C.J. (1998). Orientation discrimination and tilt aftereffects with luminance and illusory contours. *Vision Research, 39* (4), 765-775.

Bowne, S.F. (1990). Contrast discrimination cannot explain spatial frequency, orientation or temporal frequency discrimination. *Vision Research, 30*, 449-461.

Boyce, P.R. (1965). The visual perception of movement in the absence of an external frame of reference. *Acta Ophthalmologica, 12*, 47-54.

Bradley, A., & Freeman, R.D. (1985). Is reduced vernier acuity in amblyopia due to position, contrast or fixation deficits? *Vision Research, 25*, 55-66.

Brindley, G.S., & Lewin, W.S. (1968). The sensations produced by electrical stimulation of the visual cortex. *Journal of Physiology, 196*, 479-493.

Burr, D.C., & Wijesundra, S.-A. (1991). Orientation discrimination depends on spatial frequency. *Vision Research, 31* (7-8), 1449-1452.

Calvert, J.E., & Harris, J.P. (1988). Spatial frequency and duration effects on the tilt illusion and orientation acuity. *Vision Research, 28* (9), 1051-1059.

Calvert, J., Manahilov, V., Simpson, W.A., & Parker, D.M. (2005). Human cortical responses to contrast modulations of visual noise. *Vision Research, 45* (17), 2218-2230.

Carlson, C.R., Cohen, R.W., & Gorog, I. (1977). Visual processing of simple two-dimensional sine-wave luminance gratings. *Vision Research, 17* (3), 351-358.

Campbell, F.W., & Gubisch, R.W. (1966). Optical quality of the human eye. *Journal of Physiology, 186*, 558-578.

Campbell, F.W., & Robson, J.G. (1968). Application of Fourier analysis to the visibility of gratings. *Journal of Physiology, 197* (3), 551–566.

Carney, T., & Klein, S.A. (1999). Optimal spatial localization is limited by contrast sensitivity. *Vision Research, 39* (3), 503-512.

Casagrande, V.A. (1994). A third parallel visual pathway to primate area V1. *Trends in Neurosciences, 17* (7), 305-310.

Casagrande, V.A. (1999). The mystery of the visual system. *Journal of Physiology, 15; 517* (Pt3), 907-917.

Chung, S.T.L., Legge, G.E., & Tjan, B.S. (2002). Spatial-frequency characteristics of letter identification in central and peripheral vision. *Vision Research, 42* (18), 2137-2152.
Chalupa, L.M & Werner, J.S. (2004). The visual neurosciences, volume I and II, 494-505. The MIT Press, Cambridge, MA.

Connolly, M., & Van Essen, D. (1984). The representation of the visual field in parvocellular and magnocellular layers of the lateral geniculate nucleus in the macaque monkey. *Journal of Comparative Neurology, 226*, 544-564.

Cornsweet, T.N. (1962). The staircase-method in psychophysics. *American Journal of Psychology, 575*, 484-491.

Cornsweet, T.N. (1970). Visual Perception. Orland: Harcourt Brace Jovanovich, Inc.

Cowey, A., & Rolls, E.T. (1974). Human cortical magnification and its relation to visual acuity. *Experimental Brain Research, 21*, 447-454.

Curcio, C.A., & Allen, K.A. (1990). Topography of ganglion cells in human retina. *Journal of Comparative Neurology, 300*, 5-25.

Curcio, C.A., Sloan, K.R., Kalina, R.E., & Hendrickson, A.E. (1990). Human photoreceptor topography. *Journal of Comparative Neurology, 292*, 497-523.

Dakin, S.C., & Mareschal, I. (2000). Sensitivity to contrast modulation depends on carrier spatial frequency and orientation. *Vision Research, 40* (3), 311-329.

Daniel, P.M., & Whitteridge, D. (1961). The representation of the visual field on the cerebral cortex in monkeys. *Journal of Physiology, 159*, 203-221.

Derrington, A.M., & Lennie, P. (1984). Spatial and temporal contrast sensitivities of neurons in lateral geniculate nucleus of macaque. *Journal of Physiology, 357*, 219-240.

Dobelle, W.H., Turkel, J., Henderson, D.C., & Evans, J.R. (1979). Mapping representation of the visual field by electrical stimulation of human visual cortex. *American Journal of Ophthalmology, 88*, 727-735.

Dow, B.M., Snyder, A.Z., Vautin, R.G., & Bauer, R. (1981). Magnification factor and receptive field size in foveal striate cortex of the monkey. *Experimental Brain Research, 44*, 213-228.

Dow, B.M., Vautin, R.G., & Bauer, R. (1985). The mapping of visual space onto foveal striate cortex in the macaque monkey. *Journal of Neuroscience, 5*, 890-902.

Drasdo, N. (1977). The neural representation of visual space. *Nature, 266*, 554-556.

Drasdo, N. (1989). Receptive field densities of the ganglion cells of the human retina. *Vision Research, 29*, 985-988.

Drasdo, N. (1991). Neural substrates and threshold gradients in peripheral vision. In: J.J. Kulikowski, V. Walsh, & I.J. Murray (Eds.), *Limits of vision,* Vision and visual dysfunction (pp. 250-264). London: Macmillan Press.

Ellemberg, D., Allen, H.A., & Hess, R.F. (2006). Second-order spatial frequency and orientation channels in human vision. *Vision Research, 46* (17), 2798-2803.

Enroth-Cugell, C., & Robson, J.G. (1966). The contrast sensitivity of retinal ganglion cells of the cat. *Journal of Physiology, 187*, 517-552.

Fendick, M., & Westheimer, G. (1983). Effects of practice and the separation of test targets

on foveal and peripheral stereoacuity. *Vision Research, 23* (12), 145-150.

Foley, J.M., & Legge, G.E. (1981). Contrast detection and near-threshold discrimination in human vision. *Vision Research, 21* (7), 1041-1053.

Foley, J.M., Varadharajan, S., Koh, C.C., & Farias, M.C.Q. (2007). Detection of Gabor patterns of different sizes, shapes, phases and eccentricities. *Vision Research, 47* (1), 85-107.

Geisler, W.S. (1984). Physical limits of acuity and hyperacuity. *Journal of Optical Society of America A, 1* (7), 775-782.

Greenlee, M.W. (1992). Spatial frequency discrimination of band-limited periodic targets: Effects of stimulus contrast, bandwidth and retinal eccentricity. *Vision Research, 32* (2), 275-283.

Harris, J.P., & Wink, B. (2000). Invariance of the perceived spatial frequency shift of peripherally viewed gratings with manipulations of contrast, duration, and luminance. *Vision Research, 40* (8), 931-941.

Heeley, D.W., & Buchanan-Smith, H.M. (1990). Recognition of stimulus orientation. *Vision Research, 30*, 1429-1437.

Heeley, D.W., & Buchanan-Smith, H.M. (1998). The influence of stimulus shape on orientation acuity. *Experimental Brain Research, 120* (2), 217-222.

Heeley, D.W., Buchanan-Smith, H.M., Cromwell, J.A., & Wright, J.S. (1997). The oblique effect in orientation acuity. *Vision Research, 37* (2), 235-242.

Heeley, D.W., Buchanan-Smith, H.M., & Heywood, S. (1993). Orientation acuity for sine-wave gratings with random variation of spatial frequency. *Vision Research, 33* (17), 2509-2513.

Heinrich, S.P., Kromeier, M., Bach, M., & Kommerell, G. (2005). Vernier acuity for stereodisparate objects and ocular prevalence. *Vision Research, 45* (10), 1321-1328.

Hendry, S., & Reid, R. (2000). The koniocellular pathway in primate vision. *Annual Review of Neuroscience, 23*, 127-153.

Henrie, J.A., & Shapley, R.M. (2001). The relatively small decline in orientation acuity as stimulus size decreases. *Vision Research, 41* (13), 1723-1733.

Hess, R.F., & Hayes, A. (1994). The coding of spatial position by the human visual system: Effects of spatial scale and retinal eccentricity. *Vision Research, 34* (5), 625-643.

Hess, R.F., & Howell, E.R. (1977). The threshold contrast sensitivity function in strabismic amblyopia: Evidence for a two type classification. *Vision Research, 17* (9), 1049-1055.

Hoekstra, J., van der Goot, D.P.J., van den Brink, G., & Bilsen, F.A. (1974). The influence of the number of cycles upon the visual contrast threshold for spatial sine wave patterns. *Vision Research, 14* (6), 365-368.

Howell, E.R., & Hess, R.F. (1978). The functional area for summation to threshold for sinusoidal gratings. *Vision Research, 18* (4), 369-374.

Hubel, D.H. (1988). Eye, Brain, and Vision. *Scientific American Library series no 22* (New York: Scientific American Library.

Hubel, D.H., & Wiesel, T.N. (1974). Uniformity of monkey striate cortex: a parallel relationship between field size, scatter, and magnification factor. *Journal of Comparative Neurology, 158*, 295-306.

Jamar, J.H.T., & Koenderink, J.J. (1983). Sine-wave gratings: Scale invariance and spatial integration at suprathreshold contrast. *Vision Research, 23* (8), 805-810.

Jamar, J.H.T., & Koenderink, J.J. (1985). Contrast detection and detection of contrast modulation for noise gratings. *Vision Research, 25* (4), 511-521.

Jamar, J.H.T., Kwakman, L.F.T., & Koenderink, J.J. (1984). The sensitivity of the peripheral visual system to amplitude modulation and frequency modulation of sine wave patterns. *Vision Research, 24*, 243-249.

Jennings, J.A.M., & Charman, W.N. (1978). Optical image quality in the peripheral retina. *American Journal of Optometry & Physiological Optics, 55*, 582-590.

Jennings, J.A.M., & Charman, W.N. (1981). The effects of central and peripheral refraction on critical fusion frequency. *Ophthalmic and Physiological Optics, 1* (2), 91-96.

Johnston, A. (1987). Spatial scaling of central and peripheral contrast-sensitivity functions. *Journal of the Optical Society of America A, 4* (8), 1583-1593.

Johnston, A., & Wright, M.J. (1986). Matching velocity in central and peripheral vision. *Vision Research, 26*, 1099-1109.

Kandel, E.R., Schwartz, J.H., & Jessell, M.T. (2000). Principles of Neural Science, 4th, 516-519. New York, McGraw-Hill Professional Publishing.

Kaplan, E., & Shapley, R.M. (1982). X and Y cells in the lateral geniculate nucleus of macaque monkey. *Journal of Physiology, 330*, 125-143.

Kelly, D.H. (1977). Visual contrast sensitivity. *Journal of Modern Optics, 24* (2), 107-129.

Kelly, D.H. (1984). Retinal inhomogeneity. I. Spatiotemporal contrast sensitivity. *Journal of Optical Society of America A, 1*, 107-113.

Klein, S.A., & Levi, D.M. (1985). Hyperacuity thresholds of 1 sec: theoretical predictions and empirical validation. *Journal of the Optical Society of America A, 2*, 1170-1190.

Klein, S.A., & Levi, D.M. (1987). Position sense of the peripheral retina. *Journal of the Optical Society of America A, 4*, 1543-1553.

Koenderink, J.J., Bouman, M.A., Bueno de Mesquita, A.E., & Slappendel, S. (1978). Perimetry of contrast detection thresholds of moving spatial sine wave patterns. III. The target extent as sensitivity controlling parameter. *Journal of the Optical Society of America, 68*, 854-860.

Kukkonen, H., Rovamo, J., Tiippana, K., & Nasanen, R. (1993). Michelson contrast, RMS contrast and energy of various spatial stimuli at threshold. *Vision Research, 33* (10), 1431-1436.

Kulikowski, J.J., & Tolhurst, D.J. (1973). Psychophysical evidence for sustained and transient detectors in human vision. *Journal of Physiology, 232* (1), 149-162.

Kulikowski, J.J., Walsh, V., & Murray, I.J. (1991). Limits of Vision. *Vision and Visual Dysfunction,* 5 London: The Macmillan Press Ltd.

Le Grand, Y. (1967). Form and space vision. (pp. 127-145). Bloomington: Indiana University Press.

Leonova, A., Pokorny, J., & Smith, V.C. (2003). Spatial frequency processing in inferred PC- and MC-pathways. *Vision Research, 43* (20), 2133-2139.

Lesher, G.W., & Mingolla, E. (1995). The Handbook of Brain Theory and Neural Networks. Cambridge: MIT Press.

Levi, D.M., & Harwerth, R.S. (1980). Contrast sensitivity in amblyopia due to stimulus deprivation. *British Journal of Ophthalmology, 64* (1), 15-20.

Levi, D.M., & Klein, S.A. (1989). Both separation and eccentricity can limit precise position judgements: a reply to Morgan and Watt. *Vision Research, 29*, 1463.

Levi, D.M., & Klein, S.A. (1990a). Equivalent intrinsic blur in spatial vision. *Vision Research, 30*, 1971-1993.

Levi, D.M., & Klein, S.A. (1990b). The role of separation and eccentricity in encoding position. *Vision Research, 30*, 557-585.

Levi, D.M., Klein, S.A., & Aitsebaomo, A.P. (1984). Detection and discrimination of the direction of motion in central and peripheral vision of normal and amblyopic observers. *Vision Research, 24*, 789-800.

Levi, D.M., Klein, S.A., & Aitsebaomo, A.P. (1985). Vernier acuity, crowding and cortical magnification. *Vision Research, 25* (7), 963-977.

Levi, D.M., McGraw, P.V., & Klein, S.A. (2000a). Vernier and contrast discrimination in central and peripheral vision. *Vision Research, 40* (8), 973-989.

Levi, D.M., McGraw, P.V., & Klein, S.A. (2000b). Vernier and contrast discrimination in central and peripheral vision. *Vision Research, 40* (8), 973-988.

Levi, D.M., & Waugh, S.J. (1994). Spatial scale shifts in peripheral vernier acuity. *Vision Research, 34* (17), 2215-2238.

Levi, D.M., Waugh, S.J., & Beard, B.L. (1994). Spatial scale shifts in amblyopia. *Vision Research, 34* (24), 3315-3333.

Levi, D.M., & Westheimer, G. (1987). Spatial-interval discrimination in the human fovea: what delimits the interval? *Journal of the Optical Society of America A, 4*, 1304-1313.

Livingstone, M.S., & Hubel, D.H. (1988). Do the relative mapping densities of the magno and parvocellular systems vary with eccentricity? *Journal of Neuroscience, 8*, 4334-4339.

Luntinen, O., Rovamo, J., & Nasanen, R. (1995). Modelling the increase of contrast sensitivity with grating area and exposure time. *Vision Research, 35* (16), 2339-2346.

Maattanen, L.M., Koenderink, J.J., & Nienhuis, B. (1988). Contrast discrimination: Invariant to spatial parameters. *Vision Research, 28* (7), 811-818.

Makela, P., Nasanen, R., Rovamo, J., & Melmoth, D. (2001). Identification of facial images in peripheral vision. *Vision Research, 41*, 599-610.

Makela, P., Rovamo, J., & Whitaker, D. (1997). The effects of eccentricity and stimulus magnification on simultaneous performance in position and movement acuity tasks. *Vision Research, 37* (10), 1261-1270.

Makela, P., Whitaker, D., & Rovamo, J. (1993). Modelling of orientation discrimination across the visual field. *Vision Research, 33* (5-6), 723-730.

Makela, P.K. (1994). Spatial scaling in human peripheral vision. Birmingham: The University of Aston in Birmingham.

Manahilov, V., & Simpson, W.A. (2001). Energy model for contrast detection: spatial-frequency and orientation selectivity in grating summation. *Vision Research, 41* (12), 1547-1560.

Mareschal, I., & Shapley, R.M. (2004). Effects of contrast and size on orientation discrimination. *Vision Research, 44* (1), 57-67.

Martin, P.R., White, A.J.R., Goodchild, A.K., Wilder, H.D., & Sefton, A.E. (1997). Evidence that blue-on cells are part of the third geniculocortical pathway in primates. *European Journal of Neuroscience, 9*, 1115-1116.

McCann, J.J., Savoy, R.L., & Hall Jr, J.A. (1978). Visibility of low-frequency sine-wave targets: Dependence on number of cycles and surround parameters. *Vision Research, 18* (7), 891-894.

McIlhagga, W., & Peterson, R. (2006). Sinusoid = light bar+dark bar? *Vision Research, 46* (12), 1934-1945.

McKee, S.P., Levi, D.M., & Movshon, J.A. (2003). The pattern of visual deficits in amblyopia. *Journal of Vision, 3* (5), 380-405.

McKee, S.P., Welch, L., Taylor, D.G., & Bowne, S.F. (1990). Finding the common bond: stereoacuity and the other hyperacuities. *Vision Research, 30*, 879-891.

Melmoth, D.R., Kukkonen, H.T., Makela, P.K., & Rovamo, J.M. (2000a). The effect of contrast and size scaling on face perception in foveal and extrafoveal vision. *Investigative Ophthalmology & Visual Science, 41* (9), 2811-2819.

Melmoth, D.R., Kukkonen, H.T., Makela, P.K., & Rovamo, J.M. (2000b). Scaling extrafoveal detection of distortion in a face and grating. *Perception, 29* (9), 1117 - 1126.

Molavi, D.W. (1997). Neuroscience Tutorial. (*http://thalamus.wustl.edu/course/eyeret.html, Access: August,* 2008) Washington: The Washington University School of Medicine.

Morand S, Thut G, De Peralta RG, Clarks S, Khateb A, Landis T, & CM, M. (2000). Electrophysiological evidence for fast visual processing through the human koniocellular pathway when stimuli move. *Cerebral Cortex, 10* (8), 817-825.

Morgan, M.J., & Aiba, T.S. (1985). Vernier acuity predicted from the changes in the light distribution of the retinal image. *Spatial Vision, 1*, 151-161.

Morgan, M.J., & Regan, D. (1987). Opponent model for the line interval discrimination: interval and vernier performance compared. *Vision Research, 27*, 107-118.

Mussap, A.J., & Levi, D.M. (1997). Vernier acuity with plaid masks: the role of oriented filters in vernier acuity. *Vision Research, 37* (10), 1325-1340.

Nachmias, J., & Sansbury, R.V. (1974). Grating contrast: Discrimination may be better than detection. *Vision Research, 14* (10), 1039-1042.

Nasanen, R., Kukkonen, H., & Rovamo, J. (1993). Spatial integration of band-pass filtered patterns in noise. *Vision Research, 33* (7), 903-911.

Nasanen, R., & O'Leary, C. (1998). Recognition of band-pass filtered hand-written numerals in foveal and peripheral vision. *Vision Research, 38* (23), 3691-3701.

Nelson, R. (2000). Visual Responses of Ganglion Cells. (http://retina.umh.es/webvision/GCPHYS1.htm Access: May, 2007). Utah: University of Utah.

Orban, G.A., Vandenbussche, E., & Vogels, R. (1984). Human orientation discrimination tested with long stimuli. *Vision Research, 24* (2), 121-128.

Paradiso, M.A., & Carney, T. (1988). Orientation discrimination as a function of stimulus eccentricity and size: nasal/temporal retina asymmetry. *Vision Research, 28*, 867-874.

Pardhan, S. (2003). Binocular recognition summation in the peripheral visual field: contrast and orientation dependence. *Vision Research, 43* (11), 1251-1257.

Pelli, D.G., & Zhang, L. (1991). Accurate control and contrast on microcomputer displays. *Vision Research, 31*, 1337-1350.

Polat, U., Bonneh, Y., Ma-Naim, T., Belkin, M., & Sagi, D. (2005). Spatial interactions in amblyopia: Effects of stimulus parameters and amblyopia type. *Vision Research, 45* (11), 1471-1479.

Popovic, Z., & Sjostrand, J. (2001). Resolution, separation of retinal ganglion cells, and cortical magnification in humans. *Vision Research, 41* (10), 1313-1320.

Regan, D., & Beverley, K.I. (1985). Postadaptation orientation discrimination. *Journal of the Optical Society of America A: Optics and Image Science, and Vision 2*(2), 147-155.

Reisbeck, T.E., & Gegenfurtner, K.R. (1998). Effects of contrast and temporal frequency on orientation discrimination for luminance and isoluminant stimuli. *Vision Research, 38* (8), 1105-1117.

Rentschler, I., & Treutwein, B. (1985). Loss of spatial phase relationship in extrafoveal vision. *Nature, 313*, 308-310.

Robson, J.G., & Graham, N. (1981). Probability summation and regional variation in contrast sensitivity across the visual field. *Vision Research, 21* (3), 409-418.

Rodieck, R.W. (1998). The First Steps in Seeing. Sunderland, Massachusetts USA: Sinauer Associates, Inc.

Rolls, E.T., & Cowey, A. (1970). Topography of the retina and striate cortex and its relationship to visual acuity in rhesus monkeys and squirrel monkeys. *Experimental Brain Research, 10*, 298-310.

Rovamo, J., Franssila, R., & Nasanen, R. (1992). Contrast sensitivity as a function of

spatial frequency, viewing distance and eccentricity with and without spatial noise. *Vision Research, 32* (4), 631-637.

Rovamo, J., Luntinen, O., & Nasanen, R. (1993). Modelling the dependence of contrast sensitivity on grating area and spatial frequency. *Vision Research, 33* (18), 2773-2788.

Rovamo, J., Mustonen, J., & Nasanen, R. (1994). Modelling contrast sensitivity as a function of retinal illuminance and grating area. *Vision Research, 34* (10), 1301-1314.

Rovamo, J., & Raninen, A. (1984). Cortical flicker frequency and M-scaling of stimulus size and retinal illuminance. *Vision Research, 24*, 1127-1131.

Rovamo, J., & Virsu, V. (1979). An estimation and application of the human cortical magnification factor. *Experimental Brain Research, 37*, 495-510.

Rovamo, J., Virsu, V., & Nasanen, R. (1978). Cortical magnification factor predicts the photopic contrast sensitivity of peripheral vision. *Nature, 271*, 54-56.

Saarinen, J., Rovamo, J., & Virsu, V. (1989). Analysis of spatial structure in eccentric vision. *Investigative Ophthalmology & Visual Science, 30* (2), 293-296.

Saarinen, S.J. (1988). Anatomy of macaque fovea and spatial densities of neurons in foveal representation. *Journal of Comparative Neurology, 269*, 479-505.

Sally, S., & Gurnsey, R. (2007). Foveal and extra-foveal orientation discrimination. *Experimental Brain Research, 183* (3), 351-360.

Sally, S., Poirier, F., & Gurnsey, R. (2005). Orientation discrimination across the visual field: Size estimates near contrast threshold. *Perception & Psychophysics, 67* (4), 638-647.

Sally, S.L., & Gurnsey, R. (2003). Orientation discrimination in foveal and extra-foveal vision: effects of stimulus bandwidth and contrast. *Vision Research, 43* (12), 1375-1386.

Sally, S.L., & Gurnsey, R. (2004). Orientation discrimination across the visual field: matching perceived contrast near threshold. *Vision Research, 44* (23), 2719-2727.

Saylor, S.A., & Olzak, L.A. (2006). Contextual effects on fine orientation discrimination tasks. *Vision Research, 46* (18), 2988-2997.

Savoy RL, M.J. (1975). Visibility of low-spatial-frequency sine-wave targets: Dependence on number of cycles. *Journal of Optical Society of America, 65* (3), 343-350.

Sceniak, M.P., Hawken, M.J., & Shapley, R (2002). Contrast-Dependent Changes in Spatial Frequency Tuning of Macaque V1 Neurons: Effects of a Changing Receptive Field Size. *Journal of Neurophysiology 88*: 1363-1373.

Sceniak, MP, Ringach, DL, Hawken MJ, & Shapley, R (1999). Contrast's effect on spatial

summation by macaque V1 neurons. *Nature Neuroscience, 2*: 733–739

Schefrin, B.E., Hauser, M., & Werner, J.S. (2004). Evidence against age-related enlargements of ganglion cell receptive field centers under scotopic conditions. *Vision Research, 44* (4), 423-428.

Schein, S.J., & de Monasterio, F.M. (1987). Mapping of retinal and geniculate neurons onto striate cortex of macaque. *Journal of Neuroscience, 7*, 996-1009.

Schwartz, S.H. (2004). Visual Perception: A Clinical Orientation London: McGraw-Hill Professional.

Shahidi, M., Wang, Z., & Zelkha, R. (2005). Quantitative thickness measurement of retinal layers imaged by optical coherence tomography. *American Journal of Ophalmology, 139* (6), 1056-1061.

Shapley, R.M., & Perry, V.H. (1986). Cat and monkey retinal ganglion cells and their visual functional roles. *Trends in Neurosciences*, 229-235.

Sjostrand, J., Olsson, V., Popovic, Z., & Conradi, N. (1999). Quantitative estimations of foveal and extra-foveal retinal circuitry in humans. *Vision Research, 39* (18), 2987-2998.

Skottun, B.C., Bradley, A., & Freeman, R.D. (1986). Orientation discrimination in amblyopia. *Investigative Ophthalmology & Visual Science, 27*, 532-537.

Slotnick, S.D., & Yantis, S. (2003). Efficient acquisition of human retino-topic maps. *Human Brain Mapping, 18*, 22-29.

Snowden, R.J. (1992). Orientation bandwidth: The effect of spatial and temporal frequency. *Vision Research, 32* (10), 1965-1974.

Spinelli, D., Bazzeo, A., & Vicario, G.B. (1984). Orientation sensitivity in the peripheral visual field. *Perception, 13*, 41-47.

Stephenson, C.M.E., & Braddick, O.J. (1983). Discrimination of relative spatial phase in fovea and periphery. *Investigative Ophthalmology & Visual Science, Suppl. 24*, 146.

Stephenson, C.M.E., Knapp, A.J., & Braddick, O.J. (1991). Discrimination of spatial phase shows a qualitative difference between foveal and peripheral processing. *Vision Research, 31*, 1315-1326.

Stigmar, G. (1971). Blurred visual stimuli. *Acta Ophthalmologica, 49*, 364-379.

Strasburger, H., Rentschler, I., & Harvey Jr, L.O. (1991). Contrast thresholds for identification of numeric characters in direct and eccentric view. *Perception & Psychophysics, 49* (6), 495-508.

Strasburger, H., Rentschler, I., & Harvey Jr, L.O. (1994). Cortical Magnification theory fails predict visual recognition. *European Journal of Neuroscience, 6*, 1583-1588.

Sullivan, G.D., Georgeson, M.A., & Oatley, K. (1972). Channels for spatial frequency selection and the detection of single bars by the human visual system. *Vision Research, 12* (3), 383-394.

Sullivan, G.D., Oatley, K., & Sutherland, N.S. (1972). Vernier acuity as affected by target length and separation. *Perception & Psychophysics, 12*, 438-444.

Talbot, S.A., & Marshall, W.H. (1941). Physiological studies on neural mechanisms of visual localization and discrimination. *American Journal of Ophalmology, 24*, 1255-1264.

Tiippana, K., & Nasanen, R. (1999). Spatial-frequency bandwidth of perceived contrast. *Vision Research, 39* (20), 3399-3403.

Toet, A., & Levi, D.M. (1992). The two-dimensional shape of spatial interaction zones in the parafovea. *Vision Research, 32*, 1349-1357.

Toet, A., Snippe, H.P., & Koenderink, J.J. (1988). Local spatial scale for three-dot alignment acuity. *Biological Cybernetics, 59*, 319-323.

Tolhurst, D.J., & Dealy, R.S. (1975). The detection and identification of lines and edges. *Vision Research, 15* (12), 1367-1372.

Tolhurst, D.J., & Ling, L. (1988). Magnification factors and the organization of the human striate cortex. *Human Neurobiology, 6*, 247-254.

Tootell, R.B., Silverman, M.S., Switkes, E., & De Valois, R.L. (1982). Deoxyglucose analysis of retinotopic organization in primate striate cortex. *Science, 218*, 902-904.

Tootell, R.B., Switkes, E., Silverman, M.S., & Hamilton, S.L. (1988). Functional anatomy of macaque striate cortex. II. Retinotopic organization. *Journal of Neuroscience, 8*, 1531-1568.

Tyler, C.W. (2001). The symmetry magnification function varies with detection task. *Journal of Vision, 1*, 137-144.

Tyler, C.W., & Torres, J. (1972). Frequency responses characteristics for sinusoidal movement in the fovea and periphery. *Perception & Psychophysics, 12*, 232-236.

Vakrou, C., Whitaker, D., & McGraw, P.V. (2007). Extrafoveal viewing reveals the nature of second-order human vision. *Journal of Vision, 7* (14:13), 1-15.

Van Essen, D.C., Newsom, W.T., & Maunsell, J.H.R. (1984). The visual field representation in striate cortex of the macaque monkey: asymmetries, anisotropies and individual variability. *Vision Research, 24*, 429-448.

Vandenbussche, E., Vogels, R., & Orban, G.A. (1986). Human orientation discrimination: changes with eccentricity in normal and amblyopic vision. *Investigative Ophthalmology & Visual Science, 73*, 1674-1683.

Vassilev, A. (1973). Contrast sensitivity near borders: Significance of test stimulus form, size and duration. *Vision Research, 13* (4), 719-730.

Virsu, V., Nasanen, R., & Osmoviita, K. (1987). Cortical magnification and peripheral vision. *Journal of Optical Society of America A, 4* (8), 1568-1578.

Virsu, V., Rovamo, J., Laurinen, P., & Nasanen, R. (1982). Temporal contrast sensitivity and cortical magnification. *Vision Research, 22*, 1211-1217.

Watson, A.B. (1987). Estimation of local spatial scale. *Journal of the Optical Society of America A, 4*, 1579-1582.

Watson, A.B., & Robson, J.G. (1981). Discrimination at threshold: Labelled detectors in human vision. *Vision Research, 21* (7), 1115-1122.

Watt, R.J. (1987). Scanning from coarse to fine spatial scales in the human visual system after the onset of a stimulus. *Journal of the Optical Society of America A, 4* 2006-2021.

Waugh, S.J., & Levi, D.M. (1993a). Visibility, luminance and vernier acuity. *Vision Research, 33* (4), 527-538.

Waugh, S.J., & Levi, D.M. (1993b). Visibility, timing and vernier acuity. *Vision Research, 33* (4), 505-526.

Waugh, S.J., & Levi, D.M. (1999). Spatial scale of visual analysis for vernier acuity does not vary over time. *Vision Research, 40* (2), 163-164.

Waugh, S.J., Levi, D.M., & Carney, T. (1993). Orientation, masking, and vernier acuity for line targets. *Vision Research, 33* (12), 1619-1638.

Wehrhahn, C., & Dresp, B. (1998). Detection facilitation by collinear stimuli in humans: Dependence on strength and sign of contrast. *Vision Research, 38* (3), 423-428.

Wehrhahn, C., & Westheimer, G. (1990). How vernier acuity depends on contrast. *Experimental Brain Research, 80* (3), 618-620.

Weiner, Irving B. (2003). Handbook of psychology: Biological Psychology, Vol. 3. Chapter 6 (pp. 139-186). Volume Editor Michela Gallagher, Randy J. Nelson, NJ, US: John Wiley & Sons Inc.

Westheimer, G. (1967). Spatial interaction in human cone vision. *Journal of Physiology, 190*, 139-154.

Westheimer, G. (1979). The spatial sense of the eye. *Investigative Ophthalmology & Visual Science, 18*, 893-912.

Westheimer, G. (1981). Visual hyperacuity. *Progress in Sensory Physiology, 1*, 1-30.

Westheimer, G. (1982). The spatial grain of the perifoveal visual field. *Vision Research, 22*, 157-162.

Westheimer, G. (1983). Temporal order detection for foveal and peripheral visual stimuli. *Vision Research, 23*, 759-763.

Westheimer, G. (2003). The distribution of preferred orientations in the peripheral visual field. *Vision Research, 43* (1), 53-57.

Westheimer, G., & Beard, B.L. (1998). Orientation Dependency for Foveal Line Stimuli: Detection and Intensity Discrimination, Resolution, Orientation Discrimination and Vernier Acuity. *Vision Research, 38* (8), 1097-1104.

Westheimer, G., Brincat, S., & Wehrhahn, C. (1999). Contrast dependency of foveal spatial functions: orientation, vernier, separation, blur and displacement discrimination and the tilt and Poggendorff illusions. *Vision Research, 39* (9), 1631-1639.

Westheimer, G., & Hauske, G. (1975). Temporal and spatial interference with vernier acuity. *Vision Research, 15*, 1137-1141.

Westheimer, G., & Li, W. (1996). Classifying illusory contours by means of orientation discrimination. *Journal of Neurophysiology, 75* (2), 523-537.

Westheimer, G., & McKee, S.P. (1977). Spatial configurations of visual hyperacuity. *Vision Research, 17*, 941-947.

Westheimer, G., & McKee, S.P. (1979). What prior uniocular processing is necessary for stereopisis? *Investigative Ophthalmology & Visual Science, 18*, 614-621.

Westheimer, G., Shimamura, K., & McKee, S.P. (1976). Interference with line-orientation sensitivity. *Journal of Optical Society of America, 66*, 332-338.

Wertheim, T. (1891). Peripheral visual acuity. *American Journal of Optometry & Physiological Optics, 57*, 915-924, cited by Dumsky I.L. 1980.

Wetherill, G.B., & Levitt, H. (1965). Sequential estimation of points on a psychometric function. *British Journal of Mathematical and Statistical Psychology, 18*, 1-10.

Weymouth, F.W. (1958). Visual sensory units and the minimal angle of resolution. *American Journal of Ophalmology, 46*, 102-112.

Whitaker, D., Latham, K., Makela, P., & Rovamo, J. (1993). Detection and discrimination of curvature in foveal and peripheral vision. *Vision Research, 33* (16), 2215-2224.

Whitaker, D., & MacVeigh, D. (1991). Interaction of spatial frequency and separation in vernier acuity. *Vision Research, 31*, 1205-1212.

Whitaker, D., Makela, P., Rovamo, J., & Latham, K. (1992). The influence of eccentricity on position and movement acuities as revealed by spatial scaling. *Vision Research, 32* (10), 1913-1930.

Whitaker, D., Rovamo, J., MacVeigh, D., & Makela, P. (1992). Spatial scaling of vernier acuity tasks. *Vision Research, 32* (8), 1481-1491.

Whitaker, D., & Walker, H. (1988). Centroid evaluation in the vernier alignment of random dot clusters. *Vision Research, 28*, 777-784.

White, A., Solomon, S., & Martin, P. (2001). Spatial properties of koniocellular cells in the lateral geniculate nucleus of the marmoset Callithrix jacchus. *Journal of Physiology, 533* (Pt 2), 519–535.

Whittle, P. (1986). Increments and decrements: Luminance discrimination. *Vision Research, 26* (10), 1677-1691.

Williams, R.A., Enoch, J.M., & Essock, E.A. (1984). The Resistance of Selected Hyperacuity Configurations to Retinal Image Degradation. *Investigative Ophthalmology & Visual Science, 25*, 389-399.

Xing D, Shapley RM, Hawken MJ & Ringach DL (2005). Effect of stimulus size on the dynamics of orientation selectivity in Macaque V1. *Journal of Neurophysiology, 94*(1): 799-812.

Yap, L.Y., Levi, D.M., & Klein, S.A. (1989). Peripheral positional acuity: retinal and cortical constraints on a 2-dot separation discrimination under photopic and scotopic conditions. *Vision Research, 29*, 789-802.

Publications

Cui, L., Rovamo, J., & Makela, P. (2007). The Effects of Contrast and Eccentricity on Orientation Discrimination. *Investigative Ophthalmology & Visual Science*, 48: E-5895.

Cui, L., Rovamo, J., & Makela, P. (2007). Foveal and peripheral orientation discrimination for a Gaussian bar stimulus. *Cardiff Institute of Tissue Engineering and Repair*, Abergavenny, UK.

Appendix I-the details of subjects

- **Orientation discrimination for Gaussian filtered line in Chapter 3**

Subject name: LC
Age: 25
Dominant eye: Right
Best corrected vision- LogMAR:
R: -0.18 (-4.75Ds)
L: 0.08 (-4.25 Ds)
Both eyes: -0.18

Subject name: VR
Age: 20
Dominant eye: Right
Best corrected vision- LogMAR:
R: -0.10
L: -0.08
Both eyes: -0.10

- **Orientation discrimination for the 2, 4 and 16cpi gratings in Chapter 4 and 5**

Subject name: LC
Age: 26
Dominant eye: Right
Best corrected vision- LogMAR:
R: -0.18 (-4.75Ds)
L: 0.08 (-4.25 Ds)
Both eyes: -0.18

Subject name: AS
Age: 21
Dominant eye: Right
Best corrected vision- LogMAR:
R: -0.10 (-5.00Ds)
L: -0.10 (-5.00 Ds)
Both eyes: -0.10

- **Contrast threshold of orientation discrimination for Gaussian filtered line in Chapter 6**

Subject name: LC
Age: 27
Dominant eye: Right
Best corrected vision- LogMAR:
R: -0.18 (-4.75Ds)
L: 0.08 (-4.25 Ds)
Both eyes: -0.18

Subject name: YC
Age: 24
Dominant eye: Right
Best corrected vision- LogMAR:
R: -0.18 (-0.75Ds)
L: -0.10 (-1.25 Ds)
Both eyes: -0.18

- **Contrast threshold of orientation discrimination for the 2, 4 and 16cpi gratings in Chapter 7 and 8**

Subject name: LC
Age: 26
Dominant eye: Right
Best corrected vision- LogMAR:
R: -0.18 (-4.75Ds)
L: 0.08 (-4.25 Ds)
Both eyes: -0.18

Subject name: BU
Age: 21
Dominant eye: Right
Best corrected vision- LogMAR:
R: -0.18(-6.25Ds)
L: -0.18 (-6.00 Ds)
Both eyes: -0.18

Appendix II The explanation of the Gaussian filter

In this thesis, a line stimulus was used both for the orientation discrimination experiment in Chapter 3 and the contrast threshold experiment in Chapter 6. The line stimulus was filtered in Fourier space with a Gaussian weighed stimulus window equation:

$$g(x,y) = \exp\{-\ln 2[(x/x_{1/2})^2 + (y/y_{1/2})^2]\}, \qquad \textbf{Equation (1)}$$

where $x_{1/2} = h/9$ and $y_{1/2} = h$ are coordinates, at which luminance deviation had decreased to half of its maximum value. At 2.5xh the luminance deviation was so small that it could be cut abruptly without a visual effect.

When $x = x_{1/2}$ and $y = 0$,

$$g(x_{1/2},0) = \exp\{-\ln 2[(x_{1/2}/x_{1/2})^2]\}$$

$$= \exp\{-\ln(2)\}$$

$$= 1/2.$$

In the same way, when $y = y_{1/2}$ and $x = 0$,

$$g(0,y_{1/2}) = 1/2.$$

Therefore, for $x = x_{1/2}$, g =1/2, which confirms that at that point g has been halved. The same applies to y. For the Gaussian filtered window of the line stimulus in this chapter, $x_{1/2}$ is much smaller than $y_{1/2}$.

For each pixel, $p(x, y)$ in the line stimulus, the Gaussian filter window $g(x, y)$ was used to convolve with the ordinate x and y separately. The results of the convolution (x', y') were the new values of the pixel. Therefore, the sharp edge of the line stimulus was smoothed.

Appendix III Modelling scaling factors for orientation discrimination threshold

In this appendix, the procedure of the modeling of the scaling factors for orientation discrimination threshold was explained in detail, including spatial scaling factor, the vertical and horizontal scaling factors of 2D scaling.

For each stimulus, the orientation discrimination thresholds of Chapters 3-5 were superimposed on to the basic condition, the fovea and 100% contrast threshold data (E=0, C=1), by spatial scaling and 2D scaling, as explained in each experimental chapter (Chapters 3-5). Because both scaling methods were applied across eccentricity E and contrast C, their scaling factors were dependent on both variables. Therefore, the equation for calculating spatial scaling factor F=1+SE (see Chapter 1 Section 1.3.4 equation (1.1)) was modified to equation (1) so that the scaling factor became a function of eccentricity and contrast. The equation included all the necessary 2nd order polynomial parameters involving E and C, in agreement with Melmoth and Rovamo (2003).

$$F_i = 1 + E/E_2 + (\log C)^2/k_1 + \log C/k_2 + E \times \log C/k_3 + E^2/E_2^{'}, \qquad \textbf{Equation (1)}$$

The modeling of each type scaling factor was conducted by using the software Origin Pro 7.5. The procedure is as follows.

Origin Pro 7.5 provides a non linear curve fit algorithm, called 'Nonlinear Curve fit'. The algorithm can be used to fit the 2D or 3D data by the equation inputted to the fitting window, shown in the left of Fig 1.

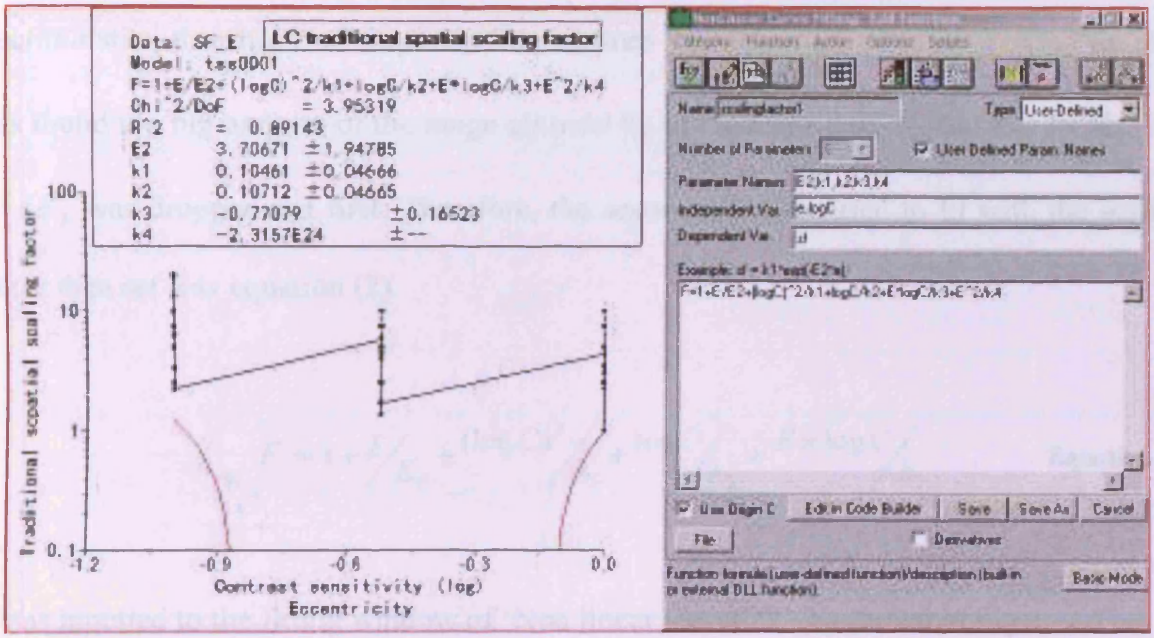

Fig 1 The results of the 'Non-linear Curve fit' algorithm of Origin Pro 7.5 by equation (1)

In the beginning of modeling of the scaling factor, the complete equation (1) was fitted to the scaling factor data set. In a text box on the right side of Fig 1 there are the fitting results, including the equation used, the Chi^2 and R^2 showing the fitting accuracy, and the parameters and their errors. Due to the parameter format of Origin, '$E_2^{'}$' in equation (1) was not allowed and therefore it was replaced by k_4. The parameter of equation (1) with poorest accuracy was first dropped out. Then the equation with inaccurate parameters and/or poor R^2 were continually modified in an iterative fashion modified until the accuracy of all remaining parameters was good while R^2 still remained high. Then the optimal equation was obtained. Actually, during the fitting for all eccentric threshold data, the

accuracy of the parameter $E_2^{'}$ was often found to be the poorest so that the item $E^2/E_2^{'}$ in equation (1) was usually dropped first.

Fig 1 shows the fitting results by equation (1) to the spatial scaling factor of the orientation discrimination thresholds of Gaussian filtered lines for subject LC. The error of k_4, i.e. $E_2^{'}$, was found too big and out of the range allowed by in the algorithm, so that the $E^2/k_4^{'}$, i.e. $E^2/E_2^{'}$ was dropped out first. Therefore, the second equation used to fit with the scaling factor data set was equation (2).

$$F_i = 1 + E/E_2 + (\log C)^2/k_1 + \log C/k_2 + E \times \log C/k_3 \qquad \textbf{Equation (2)}$$

It was inputted to the fitting window of 'Non linear Curve fit', as shown in Fig 2.

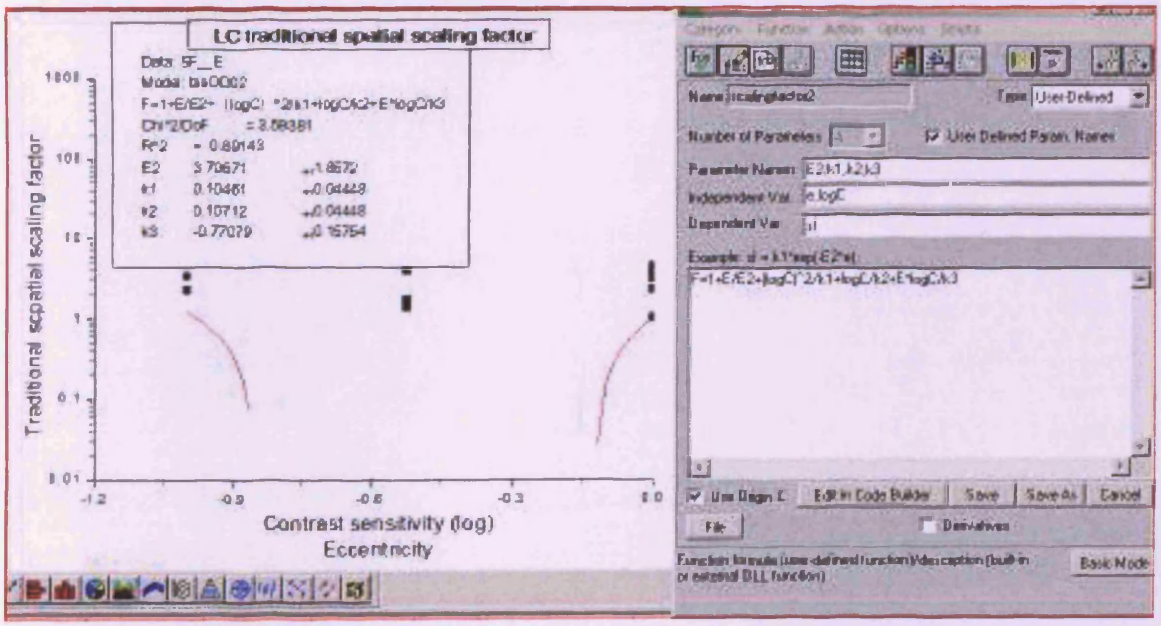

Fig 2 The results of the 'Non-linear Curve fit' algorithm of Origin Pro 7.5 by equation (2)

Such procedure was repeated in iterative fashion until the accuracy of all remaining parameters was good while R^2 still remained high and the optimal equation was obtained.

The optimal equation $F_s = 1 + E/E_2 + (\log C)^2/k_1 + E \times \log C/k_3$ was obtained to model the spatial scaling factors for all the orientation discrimination thresholds (Gaussian filtered lines in Chapter 3, the 4cpi gratings in Chapter 4, the 2 and 16cpi gratings in Chapter 5).

The optimal equation $F = 1 + E/E_2 + (\log C)^2/k_1$ was obtained to model the vertical and horizontal 2D scaling factors of all the orientation discrimination thresholds (Gaussian filtered lines in Chapter 3, the 4cpi gratings in Chapter 4, the 2 and 16cpi gratings in Chapter 5).

Appendix IV Modelling scaling factors for contrast threshold of orientation discrimination

Here, the procedure of the modeling of the scaling factors for the contrast thresholds of orientation discrimination was explained in detail, including spatial scaling factor and the vertical and horizontal scaling factors of 2D scaling, as in Appendix III.

For each stimulus, both spatial and 2D scaling were used to shift the contrast threshold for superimposing on to the basic condition, the fovea and 45 deg orientation difference data (E=0, OD=45), as explained in each corresponding experimental chapter (Chapters 6-9). Because the scaling methods were applied across eccentricity E and orientation difference OD, the scaling factors were dependent on both variables. Therefore, the equation for calculating spatial scaling factor F=1+SE (see Chapter 1 Section 1.3.4 equation (1.1)) was modified to equation (1) so that the scaling factor became a function of eccentricity and orientation difference. The equation included all the necessary 2nd order polynomial parameters involving E and OD^{-1}.

$$F_i = 1 + E/E_2 + (OD^{-2} - 45^{-2})/k_1 + E \times (OD)^{-2}/k_2 + (OD^{-1} - 45)^{-1}/k_3 + E \times (OD)^{-1}/k_4 + E^2/E_2', \quad \textbf{Equation (1)}$$

As in Appendix III, the modeling of each type scaling factor was conducted by using the software Origin Pro 7.5 and its 'Non linear curve fit' algorithm. Here the modelling started with equation (1) and its parameter with poorest accuracy was first dropped out. The equation with inaccurate parameters or poor R^2 were then continually modified in an

iterative fashion modified until the accuracy of all remaining parameters was good while R^2 still remained high. Then the optimal equation was obtained.

Equation $F_l = 1 + E/E_2 + (OD^{-2} - 45^{-2})/k_1 + E \times (OD)^{-2}/k_2 + E \times (OD)^{-1}/k_4$ was used to model both the spatial scaling factor and the horizontal scaling factor of 2D scaling for all the contrast thresholds of orientation discrimination (the Gaussian filtered lines in Chapter 6, the 4cpi gratings in Chapter 7, the 2 and 16cpi gratings in Chapter 8).

Equation $F_l = 1 + E/E_2 + E \times (OD)^{-2}/k_2 + (OD^{-1} - 45)^{-1}/k_3$ was used to model the vertical scaling factor of the 2D scaling for all the contrast thresholds of orientation discrimination (the Gaussian filtered lines in Chapter 6, the 4cpi gratings in Chapter 7, the 2 and 16cpi gratings in Chapter 8).

Appendix V The optimal curve fitting equation for eccentric orientation discrimination threshold curve

In Chapters 3-5, the orientation discrimination thresholds of the Gaussian filtered lines, 2, 4, and 16cpi gratings were measured. Due to the similar shapes of the data curves at all eccentricities and contrasts for all types stimuli and subjects, each eccentric threshold (*Th*) data at 0-10 deg eccentricities and 10-100% contrasts were fitted with equation:

$$Th = Th_{\min}(1 + H_c / H)^p, \qquad \textbf{Equation (1)}$$

where Th_{min} is the theoretical minimum threshold, H is stimulus height (i.e. line length or grating diameter in this thesis) and H_c is the critical stimulus height marking the change from the decrease to plateau. The exponent p determines the slope of the threshold curve. *Th* will always be greater than Th_{min} because the bracket portion of the equation is always greater than one. Equation (1) is consistent with the equation of $Th = \theta_{\min}(1 + L_{crit} / x)^n$ used in Sally and Gurnsey (2003, 2004).

In Tables 1-4 are listed the results of fitting with equation (1) to each eccentric orientation discrimination threshold curve (as a function of stimulus height in log-log axis), for the Gaussian filtered lines, 2, 4, and 16cpi gratings, respectively.

Subject	Contrast	Eccentricity (deg)	Th_{min}	H_c	p	R^2
LC	100%	0	0.43801	0.44938	2.00906	0.89628
	100%	2.5	0.47326	2.64837	0.94652	0.9891
	100%	5	0.54667	1.44229	1.62988	0.98476
	100%	7.5	0.72548	0.96335	2.24635	0.98767
	100%	10	0.74902	1.50951	1.80608	0.98583
	30%	0	0.48166	0.02402	36.45987	0.98179
	30%	2.5	0.63056	0.03968	35.42564	0.99102
	30%	5	0.7199	0.03307	54.02952	0.97864
	30%	7.5	0.8475	0.0411	45.07817	0.98762
	30%	10	1.00317	0.07825	23.00296	0.9937
	10%	0	0.82522	0.02635	35.8089	0.95272
	10%	2.5	0.86486	0.0394	50.17663	0.95582
	10%	5	1.46907	0.02221	31.54027	0.9402
	10%	7.5	1.48726	0.06246	42.89962	0.90592
	10%	10	1.49824	0.10299	34.96449	0.947
VR	100%	0	0.3016	1.20903	1.14529	0.97864
	100%	2.5	0.44486	0.26911	4.5656	0.9854
	100%	5	0.42345	2.64901	1.19301	0.97019
	100%	7.5	0.50271	0.86006	3.2133	0.98767
	100%	10	0.87268	0.0205	96.75502	0.96324
	30%	0	0.55192	0.4829	2.35162	0.99862
	30%	2.5	0.85048	0.64012	2.01722	0.99239
	30%	5	1.0845	0.06938	17.84338	0.9946
	30%	7.5	1.54747	0.01968	74.66115	0.92858
	30%	10	2.22014	0.07932	18.15708	0.98545
	10%	0	1.31436	0.05627	3.643501	0.99603
	10%	2.5	1.49618	3.95821	1.15815	0.99199
	10%	5	1.59862	5.01301	1.36242	0.96221
	10%	7.5	2.03077	0.10379	42.26309	0.9421
	10%	10	2.68375	0.01984	303.29264	0.9596

p	
Average	32.39
Min	0.95
Max	303.29

Table 1 The results of fitting with equation (1) to each eccentric orientation discrimination threshold curve of the Gaussian filtered lines at 0-10 deg eccentricities and 10-100% contrasts for subjects LC and VR.

Subject	Contrast	Eccentricity (deg)	Th_{min}	H_c	p	R^2
LC	100%	0	0.41238	0.00435	55.98465	0.99816
	100%	2.5	0.60848	0.00347	82.57457	0.98522
	100%	5	0.6373	0.01553	21.87394	0.99353
	100%	7.5	0.72722	0.10983	4.53491	0.99592
	100%	10	1.06624	0.00976	56.38259	0.98257
	30%	0	0.50902	0.07988	4.66606	0.9839
	30%	2.5	0.43605	1.5421	0.96788	0.97001
	30%	5	0.99733	0.01191	34.47259	0.95639
	30%	7.5	1.11138	0.00454	111.22269	0.98993
	30%	10	1.22433	0.45703	2.17465	0.99925
	10%	0	0.8897	0.02343	14.96186	0.98869
	10%	2.5	1.42367	0.01857	33.1915	0.95457
	10%	5	1.38336	0.01667	65.48333	0.98161
	10%	7.5	1.51052	0.01498	85.70975	0.97286
	10%	10	2.07294	0.01969	61.642	0.99046
AS	100%	0	0.67399	0.00422	49.14233	0.92837
	100%	2.5	1.12666	0.08515	3.86651	0.99117
	100%	5	1.20298	0.05601	5.8332	0.99325
	100%	7.5	0.82786	3.36345	0.6185	0.99622
	100%	10	1.38486	1.77688	0.86381	0.9789
	30%	0	0.70937	0.21152	1.50529	0.92809
	30%	2.5	0.70441	4.05402	0.61488	0.98168
	30%	5	1.17726	0.01419	33.76188	0.97744
	30%	7.5	0.93425	3.91354	0.5625	0.94459
	30%	10	1.57086	0.01783	48.48233	0.93153
	10%	0	1.30853	0.01089	20.9132	0.98243
	10%	2.5	1.57567	0.00831	41.11614	0.90469
	10%	5	1.67294	0.0203	29.63005	0.98738
	10%	7.5	1.31625	2.18199	1.1461	0.98637
	10%	10	0.18487	109.784	0.83362	0.95582

p	
Average	29.16
Min	0.56
Max	111.22

Table 2 The results of fitting with equation (1) to each eccentric orientation discrimination threshold data curve of the 2cpi gratings at 0-10 deg eccentricities and 10-100% contrasts for subjects LC and AS.

.

Subject	Contrast	Eccentricity (deg)	Th_{min}	H_c	p	R^2
LC	100%	0	0.37427	0.00605	55.92193	0.95886
	100%	2.5	0.18082	15.65908	0.68498	0.9522
	100%	5	0.7368	0.08105	8.52156	0.92445
	100%	7.5	0.11909	54.11079	0.71225	0.97258
	100%	10	0.98486	0.06842	12.27985	0.99544
	30%	0	0.50476	0.00906	47.55757	0.98459
	30%	2.5	0.79902	0.01681	36.89897	0.97056
	30%	5	0.82989	0.01308	59.14299	0.91248
	30%	7.5	0.90007	0.02382	37.19299	0.92297
	30%	10	1.12188	0.01361	87.90108	0.98272
	10%	0	0.54211	0.00874	63.86272	0.97962
	10%	2.5	1.10362	0.00971	68.82937	0.97766
	10%	5	1.1584	0.02485	35.18683	0.99021
	10%	7.5	0.82384	16.06013	0.54116	0.98664
	10%	10	1.03487	6.93535	0.75277	0.95689
AS	100%	0	0.48692	1.63275	0.82638	0.99635
	100%	2.5	0.69875	0.06318	8.854443	0.98423
	100%	5	0.7782	3.26884	0.70302	0.99354
	100%	7.5	0.42724	19.67435	0.6958	0.98389
	100%	10	0.47822	16.86009	0.82944	0.97389
	30%	0	0.675	0.00632	77.072472	0.92988
	30%	2.5	0.70348	2.04264	0.85488	0.99757
	30%	5	1.1965	0.21505	3.34942	0.95626
	30%	7.5	1.16618	0.72135	2.68324	0.99142
	30%	10	1.17717	1.42566	2.06528	0.99296
	10%	0	0.73269	1.05905	1.21103	0.9964
	10%	2.5	1.36711	0.15513	6.09572	0.9884
	10%	5	1.44091	0.04526	22.60764	0.97776
	10%	7.5	1.19474	4.88758	0.99837	0.9719
	10%	10	1.95661	0.08978	18.9601	0.95846

p	
Average	22.13
Min	0.54
Max	87.90

Table 3 The results of fitting with equation (1) for each eccentric orientation discrimination threshold data curve of the 4cpi gratings at 0-10 deg eccentricities and 10-100% contrasts for subjects LC and AS.

Subject	Contrast	Eccentricity (deg)	Th_{min}	H_c	p	R^2
LC	100%	0	0.3267	1.101234	1.1147	0.99288
	100%	2.5	0.60721	0.09484	15.90167	0.98892
	100%	5	0.65792	0.04432	35.35118	0.99266
	100%	7.5	0.67644	1.69792	1.59087	0.99661
	100%	10	0.7291	0.6782	4.35071	0.99975
	30%	0	0.47193	0.02018	46.24418	0.94086
	30%	2.5	0.15295	1060.4	0.34046	0.9999
	30%	5	0.72685	0.06682	28.96893	0.97875
	30%	7.5	0.78076	0.29879	10.06971	0.97972
	30%	10	0.81146	0.02956	145.35	0.98439
	10%	0	0.50979	0.03766	21.59437	0.98387
	10%	2.5	0.73599	0.19148	13.45392	0.99744
	10%	5	0.59958	20.48145	0.59055	0.99431
	10%	7.5	0.80839	0.19248	25.18283	0.99429
	10%	10	0.84487	0.19942	30.77387	0.99196
AS	100%	0	0.40955	0.98156	2.39252	0.99533
	100%	2.5	0.84515	0.01912	123.757	0.9355
	100%	5	0.89136	0.03312	93.65068	0.96623
	100%	7.5	0.9055	0.06154	68.04788	0.96753
	100%	10	0.70039	8.19232	2.22321	0.99442
	30%	0	0.40922	1.64102	1.94187	0.97276
	30%	2.5	0.95314	0.02807	76.55866	0.97565
	30%	5	1.29513	0.02803	94.14955	0.90672
	30%	7.5	1.21895	4.75808	1.30193	0.97369
	30%	10	0.16493	231.67	0.91157	0.16493
	10%	0	0.46367	8.55664	0.91092	0.91507
	10%	2.5	0.19501	1362.6	0.44549	0.99163
	10%	5	0.33502	450.2	0.5046	0.9851
	10%	7.5	0.13594	749.66	0.6933	0.97628
	10%	10	0.06693	634.2	1.06085	0.97088

p	
Average	28.31
Min	0.34
Max	145.35

Table 4 The results of fitting with equation (1) to each eccentric orientation discrimination threshold data curve of the 16cpi gratings at 0-10 deg eccentricities and 10-100% contrasts for subjects LC and AS.

With the exponent p being left to be free, the value of the exponent was found to range from 0.34 to 303 (see Tables 1-4). The large variation of the p value made it impossible to obtain an optimal equation for fitting to all the eccentric threshold curves from all eccentricities, contrasts, subjects and stimuli.

Therefore, the curve fitting of each threshold curve was conducted with the variant equation of equation (1), i.e. $Th = Th_{\min}(1 + H_c / H)^p$ where p is equal to 1-6.

p was not allowed to be greater than 6 due to the consideration that the order of the traditional threshold curve fitting function was about 1-3 in literature (Makela *et al* 1993, Melmoth *et al* 2000b, Sally and Gurnsey 2003, 2004).

The final optimal equation obtained to fitted all the eccentric threshold curve was

$$Th = Th_{\min}(1 + H_c / H)^5, \qquad \textbf{Equation (2)}$$

where p is equal to 5. The fitting R^2 with equation (2) was calculated for each eccentric threshold data curve to check the accuracy and was found to range from 0.85 to 0.99, with an average of 0.95. Therefore, equation (2) accurately describes all the eccentric threshold data curves. Tables 5-8 show the results of fitting to each eccentric threshold curve (against stimulus height in log-log axis) with equation (2), for the Gaussian filtered lines, 2, 4 and 16cpi gratings, respectively.

LC	Gaussian filtered lines			
Contrast	**Eccentricity (deg)**	Th_{min}	H_c	R^2
100%	0	0.47634	0.12954	0.89535
100%	2.5	0.66068	0.1575	0.95708
100%	5	0.61426	0.30751	0.9789
100%	7.5	0.78098	0.33449	0.98537
100%	10	0.85417	0.35884	0.98036
30%	0	0.46722	0.20545	0.97298
30%	2.5	0.59674	0.34596	0.98363
30%	5	0.69932	0.41479	0.96704
30%	7.5	0.81951	0.43325	0.97989
30%	10	0.9744	0.41213	0.9902
10%	0	0.81968	0.20269	0.94498
10%	2.5	0.84792	0.44582	0.94388
10%	5	1.46827	0.14232	0.93905
10%	7.5	1.46833	0.5822	0.89395
10%	10	1.45839	0.80843	0.93685
			Average	**0.95663**

VR	Gaussian filtered lines			
Contrast	**Eccentricity (deg)**	Th_{min}	H_c	R^2
100%	0	0.33661	0.15296	0.9617
100%	2.5	0.44729	0.2404	0.98536
100%	5	0.49547	0.32319	0.95217
100%	7.5	0.52467	0.4786	0.98704
100%	10	0.84261	0.4702	0.94639
30%	0	0.57619	0.18764	0.99668
30%	2.5	0.90651	0.1975	0.98825
30%	5	1.06567	0.27136	0.9917
30%	7.5	1.50892	0.33486	0.91319
30%	10	2.17118	0.31991	0.97994
10%	0	1.2754	0.48081	0.98966
10%	2.5	1.63258	0.563	0.98384
10%	5	1.84962	0.79158	0.94396
10%	7.5	2.0052	0.95863	0.93207
10%	10	2.62885	1.34712	0.94434
			Average	**0.96642**

Table 5 The results of the curve fitting with equation (2) for the eccentric orientation discrimination threshold data curve of the Gaussian filtered lines at 0-10 deg eccentricities and 10-100% contrasts for subjects LC and VR (see Fig 3.3 in Chapter 3).

LC	4pi gratings			
Contrast	Eccentricity (deg)	Th_{min}	H_c	R^2
100%	0	0.35330	0.08508	0.94421
100%	2.5	0.54849	0.13437	0.91858
100%	5	0.71875	0.15066	0.92380
100%	7.5	0.79203	0.16487	0.93229
100%	10	0.95186	0.18847	0.99489
30%	0	0.47595	0.10774	0.97100
30%	2.5	0.77356	0.14544	0.96480
30%	5	0.79514	0.18465	0.90326
30%	7.5	0.86674	0.21199	0.92265
30%	10	1.06913	0.29689	0.96648
10%	0	0.52125	0.13550	0.96256
10%	2.5	1.08235	0.15432	0.96728
10%	5	1.13653	0.19851	0.98472
10%	7.5	1.27438	0.26845	0.90904
10%	10	1.38742	0.30882	0.90108
			Average	**0.94444**

AS	4pi gratings			
Contrast	Eccentricity (deg)	Th_{min}	H_c	R^2
100%	0	0.60657	0.08765	0.96588
100%	2.5	0.69423	0.11791	0.98377
100%	5	0.99404	0.13599	0.96815
100%	7.5	1.13126	0.20874	0.88151
100%	10	1.35890	0.25654	0.89185
30%	0	0.65231	0.11555	0.90730
30%	2.5	0.90384	0.13332	0.97600
30%	5	1.21046	0.13468	0.95611
30%	7.5	1.27682	0.29985	0.98826
30%	10	1.46560	0.35051	0.98213
10%	0	0.77583	0.18072	0.99216
10%	2.5	1.35629	0.19562	0.98839
10%	5	1.37689	0.24224	0.97437
10%	7.5	1.68869	0.34397	0.94432
10%	10	1.87310	0.39389	0.95747
			Average	**0.95718**

Table 6 The results of the curve fitting with equation (2) for the eccentric orientation discrimination threshold data curve of the 4cpi gratings at 0-10 deg eccentricities and 10-100% contrasts for subjects LC and AS (see Fig 4.3 in Chapter 4).

LC	2pi gratings			
Contrast	Eccentricity (deg)	Th_{min}	H_c	R^2
1	0	0.40507	0.05405	0.99661
1	2.5	0.59416	0.06489	0.98001
1	5	0.62031	0.07644	0.98951
1	7.5	0.73202	0.09751	0.99591
1	10	0.98094	0.13824	0.97006
0.3	0	0.51041	0.0737	0.9839
0.3	2.5	0.66646	0.09042	0.9370
0.3	5	0.9875	0.09122	0.9496
0.3	7.5	1.09034	0.11273	0.9860
0.3	10	1.30343	0.15689	0.9974
0.1	0	0.87342	0.07738	0.9880
0.1	2.5	1.39462	0.13776	0.9447
0.1	5	1.27505	0.27423	0.9674
0.1	7.5	1.35096	0.33681	0.9523
0.1	10	1.86493	0.31408	0.9783
			Average	**0.97445**

AS	2pi gratings			
Contrast	Eccentricity (deg)	Th_{min}	H_c	R^2
1	0	0.66771	0.04485	0.91991
1	2.5	1.13637	0.06321	0.99112
1	5	1.19761	0.06670	0.99324
1	7.5	1.27301	0.07549	0.92851
1	10	1.72149	0.12669	0.95674
0.3	0	0.76032	0.04494	0.92506
0.3	2.5	1.10218	0.08013	0.91629
0.3	5	1.11434	0.11475	0.96531
0.3	7.5	1.29464	0.10329	0.89637
0.3	10	1.52506	0.20125	0.94446
0.1	0	1.29365	0.04918	0.97879
0.1	2.5	1.53870	0.07732	0.89009
0.1	5	1.52797	0.15100	0.97690
0.1	7.5	1.85127	0.19448	0.97290
0.1	10	2.77099	0.22919	0.85148
			Average	**0.94048**

Table 7 The results of the curve fitting by equation (2) for the eccentric orientation discrimination threshold data curve of the 2cpi gratings at 0-10 deg eccentricities and 10-100% contrasts for subjects LC and AS (see Fig 5.3a in Chapter 5).

LC	16pi gratings			
Contrast	Eccentricity (deg)	Th_{min}	H_c	R^2
100%	0	0.33854	0.16492	0.98852
100%	2.5	0.59356	0.33765	0.98702
100%	5	0.64524	0.34958	0.99187
100%	7.5	0.71017	0.41402	0.99408
100%	10	0.73319	0.57642	0.99973
30%	0	0.46638	0.20344	0.93168
30%	2.5	0.63055	0.33206	0.92600
30%	5	0.71698	0.42225	0.97331
30%	7.5	0.76362	0.65571	0.97939
30%	10	0.78403	0.99728	0.97913
10%	0	0.50648	0.17332	0.98101
10%	2.5	0.72511	0.56132	0.99709
10%	5	0.75413	0.76506	0.96452
10%	7.5	0.78864	1.08610	0.99375
10%	10	0.81336	1.42025	0.98664
			Average	**0.97825**

AS	16pi gratings			
Contrast	Eccentricity (deg)	Th_{min}	H_c	R^2
100%	0	0.47103	0.32796	0.98997
100%	2.5	0.65477	0.67169	0.94355
100%	5	0.75083	0.86943	0.94323
100%	7.5	0.76359	1.17244	0.94514
100%	10	1.76581	1.35900	0.99366
30%	0	0.47443	0.40245	0.96851
30%	2.5	0.90299	0.52797	0.96166
30%	5	1.24784	0.62975	0.88187
30%	7.5	1.46902	0.66501	0.96123
30%	10	1.75849	1.04468	0.94102
10%	0	0.70747	0.41623	0.85149
10%	2.5	1.38510	0.44694	0.91086
10%	5	1.79224	0.50158	0.87595
10%	7.5	1.88566	0.73442	0.87173
10%	10	2.54169	1.53610	0.87913
			Average	**0.92793**

Table 8 The results of the curve fitting by equation (2) for the eccentric orientation discrimination threshold data curve of the 16cpi gratings 0-10 deg eccentricities and 10-100% contrasts for subjects LC and AS (see Fig 5.3b in Chapter 5).

Appendix VI The optimal curve fitting equation for eccentric contrast threshold curve

Due to the similar shapes of the eccentric threshold data curves at all eccentricities and orientation differences for all subjects and stimuli, all the eccentric contrast threshold (*Th*) data (see Fig 6.1 in Chapter 6, Fig 7.1 in Chapter 7 and Fig 8.1a and 8.1b in Chapter 8) were fitted with equation (1) (Melmoth *et al.* (2000a, b) and Sally *et al.* (2005).):

$$Th = Th_{\min}(1 + (H_c / H)^p)^n, \qquad \textbf{Equation (1)}$$

where Th_{min} is the theoretical minimum threshold, H is stimulus height (i.e. line length or grating diameter in this thesis). H_c is the critical stimulus height marking the change from the decrease to plateau. Exponent p and n together determine the slope of the threshold curve. Th will always be greater than Th_{min} because the bracket portion of the equation is always greater than one.

Tables 1-4 show the results of the curve fitting with equation (1) to the each eccentric contrast threshold (against stimulus height in log-log axis) at 1.5-45 deg orientation differences, for the Gaussian filtered lines, 2, 4, and 16 cpi gratings, respectively.

LC	Gaussian filtered lines					
OD (deg)	E (deg)	Th_{min}	H_c	n	p	R^2
45	0	0.01449	0.0202	19.35108	0.70174	0.99297
45	2.5	0.01697	0.05659	25.42861	0.87375	0.98037
45	5	0.02689	7.47719	0.22392	4.23625	0.99555
45	7.5	0.0192	0.0453	22.65925	0.68766	0.99827
45	10	0.03393	11.48089	0.06024	11.93432	0.98625
15	0	0.0183	0.18205	7.28473	1.41205	0.99991
15	2.5	0.022	5.45517	0.39399	2.36085	0.99969
15	5	0.30057	7.12043	0.07809	10.42447	0.99167
15	7.5	0.03277	7.05234	0.03417	27.97613	0.99774
15	10	0.02116	17.08257	0.03095	25.33582	0.99414
5	0	0.02522	1.59094	0.78823	2.19262	0.99982
5	2.5	0.00392	0.18373	8.55306	0.3001	0.97108
5	5	0.00056	22.52017	5.70501	0.19692	0.98197
5	7.5	0.04891	8.46136	0.26647	4.04486	0.9979
5	10	0.06962	0.88386	141.06764	3.19673	0.9741
1.5	0	0.04819	3.4758	0.24052	3.70271	1
1.5	2.5	0.08275	9.51485	0.021	30.80244	0.98542
1.5	5	0.09326	9.00304	0.02245	51.54293	0.97895
1.5	7.5	0.09275	1.17342	25.30299	2.13552	0.99252
1.5	10	0.10966	4.08272	29.82746	5.48871	0.99853
			Average	**14.367**	**9.477**	**0.991**

YC	Gaussian filtered lines					
OD (deg)	E (deg)	Th_{min}	H_c	n	p	R^2
45	0	0.01283	0.0757	12.61146	0.80735	0.99927
45	2.5	0.00927	0.13076	11.73255	0.64226	0.99899
45	5	0.03042	0.84302	3.32131	1.37726	1
45	7.5	0.00947	0.00497	42.16564	0.46537	0.97739
45	10	0.00003	0.0478	18.709967	0.13995	0.99337
15	0	0.01683	3.6988	0.58599	1.8495	0.99932
15	2.5	0.01814	6.78668	0.69043	1.52162	1
15	5	0.02997	5.77541	0.16087	7.0525	0.9994
15	7.5	0.01295	0.2393	6.11901	0.41325	0.98603
15	10	0.00126	1.29414	7.81433	0.26168	0.96112
5	0	0.0305	5.61264	0.05227	14.62628	0.99986
5	2.5	0.03437	7.74071	0.04677	19.18304	0.99979
5	5	0.04939	6.54197	0.01904	56.34723	0.99373
5	7.5	0.05398	6.52177	0.03646	32.556	0.98661
5	10	0.07281	1.27502	70.34881	3.64831	0.97752
1.5	0	0.06997	1.17052	4.39852	2.2235	1
1.5	2.5	0.1039	7.50431	0.01612	49.23101	0.98374
1.5	5	0.12794	6.69605	0.03414	33.84873	0.970984
			Average	**9.937**	**12.566**	**0.990**

Table 1 The results of curve fitting with equation (1) for the eccentric contrast threshold data of the Gaussian filtered lines for subjects LC and YC.

LC	2 cpi gratings					
OD (deg)	E (deg)	Th_{min}	H_c	n	p	R^2
45	0	0.00822	0.21012	2.30814	2.577	0.9985
45	2.5	0.01707	0.07346	11.97212	1.43737	0.99063
45	5	0.01362	0.11231	6.87078	0.8899	0.99529
45	7.5	0.01444	0.01361	37.08626	0.8584	0.99279
45	10	0.01943	0.03383	27.89939	1.07531	0.99835
15	0	0.01168	0.06954	92.77014	4.01819	0.99436
15	2.5	0.02389	0.01286	482.86204	1.92505	0.97984
15	5	0.0275	0.12536	7.24563	1.43761	0.99991
15	7.5	0.02785	0.00478	21.445405	1.13166	0.9982
15	10	0.02945	0.0207	40.83355	1.07822	0.99641
5	0	0.01772	0.53704	0.22106	6.16106	0.99991
5	2.5	0.05038	0.13612	7.39144	2.47365	0.99593
5	5	0.05119	0.02855	34.38553	1.25545	0.99199
5	7.5	0.05698	0.00564	89.63086	0.94603	0.98088
5	10	0.08889	2.16013	0.01367	76.42541	0.97991
1.5	0	0.05752	0.28754	2.5257	2.92936	0.99999
1.5	2.5	0.09536	0.05691	13.77139	0.95063	0.99996
1.5	5	0.20601	1.68168	0.20463	4.84699	0.99992
1.5	7.5	0.20415	0.61633	8.88373	2.46567	0.99665
1.5	10	0.24274	0.38711	50.29531	2.71707	0.9982
			Average	**46.931**	**5.880**	**0.994**

BU	2 cpi gratings					
OD (deg)	E (deg)	Th_{min}	H_c	n	p	R^2
45	0	0.02986	1.07119	0.01599	134.74286	0.99598
45	2.5	0.01822	0.31554	2.43563	2.72321	1
45	5	0.02482	0.67251	0.11632	26.61606	0.99994
45	7.5	0.00258	10.31704	0.07356	16.83041	0.9459
45	10	0.01007	0.65182	0.05627	33.56216	0.99472
15	0	0.00963	0.12501	6.13898	1.38037	0.99967
15	2.5	0.02376	0.06513	29.73458	1.9196	0.99999
15	5	0.02705	0.94921	0.52534	2.93573	0.99652
15	7.5	0.02799	0.0151	31.04869	0.87281	0.9877
15	10	0.01771	0.04477	17.30349	0.76523	0.99815
5	0	0.02062	0.02171	76.64456	1.48264	0.99085
5	2.5	0.02108	0.2322	3.65847	0.84279	1
5	5	0.02596	0.01027	53.05469	0.8755	0.99476
5	7.5	0.02218	0.00034	356.94694	0.70804	0.99751
5	10	0.07097	1.36579	0.13574	10.72819	0.9926
1.5	0	0.1349	0.97673	0.41649	3.92671	1
1.5	2.5	0.12785	0.00197	565.61159	1.06181	0.99979
1.5	5	0.16763	0.05767	11.49876	0.85595	0.96117
			Average	**64.190**	**13.491**	**0.992**

Table 2 The results of curve fitting by equation (1) for the eccentric contrast threshold data of the 2cpi gratings for subjects LC and BU.

LC	4cpi gratings					
OD (deg)	E (deg)	Th_{min}	H_c	n	p	R^2
45	0	0.00561	0.72945	0.48256	4.50113	1
45	2.5	0.00758	0.89709	1.58933	1.86864	1
45	5	0.00987	1.5399	0.7371	2.56748	1
45	7.5	0.01096	0.22484	9.9803	1.54423	0.99997
45	10	0.01498	1.33529	0.25074	10.32027	1
15	0	0.00546	0.49521	1.53322	2.24519	1
15	2.5	0.0099	0.62383	1.8624	2.09768	0.99906
15	5	0.01487	1.34005	0.14878	13.09435	0.99995
15	7.5	0.01701	0.1539	19.91964	1.86988	0.99933
15	10	0.01942	0.09768	39.01417	1.66318	0.99873
5	0	0.0087	0.46017	1.3734	2.5133	0.9981
5	2.5	0.01918	0.85606	0.95191	3.05647	0.9996
5	5	0.02544	1.34891	0.0851	21.29445	0.99997
5	7.5	0.02053	1.4331	0.6974	3.01046	1
5	10	0.024077	4.26346	0.25591	3.19598	1
1.5	0	0.03899	2.09049	0.04501	26.34208	0.99679
1.5	2.5	0.07225	0.07407	11.64117	0.74848	0.99655
1.5	5	0.11008	4.39225	0.18773	4.50975	1
1.5	7.5	0.17639	4.00401	0.04466	21.92134	0.98562
1.5	10	0.03364	7.46181	2.95967	0.32682	0.98512
			Average	**4.898**	**6.435**	**0.998**
BU	**4cpi gratings**					
OD (deg)	**E (deg)**	Th_{min}	H_c	n	p	R^2
45	0	0.00452	0.19089	10.32915	1.25869	0.99584
45	2.5	0.00862	2.30278	0.15239	12.51411	0.99626
45	5	0.01067	2.71418	0.10489	19.04232	0.99928
45	7.5	0.00538	1.83604	2.48835	1.31486	0.98905
45	10	0.02158	2.46927	0.09393	23.39014	0.99777
15	0	0.00629	1.4954	0.62943	2.56258	1
15	2.5	0.01217	1.6917	0.06105	39.75802	0.99453
15	5	0.0159	1.41275	0.82908	3.95196	1
15	7.5	0.02289	2.09092	0.0562	37.18679	0.99997
15	10	0.02578	1.5376	0.67999	4.48911	1
5	0	0.00874	0.03222	26.79525	1.00899	0.99681
5	2.5	0.02516	1.31508	0.4332	5.9472	1
5	5	0.02106	0.24111	8.5828	1.16511	0.98869
5	7.5	0.03473	0.06344	47.04927	1.29403	0.97743
5	10	0.05158	0.26032	41.65133	2.42189	0.97433
1.5	0	0.03638	1.78203	0.8678	3.19932	0.99742
1.5	2.5	0.03372	0.65192	5.44046	1.12228	0.99961
1.5	5	0.11174	4.59949	0.13455	9.37295	1
1.5	7.5	0.02616	12.185	1.8249	0.68443	0.99968
1.5	10	0.22783	7.7339	0.34405	2.60377	0.97837
			Average	**7.813**	**8.714**	**0.994**

Table 3 The results of curve fitting by equation (1) for the eccentric contrast threshold data of the 4cpi gratings for subjects LC and BU

LC	16cpi gratings					
OD (deg)	E (deg)	Th_{min}	H_c	n	p	R^2
45	0	0.00314	1.64094	1.27936	2.49947	0.99912
45	2.5	0.00421	3.73358	1.20589	2.48223	0.99956
45	5	0.00474	2.83523	2.25655	2.99363	0.99821
45	7.5	0.00794	5.63389	0.020299	11.79459	1
45	10	0.00865	5.24873	0.33494	9.18429	1
15	0	0.00321	2.52723	0.41034	6.05934	0.99943
15	2.5	0.00577	0.57162	10.31959	1.46412	0.99963
15	5	0.00641	0.76888	11.29396	1.65474	1
15	7.5	0.00842	3.80864	1.09441	3.24022	1
15	10	0.00787	0.59302	21.78379	1.49502	0.99975
5	0	0.00521	2.89319	0.10668	16.75147	0.99982
5	2.5	0.00783	2.43456	1.77795	2.26783	0.99911
5	5	0.00923	3.17716	1.626536	2.19387	1
5	7.5	0.01118	6.5609	0.41828	4.67476	1
5	10	0.01197	6.30216	1.00955	2.44599	1
1.5	0	0.00929	4.52399	0.03856	40.83914	0.99018
1.5	2.5	0.020804	0.59935	43.88483	2.42333	0.99403
1.5	5	0.03146	6.15753	0.54289	2.97723	1
1.5	7.5	0.01877	0.61655	16.18184	0.99667	0.99319
1.5	10	0.02051	7.57638	2.07541	1.19365	0.94133
			Average	**5.883**	**5.982**	**0.996**
BU	**16cpi gratings**					
OD (deg)	E (deg)	Th_{min}	H_c	n	p	R^2
45	0	0.00294	4.70547	0.00904	22.68846	0.9996
45	2.5	0.00473	7.41191	0.04922	35.80204	0.99981
45	5	0.00604	4.73115	1.07204	2.92575	1
45	7.5	0.00751	5.17995	1.04331	3.14766	1
45	10	0.00805	6.68644	0.80636	4.25373	1
15	0	0.00455	3.06203	1.00706	2.87366	0.98295
15	2.5	0.00668	6.12518	0.07067	30.17806	0.9848
15	5	0.00956	6.79335	0.05387	37.38402	0.99345
15	7.5	0.01065	7.32341	0.035	59.20997	0.98936
15	10	0.01351	8.42761	0.10606	21.29845	1
5	0	0.00206	2.89976	2.74987	1.20745	0.99565
5	2.5	0.00674	0.45657	39.56711	1.83463	0.99127
5	5	0.01047	1.60784	5.62845	1.90958	0.99996
5	7.5	0.00137	1.97021	6.8561	0.64489	0.99127
5	10	0.01857	6.17464	0.84909	2.97593	0.99529
1.5	0	0.0142	4.02113	0.79908	2.55792	0.99876
1.5	2.5	0.01698	3.44497	1.33596	1.87518	0.99958
1.5	5	0.03074	6.0797	0.04939	34.82326	0.99872
1.5	7.5	0.05559	6.53675	0.07323	19.45281	0.96649
1.5	10	0.11786	2.37169	3.77126	2.48754	0.99964
			Average	**3.297**	**14.477**	**0.994**

Table 4 The results of curve fitting by equation (1) for the eccentric contrast threshold of the 16cpi gratings for subjects LC and BU.

Both n and p obtained through the curve fitting with equation (1) had large variations across eccentricities and orientation differences, showing in Tables (1-4). Therefore, the optimal equation could not be obtained if n and p were left to be free without limitations. Thus, the two exponents were fixed to be 1-5 and their multiplication cannot be over than 5 under the consideration that the order of the orientation discrimination threshold optimal curve fitting function obtained was 5, as well that the order of the threshold curve fitting function in literature was found to be between 1-3 (Makela *et al* 1993, Melmoth *et al* 2000b, Sally and Gurnsey 2003, 2004).

The final optimal equation obtained to fitted all the eccentric threshold curve was

$$Th = Th_{\min}(1+(H_c / H)^2)^{2.5}, \qquad \textbf{Equation (2)}$$

(see Sections 6.3, 7.3 and 8.3 in Chapters 6, 7 and 8, respectively).The fitting R^2 by equation (2) was calculated for each data curve to check the accuracy of the fit and found to range from 0.85-0.99, with the mean value of 0.96. Therefore, equation (2) describes quite accurately all the data curves. Tables 5-8 show the results of fitting with equation (2) to each eccentric contrast threshold curve (against stimulus height in log-log axis) at 1.5-45 deg orientation differences, for the Gaussian filtered lines, 2, 4, and 16 cpi gratings, respectively.

LC	Gaussian filtered lines			
OD (deg)	**E (deg)**	Th_{min}	H_c	R^2
0	45	0.02135	0.50927	0.90236
2.5	45	0.02345	1.03725	0.93624
5	45	0.03307	1.1216	0.90222
7.5	45	0.03549	1.17743	0.92898
10	45	0.03873	1.64294	0.83813
0	15	0.02021	0.456	0.99432
2.5	15	0.02776	0.93042	0.9281
5	15	0.03692	0.97121	0.86805
7.5	15	0.03964	1.09961	0.90191
10	15	0.03861	1.59687	0.92627
0	5	0.02805	0.58338	0.97488
2.5	5	0.05064	0.99402	0.86799
5	5	0.05442	1.4026	0.86455
7.5	5	0.05467	1.91742	0.94488
10	5	0.06145	2.89301	0.94084
0	1.5	0.05006	0.78083	0.97251
2.5	1.5	0.08975	1.45893	0.8652
5	1.5	0.08204	2.98938	0.90824
7.5	1.5	0.08847	3.7041	0.9895
10	1.5	0.09994	4.02615	0.86283
			Average	**0.916**

YC	Gaussian filtered lines			
OD (deg)	**E (deg)**	Th_{min}	H_c	R^2
0	45	0.02323	0.56511	0.96158
2.5	45	0.02359	1.14108	0.94208
5	45	0.03614	1.04798	0.98836
7.5	45	0.03099	1.79654	0.932
10	45	0.03528	1.95969	0.89392
0	15	0.02481	0.57863	0.87926
2.5	15	0.03169	0.99584	0.90082
5	15	0.03318	1.18395	0.92435
7.5	15	0.04233	1.46601	0.9225
10	15	0.04578	1.88036	0.8686
0	5	0.03428	0.86453	0.90537
2.5	5	0.04532	1.04287	0.85382
5	5	0.04681	1.76307	0.95468
7.5	5	0.05054	1.88098	0.94102
10	5	0.06381	2.76227	0.93019
0	1.5	0.06686	1.54948	0.99847
2.5	1.5	0.09672	2.00248	0.89367
5	1.5	0.11678	2.11838	0.85188
			Average	**0.919**

Table 5 The results of curve fitting by equation (2) for the eccentric contrast threshold data of the Gaussian filtered lines for subjects LC and YC (see Fig 6.1 in Chapter 6)

LC	2 cpi gratings			
OD (deg)	**E (deg)**	Th_{min}	H_c	R^2
0	45	0.00785	0.19244	0.99159
2.5	45	0.01872	0.2595	0.98798
5	45	0.02465	0.3031	0.96829
7.5	45	0.02544	0.3233	0.97474
10	45	0.0274	0.35786	0.99236
0	15	0.0112	0.12496	0.95925
2.5	15	0.02396	0.23621	0.97605
5	15	0.03088	0.29648	0.99787
7.5	15	0.03536	0.29981	0.99222
10	15	0.04003	0.32149	0.98886
0	5	0.01681	0.18374	0.993
2.5	5	0.04699	0.22762	0.9847
5	5	0.06033	0.28194	0.9874
7.5	5	0.07822	0.29893	0.95946
10	5	0.09306	0.45328	0.90169
0	1.5	0.04984	0.31317	0.97997
2.5	1.5	0.13163	0.42253	0.97783
5	1.5	0.20751	0.39485	0.99206
7.5	1.5	0.18898	1.07957	0.98362
10	1.5	0.23479	1.03836	0.98746
			Average	**0.979**

BU	2 cpi gratings			
OD (deg)	**E (deg)**	Th_{min}	H_c	R^2
0	45	0.00905	0.2666	0.98182
2.5	45	0.01544	0.34349	0.98686
5	45	0.01921	0.40799	0.98943
7.5	45	0.02287	0.41787	0.98622
10	45	0.0242	0.48346	0.96041
0	15	0.0112	0.26466	0.99437
2.5	15	0.02237	0.29514	0.99516
5	15	0.02873	0.32404	0.97037
7.5	15	0.04513	0.31746	0.96596
10	15	0.04578	0.44352	0.97729
0	5	0.02185	0.27344	0.98825
2.5	5	0.03877	0.27193	0.93623
5	5	0.04364	0.35349	0.97299
7.5	5	0.03964	0.46181	0.95701
10	5	0.06643	0.46154	0.98442
0	1.5	0.12805	0.38593	0.99767
2.5	1.5	0.16073	0.43121	0.98314
5	1.5	0.21169	0.59453	0.9088
			Average	**0.974**

Table 6 The results of curve fitting by equation (2) for the eccentric contrast threshold data of the 2cpi gratings for subjects LC and BU (see Fig 8.1a in Chapter 8)

LC	4cpi gratings			
OD (deg)	E (deg)	Th_{min}	H_c	R^2
0	45	0.00524	0.32139	0.99496
2.5	45	0.00967	0.48586	0.98011
5	45	0.01101	0.58231	0.98071
7.5	45	0.0117	0.65203	0.99969
10	45	0.01247	0.69601	0.99402
0	15	0.00554	0.34497	0.99888
2.5	15	0.01032	0.47925	0.99728
5	15	0.01329	0.55953	0.99511
7.5	15	0.01633	0.57223	0.99596
10	15	0.01928	0.6497	0.99617
0	5	0.00843	0.3176	0.99772
2.5	5	0.01901	0.46329	0.9941
5	5	0.02303	0.53346	0.99544
7.5	5	0.02109	0.60926	0.99089
10	5	0.02806	0.75514	0.93697
0	1.5	0.05136	0.33067	0.86052
2.5	1.5	0.11351	0.76693	0.94618
5	1.5	0.12167	0.79519	0.93656
7.5	1.5	0.18187	0.86227	0.88567
10	1.5	0.28593	0.9104	0.88938
			Average	**0.968**

BU	4cpi gratings			
OD (deg)	E (deg)	Th_{min}	H_c	R^2
0	45	0.00572	0.65582	0.99021
2.5	45	0.00887	0.77665	0.93754
5	45	0.01206	0.87785	0.94311
7.5	45	0.01259	1.01311	0.95976
10	45	0.01894	1.06427	0.97239
0	15	0.00695	0.50809	0.97828
2.5	15	0.00984	0.81582	0.9737
5	15	0.01334	0.89563	0.99811
7.5	15	0.01856	0.9295	0.97685
10	15	0.02088	0.94785	0.99521
0	5	0.01149	0.43441	0.97558
2.5	5	0.02153	0.68306	0.99625
5	5	0.02808	0.73013	0.97975
7.5	5	0.03956	0.7826	0.97246
10	5	0.04644	0.95893	0.9635
0	1.5	0.03381	1.02053	0.99488
2.5	1.5	0.04938	1.23712	0.98426
5	1.5	0.09779	1.55243	0.99515
7.5	1.5	0.11565	1.67228	0.90563
10	1.5	0.23898	2.11781	0.95974
			Average	**0.973**

Table 7 The results of curve fitting by equation (2) for the eccentric contrast threshold data of the 4cpi gratings for subjects LC and BU (see Fig 7.1 in Chapter 7)

LC	16cpi gratings			
OD (deg)	E (deg)	Th_{min}	H_c	R^2
0	45	0.00326	0.98173	0.99401
2.5	45	0.00477	1.99832	0.98984
5	45	0.00499	2.53695	0.99787
7.5	45	0.00571	2.90192	0.99454
10	45	0.00508	3.46524	0.99389
0	15	0.0032	1.06964	0.97989
2.5	15	0.00618	1.8287	0.9988
5	15	0.00658	2.27802	0.99987
7.5	15	0.0074	2.62093	0.99565
10	15	0.00823	3.21924	0.99805
0	5	0.00477	1.11138	0.99124
2.5	5	0.00777	1.91445	0.99869
5	5	0.00925	2.34521	0.99966
7.5	5	0.01087	2.56156	0.98763
10	5	0.01357	2.93759	0.98615
0	1.5	0.00954	1.30951	0.91459
2.5	1.5	0.01772	2.50492	0.97295
5	1.5	0.03359	2.08372	0.98135
7.5	1.5	0.03154	4.22463	0.98212
10	1.5	0.03699	4.58339	0.91789
			Average	**0.984**

BU	16cpi gratings			
OD (deg)	E (deg)	Th_{min}	H_c	R^2
0	45	0.00284	1.85847	0.97165
2.5	45	0.0044	2.61048	0.96572
5	45	0.00601	2.92986	0.99941
7.5	45	0.00677	3.30597	0.99921
10	45	0.00617	4.56765	0.99593
0	15	0.00453	1.68561	0.97891
2.5	15	0.00598	2.63781	0.95847
5	15	0.00865	2.72966	0.96281
7.5	15	0.00959	2.94769	0.94823
10	15	0.01074	3.98072	0.98164
0	5	0.00469	1.7837	0.96994
2.5	5	0.00588	2.73873	0.9861
5	5	0.00924	2.99172	0.99745
7.5	5	0.01124	3.06141	0.97014
10	5	0.0185	3.20908	0.98813
0	1.5	0.0169	1.46339	0.96884
2.5	1.5	0.01907	1.97706	0.98893
5	1.5	0.02758	2.2582	0.9848
7.5	1.5	0.0472	2.39896	0.91796
10	1.5	0.11295	2.52543	0.99491
			Average	**0.976**

Table 8 The results of curve fitting by equation (2) for the eccentric contrast threshold data of the 16cpi gratings for subjects LC and BU (see Fig 8.1b in Chapter 8)